

UNIVERSITÄT ROSTOCK
MATHEMATISCH-NATURWISSENSCHAFTLICHE FAKULTÄT
INSTITUT FÜR CHEMIE
ABTEILUNG PHYSIKALISCHE UND THEORETISCHE CHEMIE

SYNTHESIS AND INVESTIGATION OF CLUSTERS OF LIKE-CHARGED IONS IN OH-FUNCTIONALIZED IONIC LIQUIDS

KUMULATIVE DISSERTATION
ZUR ERLANGUNG DES AKADEMISCHEN GRADES
Doktor der Naturwissenschaften
DER MATHEMATISCH-NATURWISSENSCHAFTLICHEN FAKULTÄT DER
UNIVERSITÄT ROSTOCK

Universität
Rostock



Traditio et Innovatio

VORGELEGT DURCH M.SC. THOMAS NIEMANN
AM 18. OKTOBER 2019
VERTEIDIGT IM RAHMEN DES WISSENSCHAFTLICHEN KOLLOQUIUMS
AM 14. JANUAR 2020

https://doi.org/10.18453/rosdok_id00002639

1. Gutachter: Prof. Dr. rer. nat. habil. Ralf Ludwig
Universität Rostock
Mathematisch-Naturwissenschaftliche Fakultät
Institut für Chemie
Physikalische und Theoretische Chemie
2. Gutachter: Prof. Dr. rer. nat. habil. Markus Gerhards
Technische Universität Kaiserslautern
Fachbereich Chemie
Physikalische und Theoretische Chemie
3. Gutachter: Prof. Dr. rer. nat. habil. Roland Winter
Technische Universität Dortmund
Fakultät für Chemie und Chemische Biologie
Physikalische Chemie

Eine neue wissenschaftliche Wahrheit pflegt sich nicht in der Weise durchzusetzen, dass ihre Gegner überzeugt werden und sich als belehrt erklären, sondern vielmehr dadurch, dass ihre Gegner allmählich aussterben und dass die heranwachsende Generation von vornherein mit der Wahrheit vertraut gemacht ist.

-Max Planck, Wissenschaftliche Selbstbiographie, 1948

Acknowledgement

With a thesis as extensive as a doctoral dissertation, its success does not depend solely on the topic or person who works on it, but also to a crucial part of those who support that person. At this point I would like to take the opportunity to thank some of these people.

First and foremost, I would like to thank Professor Doctor Ralf Ludwig not only for the opportunity to make my Ph.D. in his group and for the allocation of such an exciting and varied topic, but above this for all the things he has done for me beyond that. I would like to say thank you for all the scientific freedom and the great trust that you have placed in me, for the great support in the preparation and follow-up of the research-trips and that you have always had an open ear for all concerns and scientific discussions. I will always remember the moments that make this time so family like, like the green-cabbage dinner, all the conferences that I was allowed to join and especially our annual internal group meetings in Bad Malente and the evenings in the group-dynamic practice room (beer cellar).

I thank Professor Mark A. Johnson for his warm welcome to his research group during my visit to Yale University, the opportunity to conduct research in his labs, and, overall, for a fruitful collaboration.

Also from the University of Yale, I would like to thank Helen J. Zeng and Dr. Fabian S. Menges with whom I did the experiments together in the Johnson lab and also spent a nice time in New Haven.

Next, I would like to thank another co-operation partner who has invited me to his labs: Thanks to Professor Rob Atkin from the University of Western Australia for an unforgettable and very instructive time in Down Under.

For the very dedicated introduction to the techniques of atomic force microscopy, I would like to thank Dr. Hua Li.

I would like to thank Peeter Cooper and Manuel Brunner from the Atkin group for letting me live with them during the first month of my research stay and for showing me the peculiarities of the university and the city of Perth.

Special thanks go to the analytical department of the University of Rostock. I thank Dr. Dirk Michalik and Mrs. Heike Borgwald for carrying out innumerable NMR experiments, and Mrs. Petra Dunker for carrying out the elemental analyzes. I thank Dr. Alexander Villinger, Dr. Jonas Bresien and Mrs. Isabel Schicht for the not always routine determination of the single crystal structures.

A very special thanks to Dr. Dzmitry Zaitsau for the many DSC measurements.

I would like to thank all members of the working group Ludwig and the other members of the Physical and Theoretical Chemistry of the University of Rostock for the pleasant working atmosphere and the constant helpfulness. Especially I would like to greet the

"Stammtisch crew", with whom I have spent many happy hours in the Trotzenburg. My greatest thanks go to Peter Stange, who has been instrumental in helping me through countless proofreading sessions, many scientific discussions and a constant helping hand. But besides the research, it was also nice to have you as a colleague through all the intensive literature, film and series interpretation talks we had in the last years. In this note of thanks I would also like to thank the people who have accompanied me in addition to the study and the Ph.D. through all the ups and downs. These are my fellow students and friends who were there for me at all times and all the new friends I were allowed to meet all over the world. But this is especially true for my family, who always gave me motivation and the necessary support. My parents Torsten and Martina Niemann should be especially thanked at this point, because they have earned by their steady and unconditional support a large share in the success of this work. Last but not least, I thank my partner Jenny Bödeker for her love, her understanding and her continued support, which make me realize that I am not doing all this for myself alone.

Selbstständigkeitserklärung

Ich versichere hiermit an Eides statt, dass diese Arbeit selbstständig und ausschließlich mit Hilfe der von mir angegebenen Quellen und Hilfsmittel angefertigt wurde.

Thomas Niemann
Neubramowstraße 21
18057 Rostock
thomas.niemann@uni-rostock.de

Rostock, 18. Oktober 2019

Summary

The aim of this work is the systematic investigation of different dependencies of the formation of cationic clusters in OH-functionalised ionic liquids. Cationic clusters are aggregations of several cations via hydrogen bonds. The dependencies investigated in the context of this thesis are in particular the anion dependence, cation dependence and chain length dependence. The anion dependence addresses the influence of the interaction strength of the anions on the formation of the cationic clusters. The investigations of the cation dependence show the effect of the polarizability and charge localization of the positive charge in the cations on the attractive interactions between the like-charged ions. The effects of larger distances between the center of positive charge and the OH-functional group on the formation of cationic clusters are investigated as part of the chain length dependence by successive extension of the alkyl chain of the hydroxyalkyl group.

In the comprehensive study of the counter-intuitive phenomenon of the attractive interaction between ions, which should repel each other, due to the COULOMB forces acting between them, a variety of analytical methods are used. IR spectroscopy is used to investigate all the dependencies involved in the formation of cationic clusters in the bulk phase of several large sets of specially for this purpose designed and synthesised ionic liquids. On the basis of these findings, one ionic liquid was selected to investigate the cluster distribution and the different characteristics of the hydrogen bonds between the anions and the cations and the hydrogen bonds between the cations with each other by means of neutron diffraction and molecular dynamic simulations. Detailed structure elucidation of the structures underlying the cationic clusters is provided by a combination of photoinduced predissociation spectroscopy of mass selected gas phase clusters and quantum chemical calculations. In addition, quantum-chemical calculations are used in this work to investigate structures that would not be accessible experimentally or only with disproportionate effort. These theoretical investigations investigate the thermodynamic properties and explore the limits of the attractive interactions between the cations via hydrogen bonding. In an extensive interfacial analysis by atomic force microscopy, the influence of the attractive interactions between the cations on the formed bilayer structure is shown.

Even though each of these methods has its proven specialization and strengths and weaknesses, in addition to answering central questions, they also always provide confirmations for the findings obtained with other methods, which makes the methods used very complementary. In this way a complete and comprehensive picture of the cationic clusters in OH-functionalised ionic liquids is presented in scope of this work.

Zusammenfassung

Das Ziel dieser Arbeit ist die systematische Untersuchung verschiedener Abhängigkeiten der Bildung kationischer Cluster in OH-funktionalisierten ionischen Flüssigkeiten. Bei kationischen Clustern handelt es sich um Aggregationen von mehreren Kationen über Wasserstoffbrückenbindungen. Die im Rahmen dieser Arbeit untersuchten Abhängigkeiten sind im einzelnen die Anionen-, Kationen- und Kettenlängenabhängigkeit. Die Anionenabhängigkeit adressiert den Einfluss der Wechselwirkungsstärke der Anionen auf die Bildung der Cluster. Die Untersuchungen der Kationenabhängigkeit zeigen den Effekt der Polarisierbarkeit und Lokalisation der positiven Ladung in den Kationen. Die Auswirkungen größerer Abstände zwischen dem Zentrum der positiven Ladung und der OH-funktionellen Gruppe auf die Bildung kationischer Cluster werden im Rahmen der Kettenlängenabhängigkeit durch sukzessive Verlängerung des Alkylstrangs der Hydroxyalkylgruppe untersucht.

Bei der umfassenden Untersuchung des nicht ganz intuitiven Phänomens der attraktiven Wechselwirkung zwischen Ionen, die sich wegen den zwischen ihnen wirkenden COULOMB-Kräfte abstoßen sollten, wird auf eine Vielzahl analytischer Methoden zurückgegriffen. Mittels IR-Spektroskopie werden alle vorgestellten Abhängigkeiten der Clusterbildung in der bulk-Phase mehrerer Sets aus speziell zu diesem Zweck designten und synthetisierten ionischen Flüssigkeiten untersucht. Auf Basis dieser Erkenntnisse wurde eine ionische Flüssigkeit ausgewählt. Von dieser wird die Clusterverteilung und die unterschiedlichen Charakteristika der Wasserstoffbrückenbindungen zwischen den Anionen und den Kationen und der Wasserstoffbrückenbindungen zwischen den Kationen untereinander mittels Neutronenbeugung und Molekulardynamischen Simulationen untersucht. Die Strukturaufklärung der den kationischen Clustern zugrundeliegenden Strukturen erfolgt durch eine Kombination aus photoinduzierter Predissoziationsspektroskopie massenselektierter Gasphasencluster und quantenchemischen Rechnungen. Durch quantenchemische Rechnungen werden in dieser Arbeit zudem auch Strukturen untersucht, die mit experimentellen Methoden nicht zugänglich wären. Durch diese theoretischen Untersuchungen werden die thermodynamischen Eigenschaften untersucht und die Grenzen der attraktiven Wechselwirkungen zwischen den Kationen ausgelotet. Im Rahmen einer umfangreichen Grenzflächenanalyse mittels Rasterkraftmikroskopie wird der Einfluss der attraktiven Wechselwirkungen zwischen den Kationen auf die ausgebildete Doppelschichtstruktur dargestellt.

Auch wenn jede der verwendeten Methoden Stärken und Schwächen hat, so liefern sie neben der Beantwortung zentraler Fragen auch zusätzlich immer Bestätigungen für die Befunde, die mit anderen Methoden erzielt wurden, was die verwendeten Methoden sehr komplementär macht. Auf diese Weise wird in dieser Arbeit ein umfangreiches Bild der kationischen Cluster in OH-funktionalisierten ionischen Flüssigkeiten präsentiert.

Contents

List of Tables	XI
List of Figures	XII
1. Introduction	1
1.1. Motivation	1
1.2. The concept of this study	2
2. Synthesis of ionic liquids	4
2.1. General	4
2.2. Synthesis of OH-functionalized onium halides	5
2.3. Synthesis of unfunctionalized onium halides	9
2.4. Synthesis of hydrophilic ionic liquids by anions metathesis	9
2.5. Synthesis of hydrophobic ionic liquids by anions metathesis	10
2.6. Synthesis of unfunctionalized ionic liquids without anion metathesis	11
3. Investigations of clusters of like-charged Ions in OH-functionalized ionic liquids	13
3.1. IR-studies of the bulk IL	13
3.1.1. IR spectroscopy	13
3.1.2. Dependencies of the formation of cationic clusters	15
3.1.3. Temperature dependency	15
3.1.4. Anion dependency	16
3.1.5. Cation dependency	18
3.1.6. Chain length dependency	19
3.2. ND of the bulk IL supported by MD simulations	22
3.2.1. Neutron diffraction	22
3.2.2. Molecular dynamics simulations	23
3.2.3. Cluster distribution	24
3.3. Investigations of cationic (c-c) cluster structures by means of CIVP spectroscopy	26
3.3.1. Cryogenic ion vibrational predissociation CIVP spectroscopy	26
3.3.2. (c-c) dimers	29
3.3.3. (c-c) trimers	31
3.3.4. (c-c) tetramers	34
3.4. (c-c) cluster investigations by theoretical methods	36
3.4.1. Density functional theory (DFT) calculations	36

3.4.2.	Natural bond orbital (NBO) analysis	37
3.4.3.	Controlling the kinetic and thermodynamic stability of (c-c) clusters	39
3.4.4.	Cooperative hydrogen bonding in bare (c-c) clusters	41
3.4.5.	Hydrogen bonding overcomes coulomb repulsion	43
3.5.	Atomic force microscopy study of the IL/solid interfacial structure	45
3.5.1.	Atomic force microscopy (AFM)	45
3.5.2.	Influence of hydrogen bonding on the IL/solid interfacial structure	47

4. Publications 49

A. Appendix 166

A.1.	Preparation of the Compounds	170
A.1.1.	Synthesis of 1-(2-Hydroxyethyl)pyridinium-bromide [HOC ₂ Py]Br (3 (a))	171
A.1.2.	Synthesis of 1-(2-Hydroxyethyl)pyridinium-bis(trifluoromethylsulfonyl)imide [HOC ₂ Py]NTf ₂ (3)	171
A.1.3.	Synthesis of 1-(2-Hydroxyethyl)pyridinium-methanesulfonate [HOC ₂ Py]OMs (15)	172
A.1.4.	Synthesis of 1,1-(2-Hydroxyethyl)methylpiperidinium-bromide [HOC ₂ MPip]Br (4 (a))	172
A.1.5.	Synthesis of 1,1-(2-Hydroxyethyl)methylpiperidinium-bis(trifluoromethylsulfonyl)imide [HOC ₂ MPip]NTf ₂ (4)	173
A.1.6.	Synthesis of 1,1-(2-Hydroxyethyl)methylpyrrolidinium-bromide [HOC ₂ MPyrro]Br (5 (a))	173
A.1.7.	Synthesis of 1,1-(2-Hydroxyethyl)methylpyrrolidinium-bis(trifluoromethylsulfonyl)imide [HOC ₂ MPip]NTf ₂ (5)	174
A.1.8.	Synthesis of 1-(3-Hydroxypropyl)pyridinium-chloride [HOC ₃ Py]Cl (9 a)	174
A.1.9.	Synthesis of 1-(3-Hydroxypropyl)pyridinium-bis(trifluoromethylsulfonyl)imide [HOC ₃ Py]NTf ₂ (9)	175
A.1.10.	Synthesis of 1-(3-Hydroxypropyl)pyridinium-methanesulfonate [HOC ₃ Py]OMs (16)	176
A.1.11.	Synthesis of 1-(3-Hydroxypropyl)methylpiperidinium-chloride [HOC ₃ MPip]Cl (12 (a))	176
A.1.12.	Synthesis of 1-(3-Hydroxypropyl)methylpiperidinium-bis(trifluoromethylsulfonyl)imide [HOC ₃ MPip]NTf ₂ (12)	177
A.1.13.	Synthesis of 4-Bromo-1-trimethylsiloxybutane-d _x TMSOC ₄ Br-d _x . . .	177
A.1.14.	Synthesis of 1-(4-Trimethylsiloxybutyl)-pyridinium-bromide-d _{x+y} [TMSOC ₄ Py]Br-d _{x+y}	178
A.1.15.	Synthesis of 1-(4-Hydroxybutyl)-pyridinium-bromide-d _{x+y} [HOC ₄ Py]Br-d _{x+y}	179
A.1.16.	Synthesis of 1-(4-Hydroxybutyl)-pyridinium-bis(trifluoromethylsulfonyl)imide-d _{x+y} [HOC ₄ Py]NTf ₂ -d _{x+y}	180
A.1.17.	Synthesis of 1-(4-Hydroxybutyl)-pyridinium-bis(trifluoromethylsulfonyl)imide-d _{x+y} [HOC ₄ Py]NTf ₂ -d _{x+y+1}	181
A.1.18.	Synthesis of 1-(4-Hydroxybutyl)-pyridinium-methanesulfonate [HOC ₄ Py]OMs (17)	182

A.1.19. Synthesis of 1-(4-Trimethylsiloxybutyl)-methylpiperidinium-bromide [TMSOC ₄ MPip]Br (13 (a))	182
A.1.20. Synthesis of 1-(4-Hydroxybutyl)-methylpiperidinium-bromide [HOC ₄ MPip]Br (13 (b))	183
A.1.21. Synthesis of 1-(4-Hydroxybutyl)-methylpiperidinium-bis(trifluoromethylsulfonyl)imide [HOC ₄ MPip]NTf ₂ (13 (c))	183
A.1.22. Synthesis of 5-Iodo-1-trimethylsiloxy-pentane TMSOC ₅ I (11 (a))	184
A.1.23. Synthesis of 1-(5-Trimethylsiloxy-pentyl)-pyridinium-iodide [TMSOC ₅ Py]I (11 (b))	184
A.1.24. Synthesis of 1-(5-Hydroxy-pentyl)-pyridinium-iodide [HOC ₅ Py]I (11 (c))	185
A.1.25. Synthesis of 1-(5-Hydroxy-pentyl)-pyridinium-bis(trifluoromethylsulfonyl)imide [HOC ₅ Py]NTf ₂ (11)	185
A.1.26. Synthesis of 1-(5-Hydroxy-pentyl)-pyridinium-methanesulfonate [HOC ₅ Py]OMs (18)	186
A.1.27. Synthesis of 1-(5-Trimethylsiloxy-pentyl)-methylpiperidinium-iodide [TMSOC ₅ MPip]I (14 (b))	187
A.1.28. Synthesis of 1-(5-Hydroxy-pentyl)-methylpiperidinium-iodide [HOC ₅ MPip]I (14 (c))	187
A.1.29. Synthesis of 1-(5-Hydroxy-pentyl)-methylpiperidinium-bis(trifluoromethylsulfonyl)imide [HOC ₅ Py]NTf ₂ (14)	188

Bibliography

189

List of Tables

2.1. Compilation of selected structural data from single-crystal X-ray structures	7
3.1. Advantages and disadvantages of infrared spectroscopy	14
3.2. Advantages and disadvantages of neutron diffraction.	23
3.3. Advantages and disadvantages of molecular dynamics simulations.	24
3.4. Advantages and disadvantages of molecular CIVP spectroscopy	28
3.5. Advantages and disadvantages of DFT calculations	37
3.6. Advantages and disadvantages of NBO analysis	38
3.7. Advantages and disadvantages of AFM	47
A.1. Cation dependence for the Bis(trifluoromethylsulfonyl)imide [NTf ₂] [−] anion	166
A.2. Anion dependence for the 1-(2-hydroxyethyl)-3-methylimidazolium cation	166
A.3. Chain length dependence of the cluster formation	167
A.4. List of partially deuterated ionic liquids for neutron diffraction measurements	168
A.5. List of chemicals, their provider, purification and drying method	170

List of Figures

1.1. First evidence of a cation-cation H-bond.	2
1.2. Schematic illustration of different dependencies of (c-c) cluster formation.	3
2.1. Neutral compounds of the used N-heterocycles and amines.	4
2.2. General reaction for the generation of functionalized and unfunctionalized nitrogen-based onium salts.	5
2.3. Overview of the anions used to synthesize the ionic liquids	5
2.4. Single crystal structures of [HOC ₂ Py]Br and [HOC ₂ MPip]Br.	6
2.5. Single crystal structure of [HOC ₃ Py]Cl.	6
2.6. General reaction scheme for the ring-opening reaction using TMS halides	7
2.7. Single crystal structure of [TMSOC ₄ Py]Br	8
2.8. Single crystal structure of [HOC ₄ Py]Br	8
2.9. General reaction scheme for the anion metathesis of hydrophilic ILs in non-polar aprotic solvents.	10
2.10. General reaction scheme for the anion metathesis of hydrophobic ILs in water.	11
2.11. General synthesis of esters from acid anhydrides of the anions	11
2.12. Overview of different pathways for synthesis of ionic liquids	12
3.1. Temperature dependence of the formation of cationic clusters.	16
3.2. Anion dependency of the formation of cationic clusters.	17
3.3. Cation dependency of the formation of cationic clusters.	19
3.4. Chain length-, anion- and cation-dependent VAN'T HOFF-like plots of cationic cluster formation.	21
3.5. Schematic set-up of a neutron diffraction experiment.	22
3.6. Pair distribution functions for the (c-a) and (c-c) H-bonds in the IL [HOC ₄ Py][NTf ₂] obtained from ND and MD	25
3.7. Analysis of (c-a) and (c-c) cluster populations in [HOC ₄ Py][NTf ₂]	26
3.8. Schematic set-up of the photofragmentation spectrometer used at Yale University.	28
3.9. Structure elucidation of ternary 2c, 1a gas-phase clusters.	31
3.10. Structure elucidation of quinary 3c, 2a gas-phase clusters.	33
3.11. Schematic illustration of the concept of the structural elucidation of H-bonded cyclic tetramers by means of CIVP spectroscopy.	34
3.12. Structure elucidation of quaternary 1c, 3m gas-phase clusters.	36
3.13. Stabilising effect of the addition of molecular alcohols or anions on (c-c) clusters	41

3.14. Visualized cooperativity of different sized molecular and cationic clusters.	43
3.15. Kinetic and thermodynamic stability of H-bonded cationic dimers in dependency of chain length.	45
3.16. Schematic illustration of the fundamental functionality of a beam deflection AFM.	46
3.17. Force separation profiles of chosen ILs.	48

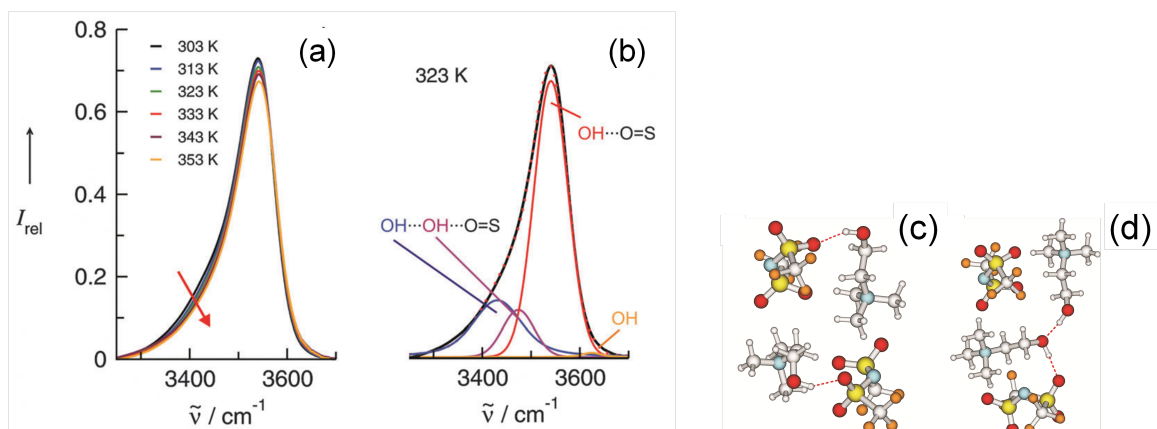
1. Introduction

1.1. Motivation

In recent years, ionic liquids (ILs) have attracted increasing interest in science and technology owing to their unique properties, which often includes a wide electrochemical window, [1, 2] very low vapour pressure, [3] and high thermal stability. [4] Per definition, a salt can be called an IL if it has a melting point below 100 °C. If the melting point is below 25 °C it is named a room temperature ionic liquid (RTIL). Although ionic liquids consist entirely of ions, and thus the COULOMB forces are dominant, their properties are often governed by a subtle balance of COULOMB interactions, hydrogen bonding and dispersion forces. [5, 6] In particular, local and directional hydrogen bonding has significant influence on IL behaviour. [7–9]

Opposite charges attract and like charges repel each other. This rule is known from COULOMB's law for the electrostatic interaction between charged particles. The pairing between oppositely charged ions is also a well-accepted concept in chemistry and plays an important role for reactions in solution, macromolecular catalysis, biochemical hydrolysis, and protein stability. [10–13] In contrast, the association of like-charged ions in solution seems to be a counter-intuitive phenomenon and for which little experimental evidence is given. The attraction between like charges has been reported for aqueous salt solutions, [14] for guanidinium ions in water, [15] for the micellation of tetraalkylammonium surfactants, [16] as well as for metastable colloidal crystallites.[17] This phenomenon is also known for biomolecular systems including oligopeptides and DNA. [18, 19] So far, large-scale structures or assemblies are prerequisites for attractive interaction between like-charged ions. For smaller systems, mediating solvent molecules, such as water, are required. For pure ionic liquids, hydrogen bonding was reported between oppositely charged ions only. [5–9, 20–23] In 2015, Knorr et al. could provide first spectroscopic evidence for attractive interaction between ions of like charge in ionic liquids via combination of IR measurements and density functional theory (DFT) calculations (Fig. 1.1). [24] This unique behaviour was somewhat surprising for ILs where all ions are solvated by counterions and the cation-anion (c-a) interaction strength mainly governs the properties of this unique liquid material. After this finding, Knorr et al. changed the IL to 1-(2-hydroxyethyl)-3-methylimidazolium tetrafluoroborate [HOC₂MIm][BF₄] which is characterised by a weakly coordinating anion and a cation with a delocalized charge. [25, 26] They found that, if the common (c-a) interaction is softened by weakly coordinating anions, the attractive cation-cation (c-c) interaction via cooperative hydrogen bonding might become more prominent in the liquid phase, resulting in more and larger (c-c) clusters. Furthermore, they studied the effect of dilution of the function-

alized IL with the unfunctionalized IL 1-propyl-3-methylimidazolium tetrafluoroborate $[\text{C}_3\text{MIm}][\text{BF}_4]$, which is almost equal in shape and size but incapable of forming hydrogen bonds due to the lack of an OH group.



(a) Mid-infrared spectrum in the OH stretching region of the ionic liquid (2-hydroxyethyl)-trimethyl-ammonium bis(trifluoromethylsulfonyl)imide as a function of temperature. The red arrow indicates the decreasing intensities of the vibrational bands slightly above 3400 cm^{-1} with increasing temperature. (b) The spectra can be deconvoluted into vibrational bands at 3431 cm^{-1} , 3474 cm^{-1} , 3541 cm^{-1} and 3624 cm^{-1} . The most intense high frequency band (red) can be assigned to the OH stretching mode along the H-bond from the cation to the anion (c-a). The low frequency bands (blue and purple) indicate cation-cation hydrogen bonding (c-c).

(c) DFT-D3 calculated structures of IL (2-hydroxyethyl)-trimethyl-ammonium bis(trifluoromethylsulfonyl)imide. I Cation-anion pairs characterised by the $\text{OH} \cdots \text{O}=\text{S}$ hydrogen bond (c-a) and the related vibrational band 3541 cm^{-1} , (d) additional cation-cation (c-c) interaction resulting in cooperative hydrogen bonding $\text{OH} \cdots \text{OH} \cdots \text{O}=\text{S}$ as observed in the mid-infrared spectrum at 3431 cm^{-1} and 3474 cm^{-1} .

Figure 1.1.: First evidence of a cation-cation H-bond in a pure ionic liquid published by Knorr et al. in 2015. [24]

After the first pieces of evidence of cationic clusters in OH-functionalized ILs and the insight that the exchange of anions and/or cations has a huge impact on the formation of cationic clusters, it quickly became obvious that it will be necessary to study the dependencies of the formation of H-bonded cationic clusters in a more systematic way.

1.2. The concept of this study

The dissertation project will investigate the formation of clusters of like-charged ions in ionic liquids. A special focus is put on the different possibilities to influence the formation of the clusters by modification of the anions and cations as well as on the structural analysis of this counterintuitive structural feature.

For the systematic investigation of this phenomenon, three sets of anion and cation combinations have been developed to address the various dependencies. By combining

cations and anions with different interaction potentials, different charge delocalizations and different chain lengths between the positive charge and functional group, the attractive interactions between ions of like charge are to be detected and quantified.

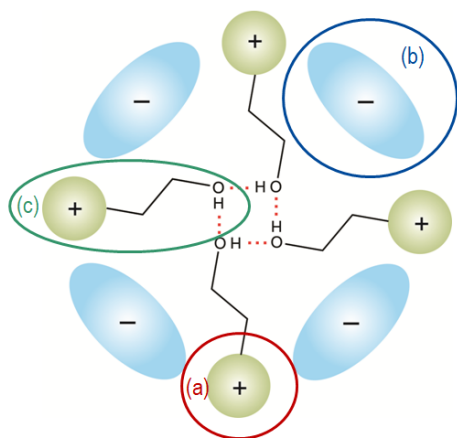


Figure 1.2: Schematic illustration of the different dependencies to be investigated by modification of the anions and cations: **(a)** Localization and delocalization of the positive charge; **(b)** Interaction strength of the anion; **(c)** Chain length of the alkyl chain between the positive charge and the OH group. [27]

In the set listed in table A.1 (see appendix), all cations have a 2-hydroxyethyl group, which on the one hand has the aim to increase the distance between the positive charge and the functional group and on the other hand enables them to form hydrogen bonds. Thus, the short-range, dipolar donor-acceptor interactions have the potential to overcome the strong, long-range electrostatic repulsions between the cations. The cations differ essentially by their different ability to delocalise the positive charge. As counterion, the bis(trifluoromethylsulfonyl)imide anion was chosen. This anion in particular is characterised by its hydrophobic nature and, due to its weak interaction with the cations, allows for an increased interaction of the cations with each other via hydrogen bonds (see Fig: 1.2 (a)).

For the second set of ILs (Tab. A.2) we chose the same $[\text{HOC}_2\text{MIm}]^+$ cation, which is known to support cation cluster formation from earlier studies. [25, 26] The set contains four different counterions to this cation: bis(trifluoromethylsulfonyl)imide ($[\text{NTf}_2]^-$); tetrafluoroborate ($[\text{BF}_4]^-$); trifluoromethylsulfonate ($[\text{OTf}]^-$); methylsulfonate ($[\text{OMs}]^-$). The interaction potential of these anions to the OH-functional group of the cations increases in this order from the $[\text{NTf}_2]^-$ to the $[\text{OMs}]^-$ anion. This procedure allows control of the attractive interaction between the cations over the counteranion (see Fig. 1.2 (b)).

The third set of ionic liquids (Tab. A.3) focuses on changing the distance between the functional group and the positive charge by enlarging the hydroxyalkyl strand. By lengthening the alkyl chain length from hydroxyethyl to hydroxypentyl, the effect on the number of cationic clusters in the ionic liquid, which is supposed to increase in the same order due to distance-induced reduction of COULOMB-repulsion between the cations, should be studied (siehe Abb. 1.2 (c)). As part of this investigation, it should also be clarified how a change in the chain length affects the anions and cation dependency of cationic cluster formation.

2. Synthesis of ionic liquids

2.1. General

Since the structural elucidation of the first ionic liquid, the onium salt ethylammonium nitrate which has a melting point of 12 °C, [28] whole generations of chemists have studied the synthesis, characterisation, and structural elucidation of this class of compounds. Most ionic liquids are formed from large, mostly unsymmetrical cations and anions with a high charge delocalization. Quaternary organic nitrogen compound (onium cations) are used predominantly. The most common ionic liquids are based on the ammonium, imidazolium, pyrrolidinium and pyridinium cations. [29–31] The most commonly used anions are the methanesulfonate, trifluoromethanesulfonate, tetrafluoroborate, hexafluorophosphate, and bis(trifluoromethanesulfonyl)imide.

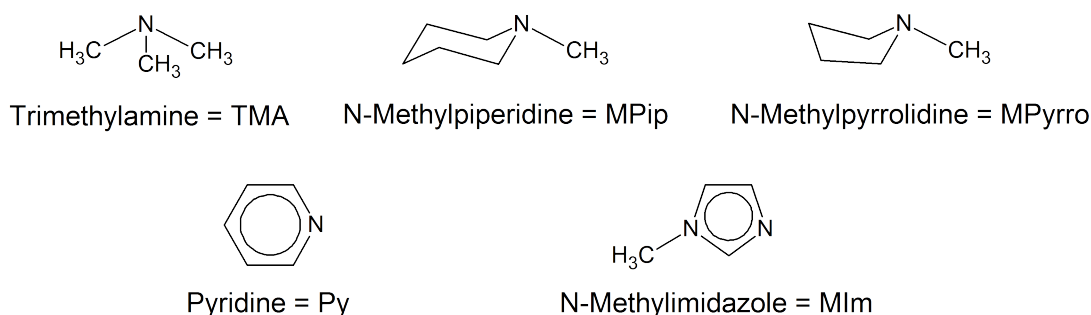


Figure 2.1.: Neutral compounds of the used N-heterocycles and amines (= $N_{Het.}$).

In most approaches, the synthesis of ionic liquids can be divided into two reaction steps. In most cases, the desired cation is first generated by alkylation of a tertiary amine or an N-heterocycle. [32] If necessary, an anion metathesis then joins in a second reaction. Various functionalized and unfunctionalized haloalkanes can be used for the formation of onium halides.

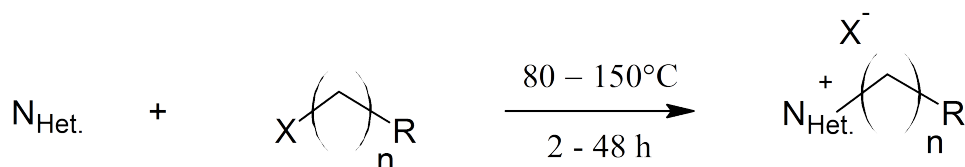


Figure 2.2.: General reaction for the generation of functionalized and unfunctionalized, nitrogen-based onium salts. ($n = (1); 2; 3; (4)$ etc., $X = -\text{Cl}; -\text{Br}; -\text{I}$, $R = -\text{H}; -\text{OH}; -\text{SH}; -\text{NH}_2$)

The reactions can be carried out without additional solvent under exclusion of water under rather mild conditions.

In the case of the listed functionalized onium salts, however, it is not possible to represent the corresponding methyl compounds due to the general reaction of (Fig. 2.2). Since the hypothetically necessary functionalized methyl halides tend to undergo elimination reactions in the sense of ERLLENMEYER's rule. Also, chain lengths of more than three carbon atoms are difficult because of occurring cyclization reactions and it becomes necessary to protect the functional group by protecting groups.

The often strongly hygroscopic and high-melting onium halide salts can, as already mentioned, be converted by an anion metathesis with the free acid or a corresponding alkali metal salt in a suitable solvent to give various ionic liquids. [33, 34] The anions used in this work are listed in figure 2.3.

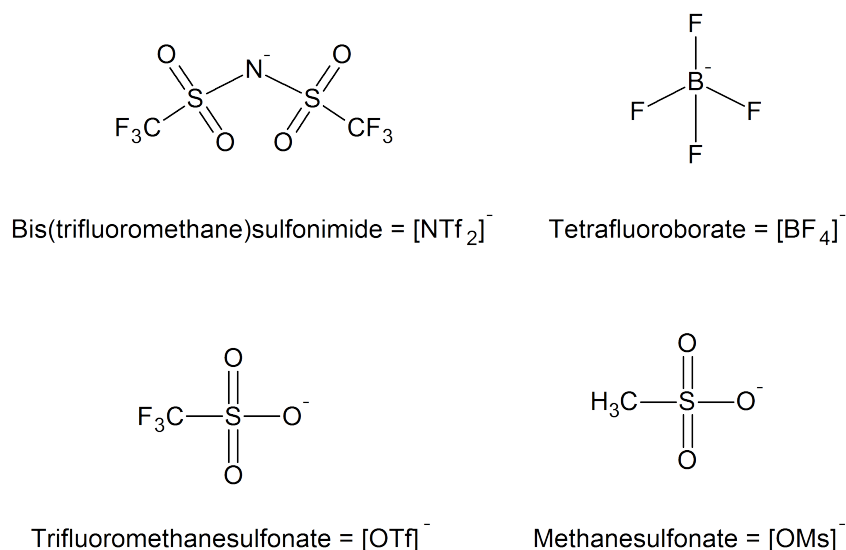


Figure 2.3.: Overview of the anions used to synthesize the ionic liquids

2.2. Synthesis of OH-functionalized onium halides

Although a large number of different heterocycles are available for the synthesis of ionic liquids, the number of halogenated alcohols suitable for the synthesis is quite small.

[30, 35] As mentioned before, the hypothetically necessary halogenated methanol for a C1 tether tends to eliminate hydrogen halide in the sense of ERLENMEYER's rule. Therefore, the smallest accessible strand is a C2 tether. The reactivity of the halogenated alcohols increases in the order of $\text{Cl} < \text{Br} < \text{I}$. [32] Fluorinated alcohols are not suitable for quaternization reactions due to their very strong C-F bond and the associated high activation energy. However, especially in the case of halogenated alcohols, the stability of the educts decreases in this sequence as well. The instability becomes even larger with increasing chain length. Therefore, it is absolutely necessary to distill the educts freshly before use. The quaternization reactions themselves are pretty simple: the amine is mixed with the desired halogenated alcohol and the mixture is then stirred and heated slowly up to about 100 °C. [36, 37] When the reaction starts, the mixture turns slightly brownish. After a few hours at the corresponding reaction temperature, the crude product is allowed to cool down to room temperature. The crude product usually starts to crystallize during the cooling. The thus obtained crude product can be recrystallized from acetonitrile/acetone mixtures to obtain the pure OH-functionalized onium halides as colourless crystalline products.

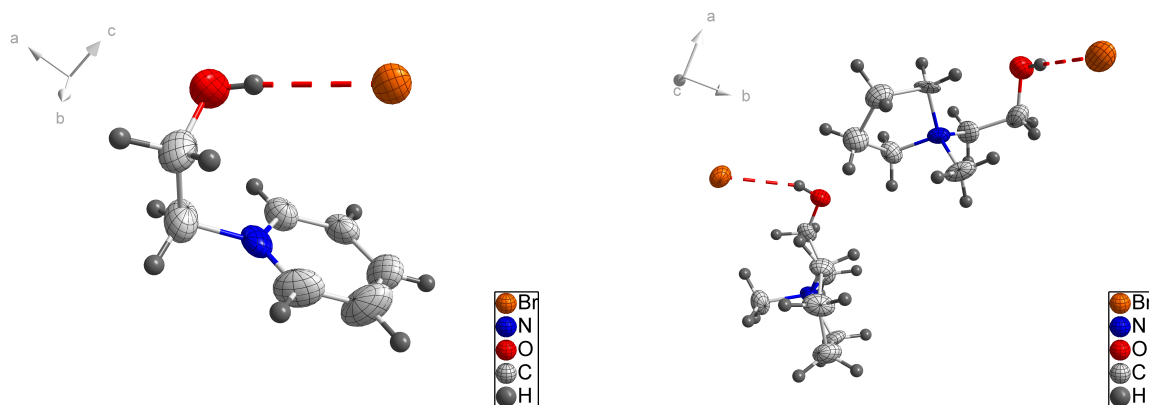


Figure 2.4.: Single crystal structures of [HOC₂Py]Br (left) and [HOC₂MPip]Br (right).

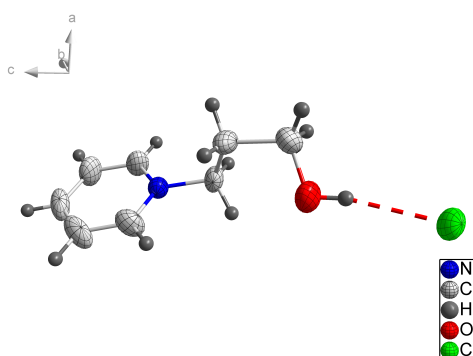


Figure 2.5.: Single crystal structure of [HOC₃Py]Cl.

Figure 2.4 and figure 2.5 show the single crystal X-ray structures of some of the

OH-functionalized onium halides synthesized in this work. All X-ray structures are characterised by a strong anion cation H-bond from the OH-group of the cation to the halide anion, indicated by the short O-X⁻ distances and the O-H...X⁻ hydrogen-bond angles close to 180 ° (see Tab. 2.1).

Table 2.1.: Compilation of selected structural data from single-crystal X-ray structures

	R_{X-O} [Å]	$\sum_{cov./ion} R_{(X^-;2H;O)}$ [Å]	α_{X-H-O} [°]	R_{X-N} [Å]	$\sum_{cov./ion} R_{(X^-;NH_3^+)}$ [Å]
[HOC ₂ Py]Br	3.20	3.22	173.7	3.52	3.38
[HOC ₂ MPip]Br(l)	3.25	3.22	156.1	4.64	3.38
[HOC ₂ MPip]Br(r)	3.22	3.22	178.7	4.93	3.38
[HOC ₃ Py]Cl	3.11	3.07	166.5	4.04	3.24
[TMSOC ₄ Py]Br	-	3.22	-	3.52	3.38
[HOC ₄ Py]Br	3.28	3.22	160.9	4.15	3.38

Chain lengths of more than three carbon atoms are difficult to synthesise because of occurring cyclization reactions. The larger (>3 C atoms) ω -halide alcohols tend to eliminate hydrogen halide to form cyclic ethers in this way. This process is accelerated in presence of bases like the amines used in the quaternization reactions. Therefore, it becomes necessary to protect the functional group by protecting groups. A novel way to make the C4 and C5 tethers accessible is to start from the cyclic ethers and use a ring-opening-reagent which reacts at the same moment as the protecting group. [38]

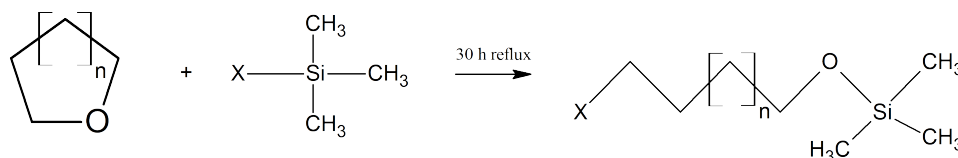


Figure 2.6.: General reaction scheme for the ring-opening reaction using trimethylsilyl halides. ($n = 1; 2$, $X = -Cl; -Br; -I$,)

The reactivity of the trimethylsilyl halides as ring-opening reagent increases in the order of $Cl < Br < I$. For $n = 1$ all trimethylsilyl halides listed in figure 2.6 can be used to obtain the corresponding 4-halido-1-trimethylsiloxybutane. [39, 40] For $n = 2$ only iodotrimethylsilane leads to the desired product 5-iodo-1-trimethylsiloxybutane, whereas the reactivity of the other two trimethylsilyl halides is too low to cause ring opening. [41, 42] The obtained ω -halido-1-trimethylsiloxyalkanes can now be used in a quaternization reaction following the reaction in figure 2.2. Since the OH group is now protected by the TMS group, no cyclization reactions can occur any more. The thus obtained onium salts are solid at room temperature and can be crystallized to obtain crystals for single crystal X-ray structural analysis (Fig. 2.7).

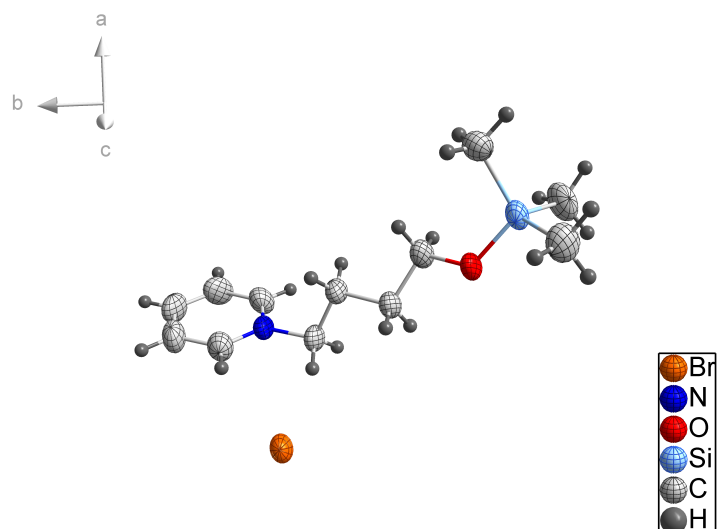


Figure 2.7.: Single crystal structure of [TMSOC₄Py]Br

As can be seen from the X-ray structure, the bromine anion is interacting exclusively with the positive charge of the pyridinium ring, because no other interaction centers, such as OH groups, are available. Because of the high chemical stability of the O-TMS bond in a neutral and alkaline environment, the trimethylsilyl (TMS) group is the ideal protecting group in quaternization reactions. The protecting group can easily be removed by water treatment. The resulting OH-functionalized onium halide can be recrystallized from acetone/acetonitrile mixtures to obtain the halides of the cations with a C4 or a C5 tether as colorless crystals of high purity.

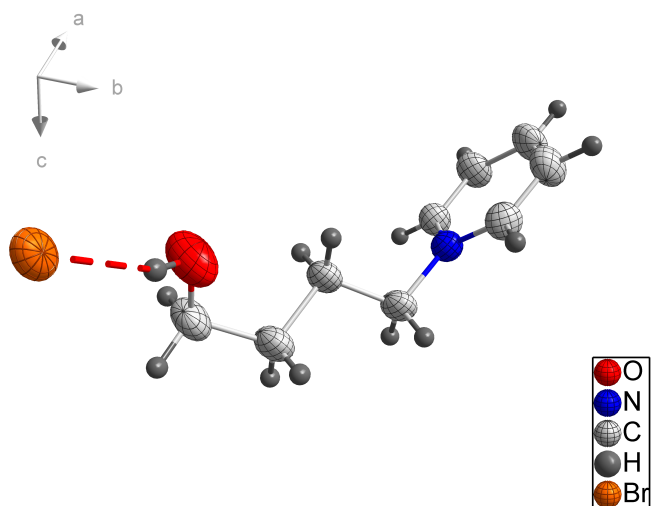


Figure 2.8.: Single crystal structure of [HOC₄Py]Br

The X-ray structure in figure 2.8 shows a hydrogen bond between the anion and the OH group of the cation, as is typical for OH-functionalized onium salts with strong

interacting anions. However, the H-bond is less strong compared to the H-bond in [HOC₂Py]Br, indicated by the longer O-Br⁻ distance and the O-H...Br⁻ hydrogen-bond angle being less close to 180 ° (see Tab. 2.1).

2.3. Synthesis of unfunctionalized onium halides

The synthesis of unfunctionalized onium halides is very similar to the synthesis of the OH-functionalized onium halides (see Fig. 2.2). The variety of the halogenated alkanes suitable for the synthesis of unfunctionalized onium halides is much greater than for the OH-functionalized onium halides since in the former no elimination reactions in the sense of a cyclization reaction or a violation of the ERLLENMEYER rule can occur. As with the OH-functionalized halogenated hydrocarbons, the reactivity increases in the order of Cl < Br < I as expected for nucleophilic substitution reactions. Fluoride salts cannot be formed in this manner either. The general synthesis is rather simple: the desired amine is mixed with an halogenated hydrocarbon of desired chain length at room temperature. The reaction mixture is then stirred and heated up slowly. A sudden clouding or discoloration of the mixture indicates the onset of reaction. After completion of the reaction, the crude product is cooled to room temperature during which it usually crystallizes. The crystalline products can be recrystallized from organic solvents, like acetonitrile or acetone. If the onium halides can not be crystallized, it is advisable to wash the crude product as thoroughly as possible with an immiscible solvent like acetone or ethyl ethanolate. Possible discolouration can be removed by treatment with activated charcoal.

2.4. Synthesis of hydrophilic ionic liquids by anions metathesis

Like the onium halides, ionic liquids with strongly coordinating anions are often characterised by the fact that they are miscible with water in any mixing ratio. [43] This hydrophilic character is further enhanced by functionalization with hydrophilic functional groups and attenuated with increasing chain length. The tetrafluoroborate ([BF₄]⁻) anion represents a kind of borderline case here. In combination with unfunctionalized cations with hydrophobic side chains, the resulting ionic liquids behave rather hydrophobic, whereas they behave hydrophilic in combination with functionalized cations with hydrophilic side chains. In case of the OH-functionalized ionic liquids investigated in this work, the tetrafluoroborate ILs can be assigned to the hydrophilic ones. However, in contrast to the onium halides and alkali metal halides, the hydrophilic ILs are very soluble in non-polar aprotic solvents, such as acetonitrile or acetone. [32, 44] In view of these facts, it is now possible to synthesize the desired ionic liquid by reacting stoichiometric amounts of the onium halide and the alkali metal salt of the desired anion in such a solvent. The insoluble starting materials and the insoluble by-product can easily be filtered off after complete anion metathesis (Fig. 2.9). The IL can then be obtained

by removing the solvent with a vacuum evaporator.

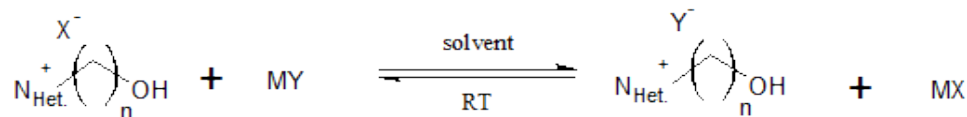


Figure 2.9.: General reaction scheme for the anion metathesis of hydrophilic ILs in non-polar aprotic solvents. (M = alkali metal, X = -Cl; -Br; -I, Y = desired anion)

As simple and cheap as it is, this procedure has a disadvantage. The ILs synthesized following this procedure often still contain residuals of educts and by-products, because they are not completely insoluble in chosen solvents. [32]

A procedure to obtain ILs without residuals of educts and by-products is to use the silver salts of the desired anions instead of the alkali metal salts. The reaction can be carried out in water, methanol or mixtures of both. [45] The very low solubility of silver halides in these solvents allow them to be separated simply by filtration, and the removal of the reaction solvent allows isolation of the IL in high yields and purities. [32] This procedure was the first reported preparation of the ILs sometimes referred to as „second generation IL“ to which all ILs considered in this work belong. It is still the most efficient synthesis of hydrophilic ILs. The disadvantage of the method is obviously the high costs of the silver salts. But this can be slightly compensated by recycling of the silver halides. [46–48]

2.5. Synthesis of hydrophobic ionic liquids by anions metathesis

In contrast to the hydrophilic ionic liquids, the hydrophobic ionic liquids are characterised by the fact that they are not miscible with water in every mixing ratio. The hydrophobic character of the ionic liquid is significantly influenced by the anion. Typical anions which lead to an increased hydrophobic character are, for example, the hexafluorophosphate $[\text{PF}_6]^-$ and the bis(trifluoromethylsulfonyl)imid $[\text{NTf}_2]^-$ frequently used in this work. [49, 50]

The procedure itself is pretty straight forward: equimolar aqueous solutions of the onium halides and the desired anion in form of alkaline metal or ammonia salt or in form of the free acids are mixed at room temperature (see Fig. 2.10) (in case of the free acids it is sometimes necessary to cool the reaction mixture as the metathesis reaction is often exothermic). During the metathesis reaction, two phases are formed, one of which is the hydrophobic IL and the other the aqueous phase containing the unreacted educts and the byproduct. The phases can now be separated in a separation funnel and the IL can be washed several times with water until no residual halide can be detected with silver nitrate solution. After drying the IL in high vacuum for several hours the hydrophobic IL can be obtained in moderate yield and high purity.

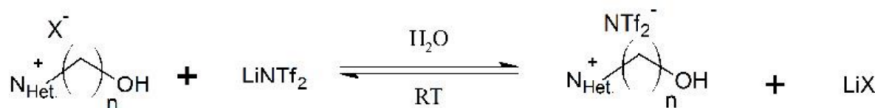


Figure 2.10.: General reaction scheme for the anion metathesis of hydrophobic ILs in water. (M = alkali metal , X = -Cl; -Br; -I)

2.6. Synthesis of unfunctionalized ionic liquids without anion metathesis

An elegant method, though limited to unfunctionalized compounds, for the synthesis of ionic liquids uses a slightly different approach. Instead of the synthesis of an onium halide as a precursor followed by an anion metathesis, this approach uses an ester. The used ester contains the desired anion and the desired hydrocarbon for the quarternization reaction with the desired amine. The benefit of this method is that both educts are molecular liquids which can be distilled to increase the purity of the product. The ester can be obtained from the reaction of the acid anhydride or acid chloride of the anion and an alcohol of the corresponding hydrocarbon (see Fig. 2.11). [51]

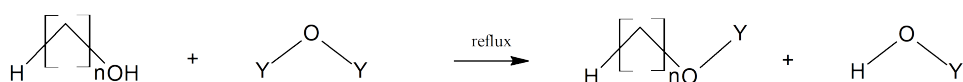


Figure 2.11.: General synthesis of esters from acid anhydrides of the anions and an alcohols of the corresponding hydrocarbons. (Y = Ms; Tf; Ac)

The unfunctionalized IL can then be obtained from a quarternization reaction with the desired amine similar to the general reaction in figure 2.2. After this, no anion metathesis is required since the desired anion has already been introduced by the ester. The only necessary purification is to remove the volatiles by drying in vacuum.

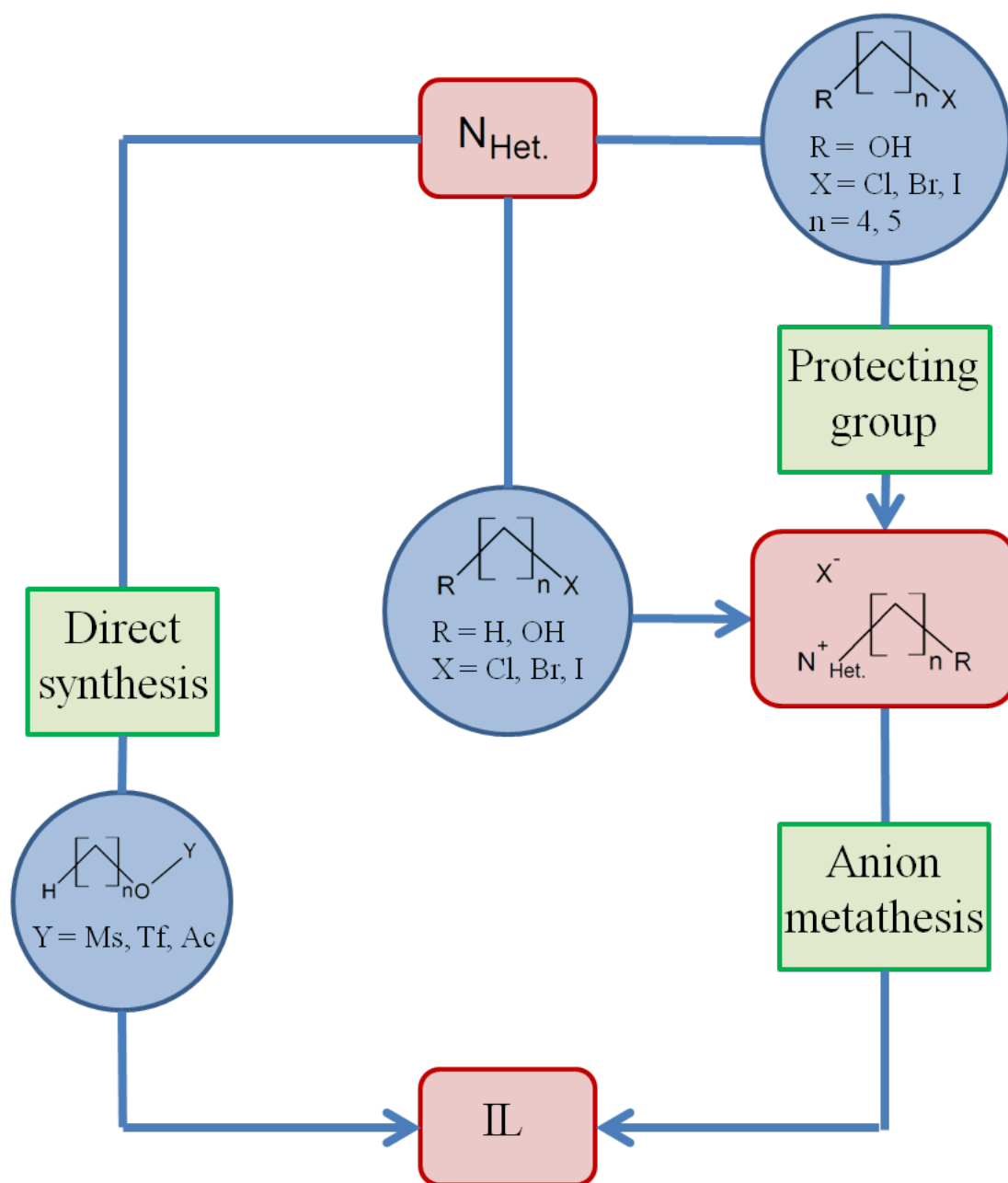


Figure 2.12.: Overview of different pathways for synthesis of ionic liquids used in this work

3. Investigations of clusters of like-charged Ions in OH-functionalized ionic liquids

In ionic liquids (ILs) the subtle energy balance between COULOMB interaction, hydrogen bonding and dispersion forces results in unique properties. To measure weak interactions and small changes in the equilibria of different structural features caused by the balance of interactions is still a challenge. In the past few years we were able to examine different dependencies for the formation of clusters of like-charged ions via H-bonding of OH-functionalized cations in ionic liquids. By combining experimental and theoretical methods we have realized a comprehensive structural analysis of differently sized cationic clusters. Furthermore, we reveal the cluster distribution of these counterintuitive structural features and their influences on the interfacial and phase behaviour.

To generate all these results, we used a variety of different experimental and theoretical methods from IR-spectroscopy and neutron diffraction over cryogenic ion vibrational predissociation spectroscopy and atomic force microscopy to molecular dynamics simulations and DFT calculations. The investigations included the liquid and solid bulk phase, the gas phase and the solid liquid interface.

3.1. IR-studies of the bulk IL

3.1.1. IR spectroscopy

Infrared (IR) spectroscopy is a subgroup of vibrational spectroscopy. If radiation from the infrared region of the electromagnetic spectrum hits a molecule, this molecule interacts with the electric field vector of the radiation and absorbs it at frequencies which correspond to the respective resonance frequencies of characteristic molecular vibrations. [52]

In the simplest case we can imagine a diatomic molecule, which can be modeled as a linear harmonic oscillator. The atoms making up the molecule are considered as point masses in the manner of classical mechanics, connected by a spring of negligible mass. [53] According to HOOK's law the restoring force \vec{F} of such a spring is given by:

$$\vec{F} = -\frac{dV(x)}{dx} = -kx \quad (3.1)$$

In the equation, $V(x)$ describes the potential energy, k is the force constant, the magnitude of which gives a measure of the strength of the bond between the atoms, and x

is the deflection from the equilibrium position along the molecular axes. By integrating from 0 to x , the relationship between the potential energy and the displacement is obtained by the following parabolic function:

$$V(x) = \frac{1}{2}kx^2 \quad (3.2)$$

The classical determination of the oscillation frequency of the harmonic oscillator is based on NEWTON's second law:

$$F = \frac{d^2x}{dt^2} \quad (3.3)$$

By equating with equation 3.1 followed by solving the resulting differential equation, we get the time t_{vib} the oscillator needs to go back to the starting position x_0 . Thus, the vibration frequency ν results as:

$$\nu = \frac{1}{t_{\text{vib}}} = \frac{1}{2\pi} \sqrt{\frac{k}{m}} \quad (3.4)$$

Equation 3.4 considers only the vibration of a single mass in x direction, but in a diatomic molecule both masses always oscillate simultaneously. Therefore, the oscillation of both masses m is reduced to that of a single reduced mass μ around the center of mass:

$$\mu = \frac{m_1 \cdot m_2}{m_1 + m_2} \quad (3.5)$$

By inserting into equation 3.5 and dividing by the speed of light c , we obtain the wave number $\tilde{\nu}$ typically used in IR-spectroscopy:

$$\tilde{\nu} = \frac{1}{2\pi c} \sqrt{\frac{k}{\mu}} \quad (3.6)$$

From equation 3.6 it is clear that larger reduced masses μ (i.e., heavier atoms, e.g., by deuteration) result in lower vibrational frequencies and that larger force constants k (i.e., stronger bonds) lead to higher vibration frequencies. This are two of the main advantages of the IR spectroscopy, because even a small change in the bond strength of the oscillator leads to a reasonable shift of the vibrational frequency. This enables IR spectroscopy to use the OH vibrations as ideal probe for describing H-bond networks qualitatively.

Table 3.1.: Advantages and disadvantages of infrared spectroscopy

Advantage	Disadvantage
Almost universal	Can't detect some molecules
Spectra are information rich	Intensity depends on change of dipole moment (no quant. comparison of different vib. bands)
Relative inexpensive, fast and easy	
Sensitive to changes of bond strengths	

Furthermore, the vibrational frequencies of many other functional groups are located in the mid-IR region of the spectra which makes this method almost universal for many substances and enables us to use different probes of one molecule to increase the amount of information. One main disadvantage of IR spectroscopy is that we observe all different compounds and species in the sample at the same time, which means for example that can't observe exclusively the OH oscillation of an OH-functional group involved in a cyclic c-c tetramer if there are linear c-c dimers, trimers and tetramers and c-a clusters present in the sample as well. This is aggravated by the disperse nature of the broad vibrational bands in bulk IR spectroscopy. Another disadvantage is reflected in the intensity of the spectral contributions, which is highly dependent on the change of transition dipole moment. This is a disadvantage because if we want to use IR spectroscopy for example to describe the binding situation of OH oscillators in different H-bonded clusters, we can't get any quantitative information from the intensity of the contribution due to the fact the dipole moments in the different shaped and sized clusters are significantly different and their magnitude is unknown.

3.1.2. Dependencies of the formation of cationic clusters

The subtle energy balance between COULOMB interaction, hydrogen bonding and dispersion forces present in ionic liquids gives us the opportunity to study not only the interaction itself, it rather gives us the chance to investigate the competition between these interactions. Such a competition is displayed by the cationic clusters investigated in this work. Cationic clusters in this context are aggregates of at least two OH-functionalized cations connected by an H-bond. The COULOMB repulsion should lead to the separation of the cations, but the attractive interaction of the H-bond between the OH functional groups overcomes the repulsive force insofar that we can detect spectral contributions in the IR, which can be assigned to (c-c) structures in equilibrium with (c-a) structures. The next section deals with the investigation of the different dependencies of the formation of cationic clusters in the bulk IL with the help of IR spectroscopy.

3.1.3. Temperature dependency

Taking into account that hydrogen bonding is a weak, directional, short range interaction and that the Coulomb interaction is an undirected, strong, long range interaction there should be a strong temperature dependency of the equilibrium between the (a-c) species and the differently sized and shaped (c-c) species. By decreasing the temperature of the IL [HOC₂MIm][NTf₂] stepwise from 80 °C (353 K) to -80 °C (193 K) in 20 K steps we can observe increasing red-shifted intensity relative to the OH vibrational band at $\approx 3550\text{ cm}^{-1}$ in the IR spectra, which can be assigned to an anion-cation H-bond (a-c) (Fig. 3.1 (a)). The red-shifted vibrational band can be assigned to O-H...O hydrogen bonds between cations (c-c). This clearly shows that the variation of temperature has a significant influence on the aggregation of like-charged ions in ionic liquids. With

the help of DFT calculations we were able to identify the responsible structures for these red-shifted bands. They arise from H-bonded dimers, trimers and tetramers of the OH-functionalized ionic liquids similar to the clusters formed in molecular solvents like water or alcohols. The highest stability was found for the cyclic tetramer. The decreasing intensity of the (a-c) band to the benefit of the (c-c) bands with decreasing temperature can be explained by an increased kinetic stabilisation of the cooperative (c-c) H-bonds. This kinetic stabilization can be determined if we remove the anions from the dimer structure and calculate the relaxed-scan potential curve for $[\text{HOC}_2\text{MIm}]_2^{2+}$ at the B3LYP-6-31+G* and MP2-6-31+G* levels of theory. We find local minimum structures at typical H-bond distances of $R_{\text{O}\cdots\text{H}} = 2.0$. The uncorrelated HF level does not show this minimum and only gives an inflection feature in this region. As shown in Figure 3.1 (b), a robust kinetic stability with a clear dissociation barrier of 3-4 kJmol⁻¹ is achieved for the B3LYP and the MP2 treatment. In this sense, the pure cationic clusters are stable up to cyclic tetramers, wherein cooperative H-bonding is maximized. Larger clusters, such as cyclic pentamers or hexamers, do not show this kinetic stability and dissociate during the geometry optimization procedure.

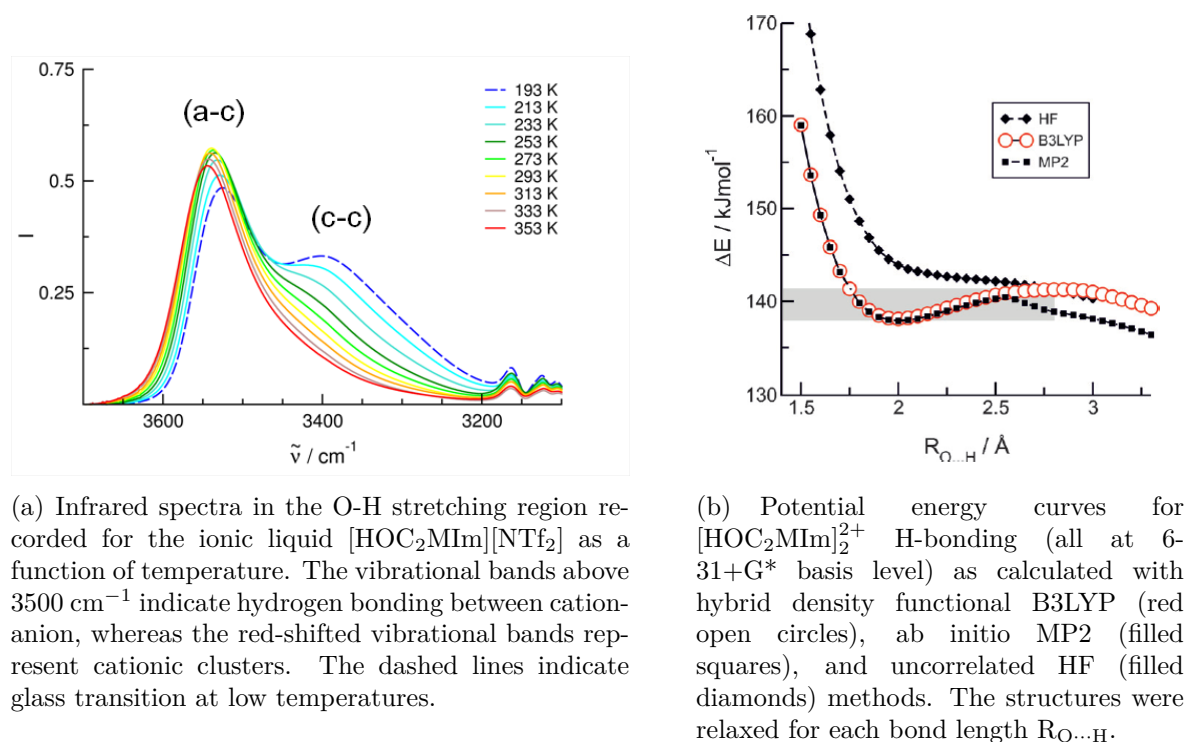


Figure 3.1.: Temperature dependence of the formation of cationic clusters.

3.1.4. Anion dependency

For our studies in **Paper I** we focused on the question how the interaction strength of the counter anion influences the formation of (c-c) clusters in OH-functionalized ILs.

For this purpose we have chosen ionic liquids which all include the 1-(2-hydroxyethyl)-3-methylimidazolium cation $[\text{HOC}_2\text{MIm}]^+$ but the four different anions tetrafluoroborate, bis-(trifluoromethanesulfonyl)imide, trifluoromethanesulfonate, and methanesulfonate, which have an increasing interaction potential in this sequence. Initially, we measured the IR spectra in the OH-stretching region of the ILs $[\text{HOC}_2\text{MIm}][\text{BF}_4]$, $[\text{HOC}_2\text{MIm}][\text{NTf}_2]$, $[\text{HOC}_2\text{MIm}][\text{OTf}]$, and $[\text{HOC}_2\text{MIm}][\text{OMs}]$ covering a large temperature range between 213 and 353 K.

In the sequence from weaker to stronger interacting anions, the frequencies shift from higher to lower wavenumbers ($\Delta\tilde{\nu} = 220 \text{ cm}^{-1}$). This finding is not surprising but supports essentially the interpretation of the spectra of the pure ILs as shown in Figure 3.2.

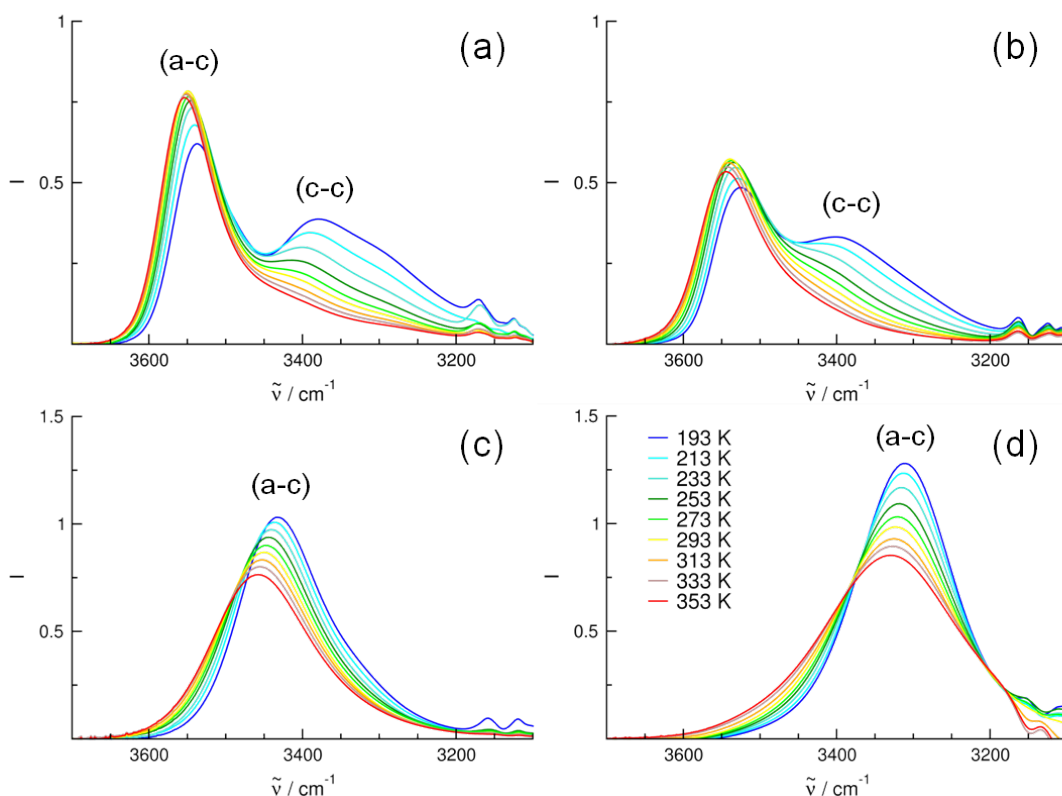


Figure 3.2.: IR spectra in the OH-stretching region recorded for the ionic liquids (a) $[\text{HOC}_2\text{MIm}][\text{BF}_4]$, (b) $[\text{HOC}_2\text{MIm}][\text{NTf}_2]$, (c) $[\text{HOC}_2\text{MIm}][\text{OTf}]$, and (d) $[\text{HOC}_2\text{MIm}][\text{OMs}]$ as a function of temperature between 213 K and 353 K.

Only for ILs $[\text{HOC}_2\text{MIm}][\text{BF}_4]$ and $[\text{HOC}_2\text{MIm}][\text{NTf}_2]$, two major vibrational signatures can be observed. Firstly, the (a-c) contributions resulting from the regular $\text{OH} \cdots \text{F}$ and $\text{OH} \cdots \text{O}$ hydrogen bonds between cations and anions and secondly, the (c-c) contributions stemming from the $\text{OH} \cdots \text{O}$ hydrogen bonds between the cations originating from like-charge attraction. The OH vibrational bands of ILs $[\text{HOC}_2\text{MIm}][\text{OTf}]$, and

$[\text{HOC}_2\text{MIm}][\text{OMs}]$ are strongly redshifted owing to the increasing anion interaction strength and fall into the range of the vibrational bands assigned to the (c-c) signatures of the cationic clusters of $[\text{HOC}_2\text{MIm}][\text{BF}_4]$ and $[\text{HOC}_2\text{MIm}][\text{NTf}_2]$. However, there is strong evidence that the vibrational band of $[\text{HOC}_2\text{MIm}][\text{OMs}]$ can be exclusively referred to (c-a) interactions, which could be shown in a dilution experiment. Clearly, the methanesulfonate anion strongly interacts with the OH group of the cation, resulting solely in cation-anion pairs of opposite-charged ions. There is no intensity which could be referred to vibrational bands of OH bonds involved in other types of interaction.

3.1.5. Cation dependency

In the study published in **Paper II**, we demonstrate by the means of IR spectroscopy that the presence of cationic clusters can be strongly supported or suppressed by specifically designed cations. The ILs are based on ammonium, piperidinium, pyrrolidinium, pyridinium, and imidazolium cations all including a hydroxyethyl group for H-bond formation to the anion or to other cations, resulting in cationic clusters. The corresponding N-heterocycles for the cations are shown in Figure 2.1. For all ILs, we have chosen the bis(trifluoromethylsulfonyl)imide $[\text{NTf}_2]^-$ as the counterion for two reasons. Firstly, this anion is flexible, resulting in low viscosities and melting points, providing room temperature ionic liquids. Secondly, the relatively hydrophobic $[\text{NTf}_2]^-$ anion forms only weak hydrogen bonds to the cation and thus supports the formation of cationic clusters. The ability for cationic cluster formation can be referred to the shape, the charge distribution and the specific interaction site of the cations. With respect to structure and charge distribution within the cation, the ILs can be divided into two groups. The ILs $[\text{HOC}_2\text{TMA}][\text{NTf}_2]$, $[\text{HOC}_2\text{MPip}][\text{NTf}_2]$ and $[\text{HOC}_2\text{MPyrro}][\text{NTf}_2]$ represent saturated compounds, characterised by positive charge localization at the nitrogen atom. In contrast, delocalized positive charge within the nitrogen heterocycle is typical for the ILs $[\text{HOC}_2\text{Py}][\text{NTf}_2]$, and $[\text{HOC}_2\text{MIm}][\text{NTf}_2]$. By tuning the properties of the cations in this way, we observe substantial cationic cluster formation already at room temperature. For the first time we can also show that the presence of cationic clusters strongly influences the properties of ionic liquids. If substantial amounts of cationic clusters are available, the ILs can be supercooled and form glasses at temperatures between 193 K and 213 K (see Fig: 3.3 (b)). If cationic clusters are only present in trace amounts, the ILs can be crystallized by forming hydrogen-bonded ion pairs between cations and anions solely. [54] The glass transition temperatures and the phase transition temperatures were measured by differential scanning calorimetry (DSC). Concerning structure and charge distribution within the cation, the ILs can be divided into two groups, they can also be divided in two groups with respect to their ability to form (c-c) clusters. Only the ILs with a delocalized positive charge are able to form substantial amounts of (c-c) clusters, which is a strong evidence that a delocalized positive charge supports and a localized positive charge suppresses the formation of cationic clusters. If crystallization occurs, the infrared spectra show the typical sharp features of cation-anion interaction only and the broad redshifted bands of the cationic clusters completely disappear (see

Fig: 3.3 (a)). For these ILs the structures could be obtained from X-ray crystallography. [53] The formation of clusters of like-charged ions is influenced by the shape and interaction strength of the ions and may provide a new path for controlling supercooling and crystallization.

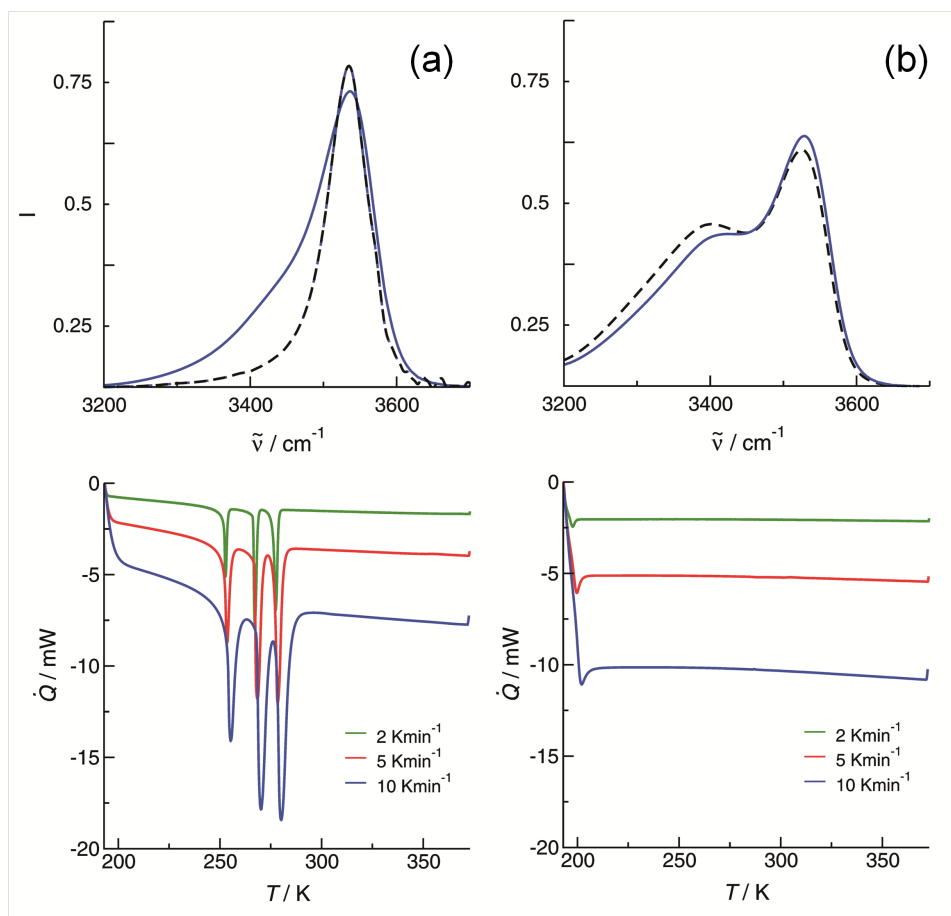


Figure 3.3.: Infrared spectra in the O-H stretching region and DSC traces recorded for the ionic liquids (a) $[\text{HOC}_2\text{MPip}][\text{NTf}_2]$ and (b) $[\text{HOC}_2\text{MIm}][\text{NTf}_2]$ for the lowest (a) 253 K, (b) 193 K) and second lowest (a) 273 K, (b) 213 K temperatures. The vibrational bands above 3500 cm^{-1} indicate hydrogen bonding between cation-anion, whereas the red-shifted vibrational bands represent cationic clusters. For IL $[\text{HOC}_2\text{MPip}][\text{NTf}_2]$ the small amount of cationic clusters disappears upon freezing, resulting in a symmetric vibrational band indicating pure (c-a) interaction. This behaviour is in accord to the DSC traces, which show phase transitions in this temperature range. For IL $[\text{HOC}_2\text{MIm}][\text{NTf}_2]$ the amount of cationic clusters further increases with decreasing temperature. No change in the vibrational signature is observed in accord with the DSC traces.

3.1.6. Chain length dependency

It was the main purpose of **Paper III** to clarify whether tethering the OH group away from the positive charge center of the cationic ring with longer hydroxyalkyl chains

compensates for unfavourable cation/anion combinations with respect to (c-c) cluster formation. Thus, we collected the IR spectra for a large set of ILs including two different $[\text{HOC}_2^-]$, $[\text{HOC}_3^-]$, $[\text{HOC}_4^-]$ and $[\text{HOC}_5^-]$ functionalised cations in combination with the $[\text{NTf}_2]^-$ anion, namely $[\text{HOC}_n\text{MPip}][\text{NTf}_2]$ and $[\text{HOC}_n\text{Py}][\text{NTf}_2]$. The intensities indicating (c-c) cluster formation constantly increase with longer hydroxyalkyl chain length. Obviously any combination of a weakly interacting anion, here $[\text{NTf}_2]^-$, with a hydroxy-functionalised cation show at least little (c-c) cluster formation. The slight preference for (c-c) interaction of polarisable versus hard cations disappears with increasing hydroxyalkyl chain length. The presence of a strongly interacting anion such as methanesulfonate completely suppresses (c-c) cluster formation and results solely in (c-a) hydrogen bonding regardless of long alkyl chain tethers. This was clearly demonstrated by the temperature dependent IR spectra of $[\text{HOC}_5\text{Py}][\text{OMs}]$ between 193 K and 353 K. Although including a polarizable cation with a long hydroxypentyl chain, we observe no (c-c) cluster formation for this IL. The symmetric shape of the vibrational band is temperature independent. Moreover, the maximum of the IR band is stronger red-shifted and its intensity further enhanced with decreasing temperature. This kind of temperature behavior is found, if only one type of hydrogen-bonded species is present in the IL, here the (c-a) clusters.

In the next step, we estimated the transition enthalpies needed to break the (c-c) hydrogen bonds shifting the equilibrium from (c-c) towards (c-a) species. We are aware that several (c-c) cluster species exist and that they transform into each other. Nevertheless, we consider the temperature dependence of the „equilibrium constant K “ as VAN’T HOFF like:

$$\ln(K) = -\frac{\Delta_R G^\ominus}{RT} = -\frac{\Delta_R H^\ominus}{RT} + \frac{\Delta_R S^\ominus}{R}$$

In particular, at low temperatures, $\Delta_R H^\ominus$ and $\Delta_R S^\ominus$ change with temperature. However, we applied the following procedure for describing the (c-c) to (c-a) transition as a function of the polarisability of the cation, the interaction strength of the anion and the alkyl chain lengths. We assume that the cation-anion (I_{c-a}) and the cation-cation (I_{c-c}) hydrogen bond IR intensities arise from cations of these two general classes of H-bonding configurations, for which relative populations are a function of absolute temperature only. Consequently, a plot of $\ln(I_{c-a}/I_{c-c})$ versus $1/T$ should yield a straight line with a negative slope that is proportional to the average difference in energy between the two classes of H-bond configurations. All ILs show an almost linear dependence between $\ln(I_{c-a}/I_{c-c})$ and $1000/T$. For the linear regression, we only excluded the data points at the lowest temperature (193 K). A negative slope and thus positive $\Delta_R H^\ominus$ show that cationic cluster formation is enthalpically favored. This is the case for ILs $[\text{HOC}_n\text{MPip}][\text{NTf}_2]$ and $[\text{HOC}_n\text{Py}][\text{NTf}_2]$ with $n=2-5$ (see Fig. 3.4). In accord with the findings above, the $\Delta_R H^\ominus$ values increase with increasing hydroxyalkyl chain lengths due to enhanced (c-c) cluster formation. The $\Delta_R H^\ominus$ of IL $[\text{HOC}_2\text{Py}][\text{NTf}_2]$ is larger than that of IL $[\text{HOC}_2\text{MPip}][\text{NTf}_2]$ because the more polarisable pyridinium cation stronger promotes (c-c) clustering as observed in the IR spectra. The $\Delta_R H^\ominus$ values for both types of ILs become similar with increasing hydroxyalkyl chain lengths overcoming the cation

effect for (c-c) cluster formation. For all ILs $[\text{HOC}_n\text{Py}][\text{OMs}]$ consisting the strongly interacting anion $[\text{OMs}]^-$ we obtain $\Delta_R H^\ominus$ values of almost zero within the experimental error indicating that the presence of (c-a) clusters is independent of temperature. The entropies $\Delta_R S^\ominus$ for ILs $[\text{HOC}_n\text{MPip}][\text{NTf}_2]$ and $[\text{HOC}_n\text{Py}][\text{NTf}_2]$ successively increase from $n = 2$ to $n = 5$. Obviously, larger structures, here (c-c) clusters, are formed with increasing chain length as observed in the strongly red-shifted and enhanced vibrational bands assigned to (c-c) cluster formation. The similar entropies $\Delta_R S^\ominus$ for all ILs $[\text{HOC}_n\text{Py}][\text{OMs}]$ show that the size of the structures are not changing with temperature which is in accord with the presence of exclusively (c-a) hydrogen bonded species.

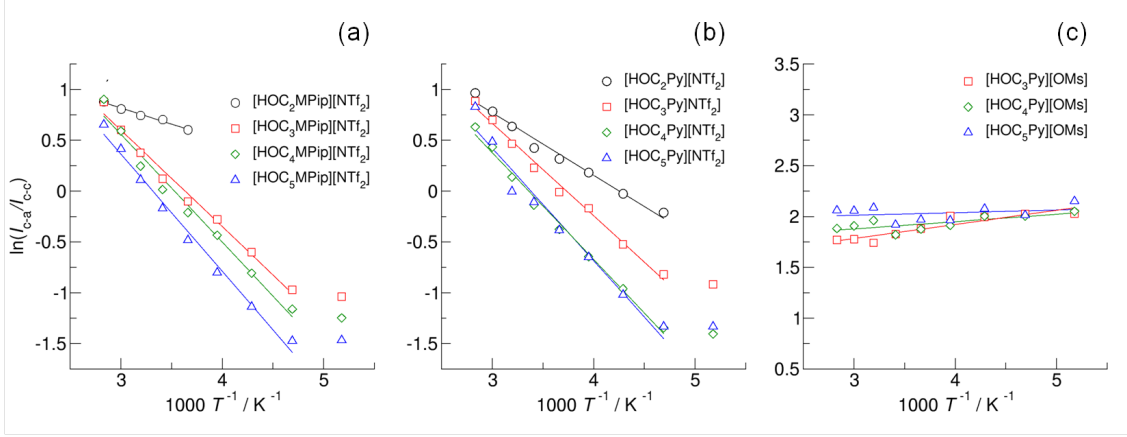


Figure 3.4.: Plots of the natural logarithm of the (c-a) to (c-c) vibrational band intensity ratios versus inverse temperature taken from the measured IR spectra between 193 K and 353 K. I_{c-a} and I_{c-c} were obtained from the integral intensities left and right of the frequency position, where the vibrational bands for the (c-a) and the (c-c) species cross. The solid lines represent linear fits ($R^2 \geq 0.98$) with slopes indicating different enthalpies of cationic cluster formation.

The differential scanning calorimetry (DSC) measurements of all ILs in **Paper III** strongly support the interpretation of the IR spectra and VAN'T HOFF-like plots as well. During cooling from 373 K to 193 K at $10 \text{ K} \cdot \text{mol}^{-1}$ cooling rates, heat capacity change corresponding to glass transitions could be observed in the DSC profiles of ILs $[\text{HOC}_n\text{MPip}][\text{NTf}_2]$ with $n=3-5$ and $[\text{HOC}_n\text{Py}][\text{NTf}_2]$ with $n=2-5$. The supercooled state of the (c-c) cluster-forming ILs is obviously fairly stable. In contrast, the phase transition behaviour is complex for IL $[\text{HOC}_2\text{MPip}][\text{NTf}_2]$, including liquid/solid ($T=276.2 \text{ K}$) and solid/solid phase transitions ($T=266.2 \text{ K}$ and 251.6 K). For the ILs $[\text{HOC}_n\text{Py}][\text{OMs}]$ with $n=2-4$ we observe clear melting transitions at $T = 362.1 \text{ K}$, 301.5 K and 325.7 K , respectively. Obviously, strong formation of cationic clusters in ILs results in supercooling and glass transition, whereas (c-a) cluster formation leads to liquid/solid phase transition. From the combined IR and DSC experiments, we have clear evidence that the formation of cationic clusters prevents the ILs from crystallization and liquid/solid phase transition. The resulting material is a glass. [55] Our findings suggest that the phase behavior of this type of ILs can be controlled by cationic cluster formation.

3.2. ND of the bulk IL supported by MD simulations

3.2.1. Neutron diffraction

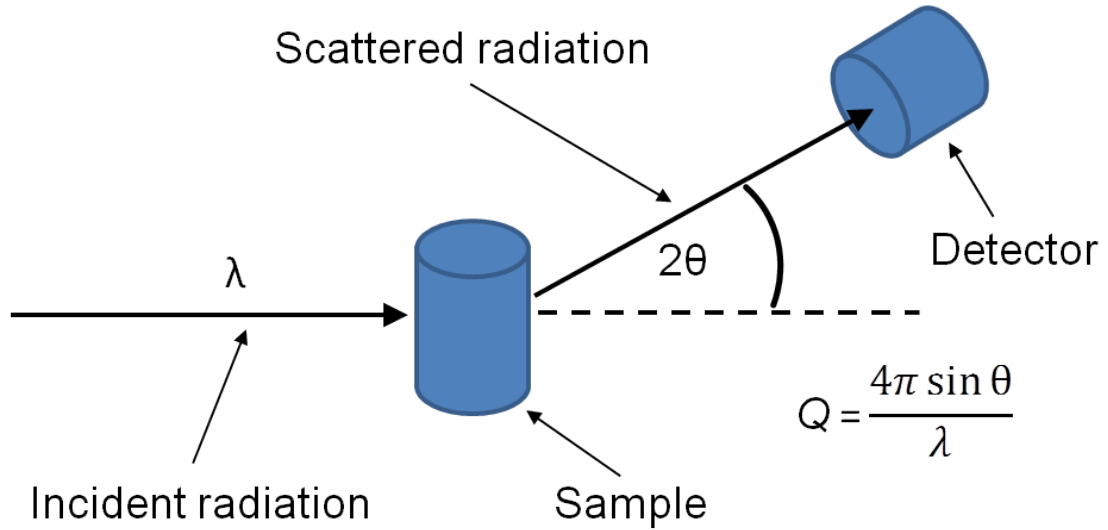


Figure 3.5.: A beam of monochromatic neutrons with wavelength λ impinges on the sample from the left, is scattered by that sample into scattering angle 2θ and then detected by the detector. The data are measured versus the variable $Q = \frac{4\pi \sin \theta}{\lambda}$. It is Q which determines the length scale that is probed by the diffraction experiment, with small Q corresponding to large distances and large Q corresponding to small distances. Any combination of θ and λ that gives the required Q values should in principle give equivalent data. The simplicity of the underlying diffraction experiment belies many of the subtleties that are associated with it. [56]

Neutrons are scattered by the atomic nucleus. In order to see diffraction effects related to the arrangement of the atoms it is necessary to use neutron wavelengths comparable to the typical spacing between atoms, 10^{-10} m. [56] This wavelength is roughly 10^4 times larger than the nuclear dimensions, so, provided the neutron energy is well away from any nuclear resonances, the scattering is called „s-wave“, which means there is no angular momentum transfer in the scattering process. (If the neutron energy is near a nuclear resonance of one of the atomic components in a material, for the most part the information obtained by scattering neutrons is not useful. Fortunately, this mostly happens only with heavier nuclei and at higher neutron energies.) To a neutron an atom therefore normally appears as an extremely small blip in space, mathematically effectively describable by a δ -function. For this reason, neutrons give arguably the most direct insight into the position and motion of atoms, both as individual particles, the self scattering, and as pairs of atoms, the distinct scattering: the neutron probes directly the site-site correlation functions between atomic centres. [57] However, because the atomic nucleus is so small, the neutron-nucleus interaction is weak, so neutrons are mostly very penetrating, and a lot of effort is required to make neutron sources which are bright

enough to perform useful diffraction and other types of neutron scattering experiments. [58]

Table 3.2.: Advantages and disadvantages of neutron diffraction.

Advantage	Disadvantage
sensitivity to light atoms	high costs
ability to distinguish isotopes	only possible at neutron sources
structure elucidation of X-ray amorphous samples	numerous isotopic substituted partials necessary
probes directly the site-site correlation functions	long measuring times
	limited temperature range

3.2.2. Molecular dynamics simulations

Molecular Dynamics (MD) refers to computer simulations in molecular modelling in which interactions between atoms and molecules and their resulting spatial movements are iteratively calculated and represented. In the modeling of complex systems with a large number of atoms involved, mainly force fields or semiempirical methods are used. The force field is the potential energy that describe the interactions between the atoms or molecules. It is defined by two parts: its mathematical form (mainly based on classic mechanics) and the atom-specific parameters (mainly obtained from spectroscopy experiments, scattering experiments or quantum mechanical calculations. [59, 60] In some cases, macroscopic properties, like viscosities or vaporization enthalpies, are used, insofar that they have to be fulfilled by the parametrised force fields. Therefore, it is not really surprising that force fields are not universally valid for the molecules for which they were developed, but are more or less parametrised for specific tasks. Hence, there may be different sets of parameters for a force field approach.

Once a suitable force field is developed, a simulation box can be filled with the chosen molecules. Then the equilibration follows: For each particle, the forces acting on it due to its neighbors are calculated, and the particles are moved according to these forces in very small time steps. [61] In order to realize the conditions of the isothermal-isobaric ensemble, both a thermostat as well as a barostat are needed. [62–65] After a few steps, the simulation box reaches a thermal equilibrium and the particles start to move "realistically". MD simulations usually use periodic boundary conditions: every particle that leaves the simulation box on one side a particle of the same type with the same momentum enters the box on the opposite side. Pressure and temperature can now be calculated from the forces and movements of the particles and changed step by step. The molecules can undergo conformational changes. From the thus obtained equilibrated simulation box thermodynamic informations can be calculated. Furthermore, structural informations, like pair correlations and pair distributions, can be calculated directly from the atomic positions in the simulated box. The big advantage of MD simulations is that dynamic information for short time scales are accessible as well.

Table 3.3.: Advantages and disadvantages of molecular dynamics simulations.

Advantage	Disadvantage
wide temperature range	results depending on chosen force fields
dynamic information	no proton transfer
direct access to structural informations	high computational effort

3.2.3. Cluster distribution

In **Paper IV** we have examined the bulk structure of 1-(4-hydroxybutyl)pyridinium bis(trifluoromethylsulfonyl)imide $[\text{HOC}_4\text{Py}][\text{NTf}_2]$ using neutron diffraction with isotopic substitution (NDIS). Neutron diffraction spectra were refined using the empirical potential structure refinement (EPSR) to extract atomic- and molecular-level structure information. [66–70] The IL $[\text{HOC}_4\text{Py}][\text{NTf}_2]$ was chosen to maximize the opportunity for like-charge hydrogen bonding: $[\text{NTf}_2]^-$ is a weakly interacting anion, whereas $[\text{HOC}_4\text{Py}]^+$ is a highly polarizable cation. In addition, the hydroxybutyl group of the cation allows for ample separation between the positively charged pyridinium ring and the hydroxy group. It is the aim of this study to characterise the (c-a) ($^+\text{O}-\text{H}\cdots\text{O}^-$) and the (c-c) ($^+\text{O}-\text{H}\cdots\text{O}^+$) hydrogen bonds in this hydroxy-functionalized IL by means of neutron diffraction, molecular dynamics (MD) simulations, and quantum chemical calculations. A similar approach combining X-ray scattering and MD simulations has been successfully applied to analyse the structure of ILs and organic phases. [71–73] The measured hydrogen-bond lengths for the two types of ionic interactions, which describe the attraction between ions of opposite and repulsion between ions of like charge, are compared to those of molecular liquids, such as water and alcohols. [74–80] In addition, we carefully address the different types of (c-a) and (c-c) clusters and their distributions in the bulk liquid. The accompanying MD simulations support the concept of the double-faced nature of hydrogen bonding in this particular class of liquids. Here, we solely focus on the intermolecular hydrogen-oxygen ($\text{H}\cdots\text{O}$) and associated oxygen-oxygen ($\text{O}\cdots\text{O}$) pair distribution functions $g_{\text{HO}}(r)$ and $g_{\text{OO}}(r)$, which describe the nature of the hydrogen bonding in the IL. As a result of the large number of isotopically labeled compounds used, both pair distribution functions could be derived confidently for the (c-a)- and the (c-c)-bound species. The first peak in the $g(r)$ functions corresponds to the first coordination shell of the nearest neighbours. Figure 3.6 a) shows the $g_{\text{HO}}(r)$ and $g_{\text{OO}}(r)$ functions for the (c-a)- and (c-c)-bound species. The maxima of the first nearest neighbour peaks in the two functions give the average hydrogen-bond lengths $r(^+\text{H}\cdots\text{O}^-)$ and $r(^+\text{O}\cdots\text{O}^-)$ for the (c-a) as well as $r(^+\text{H}\cdots\text{O}^+)$ and $r(^+\text{O}\cdots\text{O}^+)$ for the (c-c) binding motifs, respectively. The (c-c) hydrogen bonds are noticeably shorter (1.87 Å and 2.78 Å) than the (c-a) hydrogen bonds (1.95 Å and 2.88 Å), which indicates stronger attraction between ions of like charge (c-c) than between ions of opposite charge (c-a). This observation is quite remarkable because the total interaction in the (c-a)-bound species results from hydrogen bonding plus attractive COULOMB forces between the oppositely charged ions. It is evident that the (c-a) interaction is only weakly strengthened by COULOMB

attraction, whereas the (c-c) interaction is strongly enhanced by potentially cooperative hydrogen bonding. Despite the COULOMB repulsion, the hydrogen bond is shorter for the (c-c) than for the (c-a) species. [40] We complemented the NDIS measurements by MD simulations using independently derived molecular force fields. [43-45] In figure 3.6 b) we show that the $r(^+H \cdots O^-)$, $r(^+O \cdots O^-)$, $r(^+H \cdots O^+)$, and $r(^+O \cdots O^+)$ distances again show shorter hydrogen bonds for (c-c) than (c-a) and agree almost quantitatively with the geometries derived from the ND measurements. The NDIS experiments and MD simulation agree in the pair distribution functions and allow (c-a)- and (c-c)-bound species to be clearly distinguished.

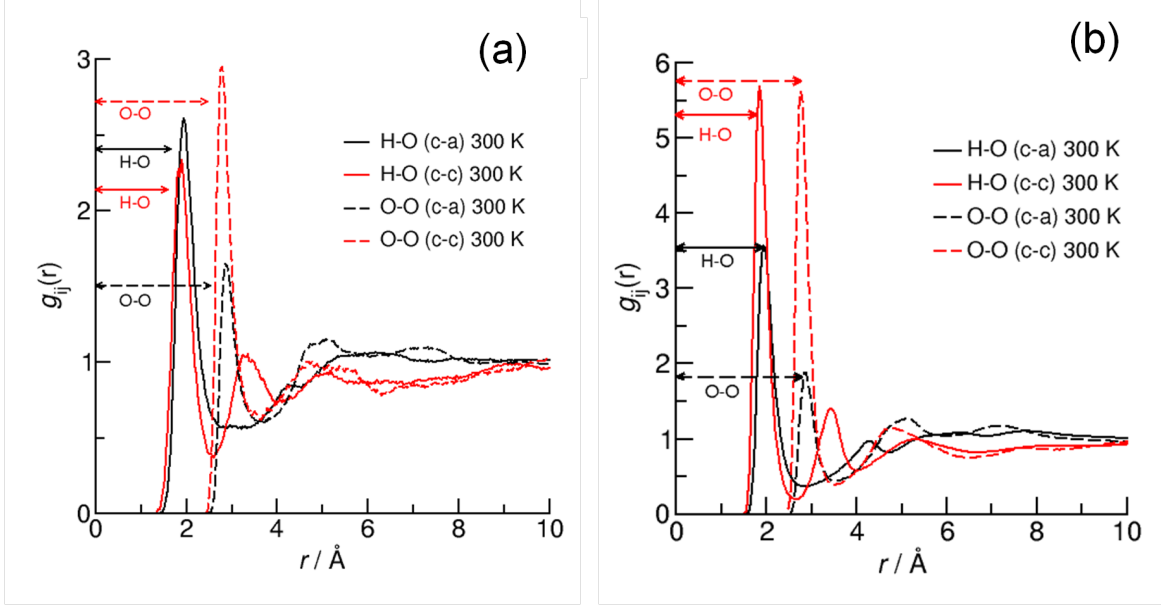
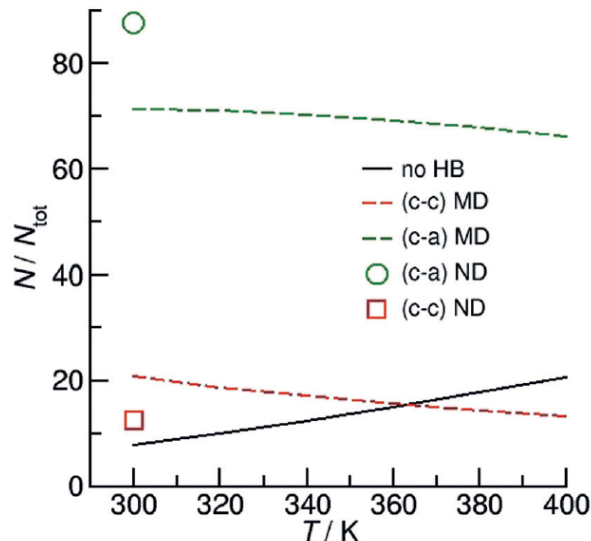


Figure 3.6.: Pair distribution functions $g_{HO}(r)$ and $g_{OO}(r)$ for the (c-a) and (c-c) hydrogen bonds in the IL $[HOC_4Py][NTf_2]$ from (a) neutron diffraction with H/D substitution and (b) molecular dynamics simulations. The nearest neighbor distances are indicated by the arrows.

The NDIS experiments and MD simulations allow quantification of the populations of these local arrangements. In figure 3.7, we show that at 300 K between 87 % (NDIS) and 75 % (MD) of the cations form (c-a) hydrogen bonds with the counterions, whereas between 13 % (NDIS) and 20 % (MD) of the cations are involved in (c-c) structural motifs. This agreement is excellent, given the possible uncertainties of the experiments and simulations (± 0.02 Å). MD simulations were performed for temperatures between 300 and 400 K to reveal the temperature dependence of the cluster populations. We observe that the (c-a) and (c-c) species decrease to the benefit of quasi-free OH groups as the temperature is increased. The decrease with temperature is more pronounced for the (c-c)- than for the (c-a)-bound species, probably for entropic reasons (formation of larger aggregates). From a VAN 'T HOFF plot of the ratio for the (c-c) and the (c-a) hydrogen-bonded species versus the inverse temperature obtained from MD simulations data we

determine the transition enthalpy from (c-c) to (c-a) to be about 3.75 kJmol^{-1} . Such a small transition enthalpy suggests that the (c-c)-bound species exist in equilibrium and that kinetic trapping is not a requirement for finding cationic clusters at room temperature.

Figure 3.7: Analysis of (c-a) and (c-c) cluster populations in $[\text{HOC}_4\text{Py}][\text{NTf}_2]$ from MD simulations as a function of temperature. The symbols show the cluster distribution obtained from NDIS experiments at 303 K.



3.3. Investigations of cationic (c-c) cluster structures by means of CIVP spectroscopy

3.3.1. Cryogenic ion vibrational predissociation CIVP spectroscopy

For our structural investigations of the cold ($\sim 35 \text{ K}$) positively charged clusters we had the privilege to use the CIVP spectrometers in a cooperation with the Johnson Lab from Yale University, which they built and developed in their labs during the past decades. The technique and experimental set-up is well described by Wolk et al.. [81] The essential requirements for CIVP spectroscopy are a source of cold ions and two stages of mass selection so that specific m/z target ions can be photoexcited and then the lighter fragment ions can be subsequently separated from their intact parents. The scheme developed at Yale over many years, which uses a time-of-flight mass spectrometer as its first analyzer and a modest resolution reflectron as the second, is illustrated in figure 3.8. The ion source is on the left, while the laser interaction and mass spectrometry components are on the right.

In the ion source, target species are extracted from solution using electrospray ionisation and transferred using radio-frequency ion guides through three stages of differential pumping to a low pressure region. The warm continuous stream of ions is then injected into a commercial three-dimensional radio-frequency ion trap modified for cryogenic operation and held at $\sim 35 \text{ K}$ with a closed cycle He cryostat. A seeded buffer gas

is pulsed into the trap just prior to ion injection, which contains a trace amount of the cryogenic solvent (N_2 in our case) to be condensed onto the ions after they are collisionally cooled. This growth period takes tens of milliseconds, and relatively large aggregates can be formed depending on the buffer gas pressure and dwell time in the trap. These weakly bound solvent molecules typically have little effect on the vibrational spectrum, as evidenced by very small incremental shifts upon addition of the first few molecules. [82] Note that the buffer gas is pulsed into the trap, so that it is slowly evacuated before the ions are extracted. This limits the collisional reheating of the cold ion upon acceleration by the extraction voltages. [83]

Tandem time-of-flight methods provide an inexpensive platform for carrying out mass-selective photofragmentation, with a typical arrangement illustrated on the right side of figure 3.8. In the basic experiment, a widely tunable IR pulse from the primary laser intercepts a single m/z ion packet from the ion distribution arriving from the source. This causes photoevaporation of weakly bound adducts, and the lighter fragment ions are then separated from their parents in a second reflectron mass spectrometer and monitored as a function of laser frequency to generate the spectrum. [81]

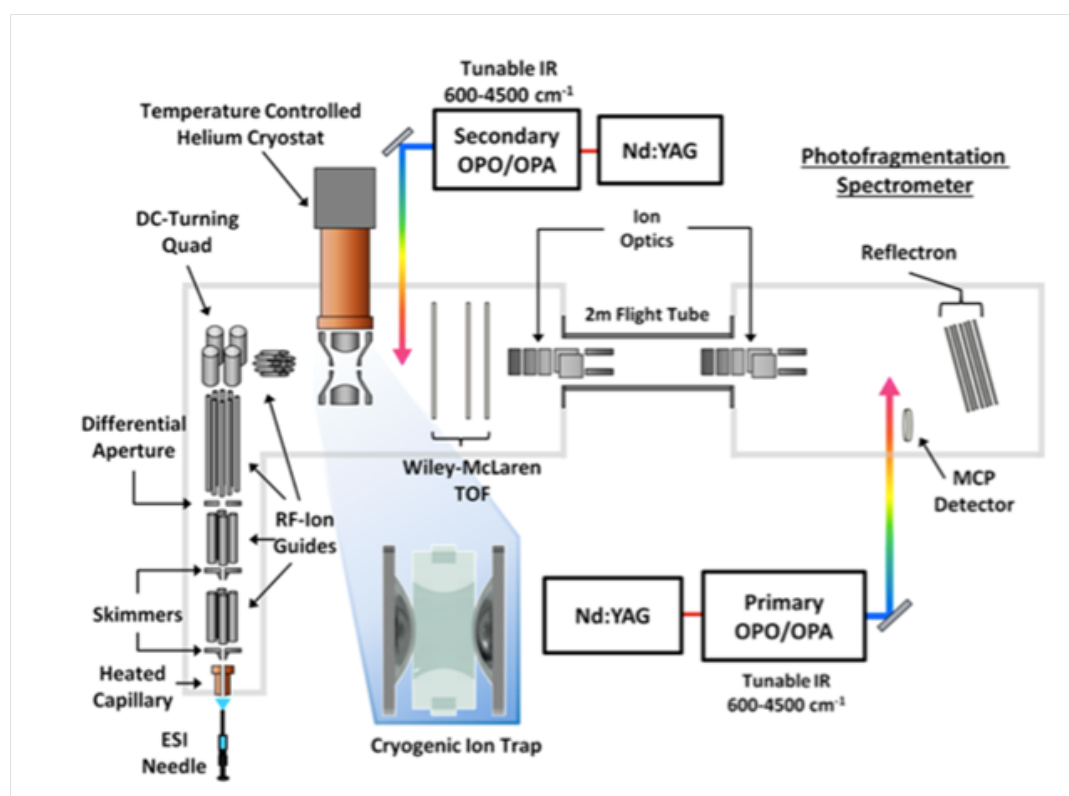


Figure 3.8.: In the Yale tandem time-of-flight photofragmentation spectrometer, ions are extracted from solution with electrospray ionisation (ESI) and guided into a 10K3D quadrupole ion trap. After collisional cooling, ions are extracted from the trap and mass selectively (to unit m/z) interrogated by one or two pulsed infrared lasers. Primary and secondary lasers are based on optical parametric oscillators and amplifiers (OPO/OPA). [81]

The Yale apparatus also includes a second laser interaction stage (labeled „secondary“ in figure 3.8), which is used to extract individual spectra when many conformers or isomers appear at the same m/z . Using IR-IR double resonance technique by fixing the „secondary“ pump laser on the excitation frequency of one spectral contribution and continuously monitoring the fragment signal while the „primary“ pump laser is scanned through the energy range of the desired spectra. The probe signal monitors the population of the conformer responsible for the band with the chosen excitation frequency, and the key to the hole-burning method is to intersect the same ion packet with a powerful pump laser before it interacts with the probe. When the pump laser drives any of the transitions associated with the conformer being isolated with the probe transition, its population will be removed by photoevaporation of its adducts. Thus, the entire spectrum associated with the conformer selected by the probe is revealed by „dips“ in the probe fragment signal as the pump laser is scanned through the spectrum.

Table 3.4.: Advantages and disadvantages of molecular CIVP spectroscopy

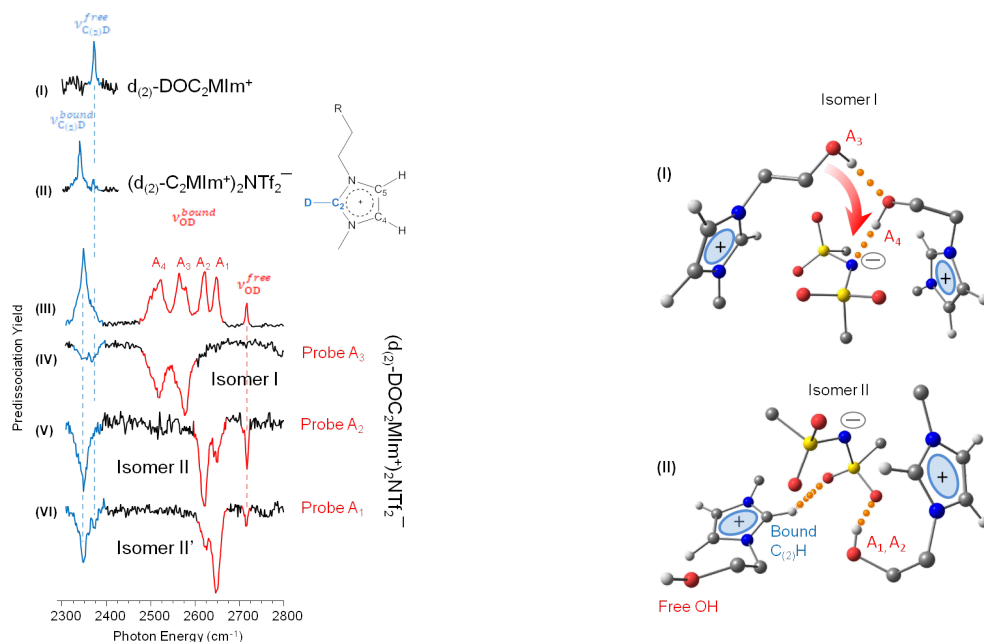
Advantage	Disadvantage
comparable to DFT spectra due to low temperatures and absence of solvents	investigated clusters have to be charged
mass selection of clusters	frequency dependency of the IR intensities
isomer selective	high experimental effort
sensitive structure elucidation	

3.3.2. (c-c) dimers

The bulk spectroscopic results (FT-IR) of the **Papers I - III** have reported strong evidence for the formation of (c-c) clusters in OH-functionalized ILs and figured out different dependencies of these formations. In those cases, the spectroscopic signatures of hydrogen bonding in the OH stretching region were observed to become more prominent at lower (~ 213 K) temperatures, but the diffuse nature of the bands allowed only a qualitative picture of the local interactions. In **Paper V** we focus on the isolated cluster ion consisting of two cations and one anion, denoted hereafter as (2,1), which are the smallest systems capable of displaying an anion-mediated, attractive interaction between molecular cations. By analysing the vibrational spectra obtained from the mass-selective, cryogenic ion trapping techniques with DFT calculations, we elucidate the gas phase structures of these ternary complexes. Recognizing that the $[\text{HOC}_2\text{MIm}]^+$ ion presents two primary contact points, the $\text{C}_{(2)}\text{H}$ and OH groups, for interaction with the anion, the key issue regards whether these docking motifs compete for attachment sites on the anion. To establish the activity of the $\text{C}_{(2)}\text{H}$ groups, we obtained the spectra of the $[\text{HOC}_2\text{MIm}]^+$ isotopologue with deuterium atom substitutions at both the $\text{C}_{(2)}$ and OH positions (denoted $[\text{d}_{(2)}\text{-DOC}_2\text{MIm}]^+$, figure 3.9 (a) (I)), its ternary complex with $[\text{NTf}_2]^-$ (figure 3.9 (a) (III)), and, for comparison, that of the analogous ternary complex with the $[\text{d}_{(2)}\text{-C}_2\text{MIm}]^+$ ion (Figure 3.9 (a) (II)). The spectral response of the $\text{C}_{(2)}\text{D}$ group

is free of the anharmonic interactions that complicate the interpretation of the coupled oscillators in the CH stretching region. As expected, the $C_{(2)}D$ fundamental appears as an isolated band in the bare ion spectrum, ($\nu_{C_{(2)}D}^{\text{free}}$ in figure 3.9 (a) (I)). Interestingly, the OD pattern in the $([d_{(2)}\text{-DOC}_2\text{MIm}]^+)_2[\text{NTf}_2]^-$ spectrum (figure 3.9 (a) (III)) is very similar to that of the OH pattern observed in the $([\text{HOC}_2\text{MIm}]^+)_2[\text{NTf}_2]^-$ case (figure 3.9 (a) (IV)). The vibrational bands in the $([d_{(2)}\text{-DOC}_2\text{MIm}]^+)_2[\text{NTf}_2]^-$ spectrum are assigned to the same series (A_1 , A_2 , A_3 , and A_4 and free OD) as those observed in the spectrum of the light isotopologue where these contributions were found to occur in the same region corresponding to fundamentals of OH groups that strongly interact with anion domains. [84–90] The $C_{(2)}D$ band near 2350 cm^{-1} appears to be asymmetrically broadened in the $([d_{(2)}\text{-DOC}_2\text{MIm}]^+)_2[\text{NTf}_2]^-$ spectrum (blue in figure 3.9 (a) (III)) with a dominant red-shifted component ($\nu_{C_{(2)}D}^{\text{bound}}$) and a weaker higher-energy shoulder. The shoulder appears at the same location as the $C_{(2)}D$ band in the isolated $[d_{(2)}\text{-DOC}_2\text{MIm}]^+$ cation ($\nu_{C_{(2)}D}^{\text{free}}$ in figure 3.9 (a) (I)) and that of $[d_{(2)}\text{-C}_2\text{MIm}]^+$, indicating that only one of the two cations attaches to the anion through the $C_{(2)}H$ group. The $C_{(2)}D$ band in the $([d_{(2)}\text{-DOC}_2\text{MIm}]^+)_2[\text{NTf}_2]^-$ spectrum (figure 3.9 (a) (III)) is broader than that in the $[d_{(2)}\text{-C}_2\text{MIm}]^+$ derivative (figure 3.9 (a) (II)). In addition, the peak maximum is blue-shifted (by 6 cm^{-1}), with the activity near the $\nu_{C_{(2)}D}^{\text{free}}$ feature merging into the overall asymmetrical shape of the band. This shift suggests that the interaction strength of the $C_{(2)}H$ group with the anion is slightly weakened upon incorporation of the hydroxyl group. To address the role of isomers in the assignments of the spectra, we carried out isomer-selective photochemical hole-burning experiments to establish whether distinct species are present and, if so, to isolate the spectrum of each. This was accomplished using a two-colour IR-IR double resonance method. The isomer-selective spectra of the $([d_{(2)}\text{-DOC}_2\text{MIm}]^+)_2[\text{NTf}_2]^-$ isotopologues are reported in figure 3.9 (a) (IV–VI)), which were obtained by probing the A_3 , A_2 , and A_1 features, respectively. Two isomer classes, denoted I and II, are resolved using double resonance. Additional frequencies were probed that yielded isomer-specific spectra consistent with one of these two classes. Most importantly, the isomer I spectrum (figure 3.9 (a) (IV)), which accounts for both the A_3 and A_4 OD features, contributes only weakly to the $C_{(2)}D$ region. Most of the $C_{(2)}D$ intensity is thus traced to the type II isomers, which also account for the free OD band as well as the moderately red-shifted A_1 and A_2 OD stretching bands. This behaviour establishes that the formation of strong bonds to the OH groups of both cations in isomer I (evidenced by the strongly red-shifted OD stretches) comes at the expense of anionic bonds to the $C_{(2)}H$ positions on the imidazolium rings. Moreover, the class II isomers display absorptions at the locations of both the free $C_{(2)}D$ ($\nu_{C_{(2)}D}^{\text{free}}$) and bound ($\nu_{C_{(2)}D}^{\text{bound}}$) regions. As such, the cations in the isomer II class bind to the anion through one $C_{(2)}H$ and one OH group. This information does not, however, resolve the question of whether or not these groups are on the same cation. Many calculated arrangements are consistent with this asymmetrical binding behaviour, with a representative structure indicated in figure 3.9 (b). In this geometry, the $[\text{NTf}_2]^-$ is in a *trans*-configuration with the $C_{(2)}H$ of the $[\text{HOC}_2\text{MIm}]^+$ (with a free OH) bound to an SO group on the anion, while the OH group on the other cation binds to the oxygen atom on the same sulfur

atom. We note that incomplete spectral separation of the two class II isomers leaves open the possibility that isomer II actually binds to the anion with both OH groups, leading to two overlapping transitions contributing to peak A_1 .



(a) Selectively deuterated N_2 -tagged photo-dissociation spectra of (I) $[d_{(2)}\text{-DOC}_2\text{Mim}]^+$, (II) $[(d_{(2)}\text{-C}_2\text{Mim})^+]_2[\text{NTf}_2]^-$, and (III) $[(d_{(2)}\text{-DOC}_2\text{Mim})^+]_2[\text{NTf}_2]^-$. Traces (IV-VI) present IR-IR double resonance spectra of $[(d_{(2)}\text{-DOC}_2\text{Mim})^+]_2[\text{NTf}_2]^-$ probed at 2578 cm⁻¹ (A_3), 2620 cm⁻¹ (A_2), and 2645 cm⁻¹ (A_1), respectively. R = OD for $[d_{(2)}\text{-DOC}_2\text{Mim}]^+$ and H for $[d_{(2)}\text{-C}_2\text{Mim}]^+$.

(b) Low-energy structures of $[(\text{HOC}_2\text{Mim})^+]_2[\text{NTf}_2]^-$ calculated at the B3LYP-D3/6-31+G(d) level of theory representing the binding motifs of isomers with (I) and without (II) direct contact between the cations. F atoms of $[\text{NTf}_2]^-$ and aliphatic H atoms of $[\text{HOC}_2\text{Mim}]^+$ are omitted for clarity.

Figure 3.9.: Structure elucidation of cold (35 K) ternary 2c, 1a gas-phase cluster by means of an IR-IR double resonance experiment combined with DFT calculations.

The calculated structure consistent with the spectral pattern displayed by isomer I (figure 3.9 (b) (I)) indeed displays this type of cooperative arrangement, and its corresponding harmonic band pattern recovers both the weak activity in the $\text{C}_{(2)}\text{D}$ region as well as the two strongly red-shifted bands (A_3 and A_4) in the OD spectral region. These results highlight the importance of the N atom in the interaction with cationic proton donors despite the fact that $[\text{NTf}_2]^-$ is often considered to be dominated by attachment to its SO groups. [91–93] Support for the role of the N atom as an H-bond acceptor can be found, however, in recent solid-state NMR results on triethylammonium-based protic ILs (PILs). [94]

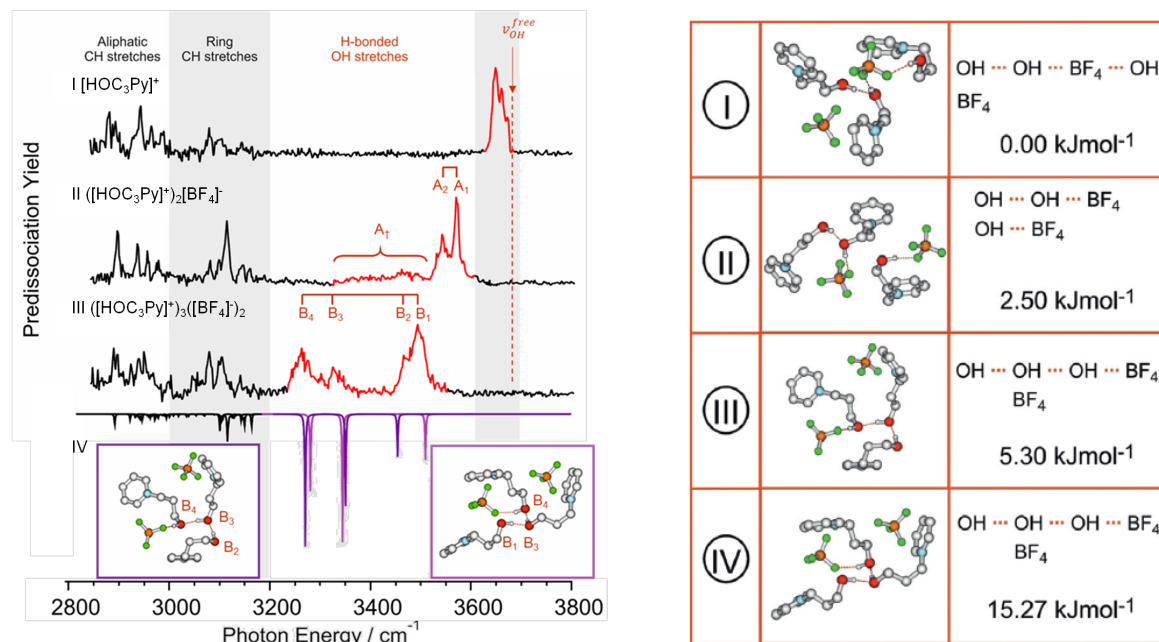
3.3.3. (c-c) trimers

After we were able to isolate three isomers of the ternary $([\text{HOC}_2\text{MIm}]^+)_2[\text{NTf}_2]^-$ complex in the 1-(2-hydroxyethyl)-3-methylimidazolium bis(trifluoromethylsulfonyl)imide IL in **Paper V**, including one in which the OH group on one cation binds to the OH group on the other, which then attaches to the basic nitrogen atom of the anion. Although we isolated the cation-cation interaction, we were not able to observe larger (c-c) bound complexes. The goal of **Paper VI** was therefore to identify an ionic liquid with cation-anion combinations that exhibit this type of (c-c) H-bond motif in larger complexes.

From the bulk phase studies of the **Papers I-III**, we learned that the formation of cationic clusters is governed by three factors that act to enhance (c-c) interactions: 1) weakly interacting anions to attenuate the (c-a) interaction, 2) polarizable cations with only one interaction site (in this case, the OH functional group) to better compensate for the negative charge of the anion, and 3) large distances between the OH functional group and the positive charge center of the cation to weaken the like-charge repulsion. We therefore switched from $[\text{HOC}_2\text{MIm}][\text{NTf}_2]$ to the 1-(3-hydroxypropyl)pyridinium tetrafluoroborate $[\text{HOC}_3\text{Py}][\text{BF}_4]$ system for the following reasons: First, we changed the $[\text{NTf}_2]^-$ counterion to a similarly weakly coordinating anion ($[\text{BF}_4]^-$) with fewer H-bond acceptors than are present in $[\text{NTf}_2]^-$ (four oxygen atoms at two sulfonyl groups and the strongly interacting nitrogen). Next, we replaced $[\text{HOC}_2\text{MIm}]^+$ with $[\text{HOC}_2\text{Py}]^+$ to suppress the hydrogen bonding that occurs via the acidic $\text{C}_{(2)}\text{H}$ position in $[\text{HOC}_2\text{MIm}]^+$ and thus isolate the interactions of the OH groups to the anions as well as to each other. In addition, the longer hydroxyalkyl group in $[\text{HOC}_2\text{Py}]^+$ allows for further separation between cationic centers linked by a hydrogen bond between OH groups.

The vibrational spectrum measured for the quinary (3,2) cluster consisting of three $[\text{HOC}_3\text{Py}]^+$ cations and two $[\text{BF}_4]^-$ anions is presented in figure 3.10 (a) III, and is compared with those of the isolated $[\text{HPPy}]^+$ cation (figure 3.10 (a) I and the corresponding (2,1) cationic complex (figure 3.10 (a) II). The key fundamentals involve the aliphatic CH ($<3000\text{ cm}^{-1}$), ring CH ($<3200\text{ cm}^{-1}$) and OH ($>3200\text{ cm}^{-1}$) stretching modes. The (2,1) and (3,2) clusters display significant redshifts and increasing intensities in the OH stretching region (red) upon complexation with $[\text{BF}_4]^-$. The spectra of the (2,1) and (3,2) complexes also include an extended suite of transitions in the OH stretching region (labelled A_1 , A_2 , and A_{\dagger} in figure 3.10 (a) II and B_1 - B_4 in figure 3.10 (a) III, respectively) that appear below the location of a free OH group (arrow in figure 3.10 (a) I. [95] The red-shifted bands A_1 , A_2 , and A_{\dagger} in the (2,1) spectrum (figure 3.10 (a) II occur at similar positions as those found in the $([\text{HOC}_2\text{MIm}]^+)_2[\text{NTf}_2]^-$ spectrum (A_1 - A_4 in Figure 3.9 (a)). This similarity suggests that bands A_1 and A_2 in the (2,1) complex can be assigned to an arrangement in which both cations bind independently to the anion through the OH groups, while the further red-shifted (but less intense) A_{\dagger} band is due to another isomer with a cooperative $\text{OH}\cdots\text{OH}\cdots\text{BF}_4^-$ H-bonding motif. This scenario is supported by harmonic frequency calculations for the $([\text{HOC}_3\text{Py}]^+)_2[\text{BF}_4]^-$ cluster. The spectrum of the quinary (3,2) complex displays vibrational bands B_3 and B_4 (figure 3.10 (a) III) which are much more red-shifted than the analogous feature A_{\dagger} in the (2,1) spectrum. This additional red-shift is important because it signals a cooperative interaction among

all three $[\text{HOC}_3\text{Py}]^+$ cations in the sense that the spectral signature of the motif in play is not established upon addition of the second cation.



(a) Photodissociation spectra of N₂-tagged I $[\text{HOC}_3\text{Py}]^+$, II $([\text{HOC}_3\text{Py}]^+)_2[\text{BF}_4]^-$, III $([\text{HOC}_3\text{Py}]^+)_3([\text{BF}_4]^-)_2$, and IV calculated harmonic spectra for $([\text{HOC}_3\text{Py}]^+)_3([\text{BF}_4]^-)_2$. The OH stretches are coloured red. The labels A₁, A₂, and A₊ denote the H-bonded OH features in the cationic (2,1) cluster and B₁–B₄ in the (3,2) cluster, respectively. Inverted traces in (d) display the calculated spectra (scaled 0.97) for isomer III (purple) and IV (pink; see caption of b) for details). The OH stretch of pure ethanol is indicated by an arrow at the right of the upper trace as a reference. [39]

(b) The lowest-energy $([\text{HOC}_3\text{Py}]^+)_3([\text{BF}_4]^-)_2$ complexes calculated at the B3LYP-D3/6-31+G* level of theory. Only the structures III and IV representing the binding motifs of isomers with triple contact between the cations show red-shifted frequencies at 3260 cm⁻¹. The aliphatic and aromatic H atoms of $[\text{HOC}_3\text{Py}]^+$ are omitted for clarity.

Figure 3.10.: Structure elucidation of cold (35 K) 3c, 2a gas-phase cluster by means of CIVP spectroscopy experiment combined with DFT calculations.

Although we could not obtain isomer-selective spectra for the (3,2) complexes because of their lower yield in the ion source, comparison with calculated vibrational band patterns provides a compelling structural assignment to $([\text{HOC}_3\text{Py}]^+)_3([\text{BF}_4]^-)_2$ complexes wherein cooperative hydrogen bonding is maximized in a homodromic $\text{OH} \cdots \text{OH} \cdots \text{OH} \cdots \text{BF}_4^-$ binding motif. Specifically, we calculated twelve (3,2) low energy structures to identify the range of H-bonded arrangements between cations and anions (c-a) and between cations themselves (c-c). The energetically most favourable (3,2) complexes are shown in figure 3.10 (b). The given clusters I: c-c-a-c, a; II: c-c-a, c-a; III: c-c-c-a, a and IV: c-c-c-a, a only differ in energy by less than 15 kJmol⁻¹,

whereas all the other calculated (3,2) isomers are energetically strongly disfavoured by more than 40 kJmol⁻¹ relative to the most stable structure (I) recovered in the search. From the calculated twelve complexes, only those showing the OH...OH...OH...BF₄⁻ binding motifs (III and IV in figure 3.10 (b)) yield the strongly red-shifted frequencies near 3260 cm⁻¹ (purple and pink inverted traces in figure 3.10 (a) IV that are observed in the measured spectra. The cooperative effect of these long chains with homodromic H-bonding appears to maximize the OH bond to the anion as well as the strengths of the linkages down the chain. The calculated (3,2) complexes III and IV, which both exhibit the OH...OH...OH...BF₄⁻ binding motif, differ in the details of their H-bonding to the anion. In complex IV, for example, the OH...BF₄⁻ interaction is weakened due to the stronger interaction of the anion with the proximal pyridinium ring. As a result, less charge can be donated from the anion into the OH antibonding orbital, leading to slightly higher frequencies (IV: 3500 cm⁻¹ vs. III: 3470 cm⁻¹). The other energetically disfavoured complexes cannot account for the large redshifts in the OH stretching bands observed experimentally. Thus, the measured spectra allow assignments to the calculated complex III with frequencies labelled B₄, B₃, and B₂ and complex IV with frequencies labelled B₄, B₃, and B₁, respectively.

3.3.4. (c-c) tetramers

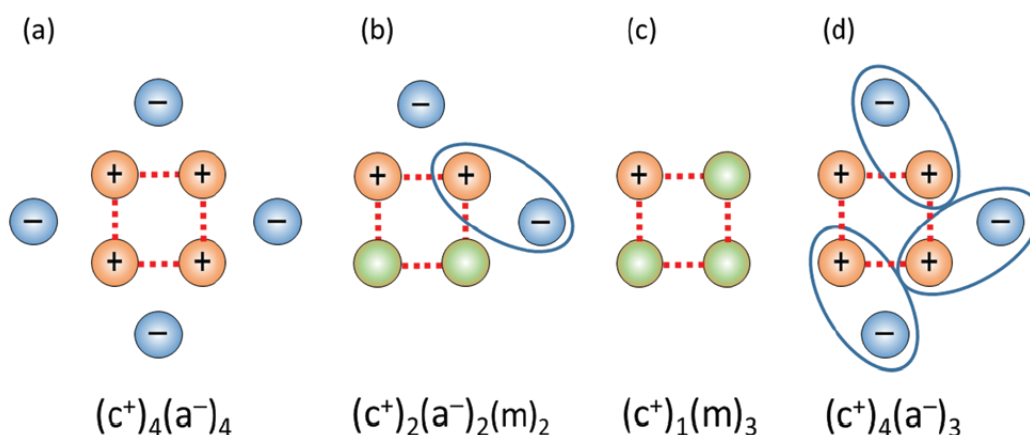
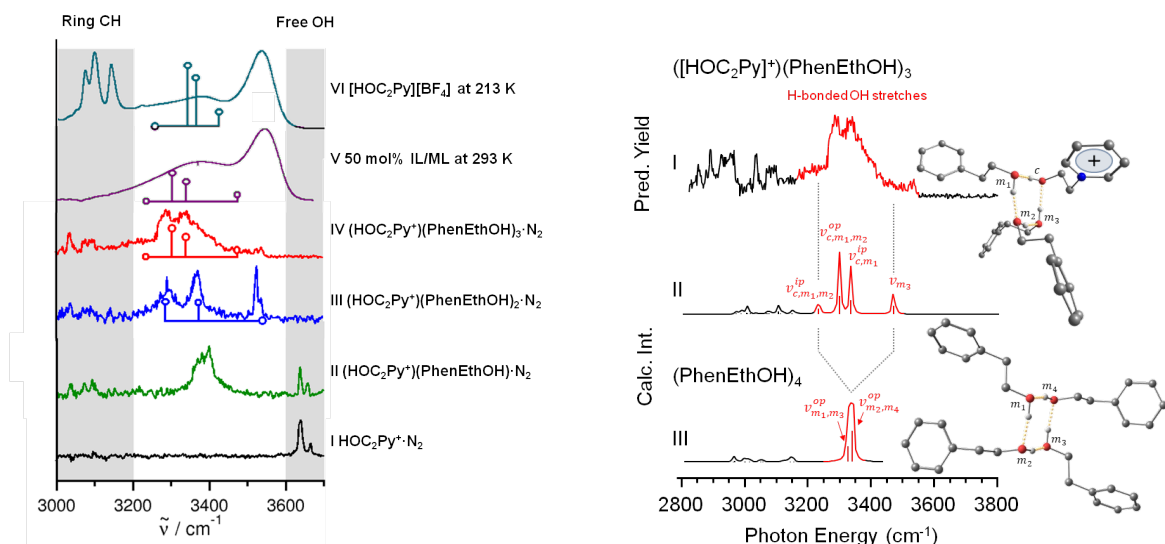


Figure 3.11.: Illustrations explaining the concept of this study. The identification of the structural motifs can be achieved by liquid and gas phase IR spectroscopies. (a) Cyclic tetramers (c⁺)₄(a⁻)₄, fully compensated by counter anions in the neutral bulk system. (b) Neutral cyclic tetramers (c⁺)₂(a⁻)₂(m)₂ in the bulk phase, wherein ion-pairs (c⁺)(a⁻) (circled in (b)) are replaced by molecules (m). (c) Positively charged cyclic tetramers (c⁺)(m)₃ in the gas phase. (d) Positively charged cyclic tetramers (c⁺)₄(a⁻)₃ in the gas phase, with stronger Coulomb repulsion by removing one counteranion.

The structural investigations of (c-c) Tetramers with the help of CIVP spectroscopy and the followed comparison to the corresponding structures in the bulk IL turns out to be more challenging. The challenge is that the most stable form of the cationic tetramer,

according to DFT calculations, is a ring of four OH groups (see Fig. 3.11 (a)) where the cooperativity between the OH groups is maximized. If we now convert this structure into a structure that we can study in a CIVP spectroscopy experiment a disadvantage of this technique comes in play, because we have to remove one counteranion to obtain a charged cluster, but that means that two cations are directly adjacent, which is energetically disfavoured with respect to the COULOMB repulsion.

For **Paper VII** we therefore developed a new strategy for the structural investigations of cyclic, tetrameric, H-bonded structural features by means of CIVP spectroscopy to compare them to the neutral cyclic (c-c) tetramers of the bulk IL (see Fig. 3.11). The spectral evolution of the cold (~ 35 K) $([\text{HOC}_2\text{Py}]^+)(\text{PhenEthOH})_n$ complexes ($n = 1-3$) are compared with that of the isolated $[\text{HOC}_2\text{Py}]^+$ cation in Figure 3.12 (a). The doublet structure of the free OH peak is due to the perturbation by the N_2 adduct. The important result is that the free OH peaks in the bare cation and binary complex (Fig. 3.12 (a) I and II) are clearly absent for the $n = 2$ and 3 clusters (Fig. 3.12 (a) III and IV), consistent with the formation of cyclic H-bond arrangements. Moreover, the band envelopes in the $n = 2$ and 3 spectra fall just on the low energy side of the red-shifted transitions observed in both the bulk IL at 213 K (Fig. 3.12 (a) V) and in the $[\text{HOC}_2\text{Py}][\text{BF}_4]/\text{PhenEthOH}$ mixture at 293 K (Fig. 3.12 (a) VI). The important advantage of comparisons with cluster results is that the isolated, cold systems can be accurately treated with electronic structure methods. This allows us to extract detailed structural information about how the local interactions are reflected in the spectra. These structures indeed correspond to homodromic H-bonded cyclic arrangements, which are analogous to those adopted by neutral cluster systems like methanol and water. [96, 97] Such cycles are known to exhibit increasingly red-shifted OH stretching fundamentals with increasing size. The character of the binary $^+\text{OH}\cdots\text{OH}$ interaction has a profound impact on the spectrum of cyclic H-bonded networks that contain a single embedded cation, as the cation is a much better donor than it is an acceptor. This manifests as a splitting in the bands. Such an effect is illustrated by comparing the $([\text{HOC}_2\text{Py}]^+)(\text{PhenEthOH})_3$ system with the symmetric (neutral) $(\text{PhenEthOH})_4$ tetramer in figure 3.12 (b). The single OH feature around 3340 cm^{-1} that is calculated for the $(\text{PhenEthOH})_4$ tetramer (Fig. 3.12 (b) III), splits into four distinct bands spanning a wide range between $3231-3470\text{ cm}^{-1}$ (Fig. 3.12 (b) II). The lower energy bands correspond to displacement of the OH group on the cation, whereas the highest frequency transition belongs to the OH of the neutral molecule in the weak $\text{OH}\cdots\text{OH}^+$ linkage (labeled ν_{m3} in Fig. 3.12 (b) II), discussed for the binary complex. Note that the dominant bands in the experimental spectrum for this cluster covers the same frequency range as the broad red-shifted OH vibrational band of the 50 mol% IL/ML mixture (Fig. 3.12 (a) V), but appears $\sim 90\text{ cm}^{-1}$ below that observed for the pure IL at 213 K (Fig. 3.12 (a) I), which is also consistent with the elimination of the repulsive interactions in the gas phase species. Taken altogether, these observations provide compelling evidence for the formation of cyclic H-bonded domains in the bulk IL at low temperature (see Fig. 3.11), which would have been more challenging to accomplish by isolated, purely ionic complexes.



(a) Vibrational predissociation spectra of N₂-tagged cation [HOC₂Py]⁺ I along with those of the ([HOC₂Py]⁺)(PhenEthOH)_n clusters with $n = 1$ II, $n = 2$ III and $n = 3$ IV at ~ 35 K. The bulk liquid IR spectra of the 50 mol % mixture of [HOC₂Py][BF₄]/PhenEthOH at 293 K V and the pure ionic liquid [HOC₂Py][BF₄] at 213 K VI. For comparison, the calculated frequencies of the monomer, dimer and the corresponding cyclic trimer and tetramers are provided whereby the lowest intensities are set to zero.

(b) Vibrational predissociation spectra of N₂-tagged I ([HOC₂Py]⁺)(PhenEthOH)₃, compared to II its calculated spectrum. Calculated spectrum of III the cyclic molecular mimic tetramer (PhenEthOH)₄ is also presented for comparison. The superscripts 'ip' and 'op' in the band labels stands for 'in-plane' and 'out-of-plane' stretches, respectively. The structures are provided on the right of the figure and H-atoms connected to carbon atoms are omitted for clarity.

Figure 3.12.: Structure elucidation of cold (35 K) 1c, 3m gas-phase cluster by means of CIVP spectroscopy experiment combined with DFT calculations and comparison to the bulk liquid.

3.4. (c-c) cluster investigations by theoretical methods

3.4.1. Density functional theory (DFT) calculations

Density Functional Theory (DFT) is a method for determining the quantum mechanical ground state of a multi-electron system, which is based on the location-dependent electron density. DFT is used to calculate fundamental properties of molecules and solids, such as bond lengths and energies. [98–100] The great importance of this theory lies in the fact that it is not necessary to solve the complete SCHRÖDINGER equation for the multi-electron system, whereby the amount of computing power drops sharply or calculations of systems with well over ten electrons are even possible.

The basis of density functional theory is the HOHENBERG-KOHN theorem: [101] The ground state of a system of N electrons (as a wave function dependent on $3N$ coordinates) is determined by the position-dependent electron density $\rho(\vec{r})$. In the density functional theory, the electron density in the ground state is now determined, from which in prin-

ciple all further properties of the ground state can be determined. The main challenge is to find the right functional, where some of the functionals can be easily derived from the corresponding classical expressions, while other functionals need approximations. This is especially necessary for the kinetic energy and the non-classical (i.e., exchange) part of the electron-electron interaction. The first suitable approximations for the kinetic energy were the KOHN-SHAM functions. With the KOHN-SHAM formalism, the problem of the multi-electron system was not really solved, but rather shifted to the exchange correlation term. In general, there are three common approached solutions to this problem: the local density approximation, LDA; the generalized gradient approximation, GGA and the Hybrid-Methods. For the latter, only part of the exchange correlation potential is calculated according to the density functional theory (e.g., with GGA), a part is calculated as the exchange energy of the KOHN-SHAM functions as in the HARTREE-FOCK method. These methods are more accurate than pure GGA calculations, especially for molecules, but the cost of the calculations is much higher than for GGA calculations. The most common hybrid method is known as B3LYP.

DFT methods can be used for the structural analysis of polyatomic systems, just like traditional quantum chemical ab initio methods. If atomic positions, nuclear charges and number of electrons are known, one can use KOHN-SHAM formalism to calculate the total energy of the system for a given core geometry. In this way, potential energy surfaces can be imaged and characterised by so-called geometry optimization of minimum or transition state geometries.

Furthermore, a number of spectroscopic properties of molecules can be calculated or even whole spectra can be predicted. Careful experimental data are used, among other things, to calibrate DFT methods. The density functional theory can thus be used for the verification or interpretation of existing data or even for prediction. However, the latter often requires the use of empirical correction schemes to achieve reliable results. [102]

Table 3.5.: Advantages and disadvantages of DFT calculations

Advantage	Disadvantage
provide detailed structural information	no mediation effects
prediction of spectroscopic observables	no temperature effects
investigation of experimentally not accessible compounds or structures	Results depending on used methods and basissets

3.4.2. Natural bond orbital (NBO) analysis

NBO analysis is based on a method for optimally transforming a given wave function into localised form, corresponding to the one-center ("lone pairs") and two-center ("bonds") elements of the LEWIS structure picture. [103] In NBO analysis, the input atomic orbital basis set is transformed via natural atomic orbitals (NAOs) and natural hybrid orbitals (NHOs) into natural bond orbitals (NBOs). [104] The NBOs obtained in this fashion correspond to the widely used LEWIS picture, in which two-center bonds

and lone pairs are localised.

Each of the NBOs (Ω_i) is expressed as linear combination of constituent NHOs (h_i), which in turn are composed of NAOs (Θ_k). [105] For example, a two center σ_{AB} bond NBO between atoms A and B can be written as

$$\sigma_{AB} = c_A h_A + c_B h_B \quad (3.7)$$

where h_A and h_B are the respective hybrids on the atoms, and c_A and c_B are the natural polarization coefficients whose squares give the percentage contributions of h_A and h_B to the NBO. The occupied σ_{AB} bond NBOs are useful to describe covalent effects. [103, 104] Furthermore, the generation of binding orbitals leads to generation of antibonding orbitals σ_{AB}^* .

$$\sigma_{AB}^* = c_A h_A - c_B h_B \quad (3.8)$$

These unoccupied orbitals are useful for the description of noncovalent effects, such as hyperconjugation or hydrogen bonding. [103]

In the LEWIS picture a hydrogen bond can generally be written as $L: \cdots H-L'$, driven by intermolecular resonance. Using NBO, the hydrogen-bonded complex can be characterised as donor-acceptor complex of „ $n_L - \sigma_{HL}^*$ “. The binary association is driven by partial intermolecular *charge-transfer* (q_{CT}) delocalisation from the lone pair (n_O) of the :L donor in the hybrid antibond (σ_{HL}^*) of the H-L' acceptor. [106] The partial occupation of the antibond (σ_{HL}^*) orbitals leads to a deviance from the LEWIS picture of localized covalent bonds. These deviances need small noncovalent corrections which can be provided in terms of a second-order perturbation. The mixing of donors and acceptors leads to an overall energy lowering, the second-order stabilization energy $\Delta E(2)_{n \rightarrow \sigma^*}$. [103, 104, 107, 108] One benefit of NBO analysis is that the descriptors q_{CT} and $\Delta E(2)_{n \rightarrow \sigma^*}$ are comparable to spectroscopic observables, like frequency shifts ($\Delta\tilde{\nu}$) in IR spectroscopy or chemical shifts (δ^1H) in NMR spectroscopy, providing a descriptive quantum mechanical explanation for a spectroscopic observation.

Table 3.6.: Advantages and disadvantages of NBO analysis

Advantage	Disadvantage
descriptors comparable to spectroscopic observables	H-bond energies are often overestimated
consistent with LEWIS picture of chemical bonding	

3.4.3. Controlling the kinetic and thermodynamic stability of (c-c) clusters

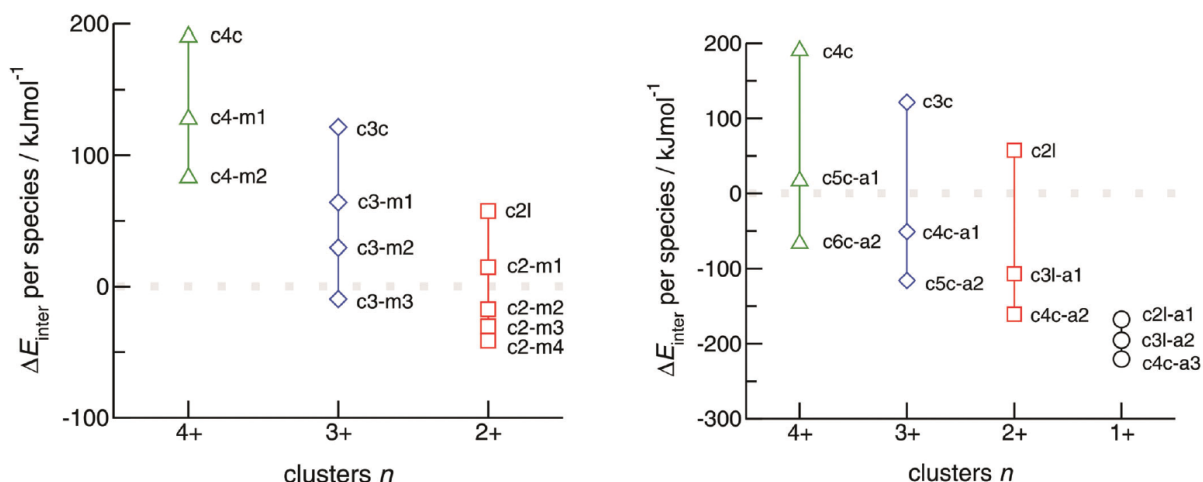
As model cation for our investigations in **Paper VIII** we have chosen (2-hydroxyethyl)-trimethylammonium $[\text{HOC}_2\text{TMA}]^+$. The related neutral species to this cation is obtained by simply replacing the nitrogen in the ammonium cation by a carbon atom, resulting in the alcohol 3-3-dimethyl-1-butanol DM1B. For the cationic clusters $[\text{HOC}_2\text{TMA}]_x^{+x}$ (cx) and the molecular clusters DM1B_y (my), linear and cyclic species up to hexamers were optimized. In a second step we added molecules or anions to the pure cationic clusters for stabilizing the overall cationic configurations. To give an example: If the cyclic cationic cluster c4c (4+) is meta-stable, we add successively molecules or counterions to strengthen kinetic stability or to achieve even thermodynamic stability. As counteranion the bis(trifluoromethylsulfonyl)imide $[\text{NTf}_2]^-$ was chosen. One part of our strategy, quite similar to the strategy of **Paper VII** is to increase the stability of the (c-c) clusters by adding molecules and the other part of our strategy is to increase the stability by addition of counterions. We optimized linear and cyclic cationic clusters of $[\text{HOC}_2\text{TMA}]^+$ from trimeric up to hexameric ($n = 3-6$) configurations. A linear cationic trimer is abbreviated as c3l, a cyclic trimer as c3c. The pure cationic clusters are kinetically stable for the cyclic trimers (c3c) and the cyclic tetramers (c4c), wherein cooperative H-bonding is maximized. Linear trimer (c3l) and tetramer (c4l) and larger cyclic clusters, such as pentamers (c5c) or hexamers (c6c), are no longer meta-stable and dissociate during the geometry optimization procedure.

What is the cause of the attractive forces between the like-charged ions? The B3LYP-D3/6-31+G* calculations suggest that the (c-c) $\text{OH} \cdots \text{OH}$ interaction is possible due to cooperative effects. [78, 80] Charge from the oxygen lone pair orbital of a first cation is donated into the OH anti-bond orbital of a second cation. The larger negative charge at the OH oxygen at the second cation can now be transferred into the OH anti-bond of another cation, further enhancing hydrogen bonding. This process leads to even stronger cooperativity in the trimers and tetramers. This way the short-range donor-acceptor covalency forces can overcome the strong long-range electrostatic repulsive forces as expected for ions of like charge. From this perspectives there are two ways to increase the stability of the (c-c) clusters, either by increasing the cooperativity without increasing the COULOMB repulsion by adding neutrals instead of cations or by compensating the repulsive forces by adding counter ions.

For the cationic clusters the energies per species are positive in the dimer (c2l), the cyclic trimer (c3c) and the cyclic tetramer (c4c). As shown by the calculated frequencies which are positive throughout, these positively charged clusters present local minimum structures on the potential energy surface. They can be „kinetically trapped“, but are far away from thermodynamic stability. To achieve better kinetic stability or even thermodynamic stability for the positively charged clusters, we added neutral molecules. As shown in figure 3.13 (a), the dimer c2l (2+) can be stabilised by adding one DM1B molecule. However, thermodynamic stability can be only achieved if a second alcohol molecule is added, resulting in the c2-m2 (2+) cyclic tetramer. By adding a third and fourth molecule we can further stabilize the 2+-charged clusters within cyclic

pentamers c2-m3 and cyclic hexamers c2-m4. With this procedure we change smoothly from the ionic to molecular systems by distributing the same positive charge over larger clusters. Two cations become thermodynamically stable if they are neighboured by only two neutral species and thus observable. Of course more molecules are needed to overcome the stronger repulsive COULOMB forces in the 3+-charged and 4+-charged configurations. Three DM1B molecules are needed within a cyclic hexamer structure c3-m3 to achieve thermodynamic stability. Cooperative hydrogen bonds within this cyclic motif of the three-fold positively charged cluster are so strong that they overcome the repulsive forces between the three cations. Thermodynamic stability can not be achieved for the 4-fold positively charged clusters. By adding one and two alcohol molecules „kinetic stability“ can be further improved within the cyclic pentamer c4-m1 and cyclic hexamer c4-m2 without approaching thermodynamic stability. In principle we could add more than two molecules to the c4c cluster. But then the ring structures exceed the size of the enthalpically and entropically favourable hexamer as known from studies of alcohol clusters. Cyclic heptamers and octamers show no further enhanced cooperativity, which is required for increasing stability. It is interesting to note that cationic clusters with charge 3+ become thermodynamically stable by adding the same number of alcohol molecules. They are in particular stable if each cation is neighboured by molecules.

The situation becomes different if we add $[\text{NTf}_2]^-$ anions to the cationic clusters but remaining the 4+, 3+ and 2+ charged species. The single positively charged clusters c2l-a1, c3l-a2 and c4c-a3 are thermodynamically stable throughout (see Fig. 3.13 (b)). Also, for the 2+-charged clusters only one additional anion is needed for thermodynamic stability. This is not surprising because each „ion pair“ in the c3l-a1 and c4c-a2 clusters contributes between 300 and 400 kJmol^{-1} of binding energy, which is well known from numerous calculations on smaller IL aggregates. [5, 6, 20, 22, 23, 109] Instead, it is remarkable that the H-bond ring in c4c-a2 is preserved during the optimization procedure and not tackled by the two weakly coordinating anions. That is even true for the 3+-charged clusters c4c-a1 and c5c-a2, wherein the cyclic cationic tetramer (c4c) and pentamer (c5c) survive. This behaviour also holds for the 4+-charged clusters. Here, two counterions are needed to achieve thermodynamic stability. It is notable that the most favourable cyclic pentamer (c5c) and hexamer (c6c) keep their motif if one and two anions are coordinated. The detection and control of clusters of like-charged ions may be regarded as support for the „anti-electrostatic hydrogen bonds“ (AEHB) as reported recently by Weinhold and Klein. [108, 110, 111] Although Frenking and Head-Gordon could show that the local minimum structures for anionic dimers can be analysed also by energy decomposition analysis (EDA) methods, AEHBs are supported by spectroscopic observables, such as vibrational frequencies, ν_{OH} , and NMR chemical shifts, $\delta^1\text{H}$. [107, 112]



(a) B3LYP-D3/6-31+G* calculated binding energies per species for the cationic clusters $c2l$, $c3c$ and $c4c$. To each of the 4+, 3+ and 2+ charged clusters 3-3-dimethyl-1-butanol molecules are added step by step, leading to lower energies of the overall clusters. In principle the cationic clusters are meta-stable and exhibit positive energies. However, 3+ and 2+ charged clusters become also thermodynamically stable, if three molecules within a cyclic hexamer ($c3-m3$) or two molecules within a cyclic tetramer ($c2-m2$) are added. Cyclic clusters larger than hexamers were not taken into account because it is known from molecular clusters that cyclic heptamers and octamers do not show further increase of cooperativity but exhibit entropic penalties. [74–78]

(b) B3LYP-D3/6-31+G* calculated binding energies per species for the cationic clusters $c4c$, $c3c$ and $c2l$. To each of the 4+, 3+, 2+ and 1+ charged clusters counterions $[\text{NTf}_2]^-$ are added step by step, leading to lower energies of the overall clusters. Except for the 4+ clusters it is shown that all positively charged clusters become thermodynamically stable by only adding one negative charge, resulting in $c4c-a1$, $c3l-a1$ and $c2l-a1$ clusters, respectively. In principle cationic clusters up to 4+ should be observable in the experiment.

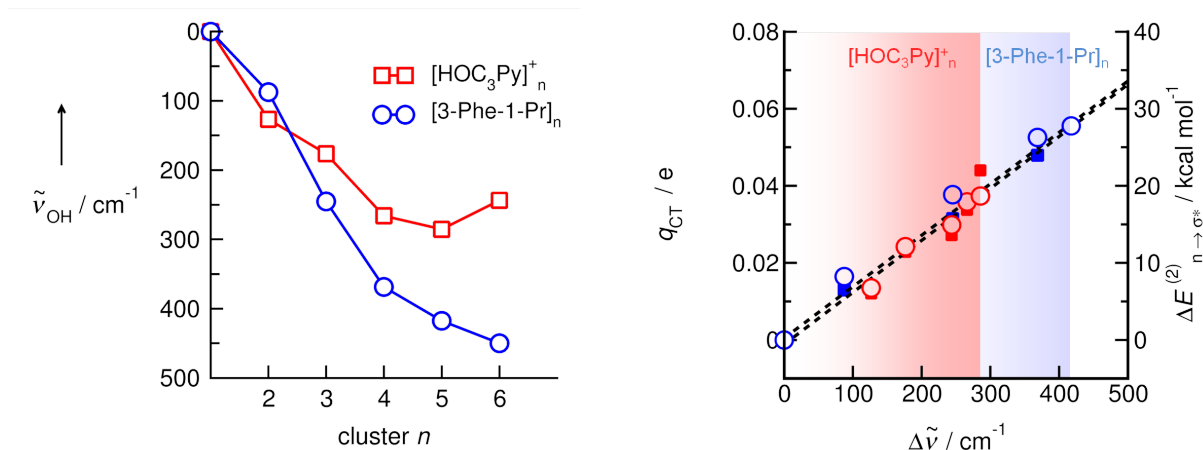
Figure 3.13.: Stabilising effect of the addition of molecular alcohols or anions on (c-c) clusters

3.4.4. Cooperative hydrogen bonding in bare (c-c) clusters

It was the purpose of **Paper IX** to study kinetically stable cationic clusters, wherein, in the absence of any mediating „solvent effects“ by molecules or counterions, the repulsive COULOMB forces can be compensated merely by cooperative hydrogen bonding between the cations. We particularly want to show that like-charge attraction also exists for cationic clusters that are much larger than the reported dimers with net charge $Q = \pm 2e$. [110, 111, 113, 114] Braga and coworkers already questioned anion-anion interaction from molecular electrostatic potential considerations and concluded that it is instead a „tugboat interaction“, controlling anion aggregation and minimizing anion-anion repulsions. [50] They claimed that the anionic dimer would fall apart if the countercations are removed. Here, we show that larger clusters of monovalent cations up to net charges $Q = + 6e$ can be kinetically trapped by cooperative hydrogen bonding. No mediating molecules, counterions or screening effects are needed to overcome the repulsive COU-

LOMB forces. The structural, spectroscopic and electronic signatures of the cationic and related molecular clusters could be related to NBO parameters, supporting the existence of „anti-electrostatic“ hydrogen bonds (AEHB) as recently suggested by Weinhold. [110, 111, 113–115] We also show that dispersion forces enhance the cationic cluster formation and compensate the long-range electrostatic repulsion. Overall, dispersion interactions shift the kinetic stability from a cyclic pentamer to a cyclic hexamer. For that purpose we have chosen the hydroxy-functionalized cation N-(3-hydroxypropyl)pyridinium [HOC_3Py^+] and its molecular mimic 3-phenyl-1-propanol [3-Phe-1-Pr] as model systems. We calculated linear clusters up to tetramers ($n = 4$) and cyclic clusters up to hexamers ($n = 6$). The hydroxy groups on the cations form hydrogen bonds and promote the aggregation into highly charged cationic clusters. We employed B3LYP/6-31+G* and B3LYP-D3/6-31+G* calculations performed with the Gaussian 09 program and analysed with the NBO 6.0 program. [116–121] For calculating all cationic and molecular clusters at the same level of theory, we have used the well balanced, but small 6-31+G* basis set. It includes polarization as well as diffuse functions, and has been shown to be suitable for calculating hydrogen-bonded clusters of like-charged ions. [24–26] [**Paper I** and **Paper VIII**]

The B3LYP-D3/6-31+G* calculations suggest that the cation-cation interaction via the $\text{OH} \cdots \text{OH}$ hydrogen bond is possible due to cooperative effects as in **Paper VIII**. Electron density from the oxygen lone pair orbital of a first cation is donated into the OH antibonding orbital of a second cation. The resulting larger negative charge at the OH oxygen at the second cation can now be transferred into the OH antibonding orbital of another cation, further enhancing hydrogen bonding. This process leads to even stronger cooperativity in the cyclic structures, such as tetramers, pentamers and hexamers. This way, the short-range donor-acceptor covalency forces can overcome the strong long-range electrostatic repulsive forces as expected for ions of like charge. These features can be rationalized in the framework of the natural bond orbital (NBO) analysis. [117, 118] NBO analysis shows typical strong $n_{\text{O}} \rightarrow \sigma_{\text{OH}}^*$ donor-acceptor interaction, corresponding to second order stabilization energies $\Delta E(2)_{n \rightarrow \sigma^*}$ and estimated total charge transfers of q_{CT} for the enhanced $\text{OH} \cdots \text{OH}$ hydrogen bonds, respectively. These typical NBO descriptors are plotted versus $\Delta\nu_{\text{OH}}$ redshifts (see figure 3.14 b)). The spectroscopic features of the cationic clusters, wherein the strong repulsive COULOMB interaction is attenuated by hydrogen bonding, can be almost linearly related to the NBO descriptors. Obviously, both properties characterise hydrogen bonding and cooperativity in a similar way. IR redshifts and downfield proton chemical shifts go along with increasing stabilization energies, $\Delta E(2)_{n \rightarrow \sigma^*}$, and enhanced charge transfer, q_{CT} . That the strongest intermolecular stabilization energies are found for the cyclic structures is well correlated to the cooperative binding energies and frequencies. These „closed-CT“ networks have highest stability, resulting in strongest interaction and largest vibrational red-shifts.



(a) Calculated O-H vibrational red-shifts, $\Delta\nu_{\text{OH}}$, for the molecular (circles) and the cationic clusters (squares) relative to the monomer values of both species. Although less pronounced, the cationic clusters show similar redshifts as the molecular clusters with increasing cluster size. Cooperative hydrogen bonding is in particular strong in the cyclic cationic tetramer.

(b) NBO-calculated second-order stabilization energies $\Delta E^{(2)}_{n \rightarrow \sigma^*}$ (open circles) and estimated total charge transfers q_{CT} (closed squares) for cationic (red) and molecular (blue) clusters $n = 2-6$ plotted versus calculated redshifts of the average OH frequency, $\Delta\tilde{\nu}_{\text{OH}}$, of the monomeric cation and molecule. The linear dependence indicates the strong relation between NBO stabilization energies and charge transfers with spectroscopic properties such as IR frequencies. The largest redshifts for the cationic and molecular clusters are indicated by the red and blue areas.

Figure 3.14.: Cooperativity of different sized molecular and cationic clusters visualized by the descriptors $\Delta\tilde{\nu}_{\text{OH}}$, $\Delta E^{(2)}_{n \rightarrow \sigma^*}$ and q_{CT} .

3.4.5. Hydrogen bonding overcomes coulomb repulsion

In principle, the COULOMB repulsion can be further attenuated by elongation of the hydroxyalkyl chain, thus increasing the distance between the positively charged centres of the cations as mentioned in **Paper VI**. This way, robust kinetically stable complexes should exist without altering the dielectric environment. An ultimate goal would be the prediction of a cationic dimer exhibiting negative binding energies that should be observable in sophisticated gas phase experiments as used in **Paper V-VII**.

It was the aim of **Paper X** to show that the interplay between attractive short-range hydrogen bonds and repulsive long-range COULOMB forces provides kinetic well-depths and barrier widths for simple cationic dimers with net charge $Q = +2e$. We demonstrate that hydrogen-bonded dimers of hydroxy-functionalized 1-(n -hydroxyalkyl)pyridinium cations exhibit substantial kinetic stability without being embedded in a dielectric medium by adding molecules or counterions as discussed in **Paper VIII**. We show that with increasing length of the hydroxyalkyl chain even absolute thermodynamic stability is achieved. In these cationic species, hydrogen bonding does not only attenuate, but also overcomes the repulsive COULOMB forces. Then, the hydrogen bond strength and geometry in the cationic dimer approaches those of familiar molecular species, such as

water and alcohols. Thus, there is a good chance for finding these like-charged dimers in gas phase experiments at low temperatures.

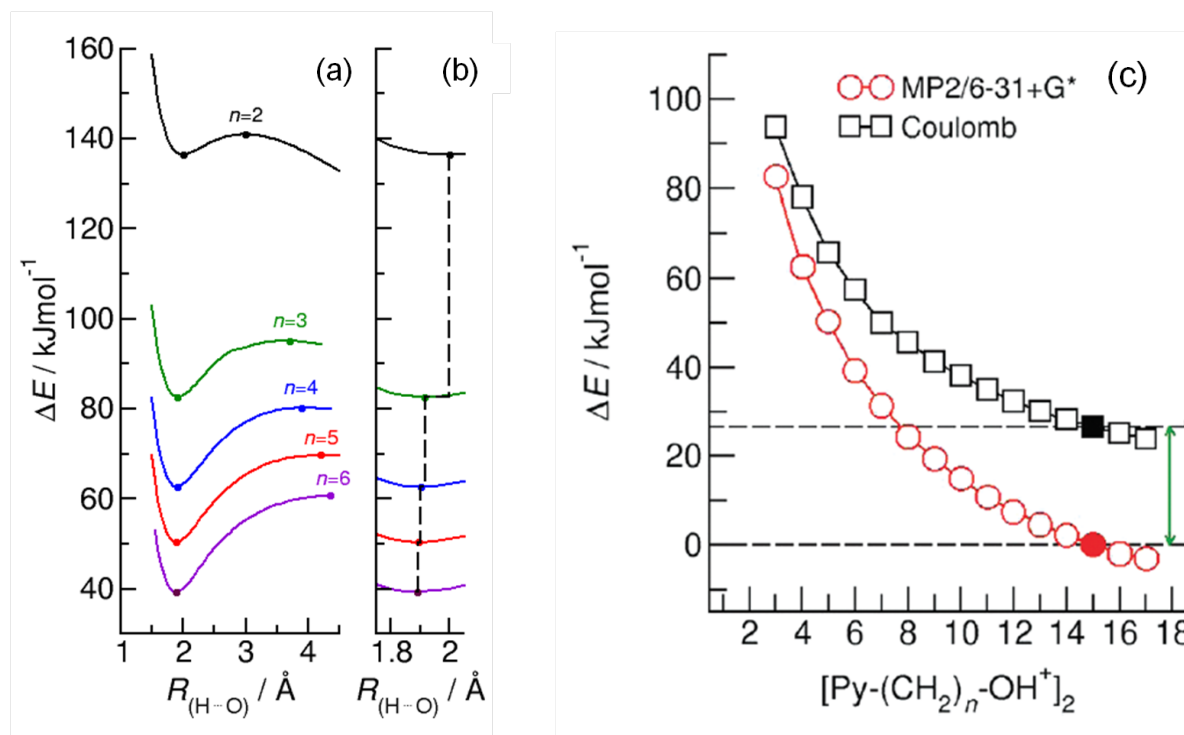
We calculated the potential energy curves for dimers of the hydroxy-functionalized cations 1-(n -hydroxyalkyl)-pyridinium $[\text{Py}-(\text{CH}_2)_n-\text{OH}^+]_2$ with $n = 2-6$ at the unrestricted second-order MØLLER–PLESSET perturbation theory (UMP2) by using the well-balanced but small 6-31+G* basis set as implemented in the Gaussian 09 program . [116] The methylene (CH_2) groups in the alkyl chains of the cations are all kept in trans position to the hydroxy functional group -OH. Analytical positive frequencies were obtained for all species $n = 2-6$ to verify the local stability of each optimized structure.

For the cationic dimers $[\text{Py}-(\text{CH}_2)_n-\text{OH}^+]_2$ with $n = 2-6$ we calculated relaxed potential energy curves by varying the $\text{H} \cdots \text{O}$ intermolecular distance and optimizing all other geometrical variables at each step of the scan. The resulting potential energy curves for each dimers $[\text{Py}-(\text{CH}_2)_n-\text{OH}^+]_2$ with $n = 2-6$ are shown in figure 3.15 (a). For each curve, we show the net energy release ΔE and the activation barrier height ΔE^* for the dissociation potentials of the cationic dimers. Additionally, we indicated the optimized equilibrium H-bond distances $R_{(\text{H} \cdots \text{O})}$. As shown in Figure 3.15 (b), robust kinetic stabilities with clear dissociation barriers are achieved for the UMP2 treatment.

For dimers with larger hydroxyalkyl tethers $n = 3-6$, the ΔE values drop from 136.4 kJmol^{-1} for $n = 2$ down to 39.3 kJmol^{-1} for $n = 6$ as shown in Fig. 3.15 (c). Thus, the equilibrium energy for the cationic dimer $[\text{Py}-(\text{CH}_2)_n-\text{OH}^+]_2$ is only moderately above that of the isolated cations. The stronger attractive interaction with increasing tether length is also reflected in shortened hydrogen bond distances $R_{(\text{H} \cdots \text{O})}$, changing from 1.9994 Å for $n = 2$ down to 1.891 Å for $n = 6$, as indicated by the dots at the potential minima in Fig. 3.15 (b). Similarly, the deep potential wells ΔE^* increase from 4.5 to 20 kJmol^{-1} , exceeding significantly the values reported for other cationic and anionic dimers. [110, 111, 114, 115]

The cationic dimers $[\text{Py}-(\text{CH}_2)_n-\text{OH}^+]_2$ including longer hydroxyalkyl chain $n = 7-16$ were fully optimized at the MP2/6-31+G* level of theory. Unfortunately, frequencies and potential energy curves could not be obtained at this demanding level of theory. For these cationic dimers we calculated the net energy release relative to the dissociated cations, ΔE , the potential energy and the $R_{(\text{H} \cdots \text{O})}$ distances that are shown along with the properties of $[\text{Py}-(\text{CH}_2)_n-\text{OH}^+]_2$ with $n = 2-6$ in Figure 3.15. In Figure 3.15 (c) we show the calculated energies ΔE for all dimers $[\text{Py}-(\text{CH}_2)_n-\text{OH}^+]_2$ which decrease from 136.4 kJmol^{-1} for $n = 2$ via 39.3 kJmol^{-1} for $n = 6$ down to -3.6 kJmol^{-1} for $n = 17$, respectively. With increasing hydroxyalkyl chain length, a robust kinetic stability switches to weak thermodynamic stability. For $[\text{Py}-(\text{CH}_2)_n-\text{OH}^+]_2$ with $n = 16, 17$ the binding energies are slightly negative. The hydrogen bond overcomes the repulsive COULOMB forces that are attenuated by the elongated alkyl chains. For $n = 15$ the energy release compared to the isolated ions is zero. In this case, the repulsive COULOMB forces are fully counter-balanced by the attractive $\text{H} \cdots \text{O}$ hydrogen bond and dispersion forces. For dissecting the amount of stabilizing energy of about 26.8 kJ mol^{-1} into hydrogen bonding and dispersion contributions, we performed additional calculations with and without including dispersion forces. Overall, the calculated dispersion energy stabilizes the (c-c) interaction by 6.7 kJ mol^{-1} and the hydrogen bond stabilizes it by 20.1 kJ

mol⁻¹.



(a) The potential energy curves for the cationic dimers $[\text{Py}-(\text{CH}_2)_n-\text{OH}^+]_2$ with $n = 2-6$ were calculated at the UMP2/6-31+G* basis level of theory relaxing the structures for each bond length $R_{(\text{H}\cdots\text{O})}$. The dissociative energy profiles show pronounced binding wells with respect to the dissociated cations and effective equilibrium well depths with respect to the transition state. (b) The bond lengths $R_{(\text{H}\cdots\text{O})}$ at the minima shift to shorter distances due to increasing hydrogen bonding.

(c) The binding energies for all cationic dimers $[\text{Py}-(\text{CH}_2)_n-\text{OH}^+]_2$ with $n = 2-17$ were calculated at the UMP2/6-31+G* basis level of theory (circles). They are compared to the long-range e^2/R behaviour of idealized COULOMB electrostatic repulsion assuming positive charges $q = +0.9e$ on the pyridinium ring (squares).

Figure 3.15.: Kinetic and thermodynamic stability of H-bonded cationic dimers in dependency of chain length.

3.5. Atomic force microscopy study of the IL/solid interfacial structure

3.5.1. Atomic force microscopy (AFM)

Laser beam deflection is the most common detection method used in modern commercial AFMs and was pioneered by Meyer and Amer. [122, 123] The cartoon in figure 3.16 (a) describes its functioning principle. [124] The cantilever deflection is measured by

monitoring the position of a laser beam reflecting from the cantilever and directed to a quadrant photodiode. The photodiode is a semiconductor device that turns the intensity of light falling on it into an electrical voltage signal. The photodiode is usually split into four sections, enabling both vertical and lateral movements of the cantilever to be differentiated. Vertical movement of the cantilever is measured as the difference in voltage between upper and lower quadrants of the photodiode. Similarly, torsional motion of the cantilever is measured as the difference in voltage between the left and right quadrants of the photodiode. Vertical movement of the cantilever originates from the so-called normal forces. The origin of torsional movement of the cantilever arises from frictional forces that originate by the lateral motion of the tip with respect to the sample during the scan. [125]

This technique causes a large amplification of the movement because for a cantilever of $l \sim 200 \mu\text{m}$ at a distance $S \sim 5 \text{ cm}$, this method amplifies the movement of the cantilever by a factor of 375, following equation 3.9.

$$D = \frac{3S}{2l}z \quad (3.9)$$

In general, the beam deflection method is less sensitive than other electronic methods, but the simplicity of the implementation makes it the preferred method to detect the cantilever deflection in air and in liquids.

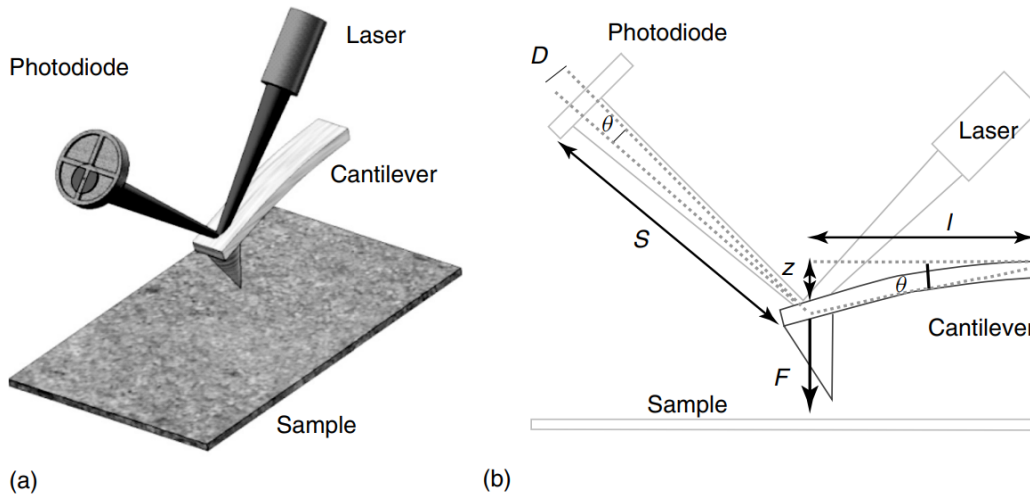


Figure 3.16.: Beam deflection method. (a) Cartoon showing the principle of the beam deflection method. A laser beam is focused on the back side of the cantilever and its reflection is directed to a photodiode that records the vertical and lateral movements of the cantilever. (b) A side view of the setup with the relevant dimensions (D = movement of laser spot at the detector, S = detector-cantilever distance, z = vertical tip movement, l = cantilever length, F = force acting on the tip). [124]

The experimental device that allows the laser beam to propagate without suffering scattering in the liquid surface is known as „liquid cell“. The importance of this device is

to ensure a steady laser spot on the detector. Because in almost any air-liquid interface, small mechanical instabilities give rise to surface waves in the liquid that scatter the light coming from a laser beam, producing a noisy spot that is useless for detecting the cantilever deflection. This problem is solved by creating a well-defined solid-liquid interface with a transparent window. The incoming laser beam is transmitted in the liquid without being affected by any surface wave, resulting in a stable spot suitable for detecting the cantilever deflection.

Table 3.7.: Advantages and disadvantages of AFM

Advantage	Disadvantage
direct measurements of distances down to atomic level	signal-to-noise worsen by surroundings vibrations
simple set up, no requirement for vacuum or inert-gas	small temperature range accessible, often limited to room temperature
viable surface potentials and different surfaces	

3.5.2. Influence of hydrogen bonding on the IL/solid interfacial structure

If the „liquid cell“ is filled with an IL we can observe that during the approach of the tip to the surface the force acting on the tip remains constant at great separations to the surface. This force is usually set to zero and indicates bulk structure. At smaller separations the force on the tip increases abruptly, then the tip jumps inward as it encounters a series of regularly-spaced, repulsive barriers. These periodic force repulsions indicate the bulk structure has transitioned into a more ordered layered structure near the negatively-charged mica surface. When the tip encounters the outermost detectable interfacial layer, it pushes against it, leading to a repulsive force. Once the force is sufficiently high, the tip breaks through the layer and „jumps“ to the next one, whereupon the force increases again and the process repeats. The closer the tip is to the surface, the more structured the interfacial layers and the higher the break through force. The jump distance is the interfacial layer thickness ($\Delta_{sep.}$). In previous studies, $\Delta_{sep.}$ has been shown to be well-approximated by the ion pair diameter, D_m , which is calculated simply from the macroscopic density and the molecular weight, assuming a cubic packing geometry. [126–129]

In **Paper XI** we have used atomic force microscopy measurements to characterise the nanoscale forces at the solid/IL interface. In particular, we have shown that the formation of (c-c) hydrogen bonds can increase the near-surface structuring of ILs and stabilise the formed layers. We investigated the influences of interaction strengths of counterions, polarisability and the chain length of the hydroxyalkyl group on the formation of ion-enriched layers at a mica surface (Fig. 3.17 (a)). Enhanced H-bonding is due to a reduced COULOMB repulsion, which is caused by a larger distance between the OH

group and the positive charge, which means interfacial layers are stabilised. However, a localised positive charge on the cation destabilises the H-bonding between the cations, due to enhanced COULOMB repulsion (comparison of Fig. 3.17 (a) and (c)). By changing the weakly coordinating $[\text{NTf}_2]^-$ anion to the strongly coordinating $[\text{OMs}]^-$ anion, we revealed the effect of the anion on the near-surface structures (comparison of Fig. 3.17 (a) and (d)). The results suggest that strongly coordinating anions form almost entirely anion-cation pairs via (a-c) H-bonds which can be moved easily by the AFM tip, leading to a decrease of the number of interfacial layers. Finally, we point out the stabilising effect of H-bonding between the functionalized cations by comparing the force separation profile of the IL $[\text{HOC}_4\text{Py}][\text{NTf}_2]$, which shows the most structuring and the highest break through forces, with the force separation profile of the unfunctionalized IL $[\text{C}_5\text{Py}][\text{NTf}_2]$, in which the ions are almost identical in size and shape (comparison of Fig. 3.17 (a) and (b)). In conclusion, ionic liquids interfacial nanostructure can be controlled by hydrogen bonding between ions of like-charge, the cation polarizability, the anion interaction strength, and hydroxylalkyl chain length.

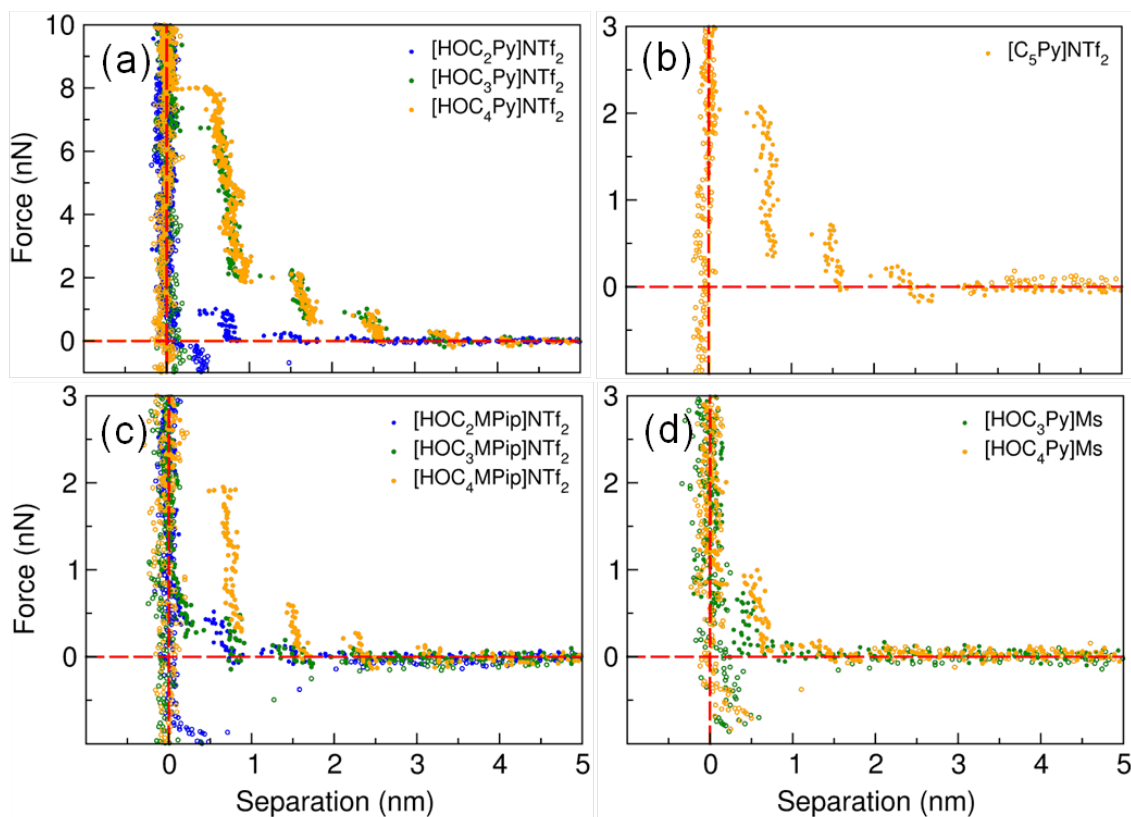


Figure 3.17.: Force separation profiles for the subsets: (a) $[\text{HOC}_n\text{Py}][\text{NTf}_2]$ (b) $[\text{HOC}_n\text{MPip}][\text{NTf}_2]$ (c) $[\text{HOC}_n\text{MPip}][\text{OMs}]$ and (d) $[\text{C}_5\text{Py}][\text{NTf}_2]$. All profiles show the approach (filled circles) of the AFM tip to the mica surface as well as the retraction (open circles).

4. Publications

Nr.	Publication	Contribution
I	A. Strate, T. Niemann, D. Michalik, R. Ludwig, <i>When Like Charged Ions Attract in Ionic Liquids: Controlling the Formation of Cationic Clusters by the Interaction Strength of the Counterions</i> , Angew. Chem. Int. Ed., 56, 496–500, 2017 Angew. Chem., 129, 510-514, 2017	Communication 15 %
II	T. Niemann, D. Zaitsau, A. Strate, A. Villinger, R. Ludwig, <i>Cationic clustering influences the phase behaviour of ionic liquids</i> , Sci. Rep., 8, 14753, 2018	Communication 50 %
III	T. Niemann, D. Zaitsau, A. Strate, P. Stange, R. Ludwig, <i>Controlling „like-likes-like“ charge attraction in hydroxy-functionalized ionic liquids by interaction strength of the anions, polarizability of the cations and varying alkyl chain length</i> , submitted to Phys. Chem. Chem. Phys.	Full Paper 50 %
IV	T. Niemann, J. Neumann, P. Stange, S. Gärtner, T. G. A. Youngs, D. Paschek, G. G. Warr, R. Atkin, R. Ludwig, <i>The double-faced nature of hydrogen bonding in hydroxyl-functionalized ionic liquids shown by neutron diffraction and molecular dynamics simulations</i> , Angew. Chem. Int. Ed., 58, 12887–12892, 2019 Angew. Chem., 131, 13019-13024, 2019	Communication 25 %
V	F. S. Menges, H. J. Zeng, P. J. Kelleher, O. Gorlova, M. A. Johnson, T. Niemann, A. Strate, R. Ludwig, <i>Structural Motifs in Cold Ternary Ion Complexes of Hydroxyl-Functionalized Ionic Liquids: Isolating the Role of Cation-Cation Interactions</i> , J. Phys. Chem. Lett., 9, 2979-2984, 2018	Communication 15 %

VI	T. Niemann, A. Strate, H. Zeng, F. Menges, M. Johnson, R. Ludwig, <i>Spectroscopic evidence for an attractive cation-cation interaction in hydroxyl-functionalized ionic liquids: The first H-bonded chain-like trimer</i> , Angew. Chem. Int. Ed., 57, 15364-15368, 2018 Angew. Chem., 130, 15590-15594, 2018	Communication 20 %
VII	T. Niemann, A. Strate, H. Zeng, F. Menges, M. Johnson, R. Ludwig, <i>Cooperatively enhanced hydrogen bonds in ionic liquids: closing the loop with molecular mimics of hydroxy-functionalized cations</i> Phys. Chem. Chem. Phys., 21, 18092–18098, 2019	Full Paper 35 %
VIII	A. Strate, T. Niemann, R. Ludwig, <i>Controlling the Kinetic and Thermodynamic Stability of Cationic Clusters by the Addition of Molecules or Counterions</i> , Phys. Chem. Chem. Phys., 19, 18854-18862, 2017	Full Paper 30 %
IX	T. Niemann, P. Stange, A. Strate, R. Ludwig, <i>Like-likes-Like: Cooperative Hydrogen Bonding Overcomes Coulomb Repulsion in Cationic Clusters with Net Charges up to $Q=+6e$</i> , ChemPhysChem, 19, 1691-1695, 2018	Communication 40 %
X	T. Niemann, P. Stange, A. Strate, R. Ludwig, <i>When hydrogen bonding overcomes Coulomb repulsion: from kinetic to thermodynamic stability of cationic dimers</i> , Phys. Chem. Chem. Phys., 21, 8215-8220, 2019	Communication 40 %
XI	T. Niemann, H. Li, G. G. Warr, R. Ludwig, R. Atkin <i>Influence of hydrogen bonding between ions of like charge on the ionic liquid interfacial structure at a mica surface</i> , submitted to J. Phys. Chem. Lett.	Communication 65 %

When Like Charged Ions Attract in Ionic Liquids: Controlling the Formation of Cationic Clusters by the Interaction Strength of the Counterions

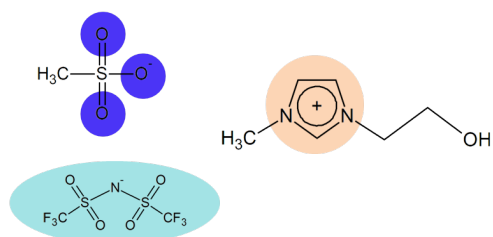
A. Strate (65 %), T. Niemann (20 %), D. Michalik (5 %), R. Ludwig (10 %)

Angew. Chem. Int. Ed., 56, 496-500, 2017

Angew. Chem., 129, 510-514, 2017

Content:

By choosing weakly coordinating anions, the attractive Coulombic interaction can be lowered leading to the formation of cationic clusters. Based on IR and NMR signatures a simple but effective spectroscopic scale for the possibility of this cluster formation is presented.



Contributions to this work:

Anne Strate had the main ideas for controlling the amount of cationic cluster formation by choosing differently strong interacting anions. She has done most of the Mid-IR measurements as well as the deconvolution of the spectra and she wrote a first draft. One IL was measured by me and I have deuterated all samples. I made a few corrections on the draft. Dirk Michalik contributed to the work with NMR measurements and Professor Ludwig received the manuscript for final corrections.

When Like Charged Ions Attract in Ionic Liquids: Controlling the Formation of Cationic Clusters by the Interaction Strength of the Counterions

Anne Strate, Thomas Niemann, Dirk Michalik, and Ralf Ludwig*

Abstract: The properties of ionic liquids are described by a subtle balance between Coulomb interaction, hydrogen bonding, and dispersion forces. We show that lowering the attractive Coulomb interaction by choosing weakly coordinating anions leads to the formation of cationic clusters. These clusters of like-charged ions are stabilized by cooperative hydrogen bonding and controlled by the interaction potential of the anion. IR and NMR spectroscopy combined with computational methods are used to detect and characterize these unusual, counter-intuitively formed clusters. They can be only observed for weakly coordinating anions. When cationic clusters are formed, cyclic tetramers are particularly stable. Therein, cooperative hydrogen-bond attraction can compete with like-charge repulsion. We present a simple but effective spectroscopic scale for the possibility of like-charge attraction in ionic liquids, based on IR and NMR signatures.

Opposite charges attract and like charges repel each other. This rule is known from Coulomb's law for the electrostatic interaction between charged particles. The pairing between oppositely charged ions is also a well-accepted concept in chemistry and plays an important role for reactions in solution, macromolecular catalysis, biochemical hydrolysis, and protein stability.^[1–3] In contrast, the association of like-charged ions in solution seems to be a counter-intuitive phenomenon and for which little experimental evidence is given. The attraction between like charges has been reported for aqueous salt solutions,^[4] for guanidinium ions in water,^[5] for the micellation of tetraalkylammonium surfactants,^[6] as well as for metastable colloidal crystallites.^[7] This phenomenon is also known for biomolecular systems including oligopeptides and DNA.^[8,9] So far, large-scale structures or assemblies are prerequisites for attractive interaction between like-charged ions. For smaller systems, mediating solvent molecules, such as water, are required. For ionic liquids (ILs), hydrogen bonding is reported between opposite charged ions only.^[10–18]

Recently, we could provide first spectroscopic evidence for attractive interaction between ions of like charge in ionic liquids (ILs).^[19] This unique behavior is somewhat surprising for ILs wherein all ions are solvated by counterions and the cation–anion interaction strength mainly governs the properties of this unique liquid material. However, if the common cation–anion interaction is softened by weakly coordinating anions, the attractive cation–cation interaction via cooperative hydrogen bonding might become possible even in the liquid phase.^[20,21]

Herein we demonstrate that the formation of cationic clusters can be controlled by the interaction potential of the counterions. Strong interacting anions prevent, and weakly interacting anions support like-charge of the cations. We could show that infrared OH stretching frequencies and the NMR proton chemical shifts are sensitive spectroscopic probes and provide a reliable measure for “like-likes-like” charge attraction. We show that the attractive interaction between like-charge ions strongly influences the structure of these ILs.

For our study we have chosen ionic liquids which all include the 1-(2-hydroxyethyl)-3-methylimidazolium cation (HEMIm) but four different anions tetrafluoroborate, bis-(trifluoromethylsulfonyl)imide, trifluoromethylsulfonate, and methylsulfonate, which have an increasing interaction potential in this sequence. Initially, we measured the IR spectra in the OH-stretch region of the ILs [HEMIm][BF₄] (**I**), [HEMIm][NTf₂] (**II**), [HEMIm][CF₃SO₃] (**III**), and [HEMIm][CH₃SO₃] (**IV**) covering a large temperature range between 213 and 353 K. In the [HEMIm] cation the OH functional group is well away from the positive charge which is located at the imidazolium ring. The idea is that this positive charge will be “neutralized” by weakly interacting anions whereas the OH bond is able to form hydrogen bonds with other OH groups resulting in H-bonded cationic clusters.

The spectra shown in Figure 1 were obtained by subtracting the spectra of the same ILs after H/D exchange at the OH groups of the cations. This way the contributions of the C–H vibrational modes from the imidazolium ring and alkyl groups could be eliminated and allowed a proper decomposition in the OH frequency range of the spectra (see Supporting Information). The measured spectra were also corrected for the varying numbers of OH oscillators arising from the different densities of ILs **I–IV**, related to the situation in IL **I**.

Additionally, we recorded the IR spectra of the 10 mol % mixtures of **I** in [PMIm][BF₄], **II** in [PMIm][NTf₂], **III** in [PMIm][CF₃SO₃], and **IV** in [PMIm][CH₃SO₃], respectively (PMIm = 1-propyl-3-methylimidazolium). With this procedure we significantly decreased the number of the OH

[*] Dipl.-Chem. A. Strate, M. Sc. T. Niemann, Prof. Dr. R. Ludwig
Universität Rostock
Institut für Chemie, Abteilung für Physikalische Chemie
Dr.-Lorenz-Weg 1, 18059 Rostock (Germany)
E-mail: ralf.ludwig@uni-rostock.de
Dr. D. Michalik, Prof. Dr. R. Ludwig
Leibniz-Institut für Katalyse an der Universität Rostock e.V.
Albert-Einstein-Strasse 29a, 18059 Rostock (Germany)
Supporting information for this article can be found under:
<http://dx.doi.org/10.1002/anie.201609799>.

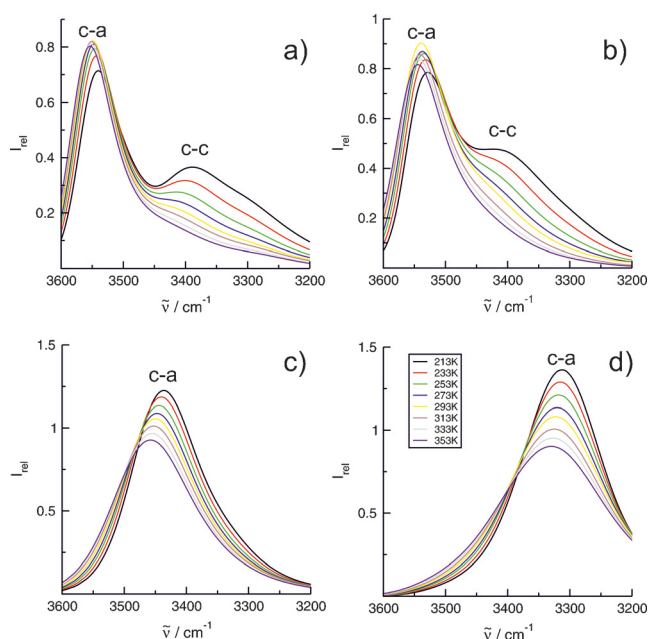


Figure 1. IR spectra in the O–H stretching region recorded for the ionic liquids a) [HEMIm][BF₄] (**I**), b) [HEMIm][NTf₂] (**II**), c) [HEMIm][CF₃SO₃] (**III**), and d) [HEMIm][CH₃SO₃] (**IV**) as a function of temperature between 213 K and 353 K.

oscillators. Consequently, the observed OH stretch vibrational bands can be almost exclusively assigned to the OH...F (**I**) and OH...O (**II–IV**) cation–anion interactions. In these mixtures, the OH vibrational bands occur at 3552 cm^{−1} for **I**, 3544 cm^{−1} for **II**, 3451 cm^{−1} for **III** and 3314 cm^{−1} for **IV** all measured at 353 K (see Supporting Information). In the sequence from weaker to stronger interacting anions, the frequencies shift from higher to lower wavenumbers ($\Delta\tilde{\nu} = 220$ cm^{−1}). This finding is not surprising but supports essentially the interpretation of the spectra of the pure ionic liquids as shown in Figure 1. Only for ILs **I** and **II**, (Figure 1 a,b) two major vibrational signatures can be observed. Firstly, the cation–anion (c-a) contributions resulting from the regular OH...F (**I**) and OH...O (**II**) hydrogen bonds between cations and anions as exclusively detected in the spectra of the 10 mol% mixtures and secondly, the cation–cation (c-c) contributions stemming from the OH...O hydrogen bonds between the cations resulting from like-charge attraction.

The OH vibrational bands of ILs **III** and **IV** are strongly redshifted owing to the increasing anion interaction strength and fall into the range of the vibrational bands assigned to the cation–cation signatures of the cationic clusters of **I** and **II** (see Figure 1 c,d). However, there is strong evidence that the vibrational band of **IV** can be exclusively referred to cation–anion interactions. For the pure IL **IV** as well as for its 10 mol% mixture in [PMIm][CH₃SO₃], the vibrational spectra can be described by a single Voigt function as shown in Figure 2a. The line shape is ideal and symmetric. If we multiply the spectrum of the 10 mol% mixture of **IV** in [PMIm][CH₃SO₃] by ten and correct for the different densities of both ILs, we obtain a spectrum showing the same spectral features and intensities as for the pure IL **IV** (Figure 2b). No shoulders occur either at the low or high

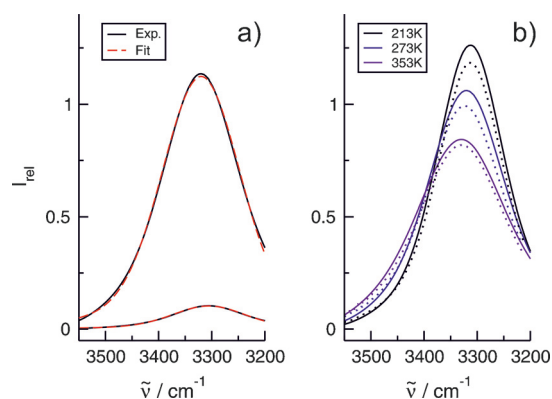


Figure 2. a) IR in the O–H stretching region recorded for the pure ionic liquid [HEMIm][CH₃SO₃] (**IV**) and for its 10 mol% mixture in [PMIm][CH₃SO₃]. Both spectra could be fitted by a single Voigt function. b) If the spectra of 10 mol% mixtures are multiplied by a factor of 10 and corrected for the densities, the resulting curves (dotted lines) nicely fit the spectra of the pure ILs, here shown for three different temperatures. Both results strongly indicate that IL **IV** consists solely of cation–anion pairs and cation–cation hydrogen bonds do not exist.

frequency site. Clearly, the methylsulfonate anion strongly interacts with the OH bond of the cation resulting solely in cation–anion pairs of opposite-charged ions. There is no intensity which could be referred to vibrational bands of OH bonds involved in other types of interaction.

The situation changes from IL **III** on. If we multiply the spectrum of the 10 mol% mixture of **III** in [C₃MIm][CF₃SO₃] by ten, we obtain lower intensity for the band assigned to the cation–anion interaction as measured for the pure IL **III**. Clearly, some of these OH bonds are now involved in other types of interaction. Likewise the spectral band becomes asymmetric indicating additional intensity at the low frequency site between $\tilde{\nu} = 3200$ and 3450 cm^{−1} (see Supporting Information). We will show below in detail that these contributions can be assigned to vibrational modes of OH bonds which form hydrogen bonds OH...O to other cations resulting in clusters of like-charged ions (c-c). However, the intensities of these vibrational bands are low and not significant for IL **III**. For the ILs **I** and **II** substantial vibrational bands occur which are redshifted relative to the cation–anion contributions between 3280 and 3500 cm^{−1}. For ILs **III** and **IV**, the cation–anion vibrational band constantly increases with decreasing temperature, whereas for ILs **I** and **II** these bands decrease with decreasing temperature in favor of vibrational bands between 3280 cm^{−1} and 3500 cm^{−1} resulting from the formation of cation–cation clusters.

As shown in Figure 3, the measured spectra of ILs **I** and **II** could be deconvoluted into one vibrational band assigned to the OH stretch of the cation–anion species and three redshifted bands all related to the cation–cation species, dimers, trimers, and tetramers (see Supporting Information). The interpretation of the deconvoluted bands is supported by DFT calculated frequencies of cation–anion and cation–cation type clusters including one up to four ion pairs at the B3LYP-D3/6-31 + G* level of theory.^[22–25] In Figure 3 it is shown that the calculated frequencies for the cationic clusters agree well with those of the deconvoluted bands of the

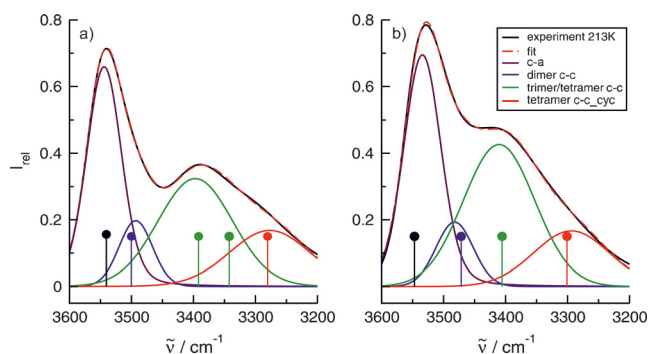


Figure 3. The IR spectra in the O–H stretching region: a) [HEMIm][BF₄] (I) and b) [HEMIm][NTf₂] (II). The spectra recorded at 213 K could be deconvoluted into four vibrational bands at $\tilde{\nu}$ = 3544, 3493, 3397, and 3277 cm^{−1} for I and $\tilde{\nu}$ = 3534, 3482, 3411, and 3294 cm^{−1} for II, respectively. The assignment of the vibrational bands to the cation–anion, the cation–cation dimer, the cation–cation trimer and tetramer as well as the cyclic cation–cation tetramer results from B3LYP/6-31 + G*-D3 calculations of clusters. The calculated average frequencies for these clusters are indicated as vertical lines in the same color as the deconvoluted bands (see Supporting Information).

measured spectra. In particular the red shifts with cation–anion cluster size are nicely reflected. Of course, all cation–anion and cation–cation structures were fully optimized and only positive frequencies were found indicating true minimum structures on the potential energy surface. The strongest redshift is found for the cyclic cation–cation cluster wherein hydrogen bonding is maximized through cooperative charge transfer from the oxygen lone pairs into the OH antibonding orbitals.^[19] The B3LYP-D3/6-31 + G* calculated structures for tetrameric clusters are shown in Figure 4. They indicate the possible H-bond structural motifs for clusters of same size.

We now assume that the intensities of the cation–anion (I_{c-a}) and the cation–cation (I_{c-c}) hydrogen-bond arise from the cations of these two general classes of H-bonding config-

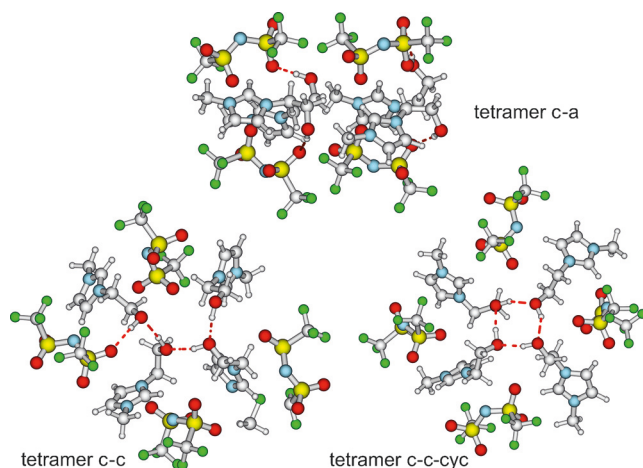


Figure 4. The calculated possible tetrameric clusters for II: tetramer c-a, including solely cation–anion pairs characterized by OH...O hydrogen bonds; tetramer c-c, with additional cation–cation interaction resulting in cooperative hydrogen bonding OH...OH...OH...OH...O; and tetramer c-c-cyc, showing a strongly cooperative H-bonded cyclic tetramer of cations via (OH...O)₄ bonds.

urations, for which relative populations are a function of absolute temperature only. Consequently a plot of $\ln(I_{c-c}/I_{c-a})$ versus $1/T$ should yield a straight line with a slope that is proportional to the average difference in energy between the two classes of H-bond configurations (ΔE). The linear fits of the data yield slopes $\Delta E/R$, where R is the universal gas constant, that gives the transfer energy between the two classes of H-bonding distribution as (3.59 ± 0.02) kJ mol^{−1} for I and (3.63 ± 0.02) kJ mol^{−1} for II (see Supporting Information). In both cases, the cation–anion configurations are only slightly favored in energy. Clearly, the repulsive Coulomb interaction between the cations is nearly overcome by attractive and cooperatively enhanced H-bond interaction in the cation–cation species.

After analyzing and quantifying the clusters of like-charged ions, we present a spectroscopic measure for like-charge attraction. In Figure 5a we plotted the square roots of

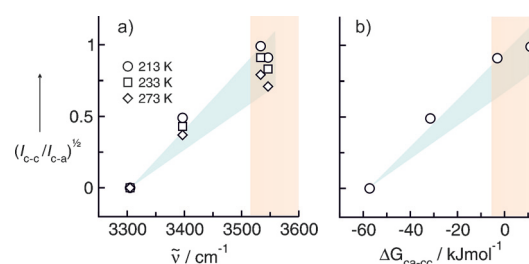


Figure 5. a) The square roots of the ratios between the intensities of c-c and c-a H-bonded clusters plotted versus the c-a OH stretch frequencies of I–IV for three different temperatures. b) The square roots of these ratios are also related to the free energy differences between calculated c-c and c-a H-bonded tetrameric clusters which were calculated for $T = 273$ K. The orange colored areas indicate the ranges of frequencies ($\tilde{\nu} = 3520$ – 3600 cm^{−1}) and free energy differences (greater than -3.7 kJ mol^{−1}), wherein like-charge attraction can be expected (as the case for I and II).

the intensity ratio I_{c-c}/I_{c-a} versus the frequencies c-a for all ILs at three different temperatures. The relation is almost linear. Clearly, substantial formation of clusters of like-charged ions can be only expected, if the OH stretch frequencies c-a are observed between $\tilde{\nu} = 3520$ and 3600 cm^{−1}. Further redshifted frequencies as for III and IV indicate the dominance of H-bonding between cation and anion. Like-charge attraction is completely suppressed from III on. This spectroscopic scale is supported by the calculated free energy differences between the c-a tetramers and c-c-cyc tetramers of I–IV as shown in Figure 5b. The ΔG_{ca-cc} values for ILs I and II between -3.7 and 11 kJ mol^{−1} allow cationic clusters formation (as indicated by the orange field in Figure 5), whereas ΔG_{ca-cc} values between -30 and -59 kJ mol^{−1} for III and IV exclude like-charge attraction and result in cation–anion clusters only.

The calculated ΔG_{ca-cc} values nicely correspond to measured frequencies between $\tilde{\nu} = 3520$ and 3600 cm^{−1} supporting IR frequencies as descriptors for like-charge attraction. Now, we show that in addition to OH vibrational frequencies, ν_{OH} , also OH proton chemical shifts, δ^1H , can be used as a measure for possible like-charge attraction. For that purpose we measured the δ^1H values of the hydroxy protons in the

10 mol % mixtures wherein only cation–anion interaction is present. We then related the proton chemical shifts (measured and calculated versus TMS) to the measured OH vibrational frequencies. As shown in Figure 6 the relation is nearly linear. Strongly downfield proton chemical shifts ($\delta = 5.6$ ppm) correlate with strongly redshifted OH frequencies

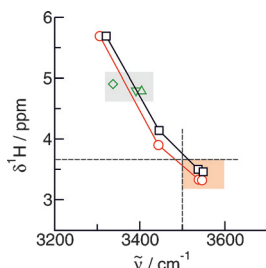


Figure 6. The relation between the measured OH proton chemical shifts, $\delta^1\text{H}$, and OH vibrational frequencies, $\tilde{\nu}_{\text{OH}}$, of the hydroxy groups of the HEMIm cations in **I–IV** is nearly linear. Both properties reflect the varying H-bond strength of the anions for the pure IL (red circles) and the 10 mol% mixture (black squares) in a similar way. The formation of clusters of like charge can be only expected for proton chemical shifts below $\delta = 3.7$ ppm (versus TMS) and for OH vibrational frequencies above 3500 cm^{-1} as indicated by the dotted lines. Additionally, we included these pairs of spectroscopic probes for molecular liquids, such as water (Δ), methanol (∇), and ethanol (\diamond).

($\tilde{\nu} = 3300\text{ cm}^{-1}$) such as given for **IV**. In contrast, the weaker cation–anion interaction as present in **I** results in moderate downfield chemical shifts ($\delta = 3.4$ ppm) and highest frequencies ($\tilde{\nu} = 3550\text{ cm}^{-1}$). This result suggests that both, the IR and the NMR spectroscopic properties reflect a similar type of electronic perturbation attributed to hydrogen bonding. For **I** and **II** both spectroscopic probes indicate a cation–anion interaction which is significantly weaker than the molecular interaction via hydrogen bonding as in water or alcohols (see Figure 6).^[26–29]

The detection and control of like-charge attraction is strong evidence for the “anti-electrostatic hydrogen bonds” (AEHB) as reported recently by Weinhold and Klein.^[30–32] Despite strong electrostatic opposition, cation–cation clusters are found to be in equilibrium with cation–anion species upon reaching typical H-bond distances and spectroscopic signatures as known for molecular liquids (see Supporting Information). If we remove the anions from the dimer structure and calculate the relaxed-scan potential curve for $[\text{HEMIm}]_2^{2+}$ at the B3LYP-6-31 + G* and MP2-6-31 + G* levels of theory, we find local minimum structures at typical H-bond distances of $R_{\text{O}\cdots\text{H}} = 2.0\text{ \AA}$. The uncorrelated HF-level does not show this minimum and only gives an inflection feature in this region. As shown in Figure 7, a robust kinetic stability with a clear dissociation barrier of $3\text{--}4\text{ kJ mol}^{-1}$ is achieved for the B3LYP and the MP2 treatment. In this sense, the pure cationic clusters are stable up to cyclic tetramers wherein cooperative H-bonding is maximized. Larger clusters, such as cyclic pentamers or hexamers, do not show this kinetic stability and dissociate during the geometry optimization procedure.

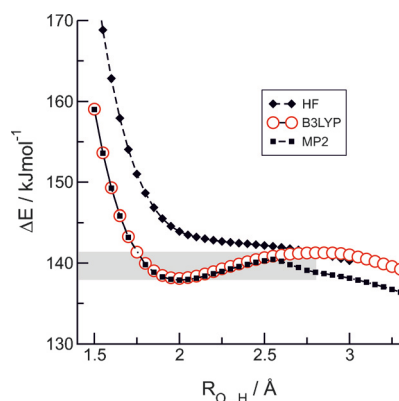


Figure 7. Potential energy curves for $[\text{HEMIm}]_2^{2+}$ H-bonding (all at 6-31 + G* basis level) as calculated with hybrid density functional B3LYP (red open circles), ab initio MP2 (filled squares), and uncorrelated HF (filled diamonds) methods. The structures were relaxed for each bond length $R_{\text{O}\cdots\text{H}}$.

Thus, it is not surprising that the ionic liquids including the counterions also give spectroscopic features that cannot be related to larger clusters than cyclic tetramers. Finally, it will be interesting to see whether typical Energy Decomposition Analysis (EDA) schemes will be able to describe the interaction between ions of like charge.^[33,34]

Herein we could provide evidence for hydrogen bonding between ions of like charge in ionic liquids. Through thus use of weakly interacting anions, the hydroxy groups of the cations can form cooperative H-bonds $\text{OH}\cdots\text{OH}$ similar to those in molecular liquids. The like-charge attraction is governed by a delicate balance of Coulomb repulsion and cooperative hydrogen bonding well beyond the simple electrostatic picture.^[33,34] We could demonstrate that the formation of the H-bonded cationic clusters can be controlled by the interaction strength of the counterions. The vibrational frequencies and the proton chemical shifts of the hydroxy groups involved in the regular H-bond between cations and anions can be used as reliable descriptor for the probability and extent of like-charge attraction. The influence of like-charge attraction on macroscopic properties, such as viscosity, electrical conductivity, and vaporization enthalpies is currently being investigated.

Acknowledgements

This work has been supported by the DFG Research Grant LU-506/14-1 and partially by the DFG Collaborative Research Center SFB 652 “Strong correlations and collective effects in radiation fields: Coulomb systems, clusters and particles”.

Conflict of interest

The authors declare no conflict of interest.

Keywords: DFT calculations · hydrogen bonding · ionic liquids · IR spectroscopy · like-charge interaction

How to cite: *Angew. Chem. Int. Ed.* **2017**, 56, 496–500
Angew. Chem. **2017**, 129, 510–514

-
- [1] J. Smid, *Angew. Chem. Int. Ed. Engl.* **1972**, 11, 112–127; *Angew. Chem.* **1972**, 84, 127–144.
- [2] C. Reichhardt, *Solvents and Solvent Effects in Organic Chemistry*, VCH, Weinheim, **1990**.
- [3] Y. Marcus, G. Hefter, *Chem. Rev.* **2006**, 106, 4585–4621.
- [4] M. Holz, K. J. Patil, *Ber. Bunsen-Ges.* **1991**, 95, 107–113.
- [5] O. Shih, A. H. England, G. C. Dallinger, J. W. Smith, K. C. Duffey, R. C. Cohen, D. Prendergast, R. J. Saykally, *J. Chem. Phys.* **2013**, 139, 035104.
- [6] M. Benrraou, B. L. Bales, R. Zana, *J. Phys. Chem. B* **2003**, 107, 13432–13440, and references therein.
- [7] A. E. Larsen, D. G. Grier, *Nature* **1997**, 385, 230–233.
- [8] M. R. Caplan, P. N. Moore, S. Zhang, R. D. Kamm, D. A. Lauffenburger, *Biomacromolecules* **2000**, 1, 627–631.
- [9] M. Kuron, A. Arnold, *Eur. Phys. J. E* **2015**, 38, 20.
- [10] K. Fumino, A. Wulf, R. Ludwig, *Angew. Chem. Int. Ed.* **2008**, 47, 3830–3834; *Angew. Chem.* **2008**, 120, 3890–3894.
- [11] K. Fumino, A. Wulf, R. Ludwig, *Angew. Chem. Int. Ed.* **2008**, 47, 8731–8734; *Angew. Chem.* **2008**, 120, 8859–8862.
- [12] S. B. C. Lehmann, M. Roatsch, M. Schöppke, B. Kirchner, *Phys. Chem. Chem. Phys.* **2010**, 12, 7473–7486.
- [13] A. S. Pensado, M. F. Costa Gomes, J. N. Canongia Lopes, P. Malfreyt, A. A. H. Pádua, *Phys. Chem. Chem. Phys.* **2011**, 13, 13518–13526.
- [14] K. Fumino, R. Ludwig, *J. Mol. Liq.* **2014**, 192, 94–102.
- [15] K. Fumino, S. Reimann, R. Ludwig, *Phys. Chem. Chem. Phys.* **2014**, 16, 21903–21929.
- [16] P. A. Hunt, C. R. Ashworth, R. P. Matthews, *Chem. Soc. Rev.* **2015**, 44, 1257–1288.
- [17] C. R. Ashworth, R. P. Matthews, T. Welton, P. A. Hunt, *Phys. Chem. Chem. Phys.* **2016**, 18, 18145–18160.
- [18] K. Fumino, T. Peppel, M. Geppert-Rybczynska, D. H. Zaitsau, J. K. Lehmann, S. P. Verevkin, M. Köckerling, R. Ludwig, *Phys. Chem. Chem. Phys.* **2011**, 13, 14064–14075.
- [19] A. Knorr, K. Fumino, A.-M. Bonsa, R. Ludwig, *Phys. Chem. Chem. Phys.* **2015**, 17, 30978–30982.
- [20] A. Knorr, R. Ludwig, *Sci. Rep.* **2015**, 5, 17505.
- [21] A. Knorr, P. Stange, K. Fumino, F. Weinhold, R. Ludwig, *ChemPhysChem* **2016**, 17, 458–462.
- [22] Gaussian 09 (Revision B.01), M. J. Frisch et al.; see the Supporting Information.
- [23] S. Grimme, J. Antony, S. Ehrlich, H. Krieg, *J. Chem. Phys.* **2010**, 132, 154104.
- [24] S. Ehrlich, J. Moellmann, W. Reckien, T. Bredow, S. Grimme, *ChemPhysChem* **2011**, 12, 3414–3420.
- [25] S. Grimme, A. Jansen, *Chem. Rev.* **2016**, 116, 5105–5154.
- [26] K. M. Murdoch, T. D. Ferris, J. C. Wright, T. C. Farrar, *J. Chem. Phys.* **2002**, 116, 5717–5724.
- [27] F. Huisken, A. Kulcke, C. Laush, J. Lisy, *J. Chem. Phys.* **1991**, 95, 3924–3929; M. Huelsekopf, R. Ludwig, *J. Mol. Liq.* **2002**, 98–99, 163–171.
- [28] R. Ludwig, F. Weinhold, T. C. Farrar, *Mol. Phys.* **1999**, 97, 465–477.
- [29] R. Ludwig, *Phys. Chem. Chem. Phys.* **2002**, 4, 5481–5487.
- [30] F. Weinhold, C. R. Landis, *Valency and Bonding A Natural Bond Orbital Donor-Acceptor Perspective*, Cambridge, University Press, Cambridge, **2005**.
- [31] a) F. Weinhold, R. A. Klein, *Angew. Chem. Int. Ed.* **2014**, 53, 11214–11217; *Angew. Chem.* **2014**, 126, 11396–11399; b) Corrigendum: F. Weinhold, R. A. Klein, *Angew. Chem. Int. Ed.* **2014**, 53, 12992; *Angew. Chem.* **2014**, 126, 13207.
- [32] F. Weinhold, C. R. Landis, E. D. Glendening, *Int. Rev. Phys. Chem.* **2016**, 35, 399–440.
- [33] K. Kitaura, K. Morokuma, *Int. J. Quantum Chem.* **1976**, 10, 325–340.
- [34] T. Ziegler, A. Rauk, *Theor. Chem. Acc.* **1977**, 46, 1–10.
-

Manuscript received: October 6, 2016

Final Article published: December 19, 2016

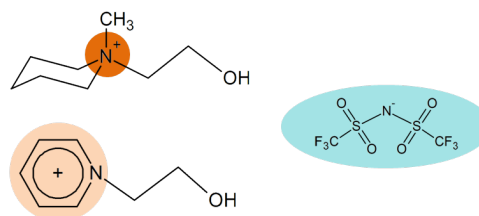
Cationic clustering influences the phase behaviour of ionic liquids

T. Niemann (50 %), D. Zaitsau (20 %), A. Strate (10 %), A. Villinger (10 %), R. Ludwig (10 %)

Sci. Rep., 8, 14753, 2018

Content:

By choosing cations with localised and delocalised positive charges at the N-heterocycle we demonstrate the role of polarisability of the center of charge on the formation of cation clusters. Based on IR and DSC results we have shown for the first time, the formation of cationic clusters protect ILs from crystallization and leads to the formation of glasses.



Contributions to this work:

I have synthesized all ILs investigated in this work and I have done all Mid-IR measurements. Dzmitry Zaitsau has done the DSC measurements. Alexander Villinger contributed with X-Ray measurements to this work. I wrote the first draft of the paper. Anne Strate had the basic idea of the chosen concept and made some corrections on the draft. Professor Ludwig received the manuscript for final corrections and submission.

SCIENTIFIC REPORTS

OPEN

Cationic clustering influences the phase behaviour of ionic liquids

Thomas Niemann¹, Dimitri Zaitsau¹, Anne Strate¹, Alexander Villinger² & Ralf Ludwig^{1,3,4} 

Received: 4 June 2018

Accepted: 19 September 2018

Published online: 03 October 2018

“Unlike charges attract, but like charges repel”. This conventional wisdom has been recently challenged for ionic liquids. It could be shown that like-charged ions attract each other despite the powerful opposing electrostatic forces. In principle, cooperative hydrogen bonding between ions of like-charge can overcome the repulsive Coulomb interaction while pushing the limits of chemical bonding. The key challenge of this solvation phenomenon is to establish design principles for the efficient formation of clusters of like-charged ions in ionic liquids. This is realised here for a set of well-suited ionic liquids including the same hydrophobic anion but different cations all equipped with hydroxyethyl groups for possible H-bonding. The formation of H-bonded cationic clusters can be controlled by the delocalization of the positive charge on the cations. Strongly localized charge results in cation-anion interaction, delocalized charge leads to the formation of cationic clusters. For the first time we can show, that the cationic clusters influence the properties of ILs. ILs comprising these clusters can be supercooled and form glasses. Crystalline structures are obtained only, if the ILs are dominantly characterized by the attraction between opposite-charged ions resulting in conventional ion pairs. That may open a new path for controlling glass formation and crystallization. The glass temperatures and the phase transitions of the ILs are observed by differential scanning calorimetry (DSC) and infrared (IR) spectroscopy.

The pairing between opposite-charged ions is a well-accepted concept in chemistry and plays an important role for reactions in solution, macromolecular catalysis, biochemical hydrolysis and protein stability^{1–5}. In contrast, establishing the theoretical foundation and experimental evidence for like-charge attraction in solution is a challenge. It seemingly contradicts conventional wisdom that like-charged ions can attract, despite the powerful opposing electrostatic forces: “Unlike charges attract, but like charges repel”. However, additional attractive forces between ions of like charge may attenuate the repulsive forces resulting in cationic or anionic cluster formation. Attractive interaction between ions of like charge has been observed for aqueous salt solutions of K/CsBr⁶, for guanidinium ions in water⁷, for tetraalkylammonium surfactants⁸, for oligopeptides and for DNA^{9–11}. Recently, McNally *et al.* reported the self-assembly of molecular ions via like-charge ion interaction and through space defined organic domains¹². Fatila *et al.* showed that hydrogen-bonded anions can stabilize each other inside macrocyclic hosts¹³. Both groups related the like-charge attraction to anti-electrostatic hydrogen bonds (AEHB) as suggested in Weinhold’s theoretical work^{14,15}. So far, this phenomenon was only reported for large-scale structures, assemblies or stabilizing frameworks. Recently, we could show for ionic liquids that hydrogen bonding can overcome the repelling forces between ions of like-charge resulting in stable cationic clusters up to cyclic tetramers (ILs)^{16–19}. Usually, the interaction between opposite-charged ions is typical for this unique liquid material, and determines its properties^{20–28}. Moreover, we could show that the appearance of cationic clusters can be controlled by the interaction strength of the counterions. Strongly interacting anions suppress and weakly interacting anions promote the cationic cluster formation²⁹. However, significant cationic cluster formation could be only observed at low temperatures, probably due to kinetic trapping.

In the present study, we demonstrate by the means of infrared (IR) spectroscopy that the presence of cationic clusters can be strongly supported or suppressed by specifically designed cations. The ability for cationic cluster formation can be referred to the shape, the charge distribution and the specific interaction site of the cations. By tuning the properties of the cations, we observe substantial cationic cluster formation already at room temperature. Here, the cationic clusters exist in equilibrium with the clusters of opposite-charged ions and ‘kinetic trapping’ is no longer a requirement for their existence²⁹. For the first time we can also show that the presence of

¹Universität Rostock, Institut für Chemie, Abteilung für Physikalische Chemie, Dr. -Lorenz-Weg 2, 18059, Rostock, Germany. ²Universität Rostock, Institut für Chemie, Abteilung für Anorganische Chemie, Albert-Einstein-Str. 3a, 18059, Rostock, Germany. ³Department Life, Light & Matter, University of Rostock, 18051, Rostock, Germany. ⁴Leibniz-Institut für Katalyse an der Universität Rostock e.V., Albert-Einstein-Str. 29a, 18059, Rostock, Germany. Correspondence and requests for materials should be addressed to R.L. (email: ralf.ludwig@uni-rostock.de)

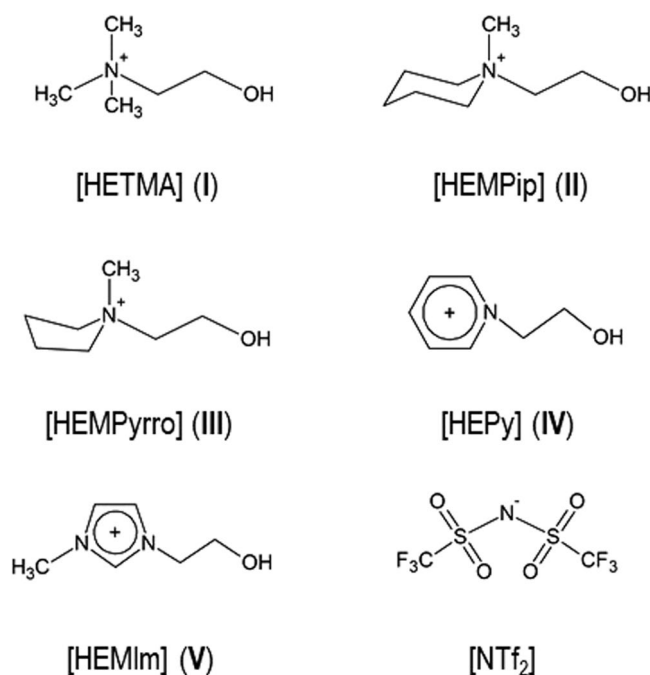


Figure 1. Structures of the cations [HETMA]⁺ (I), [HEMPip]⁺ (II), [HEMPyrro]⁺ (III), [HEPy]⁺ (IV), [HEMIm]⁺ (V) and the anion [NTf₂][−] which is present in all ILs I–V.

cationic clusters strongly influences the properties of ionic liquids. If substantial amount of cationic clusters is available, the ILs can be supercooled and form glasses at temperatures between 193 and 213 K. If cationic clusters are only present in trace amounts, the ILs can be crystallized by forming hydrogen-bonded ‘ion pairs’ between cations and anions solely³⁰. The glass transition temperatures and the phase transition temperatures were measured by differential scanning calorimetry (DSC). If crystallization occurs, the infrared spectra show the typical sharp features of cation-anion interaction only and the broad redshifted bands of the cationic clusters completely disappear. For these ILs the structures could be obtained from X-ray crystallography³⁰. The formation of clusters of like-charged ions is influenced by the shape and interaction strength of the ions and may provide a new path for controlling supercooling and crystallization.

Results and Discussion

First, we studied the formation and stability of cationic clusters for a set of specifically selected ionic liquids (see SI1). The ILs are based on ammonium, piperidinium, pyrrolidinium, pyridinium, and imidazolium cations all including a hydroxyethyl group for H-bond formation to the anion or to other cations resulting in cationic clusters. The cations are shown in Fig. 1. For all ILs, we have chosen the bis(trifluoromethylsulfonyl)imide [NTf₂][−] as the counterion for two reasons. Firstly, this anion is flexible resulting in low viscosities and melting points, finally providing room temperature ionic liquids. Secondly, the relatively hydrophobic [NTf₂][−] anion forms only weak hydrogen bonds to the cation and thus supports the formation of cationic clusters. The five ILs under investigations are [HETMA]NTf₂ (I), [HEMPip]NTf₂ (II), [HEMPyrro]NTf₂ (III), [HEPy]NTf₂ (IV), and [HEMIm]NTf₂ (V) (see Fig. 1). The ILs II, III and IV were synthesized in our lab (see SI1), the ILs I and V were purchased from IoLiTec.

In respect to structure and charge distribution within the cation, the ILs can be divided into two groups. ILs I, II and III represent saturated compounds, characterized by positive charge localization at the nitrogen atom. In contrast, delocalized positive charge within the nitrogen heterocycle is typical for ILs IV and V. The transmission infrared spectra for all ILs I–V are shown as a function of temperature in Fig. 2. We started at the highest temperature of about 353 K for all compounds and went down below the phase transition temperature for each IL ranging between 253 K for ILs I, II and III, 213 K for IL IV and 193 K for IL V.

For all ILs I–V the observed OH stretch vibrational bands above 3500 cm^{−1} can be exclusively referred to the hydrogen bond enhanced OH⋯O=S cation-anion (c-a) interaction. In all compounds I–V these vibrational bands have almost similar frequencies and intensities at 353 K, which indicates that the c-a hydrogen bonds are independent of the nature of the cation (see SI2). For all ILs vibrational intensity is also observed below 3500 cm^{−1} but to different extent depending on the type of cation in the ILs I–V. These redshifted vibrational features can be assigned to the OH⋯OH hydrogen bonds among the cations (c-c) indicating the presence of cationic clusters (see Fig. 2). Recently, both structural motifs have been observed for isolated cationic complexes of IL V by using a combined approach of photodissociation mass spectrometry and double resonance techniques³¹.

For ILs I and II the IR spectra are mainly characterized by the vibrational bands at 3540 cm^{−1} indicating pure c-a interaction along the OH⋯O=S hydrogen bond. Only little redshifted contributions can be observed for these ILs. Below their melting points, the IR spectra in the OH frequency range become highly symmetric. (see SI3) Even the trace amounts of redshifted intensities disappear and the ionic interaction is described by c-a hydrogen bonds only.

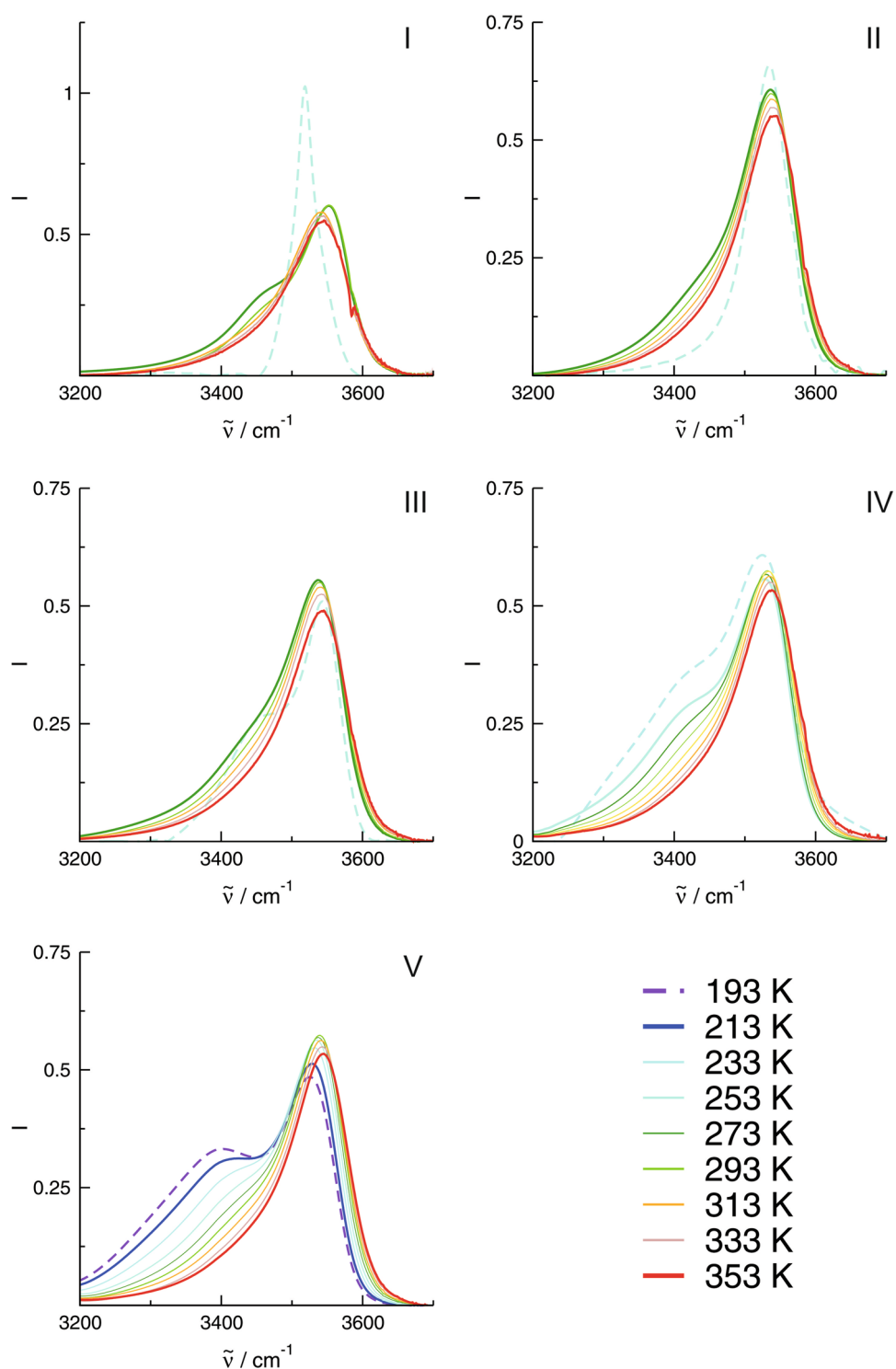


Figure 2. Infrared spectra in the O-H stretching region recorded for the ionic liquids (a) [HETMA]NTf₂ (I), (b) [HEMPip]NTf₂ (II), (c) [HEMPyrro]NTf₂ (III), (d) [HEPy]NTf₂ (IV) and (e) [HEMIm]NTf₂ (V) as a function of temperature. The vibrational bands above 3500 cm⁻¹ indicate hydrogen bonding between cation-anion, whereas the redshifted vibrational bands represent cationic clusters. In the sequence IL I–V the formation of cationic clusters strongly increases. The dashed lines indicate glass transition (II, IV, V) or phase transition (I, II) temperatures.

The interpretation of the vibrational bands is supported by DFT calculated frequencies of **c-a** and **c-c** type clusters including one up to four ion pairs at the B3LYP-D3/6-31 + G* level of theory (see SI4)^{32–35}. Figure 3 shows the spectrum of [HEMIm]NTf₂ (V) at the lowest (213 K) and highest (353 K) temperatures. Additionally the calculated averaged frequencies of a dimer, trimer and tetramer of purely **c-a** bound clusters along with those

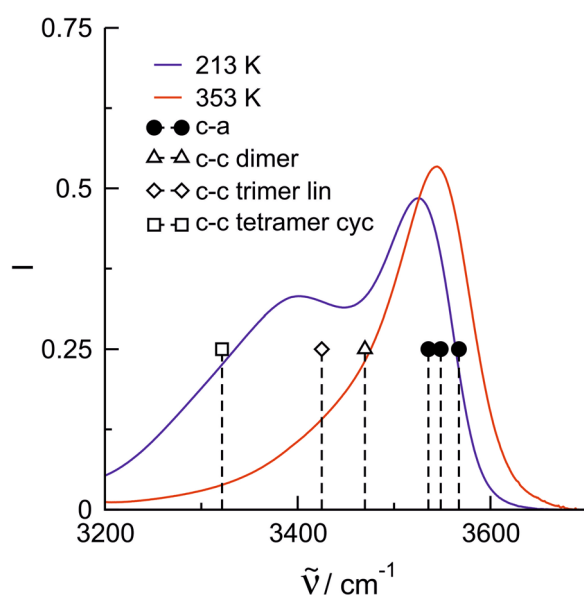


Figure 3. Infrared spectra in the O-H stretching region of the ionic liquid [HEMIm]NTf₂ (V) at 213 (blue curve) and 353 K (red curve). The vibrational bands above 3500 cm⁻¹ indicate hydrogen bonding between cation-anion (c-a), whereas the redshifted vibrational bands represent cationic (c-c) clusters. This interpretation is supported by frequency calculations at the B3LYP/6-31 + G* level of theory. We calculated dimers, trimers and tetramers of pure c-a and c-c clusters. The c-a frequencies lie above 3500 cm⁻¹ throughout (filled symbols), whereas the c-c cluster frequencies are further redshifted with increasing c-c cluster size (open symbols). The comparison with the experimental spectra suggest that linear trimer and cyclic tetramers are needed to represent the measured IR spectra. For each cluster averaged frequencies which are weighted with the calculated intensities.

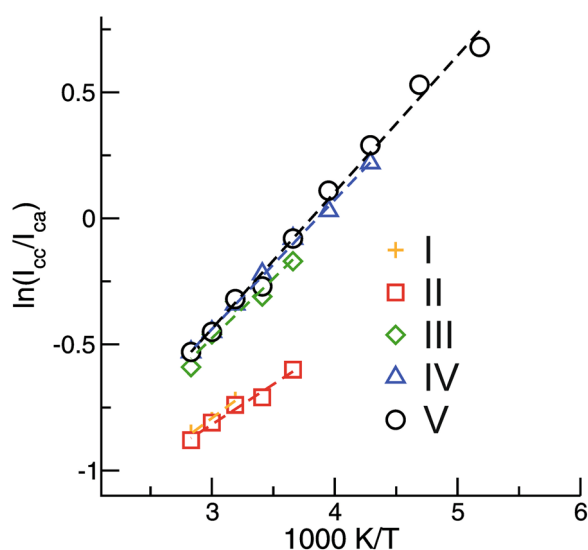


Figure 4. Plots of the natural logarithm of the c-c to c-a vibrational band intensity ratios versus inverse temperature taken from the measured spectra in Fig. 1 between 353 K and 193 K. I_{cc} and I_{ca} were obtained from the integral intensities left and right of the frequency position, where the deconvoluted vibrational bands for the ca and the cc species cross. The solid lines represent linear fits ($R^2 \geq 0.98$) with slopes indicating different enthalpies of cationic cluster formation.

of a dimer, linear trimer and cyclic tetramer of purely c-c bound clusters are shown. The calculated c-a frequencies lie clearly above 3500 cm⁻¹, whereas the c-c cluster frequencies are further redshifted with increasing cluster size strongly supporting the existence of two types of cluster species. The agreement between the calculated and measured frequencies also underlines that the c-c hydrogen bonds are stronger than those in the c-a clusters. That is quite surprising because the c-a hydrogen bonds are additionally enhanced by Coulomb attraction, whereas the c-c hydrogen bonds have to compete with the repulsive Coulomb forces between like-charged ions. Overall,

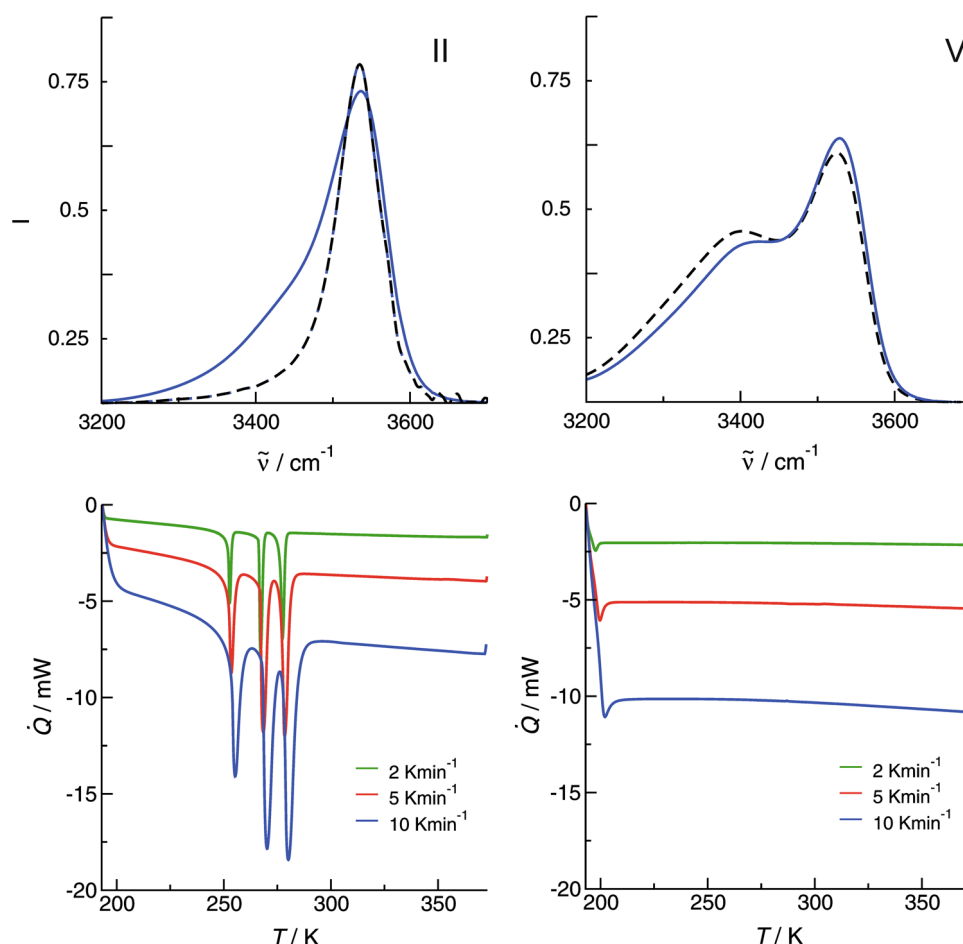


Figure 5. Infrared spectra in the O-H stretching region and DSC recorded for the ionic liquids (a) [HEMPip] NTf₂ (II) and (b) [HEMIm]NTf₂ (V) for the lowest (a) 253 K, (b) 193 K and second lowest (a) 273 K, (b) 213 K temperatures. The vibrational bands above 3500 cm⁻¹ indicate hydrogen bonding between cation-anion, whereas the redshifted vibrational bands represent cationic clusters. For IL II the small amount of cationic clusters disappears upon freezing resulting in a symmetric vibrational band indicating pure c-a interaction. This behavior is in accord to the DSC traces, which show phase transitions in this temperature range. For IL V the amount of cationic clusters further increase with decreasing temperature. No change in the vibrational signature is observed in accord with the DSC traces.

the comparison with the experimental spectra suggest that the existence of linear trimer and cyclic tetramers are required to represent the measured IR spectra.

We assume that the cation-anion (I_{ca}) and the cation-cation (I_{cc}) hydrogen bond intensities arise from cations of these two general classes of H-bonding configurations, for which relative populations are a function of absolute temperature only. Consequently, a plot of $\ln(I_{cc}/I_{ca})$ versus $1/T$ should yield a straight line with a slope that is proportional to the average difference in energy between the two classes of H-bond configurations. All ILs show a linear dependence between $\ln(I_{cc}/I_{ca})$ and $1/T$. The slope is positive for all ILs indicating that the formation of the cationic clusters resembles an exothermic reaction (see Fig. 4). Obviously, we observe two types of cations involved in different types of clusters, c-c and c-a. The slopes for IL I and II are significantly smaller than those for the other ILs (1.6 vs 1.0). The low reaction enthalpy for the ILs comprising saturated cations with localized charge indicates that only small clusters are formed in accord with the small redshifted contributions in the IR spectra. The other ILs in particular IV and V form larger clusters with enhanced stability which cannot be destroyed in favor of crystallization.

The interpretation of the IR spectra at low temperatures is also supported by the DSC measurements (see also SI5). During cooling from 373 to 193 K at 2, 5 and 10 K·min⁻¹, only a heat capacity change corresponding to the glass transition (T_g) could be observed in the DSC profiles of IL IV and V. It means that the supercooled liquids are fairly stable. For ILs I, II and III complex phase transition with melting (T_{fus}) and solid/solid phase transition (T_{ss}) are observed. Figure 5 shows the DSC traces related to the temperature dependent IR spectra of ILs II and V. After phase transition, the IR spectra for IL II only exhibit c-a vibrational bands, whereas the minor c-c spectral features typical for the liquid phase completely disappear. Obviously, the disappearance of the cationic clusters and the presence of pure c-a bonded ion pairs are related to fusion at 276.2 K and two solid/solid phase transitions at 266.2 and 251.6 K, respectively. In contrast, the strong formation of cationic clusters in IL V

is not changing the spectral features with decreasing temperature. The liquid can be supercooled and show glass transition between 195 and 198 K. From the combined IR and DSC experiments, we have clear evidence that the formation of cationic clusters prevents the ILs from crystallization and liquid/solid phase transition. The resulting material is a glass.

Both, IR and DSC experiments suggest that ILs **I** and **II** should give crystal structures. The crystal structure for IL **I** is known from the literature and shows one cation-anion pair in the asymmetric unit and four ion pairs in the unit cell³⁰. As expected, the choline cation and the $[\text{NTf}_2]^-$ anion are held together by hydrogen bonds with an interatomic distance between the hydroxyl proton and the sulfonyl oxygen atom of about $r(\text{H}\cdots\text{O}=\text{S}) = 205$ pm. Unfortunately, we failed to obtain the crystal structure for IL **II**. We found a low-temperature structure at 12 K (see SI6) that showed neither H-bonding between anions and cations, nor H-bonding among the cations. This structure showed a delocalized positive charge, which is spherically surrounded by the negative partial charges of the anions. The DSC traces show a second crystalline phase of IL **II** at 267 K between the low-temperature phase and the amorphous (glassy) phase (see Fig. 5). Probably due to high thermal motion and resulting decrease in scattering power, we were not able to solve the crystal structure of this phase.

Overall, the IR and DSC measurements clearly indicate different phase transition behavior for these two types of ILs. If substantial cationic clusters are formed, the liquid IL will supercool and becomes a glass at low temperatures as in ILs **IV** and **V**. No liquid/solid phase transition is observed. Usually, crystallization can be avoided only, if liquids are cooled sufficiently fast. Molecules will then arrange so slowly that they cannot adequately sample configurations in the available time allowed by the cooling rate. The liquid's structure, therefore, appears 'frozen'. The resulting material is a glass³⁶. Here, we show that substantial cationic cluster formation prevents crystallization and glass formation for ILs. Hydrogen bonding immobilizes the cations and no solid configurations can be formed.

Conclusions

In this work, we could show for a set of well-suited ionic liquids that the presence of like-charge attraction is governed by the charge delocalization of the cation. If the positive charge is delocalized and available to the counterion, cooperative hydrogen bonding between the like charges is possible resulting in cationic clusters up to cyclic tetramers. As shown in the IR spectra, these clusters are characterized by redshifted vibrational bands which increase in intensity with decreasing temperature. The ILs exhibiting substantial amounts of cationic clusters form glasses as shown by DSC measurements. The ILs showing only traces of these structures can be crystallized or solidified, resulting in pure cation-anion hydrogen bonds. The glass and liquid/solid phase transitions are also observed in the IR experiments. Obviously, the amount of cationic clusters influence the glass formation and crystallization. For the first time we could show, that like-charge attraction modifies the macroscopic properties of ILs. The formation of clusters of like-charged ions is influenced by the shape and interaction strength of the ions and may provide a new path for controlling crystallization and glass formation.

References

- Reichardt, C. *Solvents and Solvent Effects in Organic Chemistry*. (VCH, Weinheim 1990).
- Szwarc, M. *Ions and Ion Pairs in Organic Reactions*, **1**, (Wiley-Interscience, New York, 1972).
- Brak, K. & Jacobsen, E. N. Asymmetric Ion-Pairing Catalysis. *Angew. Chem. Int. Ed.* **52**, 534–561 (2013).
- Marcus, Y. & Hefer, G. Ion pairing. *Chem. Rev.* **106**, 4585–4621 (2006).
- Iwahara, J., Esadze, A. & Zandarashvili, L. Physicochemical Properties of Ion Pairs of Biological Macromolecules. *Biomolecules* **5**, 2435–2463 (2015).
- Holz, M. & Patil, K. J. Cation-Cation Association of Tetramethylammonium Ions in Aqueous Mixed Electrolyte Solutions. *Ber. Bunsen-Ges.* **95**, 107–113 (1991).
- Shih, O. *et al.* Cation-cation contact pairing in water: Guanidinium. *J. Chem. Phys.* **139**, 035104 (2013).
- Benraou, M., Bales, B. L. & Zana, R. Effect of the Nature of the Counterion on the Properties of Anionic Surfactants. 1. Cmc, Ionization Degree at the Cmc and Aggregation Number of Micelles of Sodium, Cesium, Tetramethylammonium, Tetraethylammonium, Tetrapropylammonium, and Tetrabutylammonium Dodecyl Sulfates. *J. Phys. Chem. B* **107**, 13432–13440 (2003).
- Caplan, M. P., Moore, P. N., Zhang, S., Kamm, R. D. & Lauffenburger, D. A. Self-Assembly of a β -Sheet Protein Governed by Relief of Electrostatic Repulsion Relative to van der Waals Attraction. *Biomacromolecules* **1**, 627–631 (2000).
- Kuron, M. & Arnold, A. Role of geometrical shape in like-charge attraction of DNA. *Eur. Phys. J. E* **38**, 20 (2015).
- Kornyshev, A. A. & Leikin, S. Theory of interaction between helical molecules. *J. Chem. Phys.* **107**, 3656–3674 (1997).
- McNally, J. S., Wag, X. P., Hoffmann, C. & Wilson, A. D. Self-assembly of molecular ions via like-charge ion interactions and through-space defined organic domains. *Chem. Commun.* **53**, 10934–37 (2017).
- Fatila, E. M. *et al.* Anions Stabilize Each Other inside Macrocyclic Hosts. *Angew. Chem. Int. Ed.* **55**, 14057–14062 (2016); *Angew. Chem.* **128**, 14263–14268 (2016).
- Weinhold, F. & Klein, R. A. Anti-Electrostatic Hydrogen Bonds. *Angew. Chem. Int. Ed.* **53**, 11214–11217 (2014); *Angew. Chem.* **126**, 11396–11399 (2014).
- Weinhold, F. & Klein, R. A. Addendum: Anti-Electrostatic Hydrogen Bonds. *Angew. Chem. Int. Ed.* **53**, 12992 (2014); *Angew. Chem.* **126**, 13207 (2014).
- Knorr, A., Fumino, K., Bansa, A.-M. & Ludwig, R. Spectroscopic evidence of 'jumping and pecking' of cholinium and H-bond enhanced cation-cation interaction in ionic liquids. *Phys. Chem. Chem. Phys.* **17**, 30978–30982 (2015).
- Knorr, A. & Ludwig, R. Spectroscopic Evidence for Clusters of Like-Charged Ions in Ionic Liquids Stabilized by Cooperative Hydrogen Bonding. *Sci. Rep.* **5**, 17505 (2015).
- Knorr, A., Stange, P., Fumino, K., Weinhold, F. & Ludwig, R. *Chem Phys Chem* **17**, 458–462 (2016).
- Strate, A., Niemann, T. & Ludwig, R. Controlling the kinetic and thermodynamic stability of cationic clusters by the addition of molecules or counterion. *Phys. Chem. Chem. Phys.* **19**, 18854–18862 (2017).
- Fumino, K., Wulf, A. & Ludwig, R. The Cation-Anion Interaction in Ionic Liquids Probed by Far-Infrared Spectroscopy. *Angew. Chem. Int. Ed.* **47**, 3830–3834 (2008); *Angew. Chem.* **120**, 3890–3894 (2008).
- Fumino, K., Wulf, A. & Ludwig, R. Strong, Localized, and Directional Hydrogen Bonds Fluidize Ionic Liquids. *Angew. Chem. Int. Ed.* **47**, 8731–8734 (2008); *Angew. Chem.* **120**, 8859–8862 (2008).

22. Lehmann, S. B. C., Roatsch, M., Schöppke, M. & Kirchner, B. On the physical origin of the cation–anion intermediate bond in ionic liquids Part I. Placing a (weak) hydrogen bond between two charges. *Phys. Chem. Chem. Phys.* **12**, 7473–7486 (2010).
23. Pensado, A. S., Costa Gomes, M. J., Canongia Lopes, J. N., Malfreyt, P. & Pádua, A. A. H. Effect of alkyl chain length and hydroxyl group functionalization on the surface properties of imidazolium ionic liquids. *Phys. Chem. Chem. Phys.* **13**, 13518–13526 (2011).
24. Fumino, K. & Ludwig, R. Analyzing the interaction energies between cation and anion in ionic liquids: The subtle balance between Coulomb forces and hydrogen bonding. *J. Mol. Liq.* **192**, 94–102 (2014).
25. Fumino, K., Reimann, S. & Ludwig, R. Probing molecular interaction in ionic liquids by low frequency spectroscopy: Coulomb energy, hydrogen bonding and dispersion forces. *Phys. Chem. Chem. Phys.* **40**, 21903–21929 (2014).
26. Hunt, P. A., Ashworth, C. R. & Matthews, R. P. Hydrogen bonding in ionic liquids. *Chem. Soc. Rev.* **44**, 1257–1288 (2015).
27. Ashwoth, C. R., Matthews, R. P., Welton, T. & Hunt, P. A. Doubly ionic hydrogen bond interactions within the choline chloride–urea deep eutectic solvent. *Phys. Chem. Chem. Phys.* **18**, 18145–18160 (2016).
28. Fumino, K. *et al.* The influence of hydrogen bonding on the physical properties of ionic liquids. *Phys. Chem. Chem. Phys.* **13**, 14064–14075 (2011).
29. Strate, A., Niemann, T., Stange, P., Michalik, D. & Ludwig, R. When Like Charged Ions Attract in Ionic Liquids: Controlling the Formation of Cationic Clusters by the Interaction Strength of the Counterions. *Angew. Chem. Int. Ed.* **56**, 496–500 (2017); *Angew. Chem.* **129**, 510–514 (2017).
30. Nockermann, P. *et al.* Temperature-Driven Mixing–Demixing Behavior of Binary Mixtures of the Ionic Liquid Choline Bis(trifluoromethylsulfonyl)imide and Water. *J. Phys. Chem. B* **113**, 1429–1437 (2009).
31. Menges, F. S. *et al.* Structural Motifs in Cold Ternary Ion Complexes of Hydroxyl-Functionalized Ionic Liquids: Isolating the Role of Cation–Cation Interactions. *J. Phys. Chem. Lett.* **9**, 2979–2984 (2018).
32. Gaussian 09 (Revision B.01), Frisch, M. J. *et al.* see the Supporting Information (2016).
33. Grimme, S., Antony, J., Ehrlich, S. & Krieg, H. A consistent and accurate ab initio parametrization of density functional dispersion correction (DFT-D) for the 94 elements H–Pu. *J. Chem. Phys.* **132**, 154104 (2010).
34. Ehrlich, S., Moellmann, J., Reckien, W., Bredow, T. & Grimme, S. System-Dependent Dispersion Coefficients for the DFT-D3 Treatment of Adsorption Processes on Ionic Surfaces. *Chem Phys Chem.* **12**, 3414–3420 (2011).
35. Grimme, S., Hansen, A., Brandenburg, J. G. & Bannwarth, C. Dispersion-Corrected Mean-Field Electronic Structure Methods. *Chem Rev.* **116**, 5105–5154 (2016).
36. Debenedetti, P. G. & Stillinger, F. H. Supercooled liquids and the glass transition. *Nature* **410**, 259–267 (2001).

Acknowledgements

This work has been supported by the DFG Research Grant LU-506/14-1.

Author Contributions

T.N., D.Z., A.S., A.V. carried out the IR, DSC and X-ray experiments. R.L. performed the quantum chemical calculations. R.L. wrote the main manuscript text and supervised the project. All authors reviewed the manuscript text.

Additional Information

Supplementary information accompanies this paper at <https://doi.org/10.1038/s41598-018-33176-6>.

Competing Interests: The authors declare no competing interests.

Publisher's note: Springer Nature remains neutral with regard to jurisdictional claims in published maps and institutional affiliations.



Open Access This article is licensed under a Creative Commons Attribution 4.0 International License, which permits use, sharing, adaptation, distribution and reproduction in any medium or format, as long as you give appropriate credit to the original author(s) and the source, provide a link to the Creative Commons license, and indicate if changes were made. The images or other third party material in this article are included in the article's Creative Commons license, unless indicated otherwise in a credit line to the material. If material is not included in the article's Creative Commons license and your intended use is not permitted by statutory regulation or exceeds the permitted use, you will need to obtain permission directly from the copyright holder. To view a copy of this license, visit <http://creativecommons.org/licenses/by/4.0/>.

© The Author(s) 2018

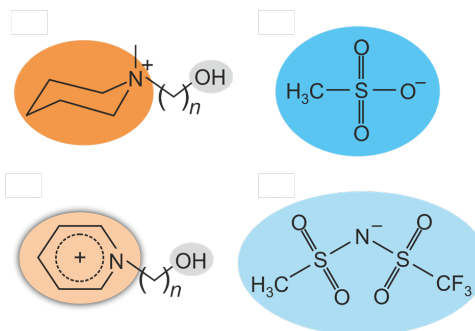
Controlling „like-likes-like“ charge attraction in hydroxy-functionalized ionic liquids by interaction strength of the anions, polarizability of the cations and varying alkyl chain length

T. Niemann (50 %), D. Zaitsau (15 %), A. Strate (10 %), P. Stange (5 %), R. Ludwig (20 %)

submitted to Phys. Chem. Chem. Phys.

Content:

The chain length dependency and its competition with the anion, cation and temperature dependency of the formation of cationic clusters is studied on a large set of ILs. The results provide a comprehensive picture of the structural and thermodynamic effects of cationic clustering.



Contributions to this work:

I have synthesized all ILs investigated in this work and I have done all Mid-IR measurements of the pure ILs. Dzmitry Zaitsau has done the DSC measurements. Anne Strate contributed with the Mid-IR measurements of the mixtures to this work. I wrote the first draft of the paper with Professor Ludwig. Peter Stange and I made some corrections on the draft. Professor Ludwig received the manuscript for final corrections and submission.

Controlling “like-likes-like” charge attraction in hydroxy-functionalized ionic liquids by interaction strength of the anions, polarizability of the cations and varying alkyl chain length

Thomas Niemann,^a Dzmitry H. Zaitsau,^{a,b}, Anne Strate,^{a,b}, Peter Stange,^a and Ralf Ludwig,^{a,b,c*}

^a Universität Rostock, Institut für Chemie, Abteilung für Physikalische Chemie, Dr.-Lorenz-Weg 2, 18059, Rostock, Germany

^b Department LL&M, University of Rostock, Albert-Einstein-Str. 25, 18059, Rostock, Germany

^c Leibniz-Institut für Katalyse an der Universität Rostock e.V., Albert-Einstein-Str. 29a, 18059 Rostock, Germany

We provide comprehensive understanding of “like-likes-like” charge attraction in hydroxy-functionalized ionic liquids (ILs) by means of infrared spectroscopy (IR), quantum chemistry and differential scanning calorimetry (DSC). We show that hydrogen bonding between cation and cation (c-c) is possible despite the repulsive forces between ions of like charge. Already at room temperature, the c-c hydrogen bonds can compete with the regular Coulomb-enhanced hydrogen bonds between cation and anion (c-a). For a large set of well-selected ILs, we show that “like-charge attraction” between the OH-functionalized cations is controllable by the polarizability of the cation, the interaction strength of the anion and the length of the hydroxyalkyl chain. In particular, we clarify whether tethering the OH group away from the positive charge center of the cationic ring with longer hydroxyalkyl chains compensates for unfavourable cation/anion combinations with respect to (c-c) cluster formation. For that purpose, we synthesized and characterized twelve ionic liquids including the differently polarizable cations, 1-(*n*-hydroxyalkyl)-1-methylpiperidinium [HOC_{*n*}MPip]⁺ and 1-(*n*-hydroxyalkyl)-pyridinium [HOC_{*n*}Py]⁺, as well as the weakly and strongly interacting anions, bis(trifluoromethanesulfonyl)imide (NTf₂[−]) and methanesulfonate (OMs[−]), respectively. On top, we varied the hydroxyalkyl chain length (HOC_{*n*}) (*n*=2-5). We systematically show how these three molecular ion parameters affect like-charge attraction. The use of polarizable cations, weakly interacting anions, and long alkyl chain tethers results in (c-c) clustering already at room temperature. Kinetic trapping is not a prerequisite for the existence of (c-c)

cluster species in ILs. Moreover, we demonstrate that micro structuring affects macroscopic behavior of this type of ILs. We observed that substantial (c-c) interaction prevents ILs from crystallizing. Instead, these ILs supercool and finally transition into a glassy state.

Introduction

A look at the literature shows that like-charge interaction has been discussed for almost a century. In the 1930s, Langmuir suggested that the required opposites might come from counter-ions situated between the like-charged particles, thus creating the attractive force.[1] He reported the role of attractive and repulsive forces in the aggregation of like-charged micelles in various sols, gels, and protein crystals. Taking up Langmuir's idea, Feynman emphasised the role of the intermediate counter-charges, sometimes paraphrased as "like-likes-like through an intermediate of unlikes".[2] Ise supported the hypothesis that the attraction of between like-charged entities lies in an intermediate of unlike charges.[3] Recently, Pollack observed attractive forces between widely separated particles of macroscopic size in aqueous solutions.[4] He claimed that "like-charge attraction should be valid not only on the colloidal scale but also at smaller scales possibly down to the nano and molecular levels."

For long time, it has been assumed that large-scale structures, assemblies or stabilizing frameworks are prerequisites for attractive interaction between like-charged ions. For example, Fatila et al. showed that hydrogen bonded anions can stabilize each other inside macrocyclic hosts.[5] They claimed that these dimer salts only survive in supramolecular capsules but probably not in solution. Meanwhile the hypothesis by Pollack is supported by the observation of attractive interaction between ions of like charge observed at molecular level for aqueous salt solutions of K/CsBr, [6] for guanidinium ions in water, [7] and in the micellation of tetraalkylammonium surfactants.[8] However, for smaller systems mediating solvent molecules such as water are required.[9]

Hydrogen bonding for ionic liquids (ILs) is mainly reported between opposite charged ions only.[10-18] Ionic liquids (ILs) attract increasing interest in science and technology due to their unique properties, which can be tailored for specific applications ranging from chemical synthesis and separation processes to media for electrochemical devices.[19-25] The properties of ILs are governed by a subtle balance of Coulombic interactions, hydrogen bonding and dispersion forces.[26,27] In particular, local and directional hydrogen bonding has significant influence on IL behavior,[28,29] leading to classification schemes based on the

character of the doubly ionic hydrogen bonds (DIHB).[30,31] This term is a pleonasm because ILs consist purely of ions and any hydrogen bonding necessarily takes place between ions.

Hydrogen bonding between ions of like-charge has been observed for hydroxyl-functionalized imidazolium cations in ionic liquids by means of from infrared (IR) and molecular dynamics simulations (MD).[32,33] Inspired by this preliminary work we developed a concept for promoting the formation of highly charged cationic clusters in hydroxyl-functionalized ILs.[34-45] The hydroxyl-functionalized ILs allow for two types of hydrogen bonding: One involving the Coulomb-enhanced interaction $\text{O}^{(-)} \cdots \text{H-O}^{(+)}$ between a cation and an anion (c-a), and another occurring between ions of like-charge $\text{O}^{(+)} \cdots \text{H-O}^{(+)}$, which in the present case involves the positively charged cations (c-c). One anticipates, that the (c-a) hydrogen bonds are significantly weaker than the (c-c) hydrogen bonds due to the repulsive Coulomb forces. In ILs, (c-c) hydrogen bonds might not appear to be important drivers of local structures because they have to compete with the repelling Coulomb forces between the cations as well as with the Coulomb enhanced (c-a) hydrogen bonds between cation and anion.

Despite this expectation, however, structural motifs involving H-bonded cationic clusters were observed in the bulk liquid phase.[34-40] In particular, FT-IR measurements clearly showed two distinct vibrational bands that are assigned to (c-a) and (c-c) hydrogen bonded species. It is interesting to note that the (c-c) hydrogen bonds are evidently stronger than those in the (c-a) case as indicated by the magnitudes of the redshifts of their corresponding vibrational bands.[34-40] The formation of these (c-c) clusters is mediated by surrounding counter ions and was observed to become more prominent at lower temperature (~213 K).

In this work, we present our full concept for supporting (c-c) cluster formation in ILs. For that purpose we synthesized hydroxyl-functionalized ILs comprising cations and anions which showed opposite behavior in terms of (c-a) and (c-c) cluster formation. The main goal of this study is to show whether the unfavourable influence of non-polarizable cations and strongly interacting anion for (c-c) like-charge attraction can be overcome by using cations with longer hydroxyalkyl chain length. Moreover, we demonstrate that (c-c) cluster formation prevents ILs from crystallizing. These ILs are supercooled and finally form glasses.

Strategy of this study

The main idea of this work is altering the dielectric background for maximizing cationic cluster formation. For this purpose, we have to create an environment for the hydroxyl groups, wherein hydrogen bonding between ions of like charge is favoured over that between ions of opposite charge, although the latter are usually preferred due to additional attractive Coulomb interaction. In recent studies we showed that the formation of cationic clusters from ILs depends on the polarizability of the cation (with only one interaction site, e.g. one functional group), the interacting strength of the anion, and the distance between the functional group and the positive charge centre of the cation.[34-45] These three dimensions are available for tuning the amount of cationic cluster formation. Based on our preliminary results we selected twelve ILs including cations and anions strongly supporting or suppressing cationic cluster formation. With short hydroxyalkyl chains (HOC_2) the pyridinium cation strengthens, and the piperidinium cation weakens (c-c) hydrogen bonding. On the counter-ion side, the bis(trifluoromethanesulfonyl)imide (NTf_2) anion weakly interacts with the hydroxyl groups of the cation, whereas the methanesulfonate $[\text{OMs}]^-$ anion strongly interacts with the OH groups, resulting in favourable (c-c) hydrogen bonding in the first and (c-a) hydrogen bonding in the latter case. For both cation/anion combinations, we systematically increased the hydroxyalkyl chain length of the cations from ethyl (HOC_2) to pentyl (HOC_5) for testing whether the alkyl chain tether compensates for the negative influence of weakly polarizable cations and/or strongly interacting anions on (c-c) cluster formation (see **Scheme I**).

The goal of our systematic study is manifold. We in particular address the following questions: What is the most relevant factor for cationic cluster formation? How does the equilibrium between (c-a) and (c-c) clusters changes with temperatures? Do the macroscopic properties depend on the alteration of local structures? Hereby, we focus on phase transition: Is the liquid/solid phase transition affected by cationic clustering?

To answer these questions, we have synthesized a suitable set of twelve hydroxy-functionalized ionic liquids (ILs) fulfilling all the requirements for controlling cationic cluster formation. This set includes the ILs 1-(*n*-hydroxyalkyl)pyridinium bis(trifluoromethanesulfonyl)imide $[\text{OHC}_n\text{Py}][\text{NTf}_2]$, 1-(*n*-hydroxyalkyl)-1-methylpiperidinium bis(trifluoromethanesulfonyl)imide $[\text{OHC}_n\text{MPip}][\text{NTf}_2]$ and 1-(*n*-hydroxyalkyl)pyridinium methanesulfonate $[\text{HOC}_n\text{Py}][\text{OMs}]$, wherein all cations are functionalized with HOC_n - groups $n=2,3,4,5$ as illustrated in **Scheme I**.

Results and Discussion

Synthesis of suitable hydroxy-functionalized ionic liquids

We synthesized the ionic liquids 1-(2-hydroxyethyl)-1-methyl-piperidinium bis(trifluoromethanesulfonyl)imide [HOC₂MPip][NTf₂] (**I**), 1-(3-hydroxypropyl)-1-methyl-piperidinium bis(trifluoromethanesulfonyl)imide [HOC₃MPip][NTf₂] (**II**), 1-(4-hydroxybutyl)-1-methyl-piperidinium bis(trifluoromethanesulfonyl)imide [HOC₄MPip][NTf₂] (**III**), 1-(5-hydroxypentyl)-1-methyl-piperidinium bis(trifluoromethanesulfonyl)imide [HOC₅MPip][NTf₂] (**IV**), 1-(2-hydroxyethyl)-pyridinium bis(trifluoromethanesulfonyl)imide [HOC₂Py][NTf₂] (**V**), 1-(3-hydroxypropyl)-pyridinium bis(trifluoromethanesulfonyl)imide [HOC₃Py][NTf₂] (**VI**), 1-(4-hydroxybutyl)-pyridinium bis(trifluoromethanesulfonyl)imide [HOC₄Py][NTf₂] (**VII**), 1-(5-hydroxypentyl)-pyridinium bis(trifluoromethanesulfonyl)imide [HOC₅Py][NTf₂] (**VIII**), 1-(2-hydroxyethyl)-pyridinium methanesulfonate [HOC₂Py][OMs] (**IX**), 1-(3-hydroxypropyl)-pyridinium methanesulfonate [HOC₃Py][OMs] (**X**), 1-(4-hydroxybutyl)-pyridinium methanesulfonate [HOC₄Py][OMs] (**XI**), 1-(5-hydroxypentyl)-pyridinium methanesulfonate [HOC₅Py][OMs] (**XII**).

The ILs were prepared in two steps: We synthesized the OH-functionalized onium halides, which were then used for the anion metathesis to create the desired cation/anion combinations. For the synthesis of the onium salts, we mixed equimolar amounts of the heterocyclic amine and the corresponding *n*-halide-alcohol and heated up to 110 °C for 1 h. In cases of the *n*-halide-alcohols with *n*= 4,5 it is important to protect the hydroxy functional group with a trimethylsilyl protecting group from a cyclization reaction, in advanced. The protecting group can be removed by water treatment. Upon cooling of the onium salt, the mixture started to crystallize. The crude products were recrystallized from acetone/acetonitrile mixtures to obtain the colorless crystalline product. For the anion (bis(trifluoromethylsulfonyl)imide, [NTf₂]⁻) metathesis we mixed equimolar amounts of the onium halide and lithium-bis(trifluoromethylsulfonyl)imide as aqueous solutions for 1 h. Two phases were obtained. The lower phase was washed several times with water until no residual bromine could be detected with silver nitrate solution. The resulting colorless ionic liquids were dried for several hours in vacuum at 60 °C. For the anion (methanesulfonate, [OMs]⁻) metathesis we mixed equimolar amounts of the onium halide and silver methanesulfonate as aqueous solutions. To remove the precipitate silver halide the suspension was then filtered. The obtained colorless solution was dried for several hours in vacuum at 60 °C to remove all volatiles. For detailed synthesis procedures and analytical data of each ILs (see the **SI**).

Hydrogen/deuterium (H/D) exchange was achieved by mixing the ILs with D₂O and removing water several times until nearly 100% deuteration was reached as proven by ¹H

NMR. All samples were dried under vacuum (at $3 \cdot 10^{-3}$ mbar) for several days and the final water concentration (< 15 ppm) was checked by Karl-Fischer titration.

Mid infrared (IR) experiments in the OH stretch region

Mid infrared (MIR) measurements were performed with a Bruker Vertex 70 FTIR spectrometer. An L.O.T.-Oriel variable-temperature cell equipped with CaF_2 windows having a path length of $12 \mu\text{m}$ was used for the variable-temperature experiments between 193 and 353 K. Cooling of the cell is achieved by means of a cooling dewar with liquid ethanol/nitrogen mixture. For each spectrum 128 scans were recorded at a spectral resolution of 1 cm^{-1} .

IR difference spectra provide interference free OH stretch vibrational bands

Using the IL $[\text{HOC}_4\text{Py}][\text{NTf}_2]$ as model system, we describe how to derive and interpret the difference spectra in the OH stretch region. We measured the IR spectra of the IL $[\text{HOC}_4\text{Py}][\text{NTf}_2]$ (blue line) and the IL $[\text{HOC}_4\text{Py-d}_1][\text{NTf}_2]$ (red line) in the frequency range between 2200 cm^{-1} and 3750 cm^{-1} (here at 253 K). As shown in **Fig.1**, we observed distinct spectral bands in the OD stretch region between 2300 cm^{-1} and 2650 cm^{-1} , and in the OH stretch region between 3165 cm^{-1} and 3750 cm^{-1} , respectively. Both ILs show similar C-H vibrational bands of the pyridinium ring and hydroxyalkyl group between 2800 cm^{-1} and 3165 cm^{-1} . Thus, subtracting the spectrum of $[\text{HOC}_4\text{Py-d}_1][\text{NTf}_2]$ from that of $[\text{HOC}_4\text{Py}][\text{NTf}_2]$, and subtracting the spectrum of $[\text{HOC}_4\text{Py}][\text{NTf}_2]$ from that of $[\text{HOC}_4\text{Py-d}_1][\text{NTf}_2]$ results in the IR difference spectra OH-OD (blue dotted line) and OD-OH (red dotted line) as shown at the bottom of **Fig.1**. This way we removed the CH stretches of the pyridinium ring and the hydroxyalkyl group, and excluded interference between CH and OH contributions as indicated by the frequency range between 2800 cm^{-1} and 3165 cm^{-1} (grey area) with almost zero intensity. The slightly different densities of both ILs are negligible, because we only change one D for one H. That this procedure is valid and applicable to all ILs considered in this study, is shown by comparing the OH-OD difference spectra (blue dotted line) with the spectrum of $[\text{HOC}_4\text{Py-d}_{13}][\text{NTf}_2]$ (d13, orange area), wherein the C-H contributions are shifted to lower frequency due to deuteration of the pyridinium ring and the hydroxyalkyl group. In **Fig.2**, we show that both IR spectra agree perfectly in the OH stretch region, justifying the approach for getting unperturbed OH vibrational bands by removing the C-H vibrational bands.

Interpretation of the OH stretch region: c-a and c-c vibrational bands

It is clearly shown in **Figs.1** and **2**, that the OH stretch region of the IL $[\text{HOC}_4\text{Py}][\text{NTf}_2]$ is characterized by a vibrational band at 3550 cm^{-1} and a significantly redshifted band at 3380 cm^{-1} , respectively. In accord with recent work, we assigned the high frequency band to the $^+\text{OH}\cdots\text{O}^-$ hydrogen bond between cation and anion (c-a), and the low frequency band to the $^+\text{OH}\cdots\text{O}^+$ hydrogen bond between cationic (c-c). For demonstrating that this assignment is reasonable, we recorded the IR spectra of $[\text{HOC}_4\text{Py}][\text{NTf}_2]$ and $[\text{C}_5\text{Py}][\text{NTf}_2]$ mixtures. Starting with 10 mol% of $[\text{HOC}_4\text{Py}][\text{NTf}_2]$, we constantly increased the number of the OH oscillators in 30 mol%, 50 mol%, 70 mol% and 90 mol% mixtures and finally in the pure 100% hydroxyl-functionalized IL. In **Fig.3a**, we show how the spectral bands change with increasing OH density. If the concentration of OH oscillators is low as in the 10mol% mixture, only the formation of (c-a) hydrogen bonds is possible indicated by large absorbance at 3550 cm^{-1} and almost no absorbance below. This situation changes visibly with increasing number of OH oscillators. The (c-a) vibrational bands increase but to minor extend for the benefit of a new strongly growing vibrational band significantly redshifted of about $\Delta\tilde{\nu}=200\text{ cm}^{-1}$. Such a vibrational band of OH oscillators can stem only from $^+\text{OH}\cdots\text{O}^+$ hydrogen bonding between cation and anion, and thus (c-c) cluster formation. In **Fig.3b**, we show exclusively the IR spectra of the 10 mol% mixture (full red line) and the pure IL (full blue line). Multiplying the OH vibrational band of the 10 mol% mixture (showing only (c-a) interaction) by ten results in an artificial vibrational band (dotted red line) representing exclusively (c-a) interaction in the pure IL. **Fig.3b** clearly shows that (c-a) cluster formation does not increase linearly with the number of OH oscillators, but grows less for the benefit of increasing (c-c) cluster formation.

Temperature dependence of (c-a) and (c-c) cluster formation: kinetic trapping?

Before studying the influence of different cations, anions and chain lengths on the cationic cluster formation for the whole set of ILs, we discuss the typical temperature dependence of the IR spectra for the model IL $[\text{HOC}_4\text{Py}][\text{NTf}_2]$. In **Fig. 4** we show the IR spectra as a function of temperature between 193 K and 353 K recorded in intervals of 20 K. As discussed later in detail, this IL exhibits redshifted vibrational bands assigned to (c-c) clusters already at the highest temperature at 353 K. Thus, kinetic trapping does not seem to be a prerequisite for (c-c) cluster formation in this type of IL with polarizable cation, weakly interacting anion and

sufficiently long hydroxyalkyl chains. We observe that the (c-a) vibrational band at 3550 cm^{-1} decreases in intensity and shifts to slightly lower wavenumbers with decreasing temperature. As expected, the (c-a) hydrogen bonds become stronger at low temperatures. However, the intensity of the c-a band strongly decreases to the benefit of substantially enhanced, redshifted vibrational bands indicating (c-c) cluster formation. At the lowest temperatures, we observe a pronounced minimum between the (c-a) and (c-c) vibrational bands allowing for the determination of the (c-a) and (c-c) cluster equilibria. In later chapter we describe how the temperature dependent equilibria behave with the molecular ion parameters.

DFT-calculated OH stretch frequencies of (c-a) and (c-c) clusters

The unexpected result that the (c-c) hydrogen bonds are stronger than the (c-a) hydrogen bonds despite the repulsive in the first and attractive Coulomb interaction in the latter case, is supported by density functional (DFT) calculations. We optimized (c-a) and (c-c) clusters of $[\text{HOC}_4\text{Py}][\text{NTf}_2]$ up to the size of tetramers at the B3LYP-D3/6-31+G* level of theory.[46-50] We have used the well-balanced, but small 6-31+G* basis set. It includes polarization as well as diffuse functions, and has been shown to be suitable for calculating hydrogen-bonded clusters of like-charged ions. The 6-31+G* basis set is also chosen for better comparison with earlier studies of molecular and ionic clusters.[51-54] We calculated the OH frequencies on the fully optimized (c-a) and (c-c) clusters. They were all positive, showing that we calculated at least local minimum structures. In **Fig. 5**, we show the calculated OH frequencies corrected for the harmonic approximation (scaling factor 0.976). The frequencies of (c-a) interaction in (c-a) monomers ($^+\text{OH}\cdots\text{O}^-$) or (c-c) linear dimers ($^+\text{OH}\cdots^+\text{OH}\cdots\text{O}^-$) and trimers ($^+\text{OH}\cdots^+\text{OH}\cdots^+\text{OH}\cdots\text{O}^-$) including one OH interaction with the oxygen (O^-) of the anion are shown by the open symbols. Describing the same type of (c-a) interaction, these frequencies are very close and nicely mimic the measured vibrational band at about 3550 cm^{-1} assigned to Coulomb enhanced hydrogen bonding between cation and anion (see **Fig.5**). The calculated ($^+\text{OH}\cdots^+\text{OH}$) frequencies in the (c-c) linear dimer, linear trimer and cyclic tetramer (given by the filled symbols) are strongly redshifted with increasing cluster size. In particular, the calculated frequencies of the cyclic tetramer almost perfectly cover the measured spectral range attributed to the cationic clusters. Of course, the broad c-c vibrational band between 3100 cm^{-1} and 3450 cm^{-1} hides the spectral signatures of differently sized and bound (c-c) clusters, and we do not know the exact cluster populations. However, that the calculated (c-a) frequencies describe the dominant vibrational band at high temperature (353 K), and the

calculated (c-c) frequencies characterize the dominant broad redshifted vibrational band at low temperature (193 K), is clear evidence for our (c-a) and (c-c) cluster assignment. As shown in **Fig.5**, we can also claim that the measured redshifted bands are assignable to larger (c-c) clusters than dimers and trimers.

Cation dependence of (c-c) cluster formation

For studying the cation dependence for (c-c) cluster formation in hydroxyl-functionalized ILs we measured the IR spectra of 1-(*n*-hydroxyalkyl)-1-methyl-piperidinium bis(trifluoromethanesulfonyl)imide ILs $[\text{HOC}_n\text{MPip}][\text{NTf}_2]$ and 1-(*n*-hydroxyalkyl)-pyridinium bis(trifluoromethanesulfonyl)imide ILs $[\text{HOC}_n\text{Py}][\text{NTf}_2]$, both with hydroxyalkyl chain lengths $n=2-5$. We show the spectra of both sets of ILs measured at 293 K in **Fig.6a** and **Fig.6b**, respectively. We observe a weak cation dependence for (c-c) cluster formation, best pronounced for the shortest hydroxyalkyl chains. For the spectrum of $[\text{HOC}_2\text{Py}][\text{NTf}_2]$ we observe slightly higher intensity in the (c-c) frequency range between 3100 cm^{-1} and 3450 cm^{-1} (indicated by the gray bar) than for that of $[\text{HOC}_n\text{MPip}][\text{NTf}_2]$. In accord with earlier findings, charge delocalization in the piperidinium cation is hardly possible and the interaction between the positively charged piperidinium ring and the $[\text{NTf}_2]^-$ anion is less favorable resulting dominantly in c-a cluster formation. In contrast, the pyridinium cation is better polarizable allowing for enhanced interaction with the counter ion. This way the anion is kept away from the OH group of the cation, which is then available for (c-c) hydrogen bonding and cluster formation. In **Fig.6a,b**, we also show that the small cationic effect on (c-c) cluster formation almost disappears with increasing length of the hydroxyalkyl chain.

Anion dependence of (c-c) cluster formation

For studying the anion dependence for (c-c) cluster formation in hydroxyl-functionalized ILs we measured the IR spectra of 1-(*n*-hydroxyalkyl)-pyridinium bis(trifluoromethanesulfonyl)imide ILs $[\text{HOC}_n\text{Py}][\text{NTf}_2]$ and 1-(*n*-hydroxyalkyl)-pyridinium methanesulfonate ILs $[\text{HOC}_n\text{Py}][\text{OMs}]$ with alkyl chain lengths $n=2-5$. The IR spectra of ILs $[\text{HOC}_n\text{Py}][\text{NTf}_2]$ we presented in **Fig.6b**. They show spectral signatures for (c-c) cluster formation already at room temperature (293 K). Here, we have favorable cation/anion combinations: a polarizable pyridinium cation is combined with a hydrophobic, weakly interacting $[\text{NTf}_2]^-$ anion, resulting in weaker (c-a) hydrogen bonds and competitive (c-c) interaction. The (c-c) cluster formation is further supported by introducing longer hydroxyalkyl chain tethers between the positively charged pyridinium ring and the OH

functional group. For studying the anion dependence for cationic cluster formation we used a strongly interacting anion such as methane sulfonate $[\text{OMs}]^-$. In **Fig.7** we show the IR spectra of $[\text{HOC}_n\text{Py}][\text{OMs}]$ with alkyl chain lengths $n=3-5$. The IL $[\text{HOC}_2\text{Py}][\text{OMs}]$ is solid at room temperature and not considered here. IR spectra of the liquid IL could be recorded only above 373 K (see SI). We observe that (c-c) cluster formation is completely suppressed in the case of strongly interacting anion, which prefer to form strong (c-a) hydrogen bonds instead. That the (c-a) spectral bands of $[\text{HOC}_2\text{Py}][\text{OMs}]$ are found in the frequency range between 3100 cm^{-1} and 3550 cm^{-1} , wherein we observed the (c-c) spectral features before, is attributed to the strongly interacting anion resulting in enormous redshifts of these bands. Regardless of the hydroxyalkyl chain lengths the vibrational bands remain symmetric and exhibit comparable intensity. As typical for c-a hydrogen bonding, the vibrational bands are redshifted and stronger enhanced for the IL with the shorter hydroxyalkyl chain. Even if we take differently OH densities for the ILs $[\text{HOC}_n\text{Py}][\text{OMs}]$ into account, this situation doesn't change (see SI). Here, we can conclude that strongly interacting anions result exclusively in (c-a) hydrogen bonding, even in the presence of polarizable cations with long hydroxyalkyl chain tethers.

Chain length dependence of (c-c) cluster formation

It was the main purpose of this study to clarify whether tethering the OH group away from the positive charge center of the cationic ring with longer hydroxyalkyl chains compensates for unfavourable cation/anion combinations with respect to (c-c) cluster formation. Thus, we show the IR spectra for the full set of ILs considered in this study separately for $[\text{HOC}_2^-]$, $[\text{HOC}_3^-]$, $[\text{HOC}_4^-]$ and $[\text{HOC}_5^-]$ decorated cations in **Figs.8a-d**. For two sets of ILs, namely $[\text{HOC}_n\text{MPip}][\text{NTf}_2]$ and $[\text{HOC}_n\text{Py}][\text{NTf}_2]$, the intensities indicating (c-c) cluster formation constantly increase with longer hydroxyalkyl chains. Obviously any combination of a weakly interacting anion, here $[\text{NTf}_2]^-$, with a hydroxyl-functionalized cation show at least little (c-c) cluster formation. The slight preference for (c-c) interaction of polarizable versus hard cations disappears with increasing hydroxyalkyl chain length. As clearly observed in **Fig.8a-d**, the presence of a strongly interacting anion such as methanesulfonate completely suppresses (c-c) cluster formation and results solely in (c-a) hydrogen bonding regardless of long alkyl chain tethers. This is clearly demonstrated in **Fig.9**, wherein we show the temperature dependent IR spectra of $[\text{HOC}_5\text{Py}][\text{OMs}]$ between 193 K and 353 K. Although including a polarizable cation with a long hydroxypentyl chain, we observe no (c-c) cluster formation for this IL. The symmetric shape of the vibrational band is temperature independent. Moreover, the maximum of the IR band is stronger redshifted and its intensity

further enhanced with decreasing temperature. This kind of temperature behavior is found, if only one type of hydrogen-bonded species is present in the IL, here the (c-a) clusters.

Van't Hoff like behavior of c-a and c-c cluster equilibrium

In the next step, we estimated the transition enthalpies needed to break the (c-c) hydrogen bonds shifting the equilibrium from (c-c) towards (c-a) species. We are aware that several (c-c) cluster species exist and that they transform into each other. Nevertheless, we consider the temperature dependence of the “equilibrium constant K ” as van't Hoff like:

$$\ln(K) = -\frac{\Delta_R G^\theta}{RT} = -\frac{\Delta_R H^\theta}{RT} + \frac{\Delta_R S^\theta}{R}$$

In particular, at low temperatures, ΔH^θ and ΔS^θ change with temperature. However, we applied the following procedure for describing the (c-c) to (c-a) transition as a function of the polarizability of the cation, the interaction strength of the anion and the alkyl chain lengths. We assume that the cation-anion (I_{c-a}) and the cation-cation (I_{c-c}) hydrogen bond IR intensities arise from cations of these two general classes of H-bonding configurations, for which relative populations are a function of absolute temperature only. Consequently, a plot of $\ln(I_{c-a}/I_{c-c})$ versus $1/T$ should yield a straight line with a negative slope that is proportional to the average difference in energy between the two classes of H-bond configurations. All ILs show an almost linear dependence between $\ln(I_{c-a}/I_{c-c})$ and $1000/T$. For the linear regression, we only excluded the data points at the lowest temperature (193 K). A negative slope and thus positive $\Delta_R H^\theta$ show that cationic cluster formation is enthalpically favored (see **Table 1**). This is the case for ILs $[\text{HOC}_n\text{MPip}][\text{NTf}_2]$ and $[\text{HOC}_n\text{Py}][\text{NTf}_2]$ with $n=2-5$ (see **Fig. 10a,b**). In accord with the findings above, the $\Delta_R H^\theta$ values increase with increasing hydroxyalkyl chain lengths due to enhanced (c-c) cluster formation. The $\Delta_R H^\theta$ of IL $[\text{HOC}_2\text{Py}][\text{NTf}_2]$ is larger than that of IL $[\text{HOC}_2\text{MPip}][\text{NTf}_2]$ because the more polarizable pyridinium cation stronger promotes c-c clustering as observed in the IR spectra (see Fig.6a,b). The $\Delta_R H^\theta$ values for both types of ILs become similar with increasing hydroxyalkyl chain lengths overcoming the cation effect for (c-c) cluster formation. For all ILs $[\text{HOC}_n\text{Py}][\text{OMs}]$ consisting the strongly interacting anion $[\text{OMs}]^-$ we obtain $\Delta_R H^\theta$ values of almost zero within the experimental error indicating that the presence of (c-a) clusters is independent of temperature. The entropies $\Delta_R S^\theta$ for ILs $[\text{HOC}_n\text{MPip}][\text{NTf}_2]$ and $[\text{HOC}_n\text{Py}][\text{NTf}_2]$ successively increase from $n=2$ to $n=5$. Obviously, larger structures, here (c-c) clusters, are

formed with increasing chain length as observed in the strongly redshifted and enhanced vibrational bands assigned to (c-c) cluster formation. The similar entropies $\Delta_R S^\theta$ for all ILs [HOC_nPy][OMs] show that the size of the structures are not changing with temperature which is in accord with the presence of exclusively (c-a) hydrogen bonded species.

Crystallization or supercooling – (c-c) cluster formation prevents crystallization

The differential scanning calorimetry (DSC) traces of all ILs **I-XII** as shown in **Fig.11a-c** strongly support the interpretation of the IR spectra (see also **SI**). The DSC measurements were carried out by using a Mettler Toledo DSC 822e with a Huber TC100MT cooler under N₂ atmosphere. The samples for DSC measurements were tightly sealed in Al pans of 40 µl volume. All handling operations with sample were carried out in a glove-box under a nitrogen atmosphere (residual concentrations of oxygen 1.0 ppm and water 0.3 ppm). Pans and samples were weighted with Sartorius MSE3.6P-000-DM microbalances with the standard uncertainty of 5·10⁻⁶ g. The calibration of Mettler Toledo DSC 822e was checked with melting behavior of the reference samples of indium, *n*-octane, and double-distilled water. The temperature of fusion agreed with recommended value better than 0.3 K and the fusion enthalpy within 0.2 kJ·mol⁻¹. Thermograms were recorded during cooling (373-193 K) and heating (193-373 K) at cooling and heating rates of 1, 5, and 10 K·min⁻¹. The glass transition temperature (*T_g*, middle point of the heat capacity change), crystallization temperature (*T_c*), and melting temperature (*T_{fus}*) were determined from DSC thermograms during the heating scans (see **Table 2**).

During cooling from 373 to 193 K at 10 K·min⁻¹ cooling rates, heat capacity change corresponding to glass transitions (*T_g*) could be observed in the DSC profiles of ILs [HOC_nMPip][NTf₂] with *n*=3-5 and [HOC_nPy][NTf₂] with *n*=2-5. The supercooled state of the (c-c) cluster-forming ILs is obviously fairly stable. In contrast, the phase transition behavior is complex for IL [HOC₂MPip][NTf₂], including melting (*T_{fus}*=276.2 K) and solid/solid phase transitions (*T_{ss}*= 266.2 K and *T_{ss}*= 251.6 K). For ILs [HOC_nPy][OMs] with *n*=2-4 we observe clear melting transitions at *T_{fus}*=362.1 K, *T_{fus}*=301.5 K and *T_{fus}*=325.7 K, respectively.

Obviously, strong formation of cationic clusters in ILs results in supercooling and glass transition, whereas (c-a) cluster formation leads to liquid/solid phase transition. From the combined IR and DSC experiments, we have clear evidence that the formation of cationic clusters prevents the ILs from crystallization and liquid/solid phase transition. The resulting

material is a glass.[55] Our findings suggest that the phase behavior of this type of ILs can be controlled by cationic cluster formation.

Conclusion

In this work, we showed for a well-suited set of hydroxy-functionalized ILs that the formation of cationic clusters can be supported by polarizable cations, weakly interacting anions and lengthening of the hydroxyalkyl chains. IR spectra provided evidence that for some cation/anion combinations (c-c) cluster formation can successfully compete with (c-a) cluster formation already at room temperature and that kinetic trapping is not a prerequisite for like-charge attraction. Strong cooperative hydrogen bonds between the hydroxyl functional groups are capable to overcome the repulsive Coulomb forces between the cations. In particular, we showed that tethering the OH functional group away from the positively charged ring of the cations allows (c-c) cluster formation for ILs with hardly polarizable cations but not for those with strongly interacting anions. ILs with these anions form (c-a) hydrogen bonds exclusively, even if the cation has a long hydroxypentyl chain. Then, (c-a) interaction is strongly enhanced by attractive Coulomb forces and (c-c) bound species are not formed. The van't Hoff plots for the temperature dependent equilibria of (c-a) and (c-c) cluster species clearly show in which way the three molecular ion parameters (cation, anion and hydroxyalkyl chain) promote or suppress (c-c) cluster formation. We also provide evidence that (c-c) micro structuring has an influence on macroscopic properties of ILs such as phase behavior. The measured DSC traces clearly show that the ILs forming substantial amounts of (c-c) clusters do not tend to crystallize and rather form glasses.

References:

- [1] I. Langmuir, *J. Chem. Phys.* **1938**, 6, 873-896.
- [2] R. P. Feynman, R. B. Leighton, M. Sands, *The Feynman Lecture on Physics*, Addison-Wesley, Reading, MA, **1963**, ch. 2, p. 2.
- [3] N. Ise, T. Okubo, *Acc. Chem. Res.* **1980**, 13, 303.
- [4] E. Nagornyak, H. Yoo, G. H. Pollack, *Soft Matter* **2009**, 3850-3857.
- [5] E. M. Fatila, E. B. Twum, A. Sengupta, M. Pink, J. A. Karty, K. Raghavachari, A. H. Flood, *Angew. Chem. Int. Ed.* **2016**, 55, 14057-14062; *Angew. Chem.* **2016**, 128, 14263–14268.

- [6] M. Holz, K. J. Patil, *Ber. Bunsen-Ges.* **1991**, 95, 107–113.
- [7] O. Shih, A. H. England, G. C. Dallinger, J. W. Smith, K. C. Duffey, R. C. Cohen, D. Prendergast, R. J. Saykally, *J. Chem. Phys.* **2013**, 139, 035104.
- [8] M. Benrraou, B. L. Bales, R. Zana, *J. Phys. Chem. B* **2003**, 107, 13432–13440, and references therein.
- [9] T. Inagaki, S. Aono, H. Nakano, T. Yamamoto, *J. Phys. Chem. B* **2014**, 118, 5499–5508;
- [10] K. Fumino, A. Wulf, R. Ludwig, *Angew. Chem* **2008**, 120, 3890–3894; *Angew. Chem. Int. Ed.* **2008**, 47, 3830–3834.
- [11] K. Fumino, A. Wulf, R. Ludwig, *Angew. Chem* **2008**, 120, 8859–8862; *Angew. Chem. Int. Ed.* **2008**, 47, 8731–8734.
- [12] Sebastian B. C. Lehmann, Martin Roatsch, Matthias Schöppke and Barbara Kirchner, *Phys. Chem. Chem. Phys.*, **2010**, 12, 7473–7486.
- [13] A. S. Pensado, M. F. Costa Gomes, J. N. Canongia Lopes, P. Malfreyt, A. A. H. Pádua, *Phys. Chem. Chem. Phys.* **2011**, 13, 13518–13526.
- [14] K. Fumino, R. Ludwig, *J. Mol. Liq.* **2014**, 192, 94–102.
- [15] K. Fumino, S. Reimann, R. Ludwig, *Phys. Chem. Chem. Phys.*, **2014**, 40, 21903–21929.
- [16] P. A. Hunt, C. R. Ashworth, R. P. Matthews, *Chem. Soc. Rev.* **2015**, 44, 1257–1288.
- [17] C. R. Ashwoth, R. P. Matthews, T. Welton, P. A. Hunt, *Phys. Chem. Chem. Phys.* **2016**, 18, 18145–18160.
- [18] K. Fumino, T. Peppel, M. Geppert-Rybczynska, D. H. Zaitsau, J. K. Lehmann, S. P. Verevkin, M. Köckerling, R. Ludwig, *Phys. Chem. Chem. Phys.* **2011**, 13, 14064–14075.
- [19] H. Weingärtner, *Angew. Chem. Int. Ed.* **2008**, 47, 654–670; *Angew. Chem.* **2008**, 120, 664–682.
- [20] F. Endres, S. Z. El Abedin, *Phys. Chem. Chem. Phys.* **2006**, 8, 2101–2116.
- [21] T. Welton, *Chem. Rev.* 1999, 99, 2077–2084.
- [22] N. V. Plechkova, K. R. Seddon, *Chem. Soc. Rev.* **2008**, 37, 123.
- [23] Sónia P. M. Ventura, Francisca A. e Silva, Maria V. Quental, Dibyendu Mondal, Mara G. Freire, and João A. P. Coutinho, *Chem. Rev.* **2017**, 117, 6984–7052.
- [24] Maciej Galiński, Andrzej Lewandowski, Izabela Stępnia, *Electrochim. Acta.* **2006**, 51, 5567–5580.

- [25] S. Mennea, J. Piresb, M. Anoutib, A. Balducci, *Electrochem. Commun.* **2013**, 31, 39–41.
- [26] K. Fumino, R. Ludwig, *J. Mol. Liq.* **2014**, 192, 94–102.
- [27] K. Fumino, S. Reimann, R. Ludwig, *Phys. Chem. Chem. Phys.* **2014**, 40, 21903–21929.
- [28] K. Fumino, A. Wulf, R. Ludwig, *Angew. Chem. Int. Ed.* **2008**, 47, 8731–8734.
- [29] K. Fumino, T. Peppel, M. Geppert-Rybczyńska, D. H. Zaitsau, J. K. Lehmann, S. P. Verevkin, M. Köckerling, R. Ludwig, *Phys. Chem. Chem. Phys.* **2011**, 13, 14064–14075.
- [30] P. A. Hunt, C. R. Ashworth, R. P. Matthews, *Chem. Soc. Rev.* **2015**, 44, 125.
- [31] C. R. Ashworth, R. P. Matthews, T. Welton, P. A. Hunt, *Phys. Chem. Chem. Phys.* **2016**, 18, 18145–18160.
- [32] S. A. Katsyuba, M. V. Vener, E. E. Zvereva, Z. F. Fei, R. Scopelliti, G. Laurenczy, N. Yan, E. Paunescu, P. J. Dyson, *J. Phys. Chem. B* **2013**, 117, 9094–9105.
- [33] M. Fakhraee, B. Zandkarimi, H. Salari, M. R. Gholami, *J. Phys. Chem. B* **2014**, 118, 14410–14428.
- [34] A. Knorr, K. Fumino, A.-M. Bonsa, R. Ludwig, *Phys. Chem. Chem. Phys.* **2015**, 17, 30978 – 30982.
- [35] A. Knorr, R. Ludwig, *Sci. Rep.* **2015**, 5, 17505.
- [36] A. Knorr, P. Stange, K. Fumino, F. Weinhold, R. Ludwig, *ChemPhysChem* **2016**, 17, 458–462.
- [37] A. Strate, T. Niemann, P. Stange, D. Michalik, R. Ludwig, *Angew. Chem. Int. Ed.* **2017**, 56, 496 –500; *Angew. Chem.* **2017**, 129, 510 –514.
- [38] A. Strate, T. Niemann, D. Michalik, R. Ludwig, *Angew. Chem., Int. Ed.* **2017**, 56, 496–500; *Angew. Chem.* **2017**, 129, 510 –514.
- [39] A. Strate, T. Niemann, R. Ludwig, *Phys. Chem. Chem. Phys.* **2017**, 19, 18854–18862
- [40] T. Niemann, D. Zaitsau, A. Strate, A. Villinger, R. Ludwig, *Sci. Rep.* **2018**, 8, 14753.
- [41] F. S. Menges, H. J. Zeng, P. J. Kelleher, O. Gorlova, M. A. Johnson, T. Niemann, A. Strate, R. Ludwig, *J. Phys. Chem. Lett.* **2018**, 9, 2979–2984.
- [42] T. Niemann, A. Strate, R. Ludwig, H. J. Zeng, F. S. Menges, M. A. Johnson, *Angew. Chem., Int. Ed.* **2018**, 57, 15364–15368; *Angew. Chem.* **2018**, 130, 15590–15594.
- [43] A. Strate, V. Overbeck, V. Lehde, J. Neumann, A. M. Bonsa, T. Niemann, D. Paschek, D. Michalik, R. Ludwig, *Phys. Chem. Chem. Phys.* **2018**, 20, 5617–5625.
- [44] T. Niemann, A. Strate, R. Ludwig, H. J. Zeng, F. Menges, M. A. Johnson, *Phys.*

- Chem. Chem. Phys.* **2019**, 21, 18092-18098.
- [45] T. Niemann, J. Neumann, P. Stange, S. Gärtner, T. G. A. Youngs, D. Paschek, R. Atkin, R. Ludwig, *Angew. Chem. Int. Ed.* **2019**, 58, 12887-12892; *Angew. Chem.* **2019**, 131, 13019-13024.
- [46] Gaussian 09, Revision A.02, M. J. Frisch, G. W. Trucks, H. B. Schlegel, G. E. Scuseria, M. A. Robb, J. R. Cheeseman, G. Scalmani, V. Barone, G. A. Petersson, H. Nakatsuji, X. Li, M. Caricato, A. Marenich, J. Bloino, B. G. Janesko, R. Gomperts, B. Mennucci, H. P. Hratchian, J. V. Ortiz, A. F. Izmaylov, J. L. Sonnenberg, D. Williams-Young, F. Ding, F. Lipparini, F. Egidi, J. Goings, B. Peng, A. Petrone, T. Henderson, D. Ranasinghe, V. G. Zakrzewski, J. Gao, N. Rega, G. Zheng, W. Liang, M. Hada, M. Ehara, K. Toyota, R. Fukuda, J. Hasegawa, M. Ishida, T. Nakajima, Y. Honda, O. Kitao, H. Nakai, T. Vreven, K. Throssell, J. A. Montgomery, Jr., J. E. Peralta, F. Ogliaro, M. Bearpark, J. J. Heyd, E. Brothers, K. N. Kudin, V. N. Staroverov, T. Keith, R. Kobayashi, J. Normand, K. Raghavachari, A. Rendell, J. C. Burant, S. S. Iyengar, J. Tomasi, M. Cossi, J. M. Millam, M. Klene, C. Adamo, R. Cammi, J. W. Ochterski, R. L. Martin, K. Morokuma, O. Farkas, J. B. Foresman, and D. J. Fox, Gaussian, Inc., Wallingford CT, 2016.
- [47] S. Grimme, J. Antony, S. Ehrlich, H. Krieg, *J. Chem. Phys.* **2010**, 132, 154104.
- [48] S. Ehrlich, J. Moellmann, W. Reckien, T. Bredow, S. Grimme, *ChemPhysChem* **2011**, 12, 3414-3420.
- [49] S. Grimme, A. Jansen, J. G. Brandenburg, C. Bannwarth, *Chem. Rev.* **2016**, 116, 5105-5154.
- [50] R. Ludwig, *Phys. Chem. Chem. Phys.* **2002**, 4, 5481-5487.
- [51] K. M. Murdoch, T. D. Ferris, J. C. Wright, T. C. Farrar, *J. Chem. Phys.* **2002**, 116, 5717.
- [52] R. Ludwig, *ChemPhysChem* **2005**, 6, 1369-1375.
- [53] A. Strate, T. Niemann, R. Ludwig, *Phys. Chem. Chem. Phys.* **2017**, 19, 18854-18862
- [54] T. Niemann, D. Zaitsau, A. Strate, A. Villinger, R. Ludwig, *Sci. Rep.* **2018**, 8, 14753.
- [55] Debenedetti, P. G., Stillinger, F. H., Supercooled liquids and the glass transition. *Nature* **2001**, 410, 259-267.

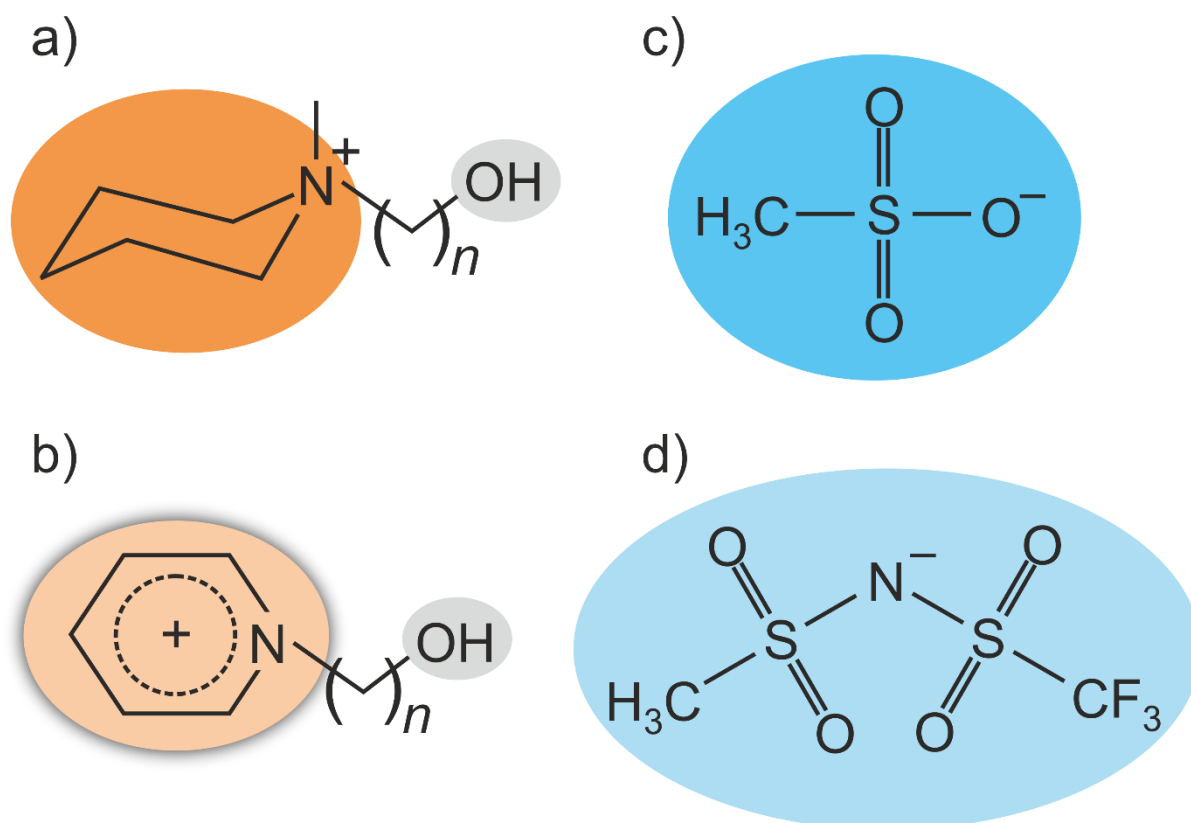
Table 2. The thermodynamic parameters of observed phase transitions for studied ILs.

Ionic liquid	Phase transition	T_{trs} , K	$\Delta_{\text{trs}}H^{\circ}_{\text{m}}$, kJ·mol ⁻¹	Comments
[HOC ₂ Py][CH ₃ SO ₃]	cr - liquid	362.1 ± 0.1	25.1 ± 0.1	
[HOC ₃ Py][CH ₃ SO ₃]	glass-liquid	214.7 ± 0.2 (1 K·min ⁻¹) 216.7 ± 0.3 (5 K·min ⁻¹) 217.6 ± 0.1 (10 K·min ⁻¹) 301.5 ± 0.1	- 15.0 ± 0.2	The crystallinity of the sample was ~ 95%
[HOC ₄ Py][CH ₃ SO ₃]	glass-liquid cr-liquid	213.4 ± 0.3 (1 K·min ⁻¹) 214.8 ± 0.2 (5 K·min ⁻¹) 216.3 ± 0.2 (10 K·min ⁻¹) 325.7 ± 0.2	- 27.3 ± 0.2	
[HOC ₅ Py][CH ₃ SO ₃]	glass-liquid	220.3 ± 0.5 (1 K·min ⁻¹) 221.8 ± 0.1 (5 K·min ⁻¹) 222.7 ± 0.5 (10 K·min ⁻¹)	-	
[HOC ₃ Py][NTf ₂]	glass-liquid	197.6 ± 0.1 (1 K·min ⁻¹) 199.8 ± 0.1 (5 K·min ⁻¹) 200.6 ± 0.1 (10 K·min ⁻¹)	-	
[HOC ₄ Py][NTf ₂]	glass-liquid	221.5 ± 0.2 (1 K·min ⁻¹) 222.8 ± 0.4 (5 K·min ⁻¹) 224.2 ± 0.1 (10 K·min ⁻¹)	-	
[HOC ₅ Py][NTf ₂]	glass-liquid	207.8 ± 0.5 (1 K·min ⁻¹) 208.7 ± 0.3 (5 K·min ⁻¹) 209.6 ± 0.1 (10 K·min ⁻¹)	-	
[HOC ₃ MPip][NTf ₂]	glass-liquid	204.4 ± 0.3 (1 K·min ⁻¹) 205.5 ± 0.1 (5 K·min ⁻¹) 206.8 ± 0.1 (10 K·min ⁻¹)	-	
[HOC ₄ MPip][NTf ₂]	glass-liquid	205.2 ± 0.1 (1 K·min ⁻¹) 205.8 ± 0.7 (5 K·min ⁻¹) 207.1 ± 0.3 (10 K·min ⁻¹)	-	
[HOC ₅ MPip][NTf ₂]	glass-	212.8 ± 0.3 (1 K·min ⁻¹)	-	

liquid	214.3 ± 0.6 (5 K·min ⁻¹)
	215.3 ± 0.1 (10 K·min ⁻¹)

Table 1. Enthalpies $\Delta_R H^\theta$ and entropies $\Delta_R S^\theta$ for the equilibrium between c-a and c-a cluster species in the ILs **I-XII**.

	$\Delta_R H^\theta$ kJmol ⁻¹	$\Delta_R S^\theta$ Jmol ⁻¹ K ⁻¹
[HOC ₂ MPip][NTf ₂]	2.644	1.772
[HOC ₃ MPip][NTf ₂]	7.8983	3.452
[HOC ₄ MPip][NTf ₂]	8.821	3.742
[HOC ₅ MPip][NTf ₂]	9.5860	3.824
[HOC ₂ Py][NTf ₂]	5.471	2,756
[HOC ₃ Py][NTf ₂]	7.565	3.396
[HOC ₄ Py][NTf ₂]	9.079	3.535
[HOC ₅ Py][NTf ₂]	9.212	3.745
[HOC ₂ Py][OMs]	-	-
[HOC ₃ Py][OMs]	-1.413	1.261
[HOC ₄ Py][OMs]	-0.524	1.692
[HOC ₅ Py][OMs]	0.150	2.085



Scheme I: a) 1-(*n*-hydroxyalkyl)-1-methyl piperidinium and b) 1-(*n*-hydroxyalkyl)pyridinium cations, c) bis(trifluoromethanesulfonyl)imide and d) methanesulfonate anions as constituents of the ILs [HOC_{*n*}MPip][NTf₂], [HOC_{*n*}Py][NTf₂] and [HOC_{*n*}Py][OMs] with *n*=2-5. The two cations differ in polarizability and the two anions exhibit different interaction strength. Moreover, we study (c-c) cluster formation by variation of the hydroxyalkyl chain length.

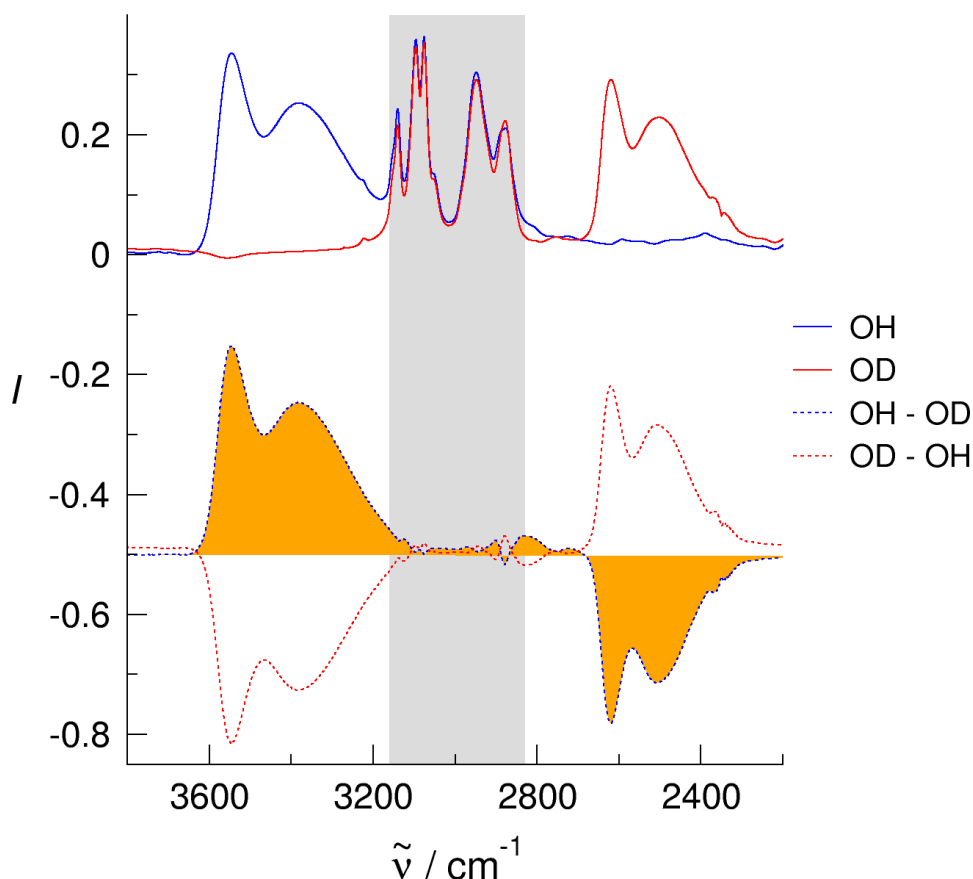


Figure 1. a) Infrared (IR) spectra of the IL $[\text{HOC}_4\text{Py}][\text{NTf}_2]$ (blue line) and the IL $[\text{HOC}_4\text{Py-d}_1][\text{NTf}_2]$ (red line) measured at 253 K in the frequency range between 2200 cm^{-1} and 3750 cm^{-1} . We observed distinct spectral bands in the OH and OD frequency regions for each IL along with the C-H vibrational bands of the pyridinium ring and hydroxyalkyl group between 2820 cm^{-1} and 3180 cm^{-1} present in both ILs (grey area). b) IR difference spectra OH-OD in the OH stretch region (dotted blue line) and OD-OH in the OD region (dotted red line) of $[\text{HOC}_4\text{Py}][\text{NTf}_2]$ and $[\text{HOC}_4\text{Py-d}_1][\text{NTf}_2]$. The spectra of the OD functionalized IL are subtracted from the corresponding spectra of the all-H species to remove the CH stretches of the pyridinium ring and exclude interference between CH and OH contributions.

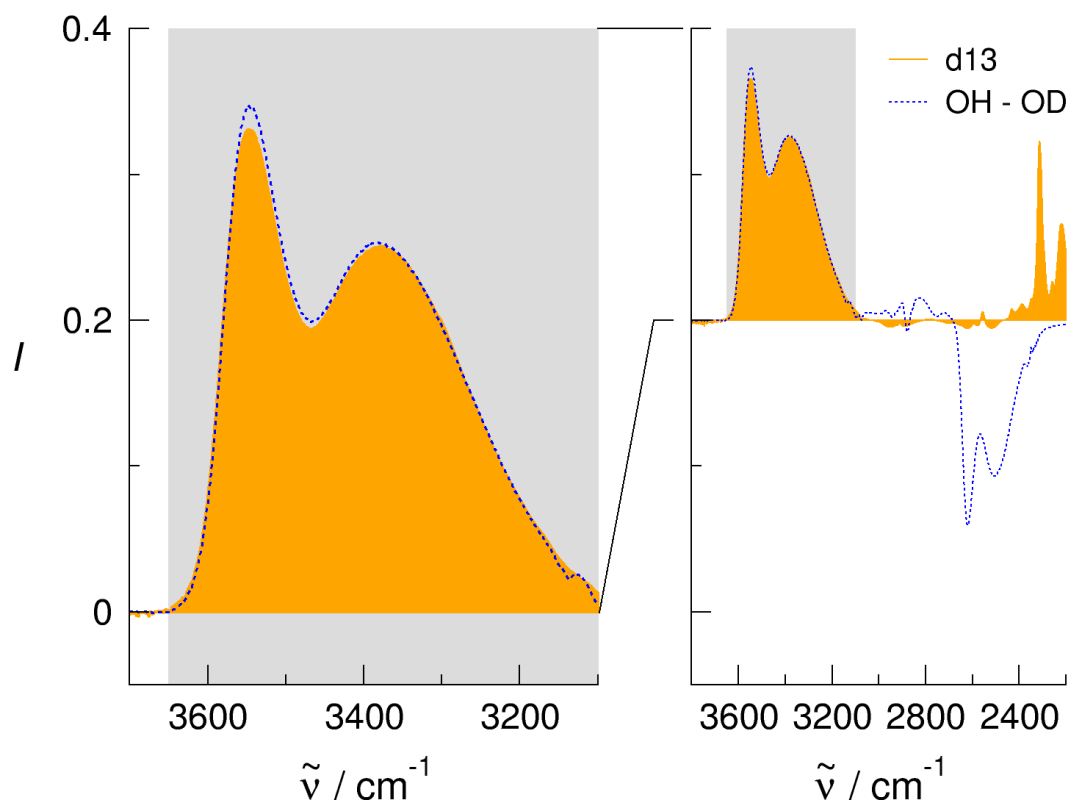


Figure 2. To show that the procedure for isolating the OH stretch region by using difference spectra is valid, we measured the IR spectra of IL $[\text{HOC}_4\text{Py-d}_{13}][\text{NTf}_2]$ (d13), which is deuterated at the pyridinium ring and the butyl chain. The IR difference spectrum (OH-OD) and the IR spectrum of $[\text{HOC}_4\text{Py-d}_{13}][\text{NTf}_2]$ (d13) agree perfectly in the OH stretch region. Thus, we can use the difference spectra between $[\text{HOC}_4\text{Py}][\text{NTf}_2]$ and $[\text{HOC}_4\text{Py-d}_1][\text{NTf}_2]$. The latter can be easily obtained by H/D exchange from the fully protonated IL, whereas the synthesis of the ring- and chain-deuterated ILs is quite challenging and time consuming.

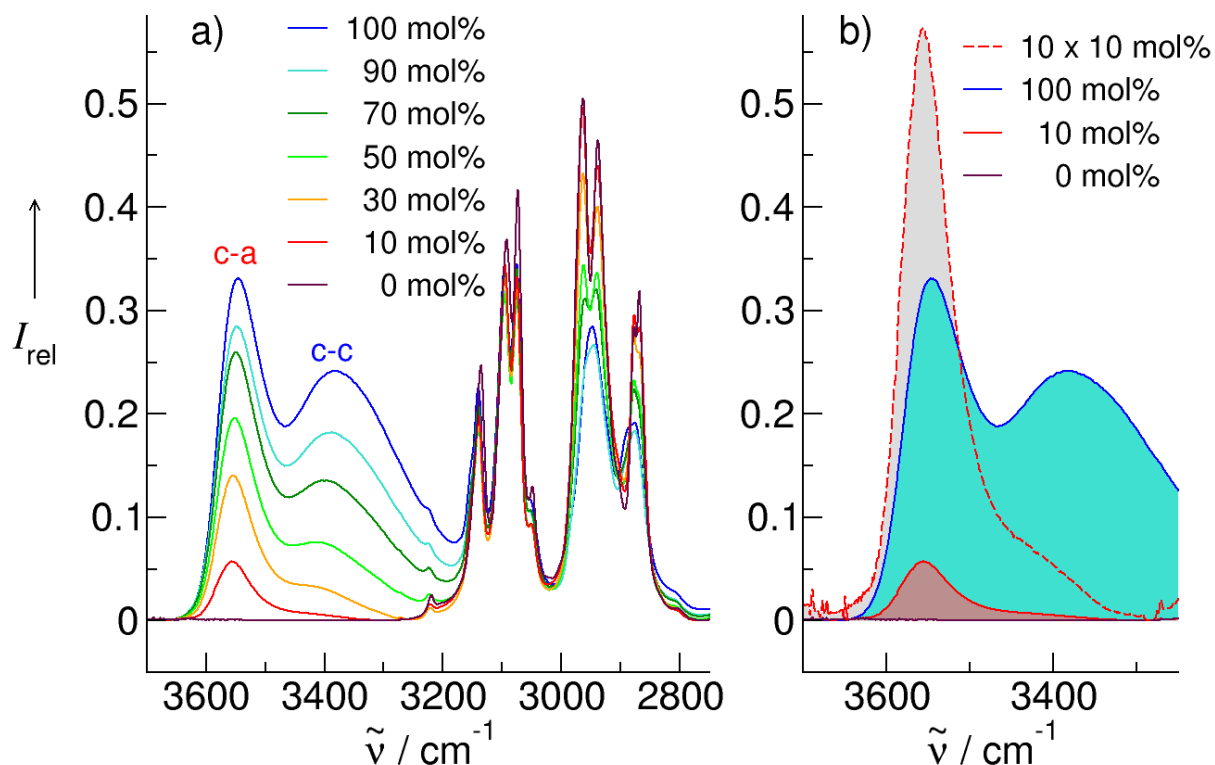


Figure 3. a) Measured infrared spectra in the OH stretch region of the IL (1-(4-hydroxybutyl)-pyridinium bis(trifluoromethanesulfonyl)imide) [HOC₄Py][NTf₂] in mixtures with the IL (1-pentylpyridinium bis(trifluoromethanesulfonyl)imide) [C₅Py][NTf₂] at 213 K. With increasing OH density, the (c-a) vibrational bands are accompanied by newly growing redshifted contributions which are assigned to (c-c) cluster formation. b) Multiplying the c-a vibrational band of the 10 mol% mixture by ten should result in a strongly enhanced spectral band (red dotted line) assuming that the pure IL solely consists of c-a clusters. Instead, we observed that in the pure IL only about 50% of the cations are involved in c-a hydrogen bonding, whereas the other half forms (c-c) hydrogen bonds among themselves.

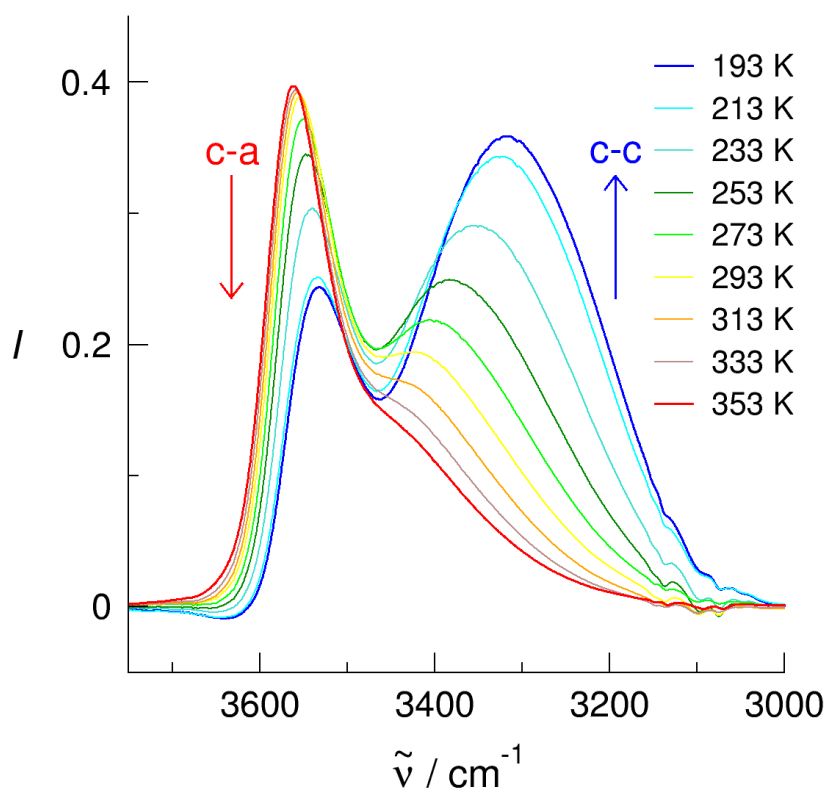


Figure 4. IR difference spectra of the IL [HOC₄Py][NTf₂] as a function of temperature between 193 K and 333 K. We show that the intensity of the (c-a) vibrational bands decrease, whereas those of the (c-c) vibrational bands strongly increase with decreasing temperature. Obviously, (c-a) clusters are reduced to the benefit (c-c) clusters. The more pronounced minimum between both bands indicates the formation of larger stronger bound c-c cluster species at low temperature.

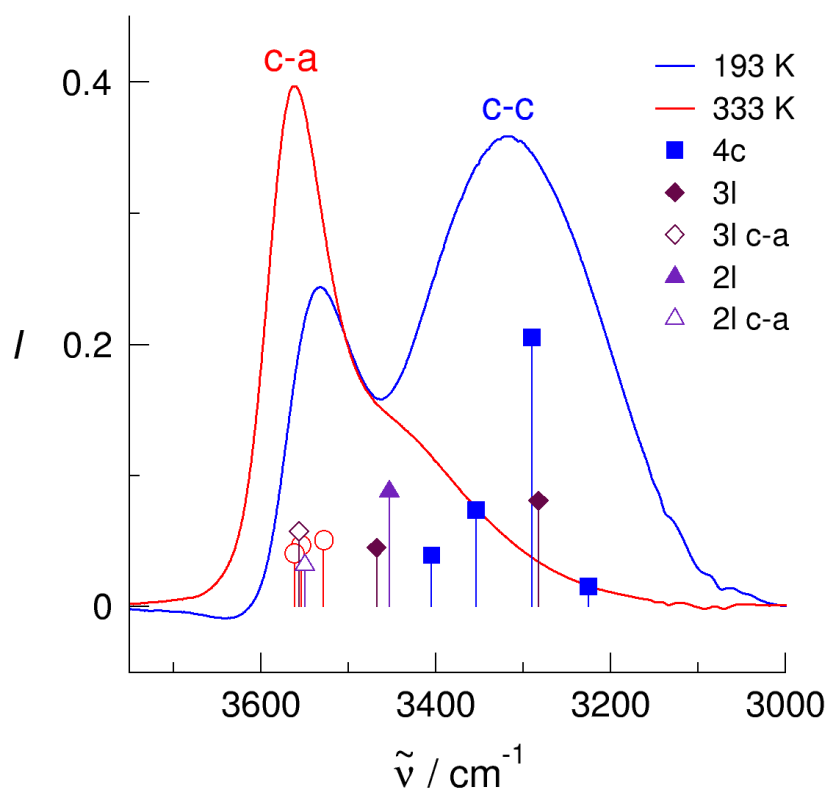


Figure 5. Calculated frequencies [B3LYP-D3/6-31+G*, scaled by 0.98] of (c-a) (open symbols) and (c-c) (filled symbols) clusters, compared to the measured IR spectra of [HOC₄Py][NTf₂] at 193 K (blue line) and 333 K (red line), respectively. Both linear and cyclic (c-c) configurations were considered. The (c-c) feature of the bulk liquid spectra is best represented by the calculated frequencies of a cyclic tetramers (blue filled squares).

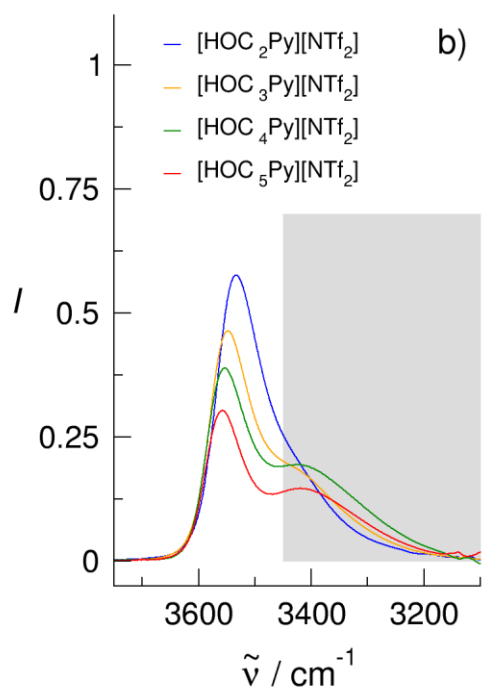
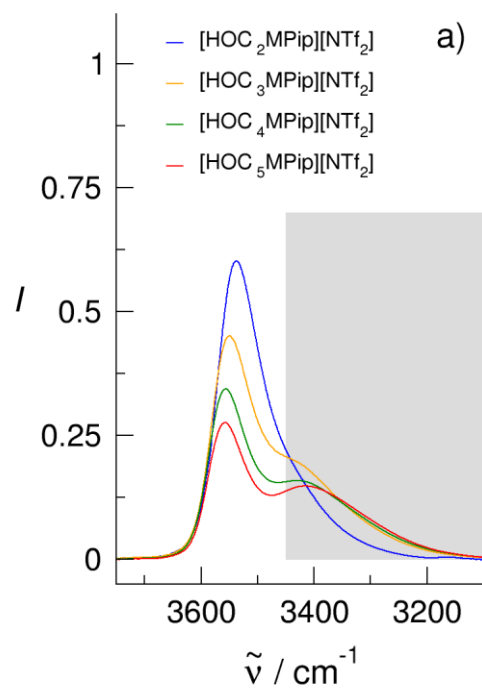


Figure 6. IR difference spectra of the ILs a) $[\text{HOC}_n\text{MPip}][\text{NTf}_2]$ and b) $[\text{HOC}_n\text{Py}][\text{NTf}_2]$ with varying hydroxy alkyl chain length $n=2-5$ at 293 K. We observe that (c-c) cluster formation indicated by the gray bar is slightly favored for the more polarizable pyridinium cation.

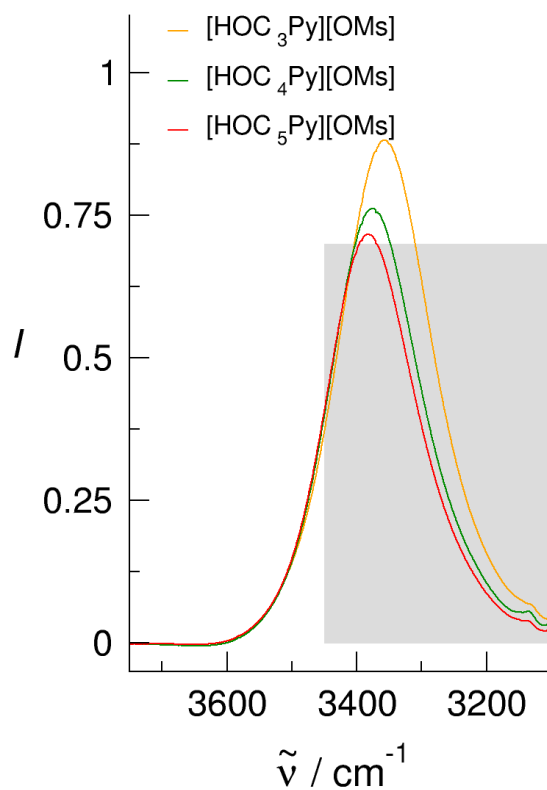
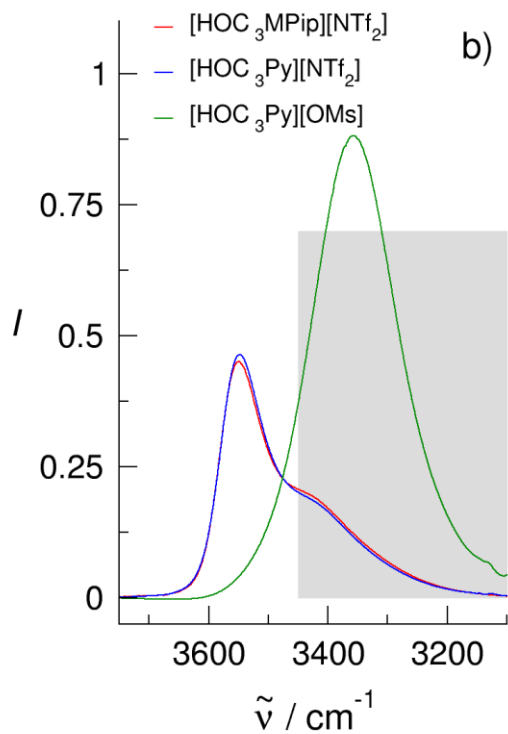
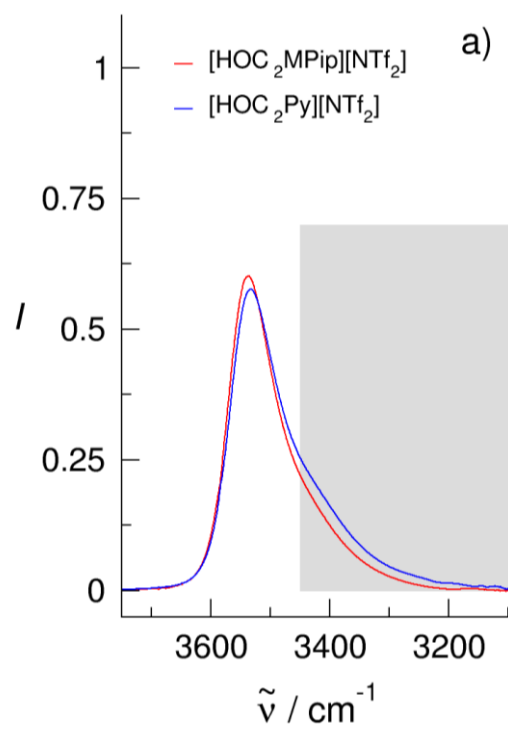


Figure 7. IR difference spectra of the IL [HOC_{*n*}Py][OMs] with varying hydroxy alkyl chain length $n=3-5$ at 293 K. We observe that (c-c) cluster formation is completely suppressed in the case of strongly interacting anion, which prefer to form strong (c-a) hydrogen bonds instead.



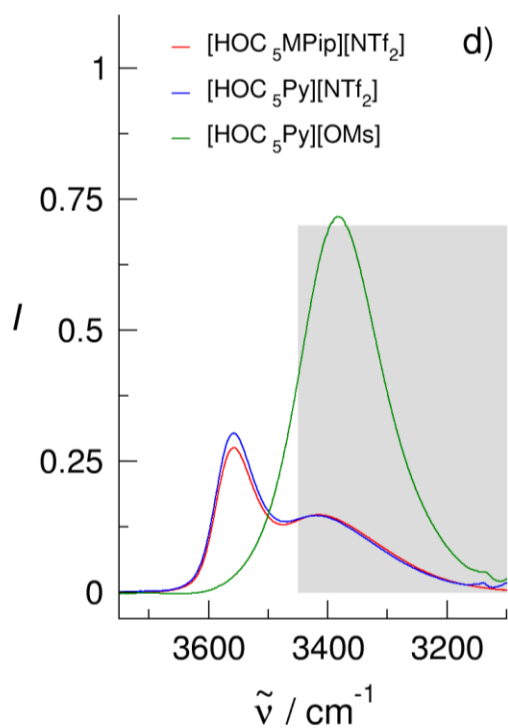
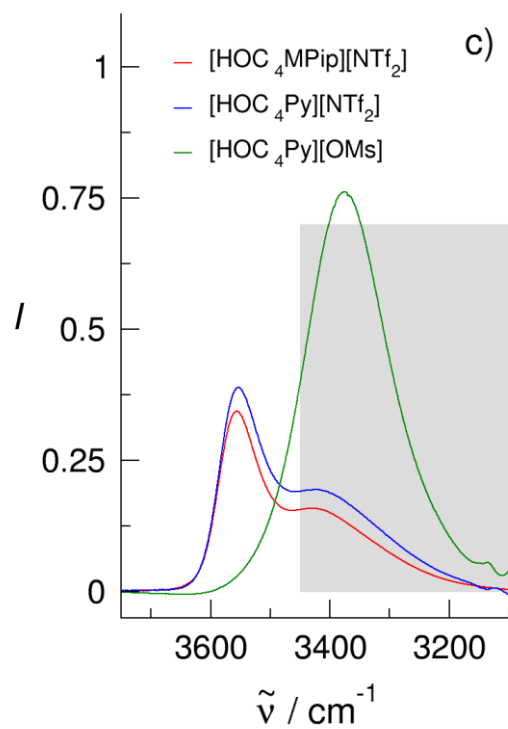


Figure 8. IR difference spectra for a) hydroxyethyl (HOC_2^-), b) hydroxypropyl (HOC_3^-), c) hydroxybutyl (HOC_4^-) and d) hydroxypentyl (HOC_5^-) functionalized cations in the ILs $[\text{HOC}_n\text{MPip}][\text{NTf}_2]$, $[\text{HOC}_n\text{Py}][\text{NTf}_2]$ and $[\text{HOC}_n\text{Py}][\text{OMs}]$, respectively.

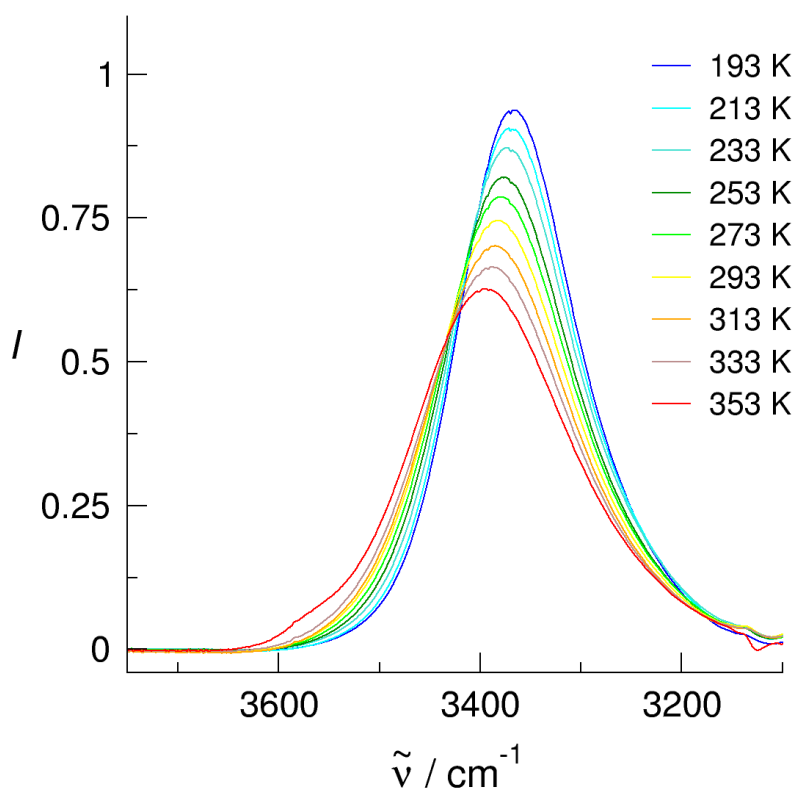
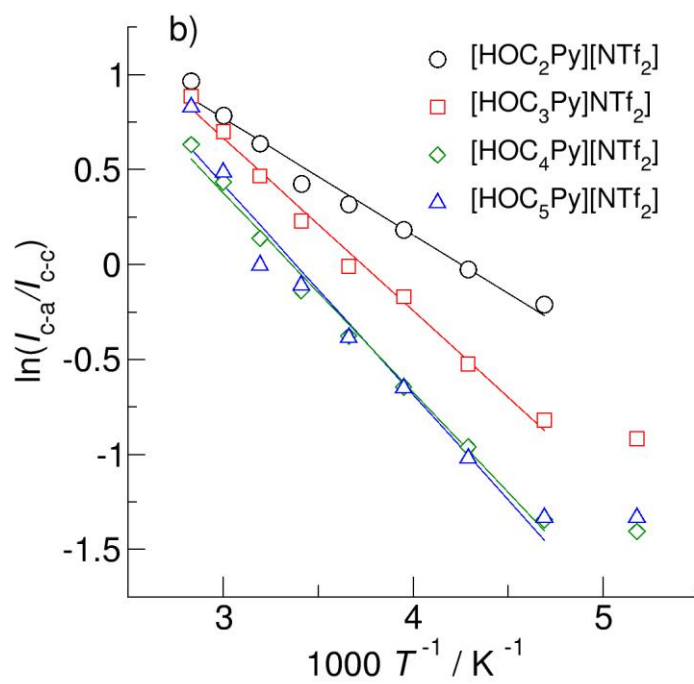
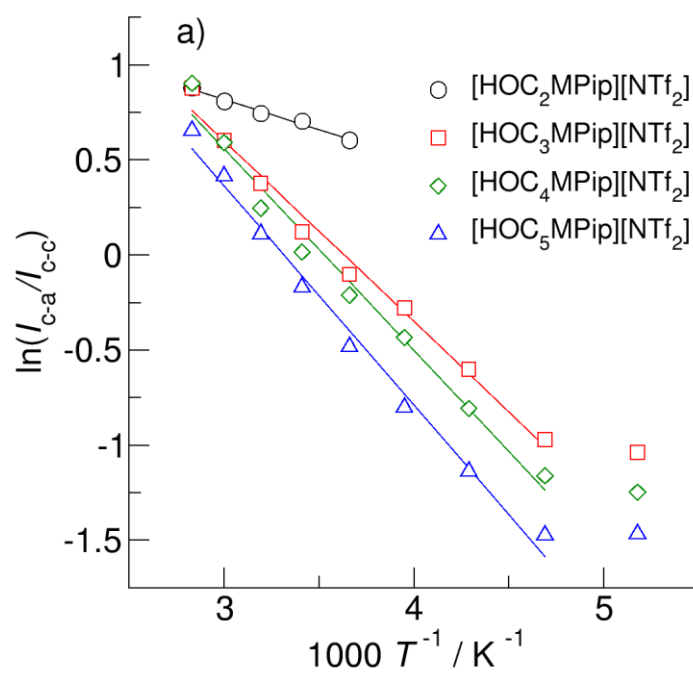


Figure 9. IR difference spectra of the IL [HOC₅Py][OMs] as a function of temperature. Even for the longest hydroxyalkyl chain (HOC₅-) and lowest temperature at 193 K, we do not observe c-c cluster formation. The symmetric shape of the vibrational band is temperature independent. Moreover, the maximum of the IR band is redshifted and its intensity enhanced with decreasing temperature, which is both typical temperature behavior for one type of hydrogen-bonded species, here the c-a clusters.



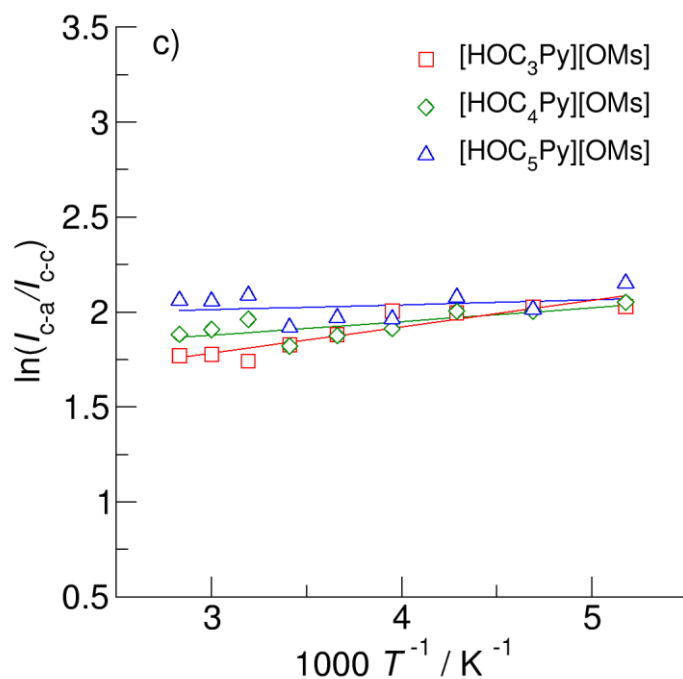
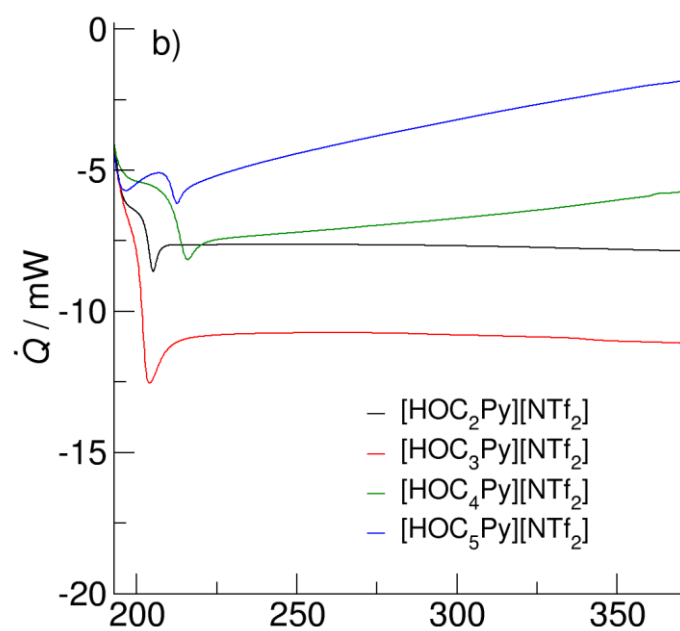
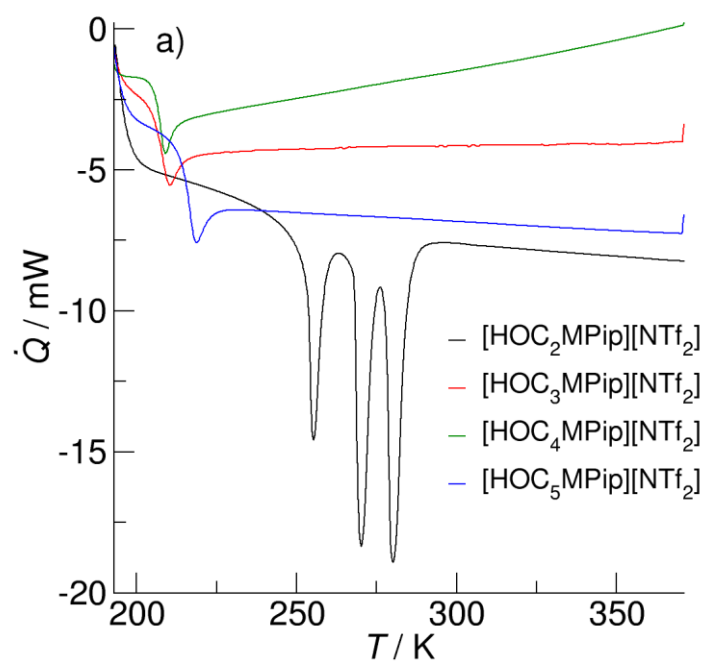


Figure 10. Plots of the natural logarithm of the (c-a) to (c-c) vibrational band intensity ratios versus inverse temperature taken from the measured IR spectra between 193 K and 353 K. I_{c-a} and I_{c-c} were obtained from the integral intensities left and right of the frequency position, where the vibrational bands for the c-a and the c-c species cross. The solid lines represent linear fits ($R^2 \geq 0.98$) with slopes indicating different enthalpies of cationic cluster formation.



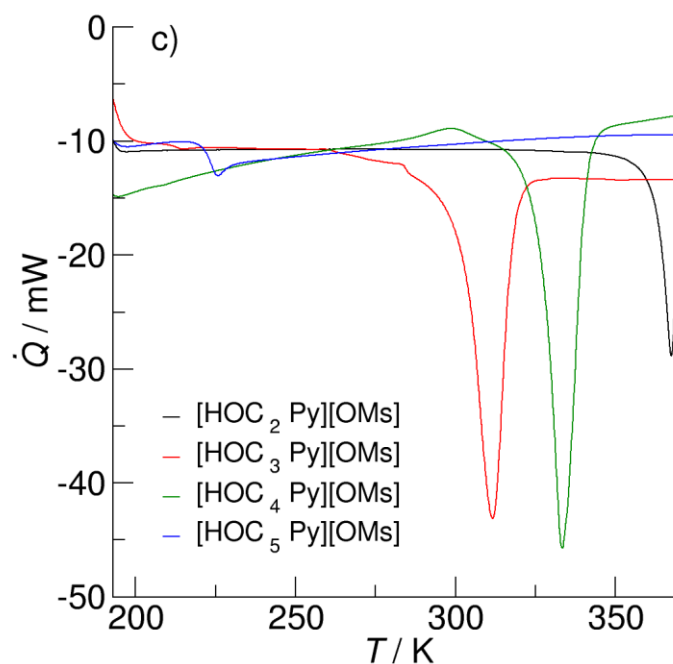


Figure 11. The DSC traces for the ILs a) $[\text{HOC}_n\text{MPip}][\text{NTf}_2]$, b) $[\text{HOC}_n\text{Py}][\text{NTf}_2]$ and c) $[\text{HOC}_n\text{Py}][\text{OMs}]$ with $n=2-5$, respectively. The heating rate is 10 Kmin^{-1} for all measurements. We observe that supercooling and glass transition is related to substantial (c-c) cluster formation as present for all ILs $[\text{HOC}_n\text{Py}][\text{NTf}_2]$ with $n=2-5$ including a polarizable cation and a weakly interacting anion. The DSC traces show liquid/solid phase transitions in ILs $[\text{HOC}_2\text{MPip}][\text{NTf}_2]$ and $[\text{HOC}_n\text{Py}][\text{OMs}]$ with $n=2-4$, for which we observed no or minor (c-c) cluster formation in the IR spectra. If the hydroxyalkyl chains exceed a particular length, e.g. in IL $[\text{HOC}_5\text{Py}][\text{OMs}]$ crystallization is also prevented for ILs with strongly interacting anions.

The double-faced nature of hydrogen bonding in hydroxyl-functionalized ionic liquids shown by neutron diffraction and molecular dynamics simulations

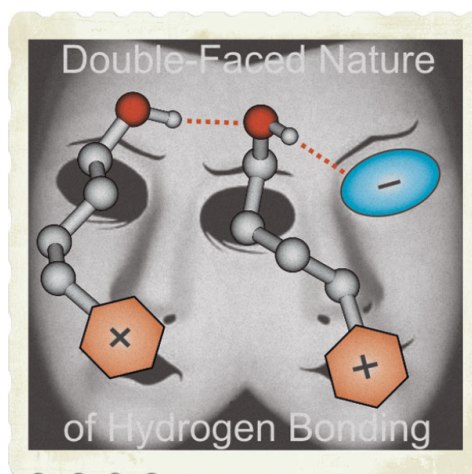
T. Niemann (25 %), J. Neumann (20 %), P. Stange (10 %), S. Gärtner (5 %), T. G. A. Youngs (5 %), D. Paschek (5 %), G. G. Warr (5 %), R. Atkin (10 %), R. Ludwig (15 %)

Angew. Chem. Int. Ed., 58, 12887–12892, 2019

Angew. Chem., 131, 13019-13024, 2019

Content:

The combination of results from neutron diffraction and molecular dynamics simulations characterise for the first time for OH-functionalised ILs the differences between the (c-c) and (c-a) H-bonds. It could be shown the (c-c) H-bond is the stronger one with respect to bond length and angle. Furthermore the cluster distribution was presented.



Contributions to this work:

I have synthesised all ILs with the specific deuterations investigated in this work. Together with Peter Stange, I have performed the ND experiments at ISIS. Sabrina Gärtner and Tristan Youngs were our local contacts at ISIS. Jan Neumann contributed to this work with the MD simulations performed by him under supervision of Dietmar Paschek. The data reduction and the on the EPSR procedure based fitting of the ND data was done by me. Professor Ludwig wrote the first draft and submitted the final manuscript after corrections from Gregory Warr, Rob Atkin and me.

Ionic Liquids

International Edition: DOI: 10.1002/anie.201904712
German Edition: DOI: 10.1002/ange.201904712

The Double-Faced Nature of Hydrogen Bonding in Hydroxy-Functionalized Ionic Liquids Shown by Neutron Diffraction and Molecular Dynamics Simulations

Thomas Niemann, Jan Neumann, Peter Stange, Sabrina Gärtner, Tristan G. A. Youngs, Dietmar Paschek, Gregory G. Warr, Rob Atkin, and Ralf Ludwig*

Abstract: We characterize the double-faced nature of hydrogen bonding in hydroxy-functionalized ionic liquids by means of neutron diffraction with isotopic substitution (NDIS), molecular dynamics (MD) simulations, and quantum chemical calculations. NDIS data are fit using the empirical potential structure refinement technique (EPSR) to elucidate the nearest neighbor H...O and O...O pair distribution functions for hydrogen bonds between ions of opposite charge and the same charge. Despite the presence of repulsive Coulomb forces, the cation–cation interaction is stronger than the cation–anion interaction. We compare the hydrogen-bond geometries of both “doubly charged hydrogen bonds” with those reported for molecular liquids, such as water and alcohols. In combination, the NDIS measurements and MD simulations reveal the subtle balance between the two types of hydrogen bonds: The small transition enthalpy suggests that the elusive like-charge attraction is almost competitive with conventional ion-pair formation.

Since the early days of Huggins, Latimer, and Rodebush, understanding hydrogen bonding in liquids and solutions has attracted much interest.^[1–9] Hydrogen bonds are local and directional with interaction strengths ranging from weak to strong. They compete with other intermolecular forces, such as Coulomb and dispersion interactions. Hydrogen bonds are key to many aspects of liquid chemistry, including dynamics, solvation, and macroscopic properties.^[6–9] In contrast to molecular liquids, ionic liquids (ILs) are composed entirely of ions, and it is expected that the cation–anion interactions dominate the structural, dynamic, and macroscopic properties of this particular class of liquids.^[10–12] However, hydrogen bonding and dispersion forces have to be taken into account to understand how the delicate balance between the different types of interactions influence the IL properties.^[13–22] In hydroxy-functionalized ILs, as investigated here, the situation may become even more complex. In this type of IL, hydrogen bonding has a double-faced nature. Two distinct types of hydrogen bonding coexist: The conventional hydrogen bonds between the cations and anions (c–a) are enhanced by attractive Coulomb interactions, whereas the elusive hydrogen bonds between like-charged ions (c–c) are presumed to be much weaker as a result of the repulsive Coulomb force.^[23–28] Despite this expectation, however, structural motifs involving hydrogen-bonded cationic clusters were recently observed in the bulk liquid and the gas phase.^[29–35] Vibrational spectroscopy clearly identified two distinct vibrational bands that were assigned to (c–a) and (c–c) hydrogen-bonded species (see Scheme 1). The magnitudes of the observed red shifts indicated that the (c–c) hydrogen bonds are evidently stronger than the (c–a) hydrogen bonds.^[33–35] However, bulk infrared (IR) spectroscopy has some shortcomings. As a consequence of the different transition dipole moments for every single hydrogen bond, the vibrational bands are broad and unspecific, and the observed red-shifts cannot be simply related to the cluster sizes and the cluster distributions. Neutron diffraction can be used to determine liquid structure at very high resolution, and H/D isotopic substitution renders it particularly sensitive to the positions of hydrogen atoms, thereby allowing the location of hydrogen atoms participating in hydrogen bonds to be unambiguously determined.

To that end we have examined the bulk structure of 1-(4-hydroxybutyl)pyridinium bis(trifluoromethylsulfonyl)imide [HOC₄Py][NTf₂] using neutron diffraction with isotopic substitution (NDIS), a well-established technique for probing inter- and intramolecular interactions in ionic and molecular

[*] M. Sc. T. Niemann, P. Stange, Prof. Dr. R. Ludwig
Universität Rostock, Institut für Chemie
Abteilung für Physikalische Chemie
Dr.-Lorenz-Weg 2, 18059, Rostock (Germany)

M. Sc. J. Neumann, Dr. D. Paschek
Universität Rostock, Institut für Chemie
Abteilung für Physikalische Chemie
Albert-Einstein-Strasse 21, 18059, Rostock (Germany)

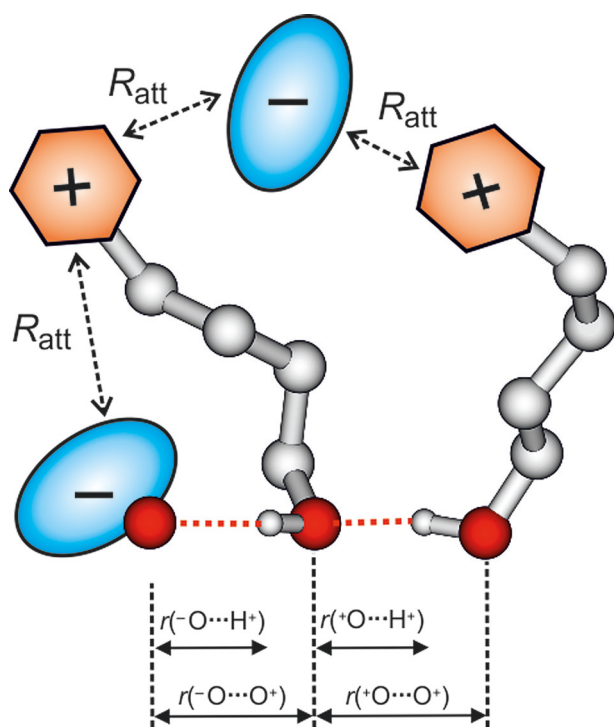
Dr. S. Gärtner, Dr. T. G. A. Youngs
ISIS Faculty, STFC, Rutherford Appleton Laboratory
Didcot OX11 0QX (UK)

Prof. G. G. Warr
School of Chemistry and Sydney Nano
The University of Sydney
NSW 2006 (Australia)

Prof. R. Atkin
School of Molecular Sciences
The University of Western Australia, Perth
Western Australia 6009 (Australia)

Prof. Dr. R. Ludwig
Department LL&M, University of Rostock
Albert-Einstein-Strasse 25, 18059, Rostock (Germany),
and
Leibniz-Institut für Katalyse an der Universität Rostock e.V.
Albert-Einstein-Strasse 29a, 18059 Rostock (Germany)

Supporting information and the ORCID identification numbers for some of the authors of this article can be found under:
<https://doi.org/10.1002/anie.201904712>.



Scheme 1. Hydrogen-bonded dimer of the hydroxy-functionalized ionic liquid $[\text{OHC}_4\text{Py}][\text{NTf}_2]$ showing both types of possible hydrogen bonding: (c–a) between cation and anion, and (c–c) between two cations. We obtained both hydrogen-bond geometries from ND experiments and MD simulations. The aliphatic and aromatic H atoms of OHC_4Py^+ are omitted for clarity.

liquids.^[36–40] Neutron diffraction spectra were refined using the empirical potential structure refinement (EPSR) to extract atomic and molecular-level structure information.^[36–40] The IL $[\text{HOC}_4\text{Py}][\text{NTf}_2]$ was chosen to maximize the opportunity for like-charge hydrogen bonding: $[\text{NTf}_2]^-$ is a weakly interacting anion, whereas $[\text{OHC}_4\text{Py}]^+$ is a highly polarizable cation. In addition, the hydroxybutyl group of the cation allows for ample separation between the positively charged pyridinium ring and the hydroxy group. Strong spectroscopic evidence for hydrogen bonding between the cations (c–c) has been found with this cation/anion combination.^[29–35]

It is the aim of this study to characterize the (c–a) ($^+\text{O}-\text{H}\cdots\text{O}^-$) and the (c–c) ($^+\text{O}-\text{H}\cdots\text{O}^+$) hydrogen bonds in this hydroxy-functionalized ionic liquid (IL) by means of neutron diffraction, molecular dynamics (MD) simulations, and quantum chemical calculations. A similar approach combining X-ray scattering and MD simulations has been successfully applied to analyze the structure of ILs and organic phases.^[41,42] The measured hydrogen-bond lengths for the two types of ionic interactions, which describe the attraction between ions of opposite and repulsion between ions of like charge, are compared to those of molecular liquids, such as water and alcohols.^[23–28] In addition, we carefully address the different types of (c–a) and (c–c) clusters and their distributions in the bulk liquid. The accompanying MD simulations support the concept of the double-faced nature of hydrogen bonding in this particular class of liquids.

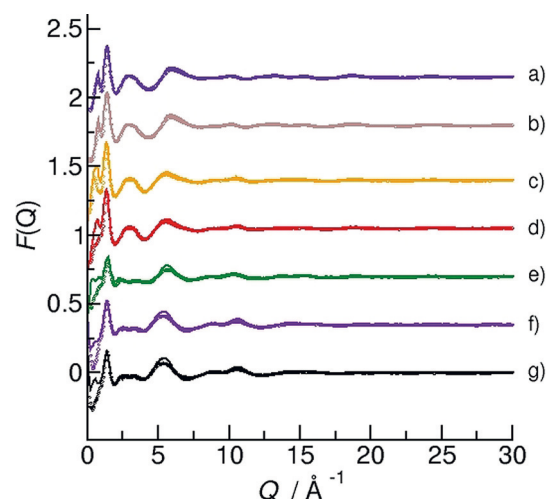


Figure 1. Measured neutron diffraction $F(Q)$ (colored circles) and fitted EPSR $F(Q)$ (solid lines) for seven deuteration schemes: a) $[\text{OHC}_4\text{Py}][\text{NTf}_2]$, b) $[\text{OHC}_4\text{Py-d}_1][\text{NTf}_2]$, c) $[\text{OHC}_4\text{Py-d}_8][\text{NTf}_2]$, d) $[\text{OHC}_4\text{Py-d}_8][\text{NTf}_2]$, e) $[\text{OHC}_4\text{Py-d}_9][\text{NTf}_2]$, f) $[\text{OHC}_4\text{Py-d}_{13}][\text{NTf}_2]$, and g) $[\text{OHC}_4\text{Py-d}_{14}][\text{NTf}_2]$. The data are offset for clarity (see also the Supporting Information).

Figure 1 shows the neutron diffraction (NDIS) data along with the EPSR-derived differential scattering cross sections $F(Q)$ (solid black lines) for momentum transfers (Q) from 0.1 to 50 \AA^{-1} . Seven chemically identical, but isotopically different IL samples were synthesized: the fully hydrogenous $[\text{HOC}_4\text{Py}][\text{NTf}_2]$ and the fully deuterated $[\text{HOC}_4\text{Py-d}_{14}][\text{NTf}_2]$ along with the compounds partially deuterated at the hydroxy group $[\text{HOC}_4\text{Py-d}_1][\text{NTf}_2]$, at the pyridinium ring and the hydroxy group $[\text{HOC}_4\text{Py-d}_6][\text{NTf}_2]$, at the butyl chain and the hydroxy group $[\text{HOC}_4\text{Py-d}_8][\text{NTf}_2]$, at the butyl chain and the hydroxy group $[\text{HOC}_4\text{Py-d}_9][\text{NTf}_2]$, and at the pyridinium ring and the butyl chain $[\text{HOC}_4\text{Py-d}_{13}][\text{NTf}_2]$. Details regarding the synthesis of the different compounds for the neutron diffraction experiments are provided in the Supporting Information. Since hydrogen and deuterium have different neutron scattering lengths, isotopic substitution enables contrast between different molecular regions of interest in a neutron diffraction experiment.

The EPSR analysis of the total structure factors $F(Q)$ yields the partial structure factors $S(Q)$, which are the Fourier transforms of the partial pair distribution functions $g(r)$ for atom–atom pairs as a function of their radial separation, normalized to the bulk density (see the Supporting Information). Here, we solely focus on the intermolecular hydrogen–oxygen ($\text{H}\cdots\text{O}$) and associated oxygen–oxygen ($\text{O}\cdots\text{O}$) pair distribution functions $g_{\text{HO}}(r)$ and $g_{\text{OO}}(r)$, which describe the nature of the hydrogen bonding in the IL. As a result of the large number of isotopically labeled compounds used, both pair distribution functions could be derived confidently for the (c–a)- and the (c–c)-bound species. The first peak in the $g(r)$ functions corresponds to the first coordination shell of the nearest neighbors. Figure 2a shows the $g_{\text{HO}}(r)$ and $g_{\text{OO}}(r)$ functions for the (c–a)- and (c–c)-bound species. The maxima of the first nearest neighbor peaks in the two functions give the average hydrogen-bond lengths $r(^+\text{H}\cdots\text{O}^-)$ and $r(^+\text{O}\cdots\text{O}^-)$

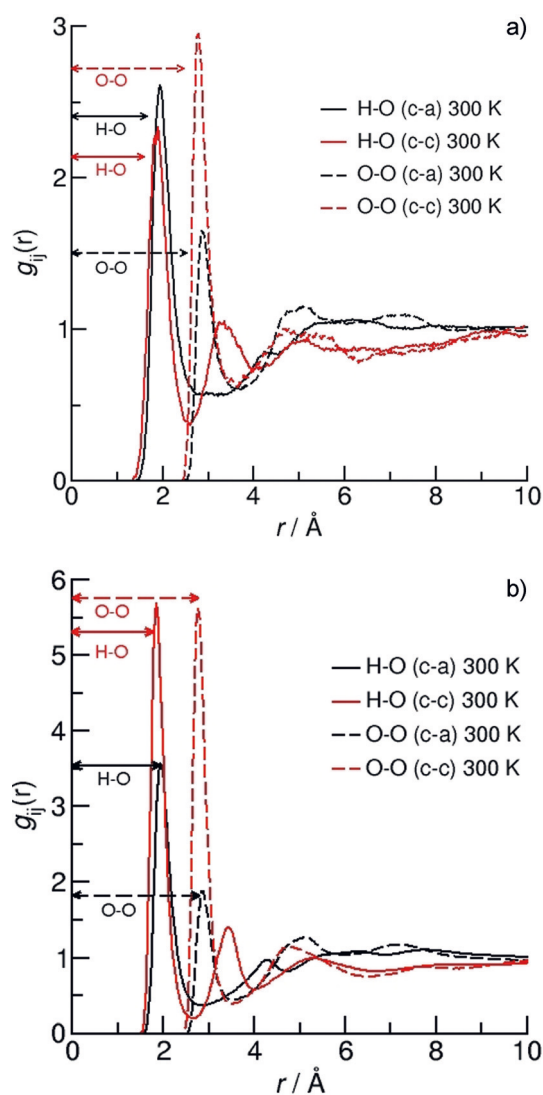


Figure 2. Pair distribution functions $g_{HO}(r)$ and $g_{OO}(r)$ for the (c-a) and (c-c) hydrogen bonds in the IL $[\text{HOC}_4\text{Py}][\text{NTf}_2]$ from a) neutron diffraction with H/D substitution and b) molecular dynamics simulations. The nearest neighbor distances are indicated by the arrows.

for the (c-a) as well as $r(^+\text{H}\cdots\text{O}^+)$ and $r(^+\text{O}\cdots\text{O}^+)$ for the (c-c) binding motifs, respectively. The (c-c) hydrogen bonds are noticeably shorter (1.87 Å and 2.78 Å) than the (c-a) hydrogen bonds (1.95 Å and 2.88 Å), which indicates stronger attraction between ions of like charge (c-c) than between ions of opposite charge (c-a). Both (c-a) and (c-c) hydrogen bonds prefer a linear configuration, as demonstrated in 2D distance/angle probability density plots derived from EPSR data, as shown in Figures S2 and S3 in the Supporting Information. Moreover, in addition to being shorter, the (c-c) hydrogen bonds are also “more linear” than the (c-a) hydrogen bonds, as revealed by a narrower distribution of the O–H \cdots O hydrogen-bond angles (see Figure S5). This observation is quite remarkable because the total interaction in the (c-a)-bound species results from hydrogen bonding plus attractive Coulomb forces between the oppositely charged ions. It is evident that the (c-a) interaction is only weakly strengthened by Coulomb attraction, whereas the (c-

c) interaction is strongly enhanced by potentially cooperative hydrogen bonding. Despite the Coulomb repulsion, the hydrogen bond is shorter for the (c-c) than for the (c-a) species.^[40] The shortening of the H \cdots O and O \cdots O distances by about 8 pm and 10 pm, respectively, is substantial and comparable to the differences in the hydrogen-bond lengths in water and ice (see Table 1). This result is in accord with

Table 1: Hydrogen-bond distances $r(\text{O}\cdots\text{O})$ and $r(\text{H}\cdots\text{O})$ for the (c-a)- and (c-c)-bound species in the IL $[\text{HOC}_4\text{Py}][\text{NTf}_2]$. For comparison, the values known for water, methanol, and ethanol in the liquid (l) and solid (s) phases are given.^[50–56]

	$r(\text{O}\cdots\text{O})/\text{\AA}$	$r(\text{H}\cdots\text{O})/\text{\AA}$
$[\text{HOC}_4\text{Py}][\text{NTf}_2]$, NDIS	2.88 (c-a), 2.78 (c-c)	1.95 (c-a), 1.87 (c-c)
$[\text{HOC}_4\text{Py}][\text{NTf}_2]$, MD	2.87 (c-a), 2.77 (c-c)	1.94 (c-a), 1.85 (c-c)
water	2.80 [l] ^[50] 2.759 [s] ^[51] 2.76 [s] ^[52] 2.825 (2) [s] ^[53]	1.880 (2) [s] ^[53]
methanol	2.798 (6) [l] ^[54] 2.792 (3) [s] ^[53]	1.804 (4) [s] ^[53]
ethanol	2.808 (8) [l] 2.716 (3) [s] ^[55] 2.730 (2) [s] ^[56]	1.93 (4) [s] ^[55]

recent IR studies in the bulk and the gas phases, which show strongly red-shifted OH vibrational bands as a result of cooperative hydrogen bonding in the (c-c) cluster species.^[29–35] However, the IR intensities of the (c-a) and (c-c) vibrational bands result from different transition dipole moments for each single hydrogen bond and does not allow determination of cluster sizes or distributions.

We complemented the NDIS measurements by MD simulations using independently derived molecular force fields (see the Supporting Information).^[43–45] In Figure 2b we show that the $r(^+\text{H}\cdots\text{O}^-)$, $r(^+\text{O}\cdots\text{O}^-)$, $r(^+\text{H}\cdots\text{O}^+)$, and $r(^+\text{O}\cdots\text{O}^+)$ distances again show shorter hydrogen bonds for (c-c) than (c-a) and agree almost quantitatively with the geometries derived from the ND measurements. In addition, the O–H \cdots O hydrogen bond angles obtained from the MD simulations behave similarly to the ND data (Figures S6–S9). Here the (c-c) hydrogen bonds are also found to be more linearly aligned than the (c-a) hydrogen bonds. Both simulated intermolecular O \cdots O distances differ by only ± 0.02 Å from the experimental geometries, thereby demonstrating the quality of the force field used in the MD simulations. The NDIS experiments and MD simulation agree in the pair distribution functions and allow (c-a)- and (c-c)-bound species to be clearly distinguished. The average $r(^+\text{O}\cdots\text{O}^-)$ and $r(^+\text{O}\cdots\text{O}^+)$ hydrogen-bond lengths of the (c-a) and (c-c) species in the liquid phase have also been compared to geometries of (c-a) and (c-c) clusters calculated by density functional theory (DFT) including Grimme’s D3 correction (see the Supporting Information).^[46–49] These calculations show that, whereas the (c-a) bond distances remain almost

constant at 2.90 Å as a function of cluster size, the distances of the (c-c) clusters decrease monotonically from 2.78 Å for the dimer to 2.75 Å for the cyclic tetramer as a result of cooperative effects. The average dimer and trimer values include the oxygen-oxygen distances derived for the liquid phase from ND experiments and MD simulations, which indicates that the present (c-c) cluster sizes range between two and three (see Figure 3a).

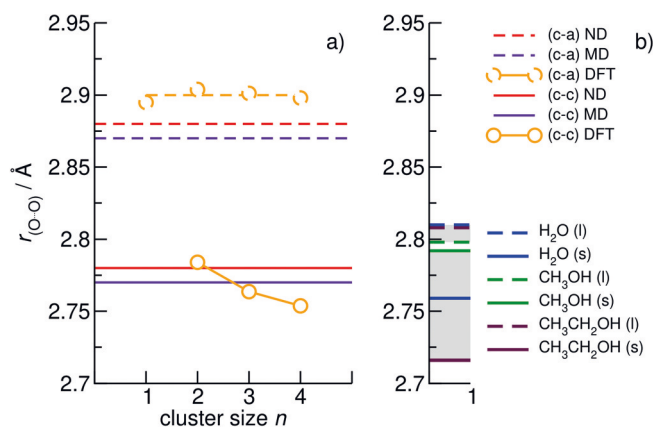


Figure 3. a) The oxygen-oxygen nearest neighbor distances $r_{(\text{O} \cdots \text{O})}$ for the (c-a) (dotted lines) and (c-c) hydrogen bonds (straight lines) of [OHC₄Py][NTf₂] from NDIS (red lines) and MD simulations (violet lines). Yellow circles: the B3LYP-D3/6-31 + G* calculated geometries of the (c-a) and (c-c) clusters for [OHC₄Py][NTf₂] versus cluster sizes n . b) The literature values for water, methanol, and ethanol for the liquid and solid phases.^[50–56] The two gray shaded areas indicate the liquid (top) and the solid-state (bottom) values.

Finally, we compare the $r(\text{O}^+ \cdots \text{O}^-)$ and $r(\text{O}^+ \cdots \text{O}^+)$ distances of this ionic liquid with those of molecular liquids. The given reference values for the O \cdots O distances of water, methanol, and ethanol in their liquid and solid phases were measured by a variety of X-ray and neutron scattering experiments.^[50–56] As shown in Figure 3b, the (c-a) hydrogen-bond length of the IL is longer than the liquid-phase hydrogen-bond lengths of the molecular liquids, thus indicating weaker hydrogen bonds despite the attractive Coulomb interaction. In contrast, the (c-c) hydrogen-bond length of the IL lies between the liquid and solid-phase values of the hydrogen-bonded molecular liquids. Apparently, the polarizable counterion fully compensates for the positive charge of the pyridinium ring, and the hydroxy groups of the cations can form cooperative hydrogen bonds with each other nearly as well as in molecular liquids. This finding is consistent with recent reports of long-range electrostatic forces in ionic liquids, similar to those found for weak electrolytes, which occur because the vast majority of cations and anions neutralize one another.^[57]

The NDIS experiments and MD simulations allow quantification of the populations of these local arrangements. In Figure 4, we show that at 300 K between 87 % (NDIS) and 75 % (MD) of the cations form (c-a) hydrogen bonds with the counterions, whereas between 13 % (NDIS) and 20 % (MD) of the cations are involved in (c-c) structural motifs. This

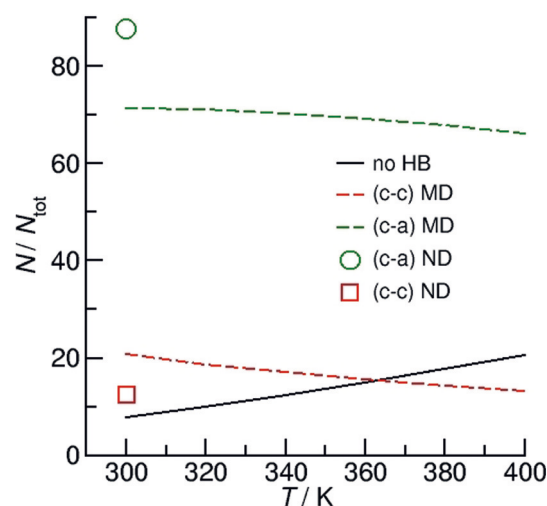


Figure 4. Analysis of (c-a) and (c-c) cluster populations in [OHC₄Py][NTf₂] from MD simulations as a function of temperature. The symbols show the cluster distribution obtained from NDIS experiments at 303 K.

agreement is excellent, given the possible uncertainties of the experiments and simulations (± 0.02 Å). MD simulations were performed for temperatures between 300 and 400 K to reveal the temperature-dependence of the cluster populations. We observe that the (c-a) and (c-c) species decrease to the benefit of quasi-free OH groups as the temperature is increased. The decrease with temperature is more pronounced for the (c-c)- than for the (c-a)-bound species, probably for entropic reasons (formation of larger aggregates). From a van't Hoff plot of the ratio for the (c-c) and the (c-a) hydrogen-bonded species versus the inverse temperature obtained from MD simulations data we determine the transition enthalpy from (c-c) to (c-a) to be about 3.75 kJ mol⁻¹. Such a small transition enthalpy suggests that the (c-c)-bound species exist in equilibrium and that kinetic trapping is not a requirement for finding cationic clusters at room temperature.

In conclusion, pair distribution functions $g_{\text{HO}}(r)$ and $g_{\text{OO}}(r)$ for both (c-a) and (c-c) hydrogen bonding in a hydroxy-functionalized ionic liquid have been revealed by ND experiments, MD simulations, and quantum chemical calculations. Each individual approach clearly distinguished hydrogen bonding between ions of opposite (c-a) and ions of like charge (c-c). The average r_{HO} and r_{OO} hydrogen-bond lengths for the (c-c)-bound species are 8 pm and 10 pm shorter than those obtained for the (c-a)-bound species. Apparently, the (c-c) hydrogen bonds are significantly stronger, despite the presence of repulsive Coulomb forces between the cations. The agreement between the NDIS and the MD results are almost quantitative. We show by means of quantum chemical calculations that cooperative effects enhance the favorable (c-c) hydrogen bonds, as has been reported earlier for clusters of water and alcohol. Our study provides strong evidence for the presence of (c-c) hydrogen bonding at room temperature. Kinetic trapping in the super-cooled state is thus not a prerequisite for like-charge attraction through hydrogen bonding. This observation is

supported by the small transition enthalpies derived from MD simulations.

Acknowledgements

R.L. thanks the Deutsche Forschungsgemeinschaft (DFG) under grant LU 506/14-1 for support of this work. T.N. thanks the “Deutscher Akademischer Austauschdienst” for supporting his research at the University of Western Australia, Perth. R.A. thanks the University of Western Australia for funding support. We gratefully acknowledge the Science and Technology Facilities Council (STFC) for access to neutron beamtime at the SANDALS instrument at the ISIS neutron and muon source, and also for the provision of sample preparation by the D-Lab. The data are available at the ISIS Neutron and Muon Source Data Journal under doi.org/10.5286/ISIS.E.RB1800066.

Conflict of interest

The authors declare no conflict of interest.

Keywords: hydrogen bonding · ionic liquids · like-charge attraction · molecular dynamics simulations · neutron diffraction

How to cite: *Angew. Chem. Int. Ed.* **2019**, *58*, 12887–12892
Angew. Chem. **2019**, *131*, 13019–13024

- [1] M. L. Huggins, *Science* **1922**, *55*, 459–460.
- [2] W. M. Latimer, W. H. Rodebush, *J. Am. Chem. Soc.* **1920**, *42*, 1419.
- [3] M. L. Huggins, *Angew. Chem. Int. Ed. Engl.* **1971**, *10*, 147–152; *Angew. Chem.* **1971**, *83*, 163–168.
- [4] L. Pauling, *The Nature of the Chemical Bond*, Cornell University Press, Ithaca, **1960**; G. A. Jeffrey, *An Introduction to Hydrogen Bonding*, Oxford University Press, New York, **1997**.
- [5] G. Gilli, P. Gilli, *The Nature of the Hydrogen Bond: Outline of a Comprehensive Hydrogen Bond Theory*, Oxford University Press, Oxford, **2009**.
- [6] G. R. Desiraju, T. Steiner, *The Weak Hydrogen Bond: In Structural Chemistry and Biology*, Oxford University Press, Oxford, **2001**.
- [7] Y. Marechal, *The Hydrogen Bond and the Water Molecule*, Elsevier, Amsterdam, **2007**.
- [8] G. A. Jeffrey, *An Introduction to Hydrogen Bonding*, Oxford University Press, New York, **1997**.
- [9] A. C. Legon, *Chem. Soc. Rev.* **1993**, *22*, 153.
- [10] K. Fumino, S. Reimann, R. Ludwig, *Phys. Chem. Chem. Phys.* **2014**, *16*, 21903–21929.
- [11] P. A. Hunt, C. R. Ashworth, R. P. Matthews, *Chem. Soc. Rev.* **2015**, *44*, 1257–1288.
- [12] C. R. Ashworth, R. P. Matthews, T. Welton, P. A. Hunt, *Phys. Chem. Chem. Phys.* **2016**, *18*, 18145–18160.
- [13] T. L. Greaves, C. J. Drummond, *Chem. Rev.* **2008**, *108*, 206.
- [14] R. Hayes, G. G. Warr, R. Atkin, *Phys. Chem. Chem. Phys.* **2010**, *12*, 1709.
- [15] M. Yoshizawa, W. Xu, C. A. Angell, *J. Am. Chem. Soc.* **2003**, *125*, 15411.
- [16] K. Fumino, A. Wulf, R. Ludwig, *Angew. Chem. Int. Ed.* **2009**, *48*, 3184; *Angew. Chem.* **2009**, *121*, 3230.
- [17] K. Fumino, A. Wulf, R. Ludwig, *Phys. Chem. Chem. Phys.* **2009**, *11*, 8790.
- [18] C. Roth, T. Peppel, K. Fumino, M. Köckerling, R. Ludwig, *Angew. Chem. Int. Ed.* **2010**, *49*, 10221; *Angew. Chem.* **2010**, *122*, 10419.
- [19] K. Fumino, E. Reichert, K. Wittler, R. Hempelmann, R. Ludwig, *Angew. Chem. Int. Ed.* **2012**, *51*, 6236; *Angew. Chem.* **2012**, *124*, 6340.
- [20] R. Hayes, N. Borisenko, B. Corr, G. B. Webber, F. Endres, R. Atkin, *Chem. Commun.* **2012**, *48*, 10246.
- [21] R. Hayes, S. Imberti, G. G. Warr, R. Atkin, *Angew. Chem. Int. Ed.* **2013**, *52*, 4623–4627; *Angew. Chem.* **2013**, *125*, 4721–4725.
- [22] R. Hayes, G. G. Warr, R. Atkin, *Chem. Rev.* **2015**, *115*, 6357–6426.
- [23] K. M. Murdoch, T. D. Ferris, J. C. Wright, T. C. Farrar, *J. Chem. Phys.* **2002**, *116*, 5717.
- [24] F. Huisken, A. Kulcke, C. Laush, J. Lisy, *J. Chem. Phys.* **1991**, *95*, 3924–3929.
- [25] M. Huelsekopf, R. Ludwig, *J. Mol. Liq.* **2002**, *98–99*, 163–171.
- [26] R. Ludwig, F. Weinhold, T. C. Farrar, *Mol. Phys.* **1999**, *97*, 465–477.
- [27] R. Ludwig, *ChemPhysChem* **2000**, *1*, 53–56.
- [28] R. Ludwig, *Phys. Chem. Chem. Phys.* **2002**, *4*, 5481–5487.
- [29] A. Knorr, K. Fumino, A.-M. Bonsa, R. Ludwig, *Phys. Chem. Chem. Phys.* **2015**, *17*, 30978–30982.
- [30] A. Knorr, R. Ludwig, *Sci. Rep.* **2015**, *5*, 17505.
- [31] A. Knorr, P. Stange, K. Fumino, F. Weinhold, R. Ludwig, *ChemPhysChem* **2016**, *17*, 458–462.
- [32] A. Strate, T. Niemann, P. Stange, D. Michalik, R. Ludwig, *Angew. Chem. Int. Ed.* **2017**, *56*, 496–500; *Angew. Chem.* **2017**, *129*, 510–514.
- [33] T. Niemann, D. Zaitsau, A. Strate, A. Villinger, R. Ludwig, *Sci. Rep.* **2018**, *8*, 14753.
- [34] F. S. Menges, H. J. Zeng, P. J. Kelleher, O. Gorlova, M. A. Johnson, T. Niemann, A. Strate, R. Ludwig, *J. Phys. Chem. Lett.* **2018**, *9*, 2979–2984.
- [35] T. Niemann, A. Strate, R. Ludwig, F. Menges, H. Zeng, P. Kelleher, O. Gorlova, M. Johnson, *Angew. Chem. Int. Ed.* **2018**, *57*, 15364–15368; *Angew. Chem.* **2018**, *130*, 15590–15594.
- [36] A. K. Soper, Empirical Potential Structure Refinement—A User's Guide, ISIS, Rutherford Appleton Laboratory, Didcot, U.K., **2006**.
- [37] A. K. Soper, *Phys. Rev. B* **2005**, *72*, 104204–104212.
- [38] C. J. Benmore, A. K. Soper, *The SANDALS Manual: A Guide to Performing Experiments on the Small Angle Neutron Diffractometer for Amorphous and Liquid Samples at ISIS*, Version 1.0, RAL Technical Reports, RAL-TR-1998-1006, 1998.
- [39] A. K. Soper, W. S. Howells, A. C. Hannon, *ATLAS-Analysis of Time-of-Flight Diffraction Data from Liquid and Amorphous Samples*, RAL-89-046 1989.
- [40] S. E. Norman, A. H. Turner, T. G. A. Youngs, *RSC Adv.* **2015**, *5*, 67220–67226.
- [41] R. Kanzaki, T. Mitsugi, S. Fukuda, K. Fujii, M. Takeuchi, Y. Soejima, T. Takamuku, T. Yamaguchi, Y. Umebayashi, S. Ishiguro, *J. Mol. Liq.* **2009**, *147*, 77–82.
- [42] G. Ferru, D. Gomes Rodrigues, L. Berthon, O. Diat, P. Baudin, P. Guilbaud, *Angew. Chem. Int. Ed.* **2014**, *53*, 5346–5350; *Angew. Chem.* **2014**, *126*, 5450–5454.
- [43] J. Neumann, B. Golub, L.-M. Odebrecht, R. Ludwig, D. Paschek, *J. Chem. Phys.* **2018**, *148*, 193828.
- [44] W. L. Jorgensen, D. S. Maxwell, J. Tirado-Rives, *J. Am. Chem. Soc.* **1996**, *118*, 11225–11236.
- [45] W. L. Jorgensen, N. A. McDonald, *J. Mol. Struct. THEOCHEM* **1998**, *424*, 145–155.
- [46] Gaussian 09, Revision A.02, M. J. Frisch, G. W. Trucks, H. B. Schlegel, G. E. Scuseria, M. A. Robb, J. R. Cheeseman, G. Scalmani, V. Barone, G. A. Petersson, H. Nakatsuji, X. Li, M.

- Caricato, A. Marenich, J. Bloino, B. G. Janesko, R. Gomperts, B. Mennucci, H. P. Hratchian, J. V. Ortiz, A. F. Izmaylov, J. L. Sonnenberg, D. Williams-Young, F. Ding, F. Lipparini, F. Egidi, J. Goings, B. Peng, A. Petrone, T. Henderson, D. Ranasinghe, V. G. Zakrzewski, J. Gao, N. Rega, G. Zheng, W. Liang, M. Hada, M. Ehara, K. Toyota, R. Fukuda, J. Hasegawa, M. Ishida, T. Nakajima, Y. Honda, O. Kitao, H. Nakai, T. Vreven, K. Throssell, J. A. Montgomery, Jr., J. E. Peralta, F. Ogliaro, M. Bearpark, J. J. Heyd, E. Brothers, K. N. Kudin, V. N. Staroverov, T. Keith, R. Kobayashi, J. Normand, K. Raghavachari, A. Rendell, J. C. Burant, S. S. Iyengar, J. Tomasi, M. Cossi, J. M. Millam, M. Klene, C. Adamo, R. Cammi, J. W. Ochterski, R. L. Martin, K. Morokuma, O. Farkas, J. B. Foresman, and D. J. Fox, Gaussian, Inc., Wallingford CT, 2016.
- [47] S. Grimme, J. Antony, S. Ehrlich, H. Krieg, *J. Chem. Phys.* **2010**, *132*, 154104.
- [48] S. Ehrlich, J. Moellmann, W. Reckien, T. Bredow, S. Grimme, *ChemPhysChem* **2011**, *12*, 3414–3420.
- [49] S. Grimme, A. Jansen, *Chem. Rev.* **2016**, *116*, 5105–5154.
- [50] L. B. Skinner, C. Huang, D. Schlesinger, L. G. M. Pettersson, A. Nilsson, C. J. Benmore, *J. Chem. Phys.* **2013**, *138*, 074506.
- [51] F. Huisken, M. Kaloudis, A. Kulcke, D. Voelkel, *Infrared Phys. Technol.* **1995**, *36*, 171.
- [52] U. Bergmann, A. Di Cicco, P. Wernet, E. Principi, P. Glatzel, A. Nilsson, *J. Chem. Phys.* **2007**, *127*, 174504.
- [53] T. Steiner, *Angew. Chem. Int. Ed.* **2002**, *41*, 48–76; *Angew. Chem.* **2002**, *114*, 50–80.
- [54] A. H. Narten, A. Habenschuss, *J. Chem. Phys.* **1984**, *80*, 3387–3391.
- [55] S. Saker, R. N. Joarder, *J. Chem. Phys.* **1994**, *100*, 5118–5122.
- [56] P.-G. Jönsson, *Acta Crystallogr. Sect. B* **1976**, *32*, 232–235.
- [57] M. A. Gebbie, A. M. Smith, H. A. Dobbs, A. A. Lee, G. G. Warr, X. Banquy, M. Valtiner, M. W. Rutland, J. N. Israelachvili, S. Perkin, R. Atkin, *Chem. Commun.* **2017**, *53*, 1214–1224.

Manuscript received: April 16, 2019

Revised manuscript received: May 25, 2019

Accepted manuscript online: June 8, 2019

Version of record online: July 9, 2019

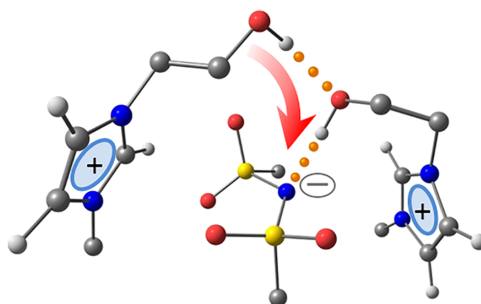
Structural Motifs in Cold Ternary Ion Complexes of Hydroxyl-Functionalized Ionic Liquids: Isolating the Role of Cation-Cation Interactions

F. S. Menges (20 %), H. J. Zeng (15 %), P. J. Kelleher (5 %), O. Gorlova (10 %), M. A. Johnson (15 %), T. Niemann (15 %), A. Strate (10 %), R. Ludwig (10 %)

J. Phys. Chem. Lett, 9, 2979-2984, 2018

Content:

The formation of (c-c) H-bonded clusters was investigated, using predissociation spectroscopy experiments on the smallest assembly that can display such an effect. Using an IR-IR double resonance experiment in combination with DFT calculations it could be shown that the initial spectra of the ternary complex consists of three structural isomers of which one shows an OH \cdots OH-bond between two cations.



Contributions to this work:

Fabian Menges (F. M.) was responsible for the CIVP experiments and has supervised Helen Zeng (H. Z.), Anne Strate (A. S.) and me. Olga Gorlova and Patrick Kelleher contributed to the work with the [C₂MIm][NTf₂] results. The DFT calculations were made by F. M., H. Z. and me. F. M. has performed the IR-IR double resonance experiments. F. M. and H. Z. wrote the first draft which was then optimized after some corrections from Prof. Ludwig, A. S. and me to the final manuscript by Prof. Johnson.

Structural Motifs in Cold Ternary Ion Complexes of Hydroxyl-Functionalized Ionic Liquids: Isolating the Role of Cation–Cation Interactions

Fabian S. Menges,^{†,§} Helen J. Zeng,[†] Patrick J. Kelleher,[†] Olga Gorlova,[†] Mark A. Johnson,^{*,†,§} Thomas Niemann,^{‡,§} Anne Strate,^{‡,§} and Ralf Ludwig^{*,‡,§}

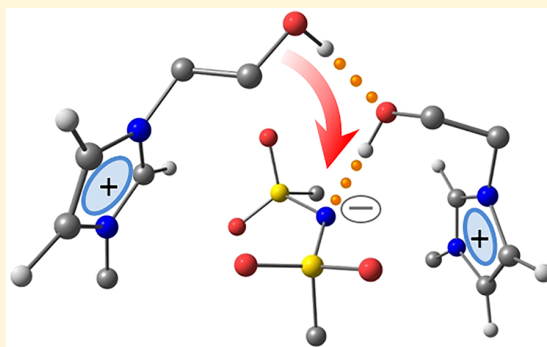
[†]Sterling Chemistry Laboratory, Yale University, New Haven, Connecticut 06520, United States

[‡]Department of Chemistry, University of Rostock, 18059 Rostock, Germany

[§]Leibniz-Institut für Katalyse e.V., Albert-Einstein-Strasse 29a, 18059 Rostock, Germany

Supporting Information

ABSTRACT: We address the competition between intermolecular forces underlying the recent observation that ionic liquids (ILs) with a hydroxyl-functionalized cation can form domains with attractive interactions between the nominally repulsive positively charged constituents. Here we show that this behavior is present even in the isolated ternary (HEMIm⁺)₂NTf₂[−] complex (HEMIm⁺ = 1-(2-hydroxyethyl)-3-methylimidazolium) cooled to about 35 K in a photodissociation mass spectrometer. Of the three isomers isolated by double resonance techniques, one is identified to exhibit direct contact between the cations. This linkage involves a cooperative H-bond wherein the OH group on one cation binds to the OH group on the other, which then attaches to the basic N atom of the anion. Formation of this motif comes at the expense of the usually dominant interaction of the acidic C₍₂₎H group on the Im ring with molecular anions, as evidenced by isomer-dependent shifts in the C₍₂₎H vibrational fundamentals.



The development of room-temperature ionic liquids (RTILs) has accelerated in recent years as their properties become increasingly tailored^{1,2} to facilitate chemical processes ranging from alternative, environmentally friendly solvents for chemical syntheses^{3–5} to spacecraft propellants.^{6–8} Because ILs are often heterogeneous at the molecular scale,^{9–12} optimizing their properties for particular applications from first-principles has proven to be challenging,^{8,13–22} and there are open fundamental questions about the intramolecular distortions and local contact motifs between the ionic constituents.^{23–25} For example, recent bulk spectroscopic results (FT-IR) have been reported that indicate direct points of contact between cations, denoted (c–c) interactions,^{26,27} that arise from cooperative hydrogen bonds involving the OH groups on hydroxyl-functionalized systems. In those cases, the spectroscopic signatures of hydrogen bonding in the OH stretching region were observed to become more prominent at lower (~213 K) temperatures, but the diffuse nature of the bands allowed only a qualitative picture of the local interactions. Here we focus on the isolated cluster ion consisting of two cations and one anion, denoted hereafter as (2,1), which are the smallest systems capable of displaying an anion-mediated, attractive interaction between molecular cations. The issues at play are indicated in the schematic arrangements of the ternary ionic complex displayed in Scheme 1. The arrangement shown on the right in

Scheme 1, with the anion sandwiched between the cations, has been observed in many (2,1) complexes that do not have OH groups.²⁸ The formation of a direct contact between the hydroxyl groups with short hydrocarbon tails (left structure in Scheme 1) requires a distortion of this quasi-symmetrical arrangement. For such a (c–c) interaction to occur, it would appear that the increased Coulomb repulsion between the positive charge centers and loss of one OH attachment to the anion would have to be somehow compensated by the H-bond linkage. Our goal in this work is therefore to identify a microscopic (2,1) system displaying this type of (c–c) motif in order to clarify the nature of the individual contacts that drive its stability.

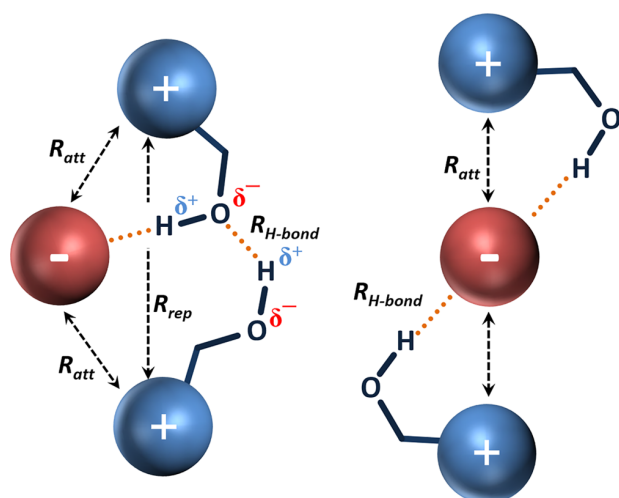
We specifically focus on the two cationic imidazolium derivatives (EMIm⁺ and HEMIm⁺) depicted in Scheme 2, complexed to NTf₂[−] (bis(trifluoromethylsulfonyl)imide), one of the most widely used anions in ILs.¹ These cations were chosen because recent studies^{17,23,24,29–34} have reported a spectroscopic way to measure the strength of the interaction between the most acidic position (C₍₂₎H) on the positively charged imidazolium ring and various anions (halides, BF₄[−]).

Received: April 11, 2018

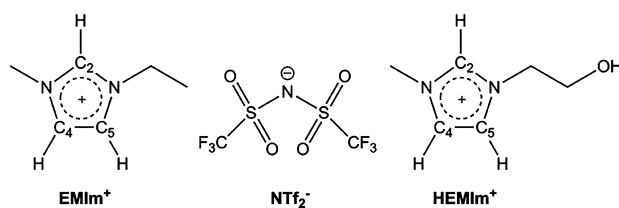
Accepted: May 11, 2018

Published: May 11, 2018

Scheme 1. Illustration of Competing Interactions at Play in an Ionic Liquid with a Hydroxyl-Functionalized Cation in the Positively Charged, Gas-Phase Ternary Complex



Scheme 2. Structures of 1-Ethyl-3-methylimidazolium (EMIm⁺), 1-(2-Hydroxyethyl)-3-methylimidazolium (HEMIm⁺), and Bis(trifluoromethylsulfonyl)imide (NTf₂⁻) Ions



This is accomplished by isolating the behavior of the vibrational fundamental associated with the isotopologue that is selectively deuterated at the C₍₂₎ position (C₍₂₎D) on the ring.^{28,31,32} When combined with the highly responsive nature of the OH stretching fundamental to its local environment, we demonstrate how the locations of the C₍₂₎H(D) and OH(D) stretching transitions provide sensitive spectroscopic reporters for the intermolecular interactions at play in the ternary ion assemblies. Specifically, by comparing the spectral behavior of the EMIm⁺ (2,1) complex with that of the hydroxylated derivative (HEMIm⁺), we establish that an H-bond linkage between the cations occurs even in this remarkably small complex. This allows us to reveal the detailed competition between the OH and CH groups for H-bonding attachment sites on NTf₂⁻ that underlie an attractive (c-c) assembly motif.

We characterize the structures of the ternary complexes with two cations and one anion by analyzing their vibrational spectra, which are obtained at low temperature (~35 K) through the use of mass-selective, cryogenic ion trapping techniques.³⁵ This method acquires spectra in a linear action mode by infrared photodissociation of weakly bound N₂ adducts.^{9,31,32,35–37} Furthermore, where appropriate, structural motifs of different isomeric structures adopted by these charged clusters are isolated through application of isomer-selective, two-color IR–IR double resonance spectroscopy.³⁸ The structural implications of the resulting band patterns are discussed in the context of calculated spectra for various

structural candidates obtained at the B3LYP-D3/6-31+G(d) level of theory.^{39–44}

Figure 1 presents the vibrational spectra measured for the EMIm⁺ and HEMIm⁺ ions (Figure 1a,c, respectively) along

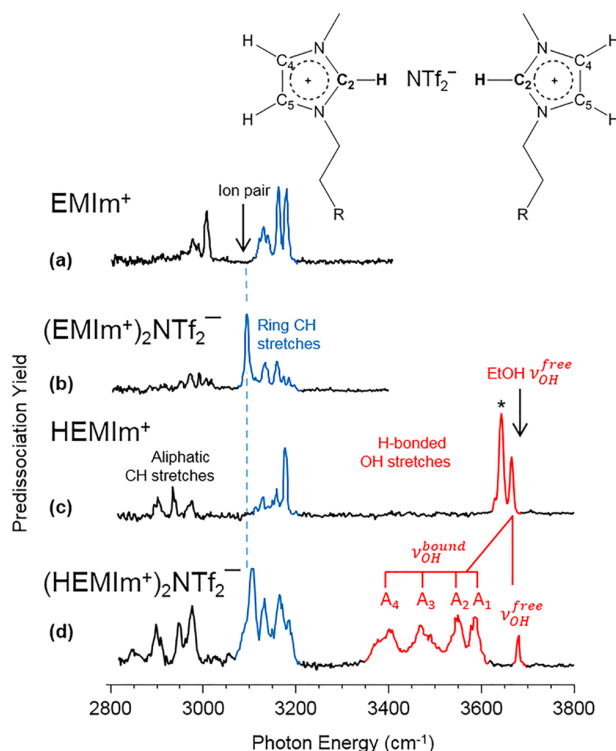


Figure 1. Photodissociation spectra of N₂-tagged (a) EMIm⁺, (b) (EMIm⁺)₂NTf₂⁻, (c) HEMIm⁺, and (d) (HEMIm⁺)₂NTf₂⁻. The OH stretches in traces (c) and (d) are colored red, with * in (c) representing an isomer where the N₂ tag is bound to the free OH (see Figure S1). The labels A₁, A₂, A₃, and A₄ denote H-bonded OH features in the ternary complex (d). In trace (b), the strongest band of the ring CH features (blue) lies close to the C₍₂₎H feature reported earlier for the [EMIm][NTf₂] neutral ion pair^{23,33,34} (arrow in trace (a)). The OH stretch fundamental of bare ethanol is indicated by an arrow at the right of trace (c).⁵⁸ R = OH for HEMIm⁺ and H for EMIm⁺. Measured transition energies are tabulated in Table S1.

with those of the corresponding (2,1) clusters with NTf₂⁻ (Figure 1b,d) in the spectral region associated with the key fundamentals involving the ring CH (blue) and OH (red) stretching modes. Energies of the key transitions are listed in Table S1. The CH multiplet near 3150 cm⁻¹ has been traced to strong mixing among the three aromatic CH stretches (labeled C₂, C₄, and C₅ in Scheme 2) as well as to Fermi-type interactions involving overtones of the corresponding bending modes.^{23,31–34,45} Nonetheless, both cations exhibit significant red shifts of these features upon complexation with the NTf₂⁻ anion, with the strongest member of the multiplet appearing lowest in energy. The fact that this feature occurs at essentially the same frequency in both ternary systems suggests that similar interactions are in play between the imidazolium ring and the anion. Moreover, we note that a similar band was observed in the [EMIm][NTf₂] neutral ion pair (arrow in Figure 1a),^{23,33,34} indicating that this is characteristic of the preferred binding motif between the EMIm⁺ ring and the NTf₂⁻ anion.

The spectrum of the ternary $(\text{HEMIm}^+)_2\text{NTf}_2^-$ complex (Figure 1d) also includes an extended suite of transitions in the OH stretching region (labeled A_1 , A_2 , A_3 , and A_4) that appear below the location of a free OH group (for example, in isolated ethanol, arrow in Figure 1c), with substructure evident on the lowest two (A_3 and A_4) features. We note that the asymmetric doublet in the HEMIm^+ spectrum near 3650 cm^{-1} arises from attachment of the N_2 tag (* in Figure 1c) to the free OH group, as discussed further in the SI (Figure S1). The red-shifted bands (A_1 – A_4) in the (2,1) spectrum occur in the region corresponding to fundamentals of OH groups that strongly interact with anionic domains.^{38,46–51} The picture that emerges from qualitative behavior of the ring CH and OH stretching bands is therefore that at least one of these two groups (available from the two cations) is strongly interacting with the anion. Moreover, the plethora of transitions in the OH stretching region raises the specter that different isomers may contribute to the pattern (as opposed to reflecting strong anharmonic coupling, which is also known to result in soft mode progressions built on OH stretching fundamentals⁵²).

Recognizing that the HEMIm^+ ion presents two primary contact points, the $\text{C}_{(2)}\text{H}$ and OH groups (Scheme 2), for interaction with the anion, the key issue regards whether these docking motifs compete for attachment sites on the anion. To establish the activity of the $\text{C}_{(2)}\text{H}$ groups, we obtained the spectra of the HEMIm^+ isotopologue with deuterium atom substitutions at both the $\text{C}_{(2)}$ and OH positions (denoted $d_{(2)}\text{-DEMIm}^+$, Figure 2a), its ternary complex with NTf_2^- (Figure 2c), and, for comparison, that of the analogous ternary complex with the $d_{(2)}\text{-EMIm}^+$ ion (Figure 2b). As mentioned above, the spectral response of the $\text{C}_{(2)}\text{D}$ group is free of the anharmonic interactions that complicate the interpretation of the coupled oscillators in the CH stretching region. As expected, the $\text{C}_{(2)}\text{D}$ fundamental appears as an isolated band in the bare ion spectrum, ($\nu_{\text{C}_{(2)}\text{D}}^{\text{free}}$ in Figure 2a). Interestingly, the OD pattern in the $(d_{(2)}\text{-DEMIm}^+)_2\text{NTf}_2^-$ spectrum (Figure 2c) is very similar to that of the OH pattern observed in the $(\text{HEMIm}^+)_2\text{NTf}_2^-$ case (Figure 1d). As such, the OD bands in the $(d_{(2)}\text{-DEMIm}^+)_2\text{NTf}_2^-$ spectrum are readily assigned to the same series (A_1 , A_2 , A_3 , and A_4 and free OD) as those observed in the spectrum of the light isotopologue. The $\text{C}_{(2)}\text{D}$ band near 2350 cm^{-1} appears to be asymmetrically broadened in the $(d_{(2)}\text{-DEMIm}^+)_2\text{NTf}_2^-$ spectrum (blue in Figure 2c) with a dominant red-shifted component ($\nu_{\text{C}_{(2)}\text{D}}^{\text{bound}}$) and a weaker higher-energy shoulder. The shoulder appears at the same location as the $\text{C}_{(2)}\text{D}$ band in the isolated $d_{(2)}\text{-DEMIm}^+$ cation ($\nu_{\text{C}_{(2)}\text{D}}^{\text{free}}$ in Figure 2a) and that of $d_{(2)}\text{-EMIm}^+$ (Figure S2a), indicating that only one of the two cations attaches to the anion through the $\text{C}_{(2)}\text{H}$ group. The $\text{C}_{(2)}\text{D}$ band in the $(d_{(2)}\text{-DEMIm}^+)_2\text{NTf}_2^-$ spectrum (Figure 2c) is broader than that in the $d_{(2)}\text{-EMIm}^+$ derivative (Figure 2b). In addition, the peak maximum is blue-shifted (by 6 cm^{-1}), with the activity near the $\nu_{\text{C}_{(2)}\text{D}}^{\text{free}}$ feature merging into the overall asymmetrical shape of the band. This shift suggests that the interaction strength of the $\text{C}_{(2)}\text{H}$ group with the anion is slightly weakened upon incorporation of the hydroxyl group.

To address the role of isomers in the assignments of the spectra, we carried out isomer-selective photochemical hole-burning experiments to establish whether distinct species are present and, if so, to isolate the spectrum of each. This was accomplished using a two-color IR–IR double resonance method described in detail by Yang et al.⁵³ Briefly, the method

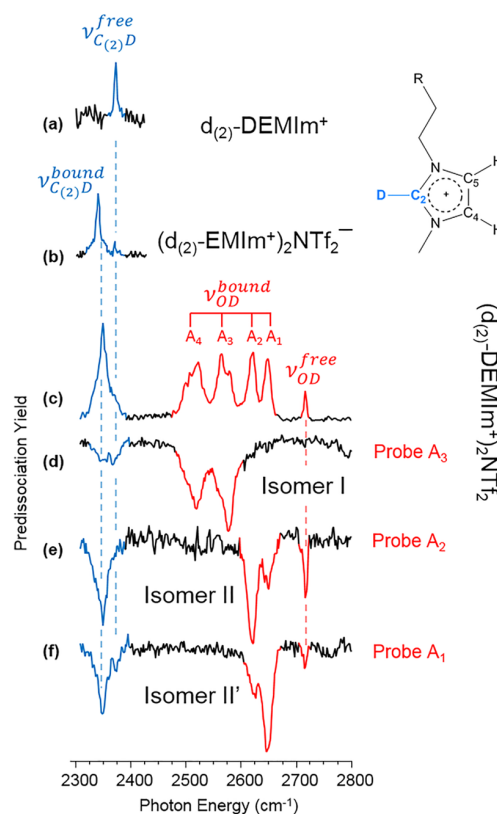


Figure 2. Selectively deuterated N_2 -tagged photodissociation spectra of (a) $d_{(2)}\text{-DEMIm}^+$, (b) $(d_{(2)}\text{-EMIm}^+)_2\text{NTf}_2^-$, and (c) $(d_{(2)}\text{-DEMIm}^+)_2\text{NTf}_2^-$. Traces (d–f) present IR–IR double resonance spectra of $(d_{(2)}\text{-DEMIm}^+)_2\text{NTf}_2^-$ probed at 2578 cm^{-1} (A_3), 2620 cm^{-1} (A_2), and 2645 cm^{-1} (A_1), respectively. R = OD for $d_{(2)}\text{-DEMIm}^+$ and H for $d_{(2)}\text{-EMIm}^+$. Measured transition energies are tabulated in Table S1.

relies on the occurrence of features that are unique to each conformer. In such a case, fixing a probe laser on a particular feature monitors the population of that isomer, while a powerful second laser is scanned through the entire spectrum upstream from the probe laser interaction. Because vibrational predissociation is a destructive method for obtaining IR spectra, pump laser excitation of resonances associated with the probed conformer yield a series of dips in the probe signal, thus isolating its spectrum. The method requires an intermediate stage of mass separation between the pump and probe and is thus denoted an IR^2MS^3 class of secondary mass analysis.³⁸

The isomer-selective spectra of the $(d_{(2)}\text{-DEMIm}^+)_2\text{NTf}_2^-$ isotopologues are reported in Figure 2d–f, which were obtained by probing the A_3 , A_2 , and A_1 features, respectively. Two isomer classes, denoted I and II, are resolved using double resonance. Additional frequencies were probed that yielded isomer-specific spectra consistent with one of these two classes (Figure S4). Most importantly, the isomer I spectrum (Figure 2d), which accounts for both the A_3 and A_4 OD features, contributes only weakly to the $\text{C}_{(2)}\text{D}$ region. Most of the $\text{C}_{(2)}\text{D}$ intensity is thus traced to the type II isomers, which also account for the free OD band as well as the moderately red-shifted A_1 and A_2 OD stretching bands. This behavior establishes that the formation of strong bonds to the OH groups of both cations in isomer I (evidenced by the strongly red-shifted OD stretches) comes at the expense of anionic

bonds to the $C_{(2)}H$ positions on the imidazolium rings. Moreover, the class II isomers display absorptions at the locations of both the free $C_{(2)}D$ ($\nu_{C_{(2)}D}^{free}$) and bound ($\nu_{C_{(2)}D}^{bound}$) regions. As such, the cations in the isomer II class bind to the anion through one $C_{(2)}H$ and one OH group. This information does not, however, resolve the question of whether or not these groups are on the same cation.

The large number of local minima available for the (2,1) clusters that have similar contact modalities does not allow unambiguous structural assignment by comparison with calculated vibrational band patterns, even when simplified by isotopomer-selective spectroscopy. This is especially true given the fact that the simpler binary ion pairs involving $[EMIm]^+ \cdot [NTf_2]^-$ are analyzed in terms of contributions from several isomers^{23,33,34} involving interactions of the $C_{(2)}H$ group with various SO groups on the cis and trans forms of the NTf_2^- scaffold. Attachment of the $C_{(2)}H$ group to the central N atom, the most basic site on the anion (which is protonated in the conjugate $HNTf_2$ acid),⁵⁴ has also been identified as a minimum-energy structure in calculations⁵⁵ but not invoked in prior experimental studies.^{23,33,34} In our survey of calculated structures (six selected structures in Figure S5 with XYZ coordinates in Table S2 and rotatable .pdf structures in Figure S7), we note that all strong $C_{(2)}H$ interactions occur at an SO group on the NTf_2^- anion, with the OH group of the corresponding $HEMIm^+$ cation adopting a nonbonding configuration. This would therefore suggest that one $HEMIm^+$ cation is responsible for both the strongly red-shifted $C_{(2)}D$ feature and the free OD feature observed in the spectrum of the ternary complex. As such, the second cation must bind in a different contact motif where the OH group binds to the anion rather than the $C_{(2)}H$ group, accounting for the weak band ($\nu_{C_{(2)}D}^{free}$) in the isomer-selective spectrum (Figure 2f). Many calculated arrangements are consistent with this asymmetrical binding behavior (Figure S5), with a representative structure indicated in Figure 3b. In this geometry, the NTf_2^- is in a trans configuration with the $C_{(2)}H$ of the $HEMIm^+$ (with a free OH) bound to an SO group on the anion, while the OH group on the other cation binds to the oxygen atom on the same sulfur atom. We note that incomplete spectral separation of the two class II isomers leaves open the possibility that isomer II' actually binds to the anion with both OH groups, leading to two overlapping transitions contributing to peak A_1 .

The situation regarding the local interactions in isomer I is more interesting because both cations bind to the anion through their OH groups, raising the possibility that they also interact with each other. The much larger red shifts associated with these OD features (A_3 and A_4 in Figure 2c) relative to those (A_1 and A_2) identified for single OH contacts in isomer II are indeed consistent with cooperative H-bonding to the anion. Harmonic calculations (Figure S3) indicate that such large shifts require a cooperative interaction between the two OH groups that acts to enhance the H-bonding interaction with the central N atom on the NTf_2^- anion. The spectral signature of this type of cooperative H-bond to an anion has been reported earlier⁵¹ for methanol attachment to the iodide ion in the $(CH_3OH)_2 \cdot I^-$ cluster. In that case, two isomers were observed: one in which both OH groups directly bind to the anion and another in which one OH attaches to the oxygen of the second to give an $OH \cdots OH \cdots I^-$ motif. This yields two OH bands split apart by 206 cm^{-1} , with the OH in contact with the ion

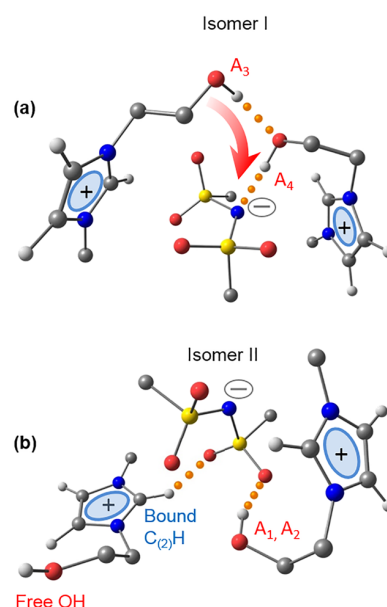


Figure 3. Low-energy structures of $(HEMIm^+)_2NTf_2^-$ calculated at the B3LYP-D3/6-31+G(d) level of theory representing the binding motifs of isomers with (a) and without (b) direct contact between the cations. F atoms of NTf_2^- and aliphatic H atoms of $HEMIm^+$ are omitted for clarity. Labels indicate groups nominally assigned to bands indicated in Figures 1 and 2.

appearing 197 cm^{-1} below that which results from attachment of a single methanol to iodide. The calculated structure consistent with the spectral pattern displayed by isomer I (Figure 3a) indeed displays this type of cooperative arrangement, and its corresponding harmonic band pattern (shown in Figure S3e) recovers both the weak activity in the $C_{(2)}D$ region as well as the two strongly red-shifted bands (A_3 and A_4) in the OD spectral region. These results highlight the importance of the N atom in the interaction with cationic proton donors despite the fact that NTf_2^- is often considered to be dominated by attachment to its SO groups.^{23,33,34,56} Support for the role of the N atom as an H-bond acceptor can be found, however, in recent solid-state NMR results on triethylammonium-based protic ILs (PILs),⁵⁷ which established that H-bonding from the cation to the central nitrogen atom on NTf_2^- is stronger than that to the oxygen. Calculations also indicate that this binding motif occurs with weakly acidic protons, as illustrated by the structure of the complex formed by attachment of a carboxylic acid-functionalized $EMIm^+$ cation to NTf_2^- , as presented in Figure S6.

Vibrational spectra of the bulk $[HEMIm][NTf_2]$ ionic liquids, with a hydroxyl-functionalized hydrocarbon tail on the cation, have been interpreted in the context of an attractive, H-bonding interaction between the cations. We trace this behavior to the smallest assembly that can display such an effect, the isolated ternary $(HEMIm^+)_2NTf_2^-$ complex, cooled to about 35 K in a photodissociation mass spectrometer. Of the three isomers isolated by double resonance techniques, the one with direct contact between the cations involves a cooperative H-bond in which the OH group on one cation binds to the OH group on the other, which then attaches to the N position at the center of the NTf_2^- anion. This can be formally regarded as an acid–base interaction motif involving cooperativity-enhanced acidity of an OH group interacting with the

protonation site of the NTf_2^- anion. This behavior is thus a microscopic example of a growing class of interactions in hydroxyl-functionalized ionic liquids in which cationic constituents bind together in hydrogen-bonded domains surrounded by anionic counterions.

■ ASSOCIATED CONTENT

Supporting Information

The Supporting Information is available free of charge on the ACS Publications website at DOI: 10.1021/acs.jpclett.8b01130.

Supporting experimental and computational data, as well as rotatable structures (PDF)

■ AUTHOR INFORMATION

Corresponding Authors

*E-mail: mark.johnson@yale.edu (M.A.J.).

*E-mail: ralf.ludwig@uni-rostock.de (R.L.).

ORCID

Fabian S. Menges: 0000-0002-5859-9197

Mark A. Johnson: 0000-0002-1492-6993

Notes

The authors declare no competing financial interest.

■ ACKNOWLEDGMENTS

M.A.J. gratefully acknowledges the U.S. Department of Energy under Grant DE-FG02-06ER15800 for support of the characterization of ionic liquid structure and the Air Force Office of Scientific Research (Grant FA9550-17-1-0267) for the two-color IR–IR capability of the cryogenic ion vibrational spectrometer critical for this study. P.J.K. thanks the National Science Foundation's Center for Aerosol Impacts on Chemistry of the Environment (CAICE) under grant number CHE-1305427 for funding the work on the laser systems critical for these experiments. R.L. gratefully acknowledges financial support from the Deutsche Forschungsgemeinschaft (DFG) under Grant LU 506/14-1. T.N. and A.S. thank the "HERMES-Forschungsförderung" and the "Frauenförderprogramm" of the University of Rostock for supporting their research stays at Yale University. The authors thank Chinh H. Duong and Nan Yang for their help with the double resonance measurements, as well as Profs. E. Castner and M. Maroncelli for their very helpful remarks regarding the presentation of this work.

■ REFERENCES

- Castner, E. W.; Margulis, C. J.; Maroncelli, M.; Wishart, J. F. Ionic Liquids: Structure and Photochemical Reactions. *Annu. Rev. Phys. Chem.* **2011**, *62*, 85–105.
- Tang, S.; Baker, G. A.; Zhao, H. Ether- and Alcohol-Functionalized Task-Specific Ionic Liquids: Attractive Properties and Applications. *Chem. Soc. Rev.* **2012**, *41* (10), 4030–66.
- Vekariya, R. L. A Review of Ionic Liquids: Applications towards Catalytic Organic Transformations. *J. Mol. Liq.* **2017**, *227*, 44–60.
- Dorjnamjin, D.; Ariunaa, M.; Shim, Y. K. Synthesis of Silver Nanoparticles using Hydroxyl Functionalized Ionic Liquids and their Antimicrobial Activity. *Int. J. Mol. Sci.* **2008**, *9* (5), 807–819.
- Janiak, C. Metal Nanoparticle Synthesis in Ionic Liquids. *Top. Organomet. Chem.* **2013**, *51*, 17–53.
- Gao, H. X.; Joo, Y. H.; Twamley, B.; Zhou, Z. Q.; Shreeve, J. M. Hypergolic Ionic Liquids with the 2,2-Dialkyltriazanium Cation. *Angew. Chem., Int. Ed.* **2009**, *48* (15), 2792–2795.
- Schneider, S.; Hawkins, T.; Rosander, M.; Vaghjiani, G.; Chabreau, S.; Drake, G. Ionic Liquids as Hypergolic Fuels. *Energy Fuels* **2008**, *22* (4), 2871–2872.
- Zhang, Y. Q.; Gao, H. X.; Joo, Y. H.; Shreeve, J. M. Ionic Liquids as Hypergolic Fuels. *Angew. Chem., Int. Ed.* **2011**, *50* (41), 9554–9562.
- Hanke, K.; Kaufmann, M.; Schwaab, G.; Havenith, M.; Wolke, C. T.; Gorlova, O.; Johnson, M. A.; Kar, B. P.; Sander, W.; Sanchez-Garcia, E. Understanding the Ionic Liquid $[\text{NC}_{4111}][\text{NTf}_2]$ from Individual Building Blocks: An IR-Spectroscopic Study. *Phys. Chem. Chem. Phys.* **2015**, *17* (13), 8518–8529.
- Wang, Y. T.; Voth, G. A. Unique Spatial Heterogeneity in Ionic Liquids. *J. Am. Chem. Soc.* **2005**, *127* (35), 12192–12193.
- Hayes, R.; Warr, G. G.; Atkin, R. Structure and Nanostructure in Ionic Liquids. *Chem. Rev. (Washington, DC, U. S.)* **2015**, *115* (13), 6357–6426.
- Triolo, A.; Russina, O.; Bleif, H. J.; Di Cola, E. Nanoscale Segregation in Room Temperature Ionic Liquids. *J. Phys. Chem. B* **2007**, *111* (18), 4641–4644.
- Wishart, J. F. Energy Applications of Ionic Liquids. *Energy Environ. Sci.* **2009**, *2* (9), 956–961.
- Shkrob, I. A.; Wishart, J. F. Charge Trapping in Imidazolium Ionic Liquids. *J. Phys. Chem. B* **2009**, *113* (16), 5582–5592.
- Armand, M.; Endres, F.; MacFarlane, D. R.; Ohno, H.; Scrosati, B. Ionic-Liquid Materials for the Electrochemical Challenges of the Future. *Nat. Mater.* **2009**, *8* (8), 621–629.
- Galinski, M.; Lewandowski, A.; Stepniak, I. Ionic Liquids as Electrolytes. *Electrochim. Acta* **2006**, *51* (26), 5567–5580.
- Lei, Z. G.; Dai, C. N.; Chen, B. H. Gas Solubility in Ionic Liquids. *Chem. Rev. (Washington, DC, U. S.)* **2014**, *114* (2), 1289–1326.
- Hapiot, P.; Lagrost, C. Electrochemical Reactivity in Room-Temperature Ionic Liquids. *Chem. Rev. (Washington, DC, U. S.)* **2008**, *108* (7), 2238–2264.
- Weingartner, H.; Cabrele, C.; Herrmann, C. How Ionic Liquids Can Help to Stabilize Native Proteins. *Phys. Chem. Chem. Phys.* **2012**, *14* (2), 415–426.
- Rogers, R. D.; Seddon, K. R. Ionic Liquids - Solvents of the Future? *Science* **2003**, *302* (5646), 792–793.
- Leal, J. P.; Esperanca, J. M. S. S.; Minas da Piedade, M. E.; Canongia Lopes, J. N.; Rebelo, L. P. N.; Seddon, K. R. The Nature of Ionic Liquids in the Gas Phase. *J. Phys. Chem. A* **2007**, *111* (28), 6176–6182.
- Earle, M. J.; Esperanca, J. M. S. S.; Gilea, M. A.; Canongia Lopes, J. N.; Rebelo, L. P. N.; Magee, J. W.; Seddon, K. R.; Widegren, J. A. The Distillation and Volatility of Ionic Liquids. *Nature* **2006**, *439* (7078), 831–834.
- Booth, R. S.; Annesley, C. J.; Young, J. W.; Vogelhuber, K. M.; Boatz, J. A.; Stearns, J. A. Identification of Multiple Conformers of the Ionic Liquid $[\text{Emim}][\text{Tf}_2\text{N}]$ in the Gas Phase using IR/UV Action Spectroscopy. *Phys. Chem. Chem. Phys.* **2016**, *18* (25), 17037–17043.
- Hunt, P. A.; Ashworth, C. R.; Matthews, R. P. Hydrogen Bonding in Ionic Liquids. *Chem. Soc. Rev.* **2015**, *44* (5), 1257–1288.
- Weingartner, H. Understanding Ionic Liquids at the Molecular Level: Facts, Problems, and Controversies. *Angew. Chem., Int. Ed.* **2008**, *47* (4), 654–70.
- Knorr, A.; Stange, P.; Fumino, K.; Weinhold, F.; Ludwig, R. Spectroscopic Evidence for Clusters of Like-Charged Ions in Ionic Liquids Stabilized by Cooperative Hydrogen Bonding. *ChemPhysChem* **2016**, *17* (4), 458–462.
- Katsyuba, S. A.; Vener, M. V.; Zvereva, E. E.; Fei, Z. F.; Scopelliti, R.; Laurenczy, G.; Yan, N.; Paunescu, E.; Dyson, P. J. How Strong Is Hydrogen Bonding in Ionic Liquids? Combined X-ray Crystallographic, Infrared/Raman Spectroscopic, and Density Functional Theory Study. *J. Phys. Chem. B* **2013**, *117* (30), 9094–9105.
- Gorlova, O.; Craig, S. M.; Johnson, M. A. Communication: Spectroscopic Characterization of a Strongly Interacting C_2H Group on the EMIM^+ Cation in the $(\text{EMIM}^+)_2\text{X}^-$ ($\text{X} = \text{BF}_4, \text{Cl}, \text{Br}$, and I) Ternary Building Blocks of Ionic Liquids. *J. Chem. Phys.* **2017**, *147* (23), 231101.
- Tsuzuki, S.; Tokuda, H.; Mikami, M. Theoretical Analysis of the Hydrogen Bond of Imidazolium C_2H with Anions. *Phys. Chem. Chem. Phys.* **2007**, *9* (34), 4780–4784.

- (30) Strate, A.; Niemann, T.; Michalik, D.; Ludwig, R. When Like Charged Ions Attract in Ionic Liquids: Controlling the Formation of Cationic Clusters by the Interaction Strength of the Counterions. *Angew. Chem., Int. Ed.* **2017**, *56* (2), 496–500.
- (31) Johnson, C. J.; Fournier, J. A.; Wolke, C. T.; Johnson, M. A. Ionic Liquids from the Bottom Up: Local Assembly Motifs in [EMIM][BF₄] through Cryogenic Ion Spectroscopy. *J. Chem. Phys.* **2013**, *139* (22), 224305.
- (32) Fournier, J. A.; Wolke, C. T.; Johnson, C. J.; McCoy, A. B.; Johnson, M. A. Comparison of the Local Binding Motifs in the Imidazolium-Based Ionic Liquids [EMIM][BF₄] and [EMMIM][BF₄] through Cryogenic Ion Vibrational Predissociation Spectroscopy: Unraveling the Roles of Anharmonicity and Intermolecular Interactions. *J. Chem. Phys.* **2015**, *142* (6), 064306.
- (33) Cooper, R.; Zolot, A. M.; Boatz, J. A.; Sporleder, D. P.; Stearns, J. A. IR and UV Spectroscopy of Vapor-Phase Jet-Cooled Ionic Liquid [Emim]⁺[Tf₂N][−]: Ion Pair Structure and Photodissociation Dynamics. *J. Phys. Chem. A* **2013**, *117* (47), 12419–12428.
- (34) Obi, E. I.; Leavitt, C. M.; Raston, P. L.; Moradi, C. P.; Flynn, S. D.; Vaghjiani, G. L.; Boatz, J. A.; Chambreau, S. D.; Doublerly, G. E. Helium Nanodroplet Isolation and Infrared Spectroscopy of the Isolated Ion-Pair 1-Ethyl-3-Methylimidazolium Bis-(trifluoromethylsulfonyl)imide. *J. Phys. Chem. A* **2013**, *117* (37), 9047–9056.
- (35) Wolk, A. B.; Leavitt, C. M.; Garand, E.; Johnson, M. A. Cryogenic Ion Chemistry and Spectroscopy. *Acc. Chem. Res.* **2014**, *47* (1), 202–210.
- (36) Craig, S. M.; Menges, F. S.; Johnson, M. A. Application of Gas Phase Cryogenic Vibrational Spectroscopy to Characterize the CO₂, CO, N₂ and N₂O Interactions with the Open Coordination Site on a Ni(I) Macrocyclic using Dual Cryogenic Ion Traps. *J. Mol. Spectrosc.* **2017**, *332*, 117–123.
- (37) Menges, F. S.; Craig, S. M.; Totsch, N.; Bloomfield, A.; Ghosh, S.; Kruger, H. J.; Johnson, M. A. Capture of CO₂ by a Cationic Nickel(I) Complex in the Gas Phase and Characterization of the Bound, Activated CO₂ Molecule by Cryogenic Ion Vibrational Predissociation Spectroscopy. *Angew. Chem., Int. Ed.* **2016**, *55* (4), 1282–1285.
- (38) Leavitt, C. M.; Wolk, A. B.; Fournier, J. A.; Kamrath, M. Z.; Garand, E.; Van Stipdonk, M. J.; Johnson, M. A. Isomer-Specific IR-IR Double Resonance Spectroscopy of D₂-Tagged Protonated Dipeptides Prepared in a Cryogenic Ion Trap. *J. Phys. Chem. Lett.* **2012**, *3* (9), 1099–1105.
- (39) Grimme, S.; Hansen, A.; Brandenburg, J. G.; Bannwarth, C. Dispersion-Corrected Mean-Field Electronic Structure Methods. *Chem. Rev. (Washington, DC, U. S.)* **2016**, *116* (9), 5105–5154.
- (40) Ehrlich, S.; Moellmann, J.; Reckien, W.; Bredow, T.; Grimme, S. System-Dependent Dispersion Coefficients for the DFT-D3 Treatment of Adsorption Processes on Ionic Surfaces. *ChemPhysChem* **2011**, *12* (17), 3414–3420.
- (41) Grimme, S.; Bannwarth, C. Ultra-Fast Computation of Electronic Spectra for Large Systems by Tight-Binding Based Simplified Tamm-Dancoff Approximation (sTDA-xTB). *J. Chem. Phys.* **2016**, *145* (5), 054103.
- (42) Grimme, S.; Antony, J.; Ehrlich, S.; Krieg, H. A Consistent and Accurate Ab Initio Parametrization of Density Functional Dispersion Correction (DFT-D) for the 94 Elements H–Pu. *J. Chem. Phys.* **2010**, *132* (15), 154104.
- (43) Knorr, A.; Ludwig, R. Cation-Cation Clusters in Ionic Liquids: Cooperative Hydrogen Bonding Overcomes Like-Charge Repulsion. *Sci. Rep.* **2015**, DOI: 10.1038/srep17505.
- (44) Heimer, N. E.; Del Sesto, R. E.; Meng, Z. Z.; Wilkes, J. S.; Carper, W. R. Vibrational Spectra of Imidazolium Tetrafluoroborate Ionic Liquids. *J. Mol. Liq.* **2006**, *124* (1–3), 84–95.
- (45) Roth, C.; Chatzipapadopoulos, S.; Kerle, D.; Friedriszik, F.; Lutgens, M.; Lochbrunner, S.; Kuhn, O.; Ludwig, R. Hydrogen Bonding in Ionic Liquids Probed by Linear and Nonlinear Vibrational Spectroscopy. *New J. Phys.* **2012**, *14*, 105026.
- (46) DePalma, J. W.; Kelleher, P. J.; Tavares, L. C.; Johnson, M. A. Coordination-Dependent Spectroscopic Signatures of Divalent Metal Ion Binding to Carboxylate Head Groups: H₂[−] and He-Tagged Vibrational Spectra of M²⁺·RCO₂[−] (M = Mg and Ca, R = −CD₃, −CD₂CD₃) Complexes. *J. Phys. Chem. Lett.* **2017**, *8* (2), 484–488.
- (47) Roscioli, J. R.; Diken, E. G.; Johnson, M. A.; Horvath, S.; McCoy, A. B. Prying Apart a Water Molecule with Anionic H-Bonding: A Comparative Spectroscopic Study of the X·H₂O (X = OH, O, F, Cl, and Br) Binary Complexes in the 600–3800 cm^{−1} Region. *J. Phys. Chem. A* **2006**, *110* (15), 4943–4952.
- (48) Gorlova, O.; DePalma, J. W.; Wolke, C. T.; Brathwaite, A.; Odbadrakh, T. T.; Jordan, K. D.; McCoy, A. B.; Johnson, M. A. Characterization of the Primary Hydration Shell of the Hydroxide Ion with H₂ Tagging Vibrational Spectroscopy of the OH[−]·(H₂O)_{n=2,3} and OD[−]·(D₂O)_{n=2,3} Clusters. *J. Chem. Phys.* **2016**, *145*, 134304.
- (49) Robertson, W. H.; Weddle, G. H.; Kelley, J. A.; Johnson, M. A. Solvation of the Cl[−]·H₂O Complex in CCl₄ Clusters: The Effect of Solvent-Mediated Charge Redistribution on the Ionic H-Bond. *J. Phys. Chem. A* **2002**, *106*, 1205–1209.
- (50) Robertson, W. H.; Diken, E. G.; Price, E. A.; Shin, J.-W.; Johnson, M. A. Spectroscopic Determination of the OH[−] Solvation Shell in the OH[−]·(H₂O)_n Clusters. *Science* **2003**, *299*, 1367.
- (51) Robertson, W. H.; Karapetian, K.; Ayotte, P.; Jordan, K. D.; Johnson, M. A. Infrared Predissociation Spectroscopy of I[−]·(CH₃OH)_n, n = 1, 2: Cooperativity in Asymmetric Solvation. *J. Chem. Phys.* **2002**, *116*, 4853–4857.
- (52) Robertson, W. H.; Price, E. A.; Weber, J. M.; Shin, J.-W.; Weddle, G. H.; Johnson, M. A. Infrared Signatures of a Water Molecule Attached to Triatomic Domains of Molecular Anions: Evolution of the H-bonding Configuration with Domain Length. *J. Phys. Chem. A* **2003**, *107*, 6527–6532.
- (53) Yang, N.; Duong, C. H.; Kelleher, P. J.; Johnson, M. A.; McCoy, A. B. Isolation of Site-Specific Anharmonicities of Individual Water Molecules in the I[−]·(H₂O)₂ Complex using Tag-Free, Isotopomer Selective IR-IR Double Resonance. *Chem. Phys. Lett.* **2017**, *690*, 159–171.
- (54) Akai, N.; Parazs, D.; Kawai, A.; Shibuya, K. Cryogenic Neon Matrix-isolation FTIR Spectroscopy of Evaporated Ionic Liquids: Geometrical Structure of Cation-Anion 1:1 Pair in the Gas Phase. *J. Phys. Chem. B* **2009**, *113* (14), 4756–4762.
- (55) Zhang, S. G.; Qi, X. J.; Ma, X. Y.; Lu, L. J.; Zhang, Q. H.; Deng, Y. Q. Investigation of Cation-Anion Interaction in 1-(2-Hydroxyethyl)-3-Methylimidazolium-Based Ion Pairs by Density Functional Theory Calculations and Experiments. *J. Phys. Org. Chem.* **2012**, *25* (3), 248–257.
- (56) Lall-Ramnarine, S. I.; Zhao, M.; Rodriguez, C.; Fernandez, R.; Zmich, N.; Fernandez, E. D.; Dhiman, S. B.; Castner, E. W.; Wishart, J. F. Connecting Structural and Transport Properties of Ionic Liquids with Cationic Oligoether Chains. *J. Electrochem. Soc.* **2017**, *164* (8), H5247–H5262.
- (57) Khudozhnikov, A. E.; Stange, P.; Golub, B.; Paschek, D.; Stepanov, A. G.; Kolokolov, D. I.; Ludwig, R. Characterization of Doubly Ionic Hydrogen Bonds in Protic Ionic Liquids by NMR Deuteron Quadrupole Coupling Constants: Differences to H-bonds in Amides, Peptides, and Proteins. *Angew. Chem., Int. Ed.* **2017**, *56* (45), 14310–14314.
- (58) Plyler, E. K. Infrared Spectra of Methanol, Ethanol, and Normal-Propanol. *J. Res. Natl. Bur. Stand. (U. S.)* **1952**, *48* (4), 281–286.

Spectroscopic evidence for an attractive cation-cation interaction in hydroxyl-functionalized ionic liquids: The first H-bonded chain-like trimer

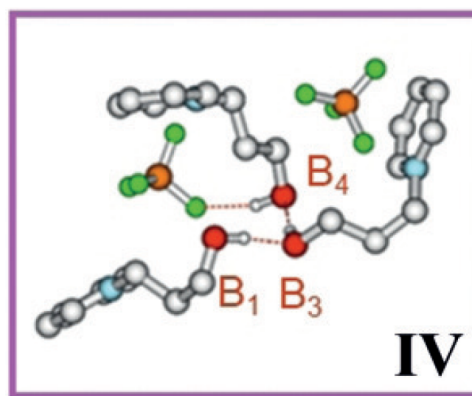
T. Niemann (20 %), A. Strate (10 %), R. Ludwig (20 %), H. J. Zeng (20 %), F. S. Menges (15 %), M. A. Johnson (15 %)

Angew. Chem. Int. Ed., 57, 47, 15364-15368, 2018

Angew. Chem., 130, 47, 15590-15594, 2018

Content:

The vibrational spectrum of the $[\text{HOC}_3\text{Py}^+]_3[\text{BF}_4^-]_2$ complex exhibits spectral features which are consistent with the formation of an $\text{OH}\cdots\text{OH}\cdots\text{OH}\cdots\text{BF}_4^-$ binding motive. We rationalised this behaviour in the context of strong cooperative hydrogen bonding. This was the largest H-bonded cationic cluster reported so far.



Contributions to this work:

I have synthesised the IL investigated in this work. Fabian Menges (F. M.) was responsible for the CIVP experiments and has supervised Helen Zeng (H. Z.), Anne Strate and me during them. The DFT calculations were made by Prof. Ludwig and me. Prof. Ludwig wrote the first draft to which I have contributed in some parts. It was then optimized after some corrections from Prof. Johnson, F. M., H. Z. and me to the final manuscript by Prof. Ludwig.

Ionic Liquids

International Edition: DOI: 10.1002/anie.201808381
German Edition: DOI: 10.1002/ange.201808381

Spectroscopic Evidence for an Attractive Cation–Cation Interaction in Hydroxy-Functionalized Ionic Liquids: A Hydrogen-Bonded Chain-like Trimer

Thomas Niemann, Anne Strate, Ralf Ludwig,* Helen J. Zeng, Fabian S. Menges, and Mark A. Johnson*

Abstract: We address the formation of hydrogen bonded domains among the cationic constituents of the ionic liquid (IL) 1-(3-hydroxypropyl)pyridinium tetrafluoroborate [HPPy][BF₄] by means of cryogenic ion vibrational predissociation spectroscopy of cold (ca. 35 K) gas-phase cluster ions and quantum chemistry. Specifically, analysis of the OH stretching bands reveals a chain-like OH...OH...OH...BF₄[−] binding motif involving the three cations in the cationic quinary cluster ion (HPPy⁺)₃(BF₄[−])₂. Calculations show that this cooperative H-bond attraction compensates for the repulsive Coulomb forces and results in stable complexes that successfully compete with those in which the OH groups are predominantly attached to the counter anions. Our combined experimental and theoretical approach provides insight into the cooperative effects that lead to the formation of hydrogen bonded domains involving the cationic constituents of ILs.



Ionic liquids (ILs) attract increasing interest in science and technology owing to their unique properties, which can be tailored for specific applications ranging from chemical synthesis and separation processes to media for electrochemical devices.^[1–7] The properties of ILs are governed by a subtle balance of Coulombic interactions, hydrogen bonding, and dispersion forces.^[8,9] In particular, local and directional hydrogen bonding has significant influence on IL behavior,^[10,11] leading to classification schemes based on the character of the doubly ionic hydrogen bonds (DIHB).^[12,13] This term is a pleonasm because ILs consist purely of ions and any hydrogen bonding necessarily takes place between ions.

In principle, two main types of hydrogen bonding are possible: One involving the Coulomb-enhanced interaction between a cation and an anion (c–a), and another occurring between ions of like-charge, which in the present case involves the positively charged cations (c–c). It is anticipated that the (c–c) hydrogen bonds are significantly weakened by repulsive Coulomb forces, and the strengths of both types of H-bonds in ILs differ from the regular hydrogen bonds observed for neutral molecular clusters of water or alcohols.^[14–17] In ILs, (c–c) hydrogen bonds might not appear to be important drivers of local structures because they have to compete with the repelling Coulomb forces between the cations as well as with the Coulomb enhanced (c–a) hydrogen bonds between cation and anion. Despite this expectation, however, structural motifs involving H-bonded cationic clusters were observed in the bulk liquid phase.^[18–21] In particular, FT-IR measurements clearly showed two distinct vibrational bands that are assigned to (c–a) and (c–c) hydrogen bonded species. Note that the (c–c) hydrogen bonds are evidently stronger than those in the (c–a) case as indicated by the magnitudes of the redshifts of their corresponding vibrational bands.^[18–21] The formation of these (c–c) clusters is mediated by surrounding counterions and was observed to become more prominent at lower temperature (ca. 213 K).

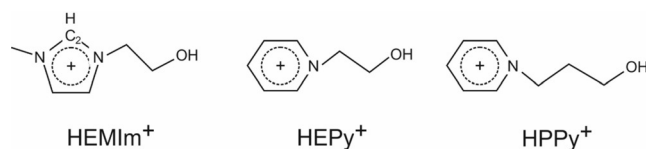
Because the diffuse nature of the vibrational bands from bulk ILs allows only a qualitative picture of the local interactions, we recently focused on the isolated cluster ions in the gas-phase consisting of two cations and one anion, denoted as (2,1).^[22] We were able to isolate three isomers of the ternary (HEMIm⁺)₂NTf₂[−] complex in the 1-(2-hydroxyethyl)-3-methylimidazolium bis(trifluoromethylsulfonyl)imide IL, including one in which the OH group on one cation binds to the OH group on the other, which then attaches to the basic nitrogen atom of the anion. Although we isolated the cation–cation interaction, we were not able to observe larger (c–c) bound complexes. The goal of this work is therefore to identify an ionic liquid with cation–anion combinations that exhibit this type of (c–c) H-bond motif in larger complexes.

From recent bulk phase studies on ILs, we learned that the formation of cationic clusters is governed by three factors that act to enhance (c–c) interactions: 1) weakly interacting anions to attenuate the (c–a) interaction, 2) polarizable cations with only one interaction site (in this case, the OH functional group) to better compensate for the negative charge of the anion, and 3) large distances between the OH functional

[*] M. Sc. T. Niemann, Dr. A. Strate, Dr. R. Ludwig
Department of Chemistry, University of Rostock
18059 Rostock (Germany)
and
Department Life, Light & Matter, University of Rostock
18051 Rostock (Germany)
E-mail: ralf.ludwig@uni-rostock.de
Dr. R. Ludwig
Leibniz-Institut für Katalyse e.V.
Albert-Einstein-Str. 29a, 18059 Rostock (Germany)
M. Sc. H. J. Zeng, Dr. F. S. Menges, Dr. M. A. Johnson
Sterling Chemistry Laboratory, Yale University
New Haven, CT 06520 (USA)
E-mail: mark.johnson@yale.edu

 Supporting information and the ORCID identification number(s) for the author(s) of this article can be found under:
 <https://doi.org/10.1002/anie.201808381>.

group and the positive charge center of the cation to weaken the like-charge repulsion.^[22] We therefore switched from [HEMIm][NTf₂] to the 1-(3-hydroxypropyl)pyridinium tetrafluoroborate [HPPy][BF₄] system (see Scheme 1) for the following reasons: First, we changed the NTf₂[−] counterion to a similarly weakly coordinating anion (BF₄[−]) with fewer H-bond acceptors than are present in NTf₂[−] (four oxygen atoms at two sulfonyl groups and the strongly interacting nitrogen). Next, we replaced HEMIm⁺ with HPPy⁺ to suppress the hydrogen bonding that occurs via the acidic C₂H position in HEMIm⁺ and thus isolate the interactions of the OH groups to the anions as well as to each other. In addition, the longer hydroxyalkyl group in HPPy⁺ allows for further separation between cationic centers linked by a hydrogen bond between OH groups.



Scheme 1. Structures of HEMIm⁺, HEPy⁺, and HPPy⁺ cations.

The efficacies of these design strategies for the cationic components were tested with quantum chemical calculations of the potential energy curves of the cationic dimers 1-(2-hydroxyethyl)-3-methylimidazolium (HEMIm⁺)₂, 1-(2-hydroxyethyl)pyridinium (HEPy⁺)₂ and 1-(3-hydroxypropyl)pyridinium (HPPy⁺)₂. These were calculated using unrestricted second-order Møller-Plesset perturbation theory (UMP2) with the well-balanced, but small 6-31 + G* basis set.^[23–25] It includes polarization as well as diffuse functions and has been shown to be suitable for calculating hydrogen bonded clusters of like-charged ions.^[26,27] Although we were not able to isolate the (HPPy⁺)₂ dications experimentally, we note that diatomic dications (e.g., N₂²⁺) have been directly observed and spectroscopically characterized in other experiments.^[28] Interestingly, these curves often feature a local minimum at small internuclear distances that enable metastable bound states far into the continuum arising from separation of the two positively charged atoms.

Figure 1 presents the potential energy curves for the dissociation of the dicationic dimers (HEMIm⁺)₂, (HEPy⁺)₂ and (HPPy⁺)₂, along the $R_{(\text{H}\cdots\text{O})}$ hydrogen-bond stretching coordinate (with relaxation of the other variables), plotted with energies relative to that of the isolated cations at $\Delta E = 0$. Like the doubly charged diatomic molecules,^[28] these curves also feature shallow local minima, and the vertical arrows show the calculated equilibrium well energies at this level of theory for the three dimers in the sequence above: $\Delta E = 137.8 \text{ kJ mol}^{-1}$, $\Delta E = 136.4 \text{ kJ mol}^{-1}$, and $\Delta E = 82.4 \text{ kJ mol}^{-1}$. In each case, the effective well depth is measured with respect to the transition state (at about $R_{(\text{H}\cdots\text{O})} = 2.5 \text{ \AA}$, $R_{(\text{H}\cdots\text{O})} = 3.0 \text{ \AA}$, and $R_{(\text{H}\cdots\text{O})} = 3.55 \text{ \AA}$, respectively) that signals the descent towards separated cations. These local minima correspond to binding energies of 3.1 kJ mol^{-1} , 4.52 kJ mol^{-1} , and $12.14 \text{ kJ mol}^{-1}$ respectively. From these calculations it becomes clear that the binding energy is only slightly

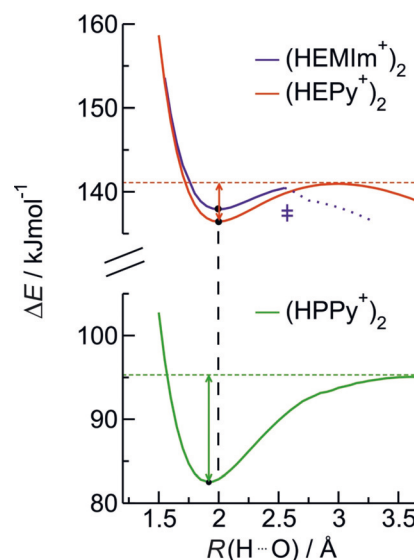


Figure 1. Calculated (UMP2/6-31 + G*) potential energy curves for the dicationic dimers (HEMIm⁺)₂, (HEPy⁺)₂, and (HPPy⁺)₂, along the $R_{(\text{H}\cdots\text{O})}$ hydrogen-bond stretching coordinate. The equilibrium bond lengths, $R_{(\text{H}\cdots\text{O})}$, for the fully relaxed structures are shown as dots and included in Table S1.

increased from (HEMIm⁺)₂ to (HEPy⁺)₂, but increases substantially from (HEPy⁺)₂ to (HPPy⁺)₂ owing to elongation of the hydroxyalkyl chain tether, thus weakening the repulsive Coulomb forces. Moreover, the effective well depth and the width of the potential barrier opposing tunneling-type dissociation are significantly larger for (HPPy⁺)₂ compared to (HEPy⁺)₂. The equilibrium distances are also shortened from $R_{(\text{H}\cdots\text{O})} = 1.9994 \text{ \AA}$ to $R_{(\text{H}\cdots\text{O})} = 1.91745 \text{ \AA}$ with increasing alkyl chain tether (see Figure 1). We note that the relaxed potential energy curve for (HEMIm⁺)₂ exhibits numerical anomalies (denoted by ‡ in Figure 1). This situation is easily understood, however, as a consequence of the weakening of the intermolecular H-bond when the two moieties are stretched to an $R_{(\text{H}\cdots\text{O})}$ distance of about 2.5 \AA . At that point, the decrease in energy reflects the internal rearrangements within the individual cations, leading to intramolecular H-bonds between the C₂H donors and the hydroxy oxygen acceptors. This is also in agreement with our earlier experimental result for the ternary complexes of this IL.^[22] Usually, OH groups win the competition with CH groups for H-bonding attachment sites on NTf₂[−]. However, simply the presence of the CH attachment site allows the formation of species for which one OH group is free and not involved in a desired (c–c) complex. In conclusion, the quantum chemical calculations fully support our hypothesis that [HPPy][BF₄] may provide the largest (c–c) complexes ever observed. Based on these results we synthesized the IL [HPPy][BF₄] following well known methods (see Supporting Information). The IL was properly purified and the water content has been determined by Karl-Fischer titration.

We characterized the structures of the ternary complexes with two cations and one anion (2,1), and those of the quinary complexes with three cations and two anions (3,2) by analyzing their vibrational spectra displayed in Figure 2b,c.

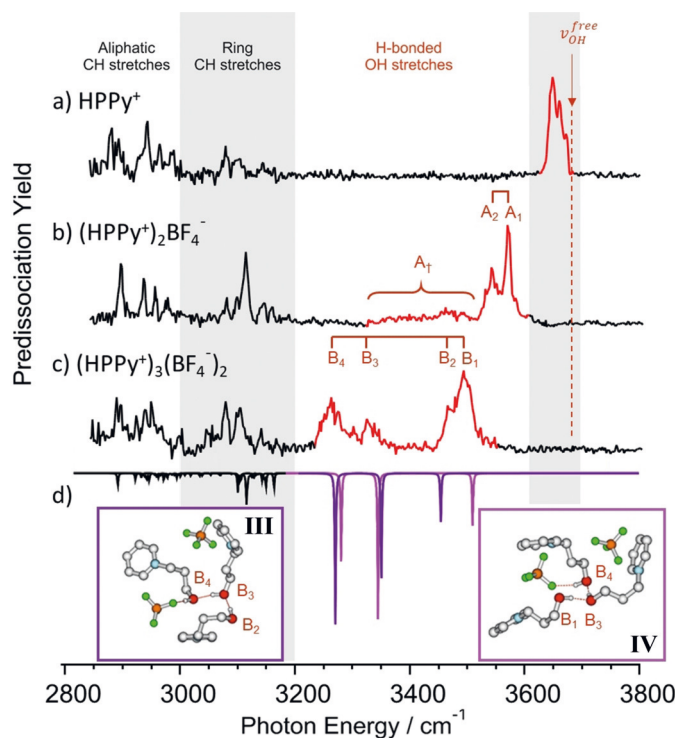


Figure 2. Photodissociation spectra of N_2 tagged a) $HPPy^+$, b) $(HPPy^+)_2BF_4^-$, c) $(HPPy^+)_3(BF_4^-)_2$, and d) calculated harmonic spectra for $(HPPy^+)_3(BF_4^-)_2$. The OH stretches are colored red. The labels A_1 , A_2 , and A_3 denote the H-bonded OH features in the cationic (2,1) cluster and B_1 – B_4 in the (3,2) cluster, respectively. Inverted traces in (d) display the calculated spectra (scaled 0.97) for isomer **III** (purple) and **IV** (pink; see caption of Figure 3 for details). The OH stretch of pure ethanol is indicated by an arrow at the right of the upper trace as a reference.^[34]

These were obtained at low temperature (ca. 35 K) through the use of mass-selective, cryogenic ion-trapping techniques.^[22] This method acquires spectra in a linear action mode by infrared photodissociation of weakly bound N_2 adducts. The structural implications of the resulting band patterns are discussed in the context of calculated spectra for various structural candidates obtained at the B3LYP-D3/6-31 + G* level of theory.^[29–33] For cationic dimers, this method gave similar results to those obtained with the more demanding MP2 method.

The vibrational spectrum measured for the (3,2) cluster of $HPPy^+$ cations with BF_4^- anions is presented in Figure 2c, and is compared with those of the isolated $HPPy^+$ cation (Figure 2a) and the corresponding (2,1) cationic complex (Figure 2b). The key fundamentals involve the aliphatic CH (<3000 cm^{-1}), ring CH (<3200 cm^{-1}) and OH (>3200 cm^{-1}) stretching modes. The (2,1) and (3,2) clusters display significant red shifts and increasing intensities in the OH stretching region (red) upon complexation with BF_4^- . The spectra of the (2,1) and (3,2) complexes also include an extended suite of transitions in the OH stretching region (labelled A_1 , A_2 , and A_3 in Figure 2b and B_1 – B_4 in Figure 2c, respectively) that appear below the location of a free OH group (arrow in Figure 2a).^[34] The red shifted bands (A_1 , A_2 , and A_3) in the (2,1) spectrum (Figure 2b) occur at similar positions as those

found in the $(HEMIm^+)_2NTf_2^-$ spectrum (A_1 – A_4 in Figure S2a).^[22] This similarity suggests that bands A_1 and A_2 in the (2,1) complex can be assigned to an arrangement in which both cations bind independently to the anion through the OH groups, while the further red shifted (but less intense) A_3 band is due to another isomer with a cooperative $OH\cdots OH\cdots BF_4^-$ H-bonding motif. This scenario is supported by harmonic frequency calculations for the $HPPy^+/BF_4^-$ (2,1) cluster as shown in Figure S3b. Surprisingly, however, the vibrational features of the isomer with the direct contact between the cations is barely evident in the spectrum, indicating that the longer alkyl chain tether does not enhance the generation of this isomer in the (2,1) complexes as expected. However, the spectrum of the quinary (3,2) complex displays vibrational bands B_3 and B_4 (Figure 2c) which are much more red shifted than the analogous feature A_3 in the (2,1) spectrum. This additional red shift is important because it signals a cooperative interaction among all three $HPPy^+$ cations in the sense that the spectral signature of the motif in play is not established upon addition of the second cation.

Although we could not obtain isomer-selective spectra for the (3,2) complexes because of their lower yield in the ion source,^[22] comparison with calculated vibrational band patterns provides a compelling structural assignment to $(HPPy^+)_3(BF_4^-)_2$ complexes wherein cooperative hydrogen bonding is maximized in a homodromic (that is, in the same sense) $OH\cdots OH\cdots OH\cdots BF_4^-$ binding motif. Specifically, we calculated twelve (3,2) low energy structures to identify the range of H-bonded arrangements between cations and anions (c–a) and between cations themselves (c–c) (see Supporting Information). The energetically most favorable (3,2) complexes are shown in Figure 3. The given clusters **I**: c–c–a, a; **II**: c–c–a, c–a; **III**: c–c–c–a, a and **IV**: c–c–c–a, a only differ in energy by less than 15 $kJ\ mol^{-1}$, whereas all the other calculated (3,2) isomers are energetically strongly disfavored by more than 40 $kJ\ mol^{-1}$ relative to the most stable structure (**I**) recovered in the search. From the calculated twelve complexes, only those showing the $OH\cdots OH\cdots OH\cdots BF_4^-$ binding motifs (**III** and **IV** in Figure 3) yield the strongly redshifted frequencies near 3260 cm^{-1} (purple and pink inverted traces in Figure 2d) that are observed in the measured spectra. The cooperative effect of these long chains with homodromic H-bonding appears to maximize the OH bond to the anion as well as the strengths of the linkages down the chain. The calculated (3,2) complexes **III** and **IV**, which both exhibit the $OH\cdots OH\cdots OH\cdots BF_4^-$ binding motif, differ in the details of their H-bonding to the anion. In complex **IV**, for example, the $OH\cdots BF_4^-$ interaction is weakened due to the stronger interaction of the anion with the proximal pyridinium ring. As a result, less charge can be donated from the anion into the OH antibonding orbital, leading to slightly higher frequencies (**IV**: 3500 cm^{-1} vs. **III**: 3470 cm^{-1}). The other energetically disfavored complexes (see Supporting Information) cannot account for the large redshifts in the OH stretching bands observed experimentally. Thus, the measured spectra allow assignments to the calculated complex **III** with frequencies labelled B_4 , B_3 , and B_2 and complex **IV** with frequencies labelled B_4 , B_3 , and B_1 , respectively.

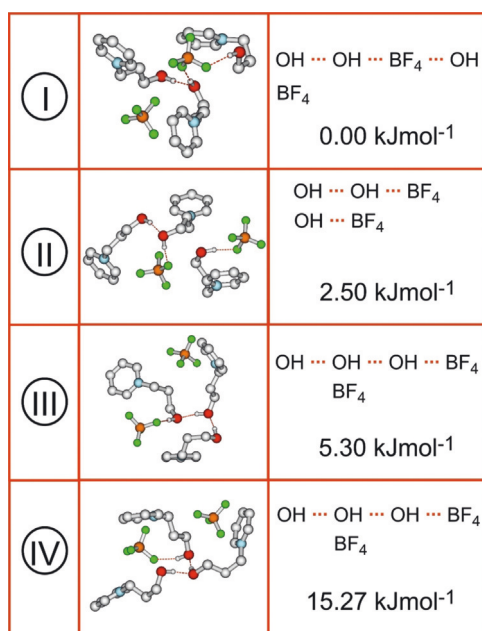


Figure 3. The lowest-energy (HPPy⁺)₃(BF₄⁻)₂ complexes calculated at the B3LYP-D3/6-31 + G* level of theory. Only the structures III and IV representing the binding motifs of isomers with triple contact between the cations show redshifted frequencies at 3260 cm⁻¹. The aliphatic and aromatic H atoms of HPPy⁺ are omitted for clarity.

Summarizing, the vibrational spectrum of the (HPPy⁺)₃(BF₄⁻)₂ complex exhibits spectral features in the OH stretching region that are consistent with formation of an OH...O-H...OH...BF₄⁻ binding motif. In this arrangement, the OH group on the first cation binds to the OH group on a second cation, which in turn binds to the OH group of a third cation that attaches to the basic F atom of the anion. We rationalize this behavior in the context of strong cooperative hydrogen bonding and weakly interacting anions that compensate for the repulsive Coulomb forces between cations and allow the formation of H-bonded chain-like cationic trimers. The subtle balance of long- and short-range, directional and non-directional interactions between ions in IL results in the largest H-bonded cationic clusters reported so far.

Acknowledgements

M.A.J. thanks the Department of Energy (DOE) under grant DE-FG02-06ER15800 for support of this work. The cryogenic ion spectrometer critical to these measurements was provided by the Air Force Office of Scientific Research (AFOSR) under grants FA9550-17-1-0267 (DURIP) and FA9550-18-1-0213. R.L. thanks for the financial support from the Deutsche Forschungsgemeinschaft (DFG) under grant LU 506/14-1. TN and AS thank the “HERMES-Forschungsförderung” and the “Frauenförderprogramm” of the University of Rostock for supporting their research stays at Yale University.

Conflict of interest

The authors declare no conflict of interest.

Keywords: clusters · hydrogen bonding · ion spectroscopy · ionic liquids · quantum chemistry

How to cite: *Angew. Chem. Int. Ed.* **2018**, *57*, 15364–15368
Angew. Chem. **2018**, *130*, 15590–15594

- [1] H. Weingärtner, *Angew. Chem. Int. Ed.* **2008**, *47*, 654–670; *Angew. Chem.* **2008**, *120*, 664–682.
- [2] F. Endres, S. Z. El Abedin, *Phys. Chem. Chem. Phys.* **2006**, *8*, 2101–2116.
- [3] T. Welton, *Chem. Rev.* **1999**, *99*, 2071–2084.
- [4] N. V. Plechkova, K. R. Seddon, *Chem. Soc. Rev.* **2008**, *37*, 123.
- [5] S. P. M. Ventura, F. A. e Silva, M. V. Quental, D. Mondal, M. G. Freire, J. A. P. Coutinho, *Chem. Rev.* **2017**, *117*, 6984–7052.
- [6] M. Galiński, A. Lewandowski, I. Stepniak, *Electrochim. Acta* **2006**, *51*, 5567–5580.
- [7] S. Mennea, J. Piresb, M. Anoutib, A. Balducci, *Electrochem. Commun.* **2013**, *31*, 39–41.
- [8] K. Fumino, R. Ludwig, *J. Mol. Liq.* **2014**, *192*, 94–102.
- [9] K. Fumino, S. Reimann, R. Ludwig, *Phys. Chem. Chem. Phys.* **2014**, *16*, 21903–21929.
- [10] K. Fumino, A. Wulf, R. Ludwig, *Angew. Chem. Int. Ed.* **2008**, *47*, 8731–8734; *Angew. Chem.* **2008**, *120*, 8859–8862.
- [11] K. Fumino, T. Peppel, M. Geppert-Rybczyńska, D. H. Zaitsau, J. K. Lehmann, S. P. Verevkin, M. Köckerling, R. Ludwig, *Phys. Chem. Chem. Phys.* **2011**, *13*, 14064–14075.
- [12] P. A. Hunt, C. R. Ashworth, R. P. Matthews, *Chem. Soc. Rev.* **2015**, *44*, 1257.
- [13] C. R. Ashworth, R. P. Matthews, T. Welton, P. A. Hunt, *Phys. Chem. Chem. Phys.* **2016**, *18*, 18145–18160.
- [14] F. N. Keutsch, R. J. Saykally, *Proc. Natl. Acad. Sci. USA* **2001**, *98*, 10533–10540.
- [15] R. Ludwig, *Angew. Chem. Int. Ed.* **2001**, *40*, 1808–1827; *Angew. Chem.* **2001**, *113*, 1856–1876.
- [16] F. Huisken, M. Stemmler, *Chem. Phys. Lett.* **1988**, *144*, 391–395.
- [17] H. L. Han, C. Camacho, H. A. Witek, Y. P. Lee, *J. Chem. Phys.* **2011**, *134*, 144309.
- [18] A. Knorr, R. Ludwig, *Sci. Rep.* **2015**, *5*, 17505.
- [19] A. Knorr, P. Stange, K. Fumino, F. Weinhold, R. Ludwig, *ChemPhysChem* **2016**, *17*, 458–462.
- [20] A. Strate, T. Niemann, D. Michalik, R. Ludwig, *Angew. Chem. Int. Ed.* **2017**, *56*, 496–500; *Angew. Chem.* **2017**, *129*, 510–514.
- [21] T. Niemann, D. Zaitsau, A. Strate, A. Villinger, R. Ludwig, *Sci. Rep.* **2018**, *8*, 14753.
- [22] F. S. Menges, H. J. Zeng, P. J. Kelleher, O. Gorlova, M. A. Johnson, T. Niemann, A. Strate, R. Ludwig, *J. Phys. Chem. Lett.* **2018**, *9*, 2979–2984.
- [23] Gaussian 09 (Revision B.01), M. J. Frisch et al.; see the Supporting Information.
- [24] C. Møller, M. S. Plesset, *Phys. Rev.* **1934**, *46*, 618–622.
- [25] M. Head-Gordon, J. A. Pople, M. J. Frisch, *Chem. Phys. Lett.* **1988**, *153*, 503–506.
- [26] A. Strate, T. Niemann, R. Ludwig, *Phys. Chem. Chem. Phys.* **2017**, *19*, 18854–18862.
- [27] A. Strate, V. Overbeck, V. Lehde, J. Neumann, A.-M. Bónsa, T. Niemann, D. Paschek, D. Michalik, R. Ludwig, *Phys. Chem. Chem. Phys.* **2018**, *20*, 5617–5625.
- [28] R. W. Wetmore, R. K. Boyd, *J. Phys. Chem.* **1986**, *90*, 5540–5551.
- [29] S. Grimme, J. Antony, S. Ehrlich, H. Krieg, *J. Chem. Phys.* **2010**, *132*, 154104.

- [30] S. Ehrlich, J. Moellmann, W. Reckien, T. Bredow, S. Grimme, *ChemPhysChem* **2011**, *12*, 3414–3420.
- [31] S. Grimme, A. Jansen, J. G. Brandenburg, C. Bannwarth, *Chem. Rev.* **2016**, *116*, 5105–5154.
- [32] S. Grimme, C. Bannwarth, *J. Chem. Phys.* **2016**, *145*, 054103.
- [33] T. Niemann, P. Stange, A. Strate, R. Ludwig, *ChemPhysChem* **2018**, *19*, 2979–2984.
- [34] E. K. Plyler, *J. Res. Natl. Bur. Stand.* **1952**, *48*, 281–286.
- Manuscript received: July 23, 2018
Accepted manuscript online: October 10, 2018
Version of record online: October 24, 2018
-

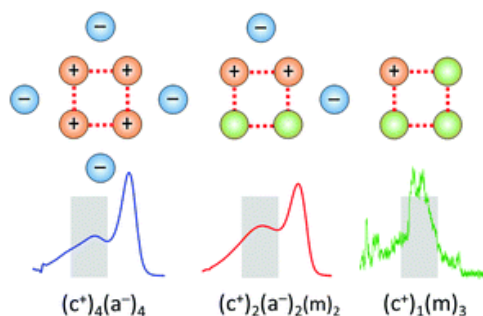
Cooperatively enhanced hydrogen bonds in ionic liquids: closing the loop with molecular mimics of hydroxy-functionalized cations

T. Niemann (35 %), A. Strate (5 %), R. Ludwig (15 %), H. J. Zeng (20 %), F. S. Menges (10 %), M. A. Johnson (15 %)

Phys. Chem. Chem. Phys., 21, 18092–18098, 2019

Content:

The combined experimental and theoretical approach using IR spectroscopy, CIVP spectroscopy, and DFT calculations for the gas and the liquid phases, provides a quantitative understanding of the competition between differently H-bonded and charged constituents in liquids. The cationic cyclic tetramer $(\text{HEPy}^+)(\text{PhenEthOH})_3$ exhibits vibrational bands similar to cyclic (c-c) tetramers in the IL and the IL/ML mixtures.



Contributions to this work:

I have synthesised the ILs investigated in this work and I have done all Mid-IR experiments of the bulk IL and IL/ML mixtures. Helen Zeng (H. Z.) was responsible for the CIVP experiments under supervision of Fabian Menges. The DFT calculations were made by Prof. Ludwig and me. I wrote the first draft with support of Prof. Ludwig. It was then optimized after major corrections from Prof. Johnson, H. Z. to the final manuscript by Prof. Ludwig.



Cite this: *Phys. Chem. Chem. Phys.*,
2019, 21, 18092

Cooperatively enhanced hydrogen bonds in ionic liquids: closing the loop with molecular mimics of hydroxy-functionalized cations†

Thomas Niemann,^{ab} Anne Strate,^{ab} Ralf Ludwig,^{id} *^{abc} Helen J. Zeng,^{id} ^d
Fabian S. Menges^{id} ^d and Mark A. Johnson^{id} *^d

We address the cooperative hydrogen bonding interactions in play between the ionic constituents of ionic liquids (ILs) with particular attention to those involving the attractive interactions between two cations in the system 1-(2-hydroxyethyl)pyridinium tetrafluoroborate [HEPy][BF₄]. This is accomplished by comparing the temperature-dependent linear infrared spectra of [HEPy][BF₄] with that of the molecular mimic of its cation, 2-phenylethanol (PhenEthOH). We then explored the structural motifs of these H-bonded configurations at the molecular level by analyzing the cryogenic ion vibrational predissociation spectroscopy of cold (~35 K) gas phase cluster ions with quantum chemical methods. The analysis of the OH stretching bands reveals the formation of the various binding motifs ranging from the common ⁺OH...BF₄[−] interaction in ion-pairs (c-a) to the unusual ⁺OH...⁺OH interaction (c-c) in linear and cyclic, homodromic H-bonding domains. Replacing ion-pairs by the molecular (neutral) analogue of the IL cation also results in the formation of positively charged cyclic motifs, with the bands of the gas phase cationic cyclic tetramer (HEPy⁺)(PhenEthOH)₃ appearing quite close to those assigned previously to cyclic tetramers in the liquid. These conclusions are supported by density functional theory (DFT) calculations of the cationic and neutral clusters as well as the local structures in the liquid. Our combined experimental and theoretical approach for the gas and the liquid phases provides important insight into the competition between differently H-bonded and charged constituents in liquids.

Received 11th June 2019,
Accepted 30th July 2019

DOI: 10.1039/c9cp03300a

rsc.li/pccp

Introduction

Hydrogen bonding is key to many processes in the chemistry and physical properties of molecular liquids,^{1–10} and this interaction also plays an especially critical role in the rational design of ionic liquids (ILs), which solely consist of ions.^{11–23} Coulomb enhanced hydrogen bonding between cation and anion in ILs has been examined in a plethora of infrared (IR) and Raman studies.^{24–32} However, in the special case of hydroxy-functionalized ILs, two distinct types of H-bonds have been reported: one corresponding to the common, Coulomb-enhanced interaction between cations and anions (c-a), and a second that creates an attractive interaction between two cations (c-c).^{33–41} For these ILs, structural motifs involving H-bonded cationic clusters were evidenced in the bulk liquid

phase by means of linear infrared (IR) measurements, which displayed two distinct vibrational band envelopes that could be assigned to (c-a) and (c-c) hydrogen bond motifs. An interesting, and counterintuitive aspect of the (c-c) hydrogen bonds is that their characteristic OH stretching bands are more redshifted than those found in the (c-a) contacts, suggesting that the (c-c) bonds are stronger than those in the (c-a) case.^{33–41} The formation of these (c-c) clusters is mediated by surrounding counter ions and was observed to become more prominent at lower temperature (~213 K).

Although it is expected that the H-bonds in ILs differ from those that are well studied in neutral clusters of water or alcohol molecules,^{42–46} the diffuse nature of the vibrational bands from bulk ILs allows only a qualitative picture of the local interactions. Consequently, our recent classification of the broad, redshifted spectral bands of hydroxy-functionalized ILs to the formation of (c-c) dimers, trimers and cyclic tetramers was somewhat speculative, being guided primarily by DFT-calculated frequencies of related clusters.^{34–37} Hence, the purpose of the present study is to combine linear infrared (IR) spectroscopy and cryogenic ion vibrational predissociation (CIVP) spectroscopy to quantify the spectral signatures of local (c-a), (c-c) and (c-m)

^a Department of Chemistry, University of Rostock, 18059 Rostock, Germany.

E-mail: ralf.ludwig@uni-rostock.de

^b Department Life, Light & Matter – University of Rostock, 18051 Rostock, Germany

^c Leibniz-Institut für Katalyse e.V., Albert-Einstein-Str. 29a, 18059 Rostock, Germany

^d Sterling Chemistry Laboratory, Yale University, New Haven, CT 06520, USA.

E-mail: mark.johnson@yale.edu

† Electronic supplementary information (ESI) available. See DOI: 10.1039/c9cp03300a

[m = neutral molecule] H-bond motifs in ILs and molecular liquids (MLs) by comparing the bands in the liquid phase with those displayed by well defined, composition selected gas phase cluster ions. The combined experimental approach, together with quantum chemical calculations, provides a detailed understanding of the interplay among H-bonding interactions between cations, anions and neutral molecules and allows inferences to be made about the likely structural candidates that exist in the bulk.

Strategy of this study

We illustrate the concept of this study in Scheme 1:

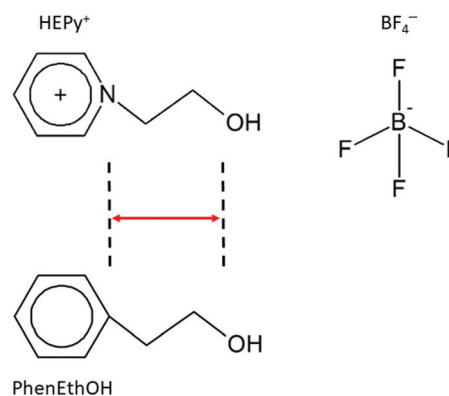
(a) Temperature-dependent, low energy vibrational bands in the OH stretching region displayed by hydroxy-functionalized ILs are attributed to H-bond formation between cations, creating cationic clusters up to cyclic tetramers $(c^+)_4(a^-)_4$ that are fully compensated by counter anions in the neutral bulk system.

(b) Promote the formation of extended H-bond networks by replacing the ion-pairs $(c^+)(a^-)$ by molecules (m) in IL/ML mixtures.

(c) Isolate the spectral signatures of local H-bonding motifs in cold, gas phase ions with precisely controlled compositions with special attention to determine the intrinsic signatures of cyclic structures in the $(c^+)(m)_3$ complexes.

(d) Extend the gas phase cluster study to the $(c^+)_4(a^-)_3$ cationic complex to compare with the bulk spectra from (a).

Our earlier studies showed that the formation of cationic clusters from ILs is enhanced by weakly interacting anions, polarizable cations with only one interaction site (e.g. one functional group) and large distances between the functional group and the positive charge centre of the cation.^{34–39} For this reason, we have chosen the 1-(2-hydroxyethyl)pyridinium tetrafluoroborate $[\text{HEPy}][\text{BF}_4]$ (see Scheme 2) as a model IL to study. Specifically, the $[\text{HEPy}][\text{BF}_4]$ system provides a weakly interacting anion (BF_4^-), a polarizable pyridinium ring (Py^+), and a hydroxyethyl tether (HE) between the positively charged pyridinium ring and the OH functional group. This is in contrast to the situation

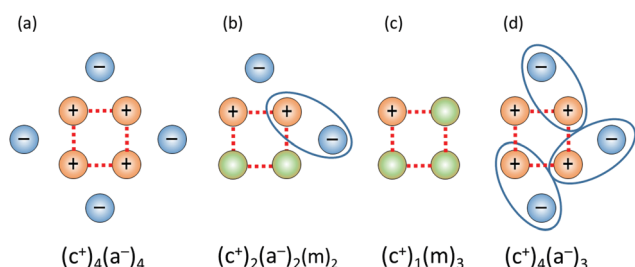


Scheme 2 The 1-(2-hydroxyethyl)pyridinium (HEPy^+) cation and the tetrafluoroborate (BF_4^-) anion as constituents of $[\text{HEPy}][\text{BF}_4]$ IL. The molecular mimic of the cation, 2-phenylethanol (PhenEthOH), has a similar distance between the aromatic ring and the hydroxyl group as indicated by the red double-headed arrow.

in the 1-(2-hydroxyethyl)-3-methylimidazolium tetrafluoroborate $[\text{HEMIm}][\text{BF}_4]$ reported earlier, in which the acidic $\text{C}_{(2)}\text{H}$ at the imidazolium ring allowed for an additional interaction with the anion as well as with their own OH group or those of other cations, all interactions that would act to suppress cationic cluster formation.^{38,39} The HEPy^+ cation in $[\text{HEPy}][\text{BF}_4]$, on the other hand, provides a single proton donor function with its OH group. To bridge the behavior of ionic liquids to their molecular analogues, we also follow the spectroscopic consequences when the IL cation is replaced by the 2-phenylethanol (PhenEthOH) molecular mimic. That modification was chosen because it likely acts to reduce the attractive and repulsive Coulomb forces at play in the systems and enhance the cooperative H-bond interactions for spectroscopic analysis. Such cooperative effects stem from non-pairwise-additive charge transfer and are characterized by strongly enhanced redshifts in IR spectra as observed with increasing size of water and alcohol clusters.^{42–46}

Features of cyclic cationic tetramers in the IR spectra of the ionic liquid $[\text{HEPy}][\text{BF}_4]$

Fig. 1 presents the infrared (IR) spectra of the pure IL $[\text{HEPy}][\text{BF}_4]$ as a function of temperature between 213 K and 353 K. To avoid congestion from aliphatic and ring CH vibrational bands and prevent possible overlap with strongly redshifted OH vibrational bands, these spectra are obtained after subtraction of that from the related OD functionalized IL. The OH group of the HEPy^+ cation provides hydrogen bonding either to the BF_4^- anion, resulting in (c–a) clusters, and/or to the hydroxyl groups of other cations, giving (c–c) clusters. At the highest temperature (353 K), we observe a main OH vibrational band at 3549 cm^{-1} , which can be easily assigned to the expected $^+\text{OH} \cdots \text{BF}_4^-$ hydrogen bond between the counter ions. The high wavenumber indicates that the cation–anion hydrogen bond is relatively weak in spite of the expected enhancement by their Coulombic attraction. In fact, the implied interaction strength is on the same order as those of water and methanol in similar ionic liquids with BF_4^- anions.^{18,19} However, the envelope of the observed vibrational band is not symmetric with extended



Scheme 1 Illustrations explaining the concept of this study. The identification of the structural motifs can be achieved by liquid and gas phase IR spectroscopies. (a) Cyclic tetramers $(c^+)_4(a^-)_4$, fully compensated by counter anions in the neutral bulk system. (b) Neutral cyclic tetramers $(c^+)_2(a^-)_2(m)_2$ in the bulk phase, wherein ion-pairs $(c^+)(a^-)$ (circled in (b)) are replaced by molecules (m). (c) Positively charged cyclic tetramers $(c^+)(m)_3$ in the gas phase. (d) Positively charged cyclic tetramers $(c^+)_4(a^-)_3$ in the gas phase, with stronger Coulomb repulsion by removing one counter anion.

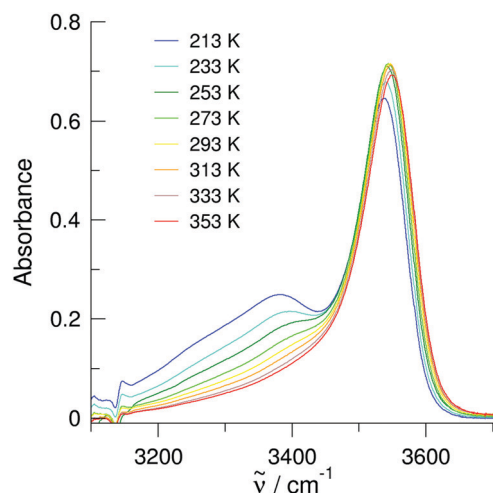


Fig. 1 Infrared difference spectra in the OH stretch region of [HEPy][BF₄] as a function of temperature between 213 K and 353 K. The spectra of the OD functionalized IL are subtracted from the corresponding spectra of the all-H species to remove the CH stretches of the pyridinium ring and exclude interference between CH and OH contributions.

intensity at the low frequency site. With decreasing temperature, this shoulder evolves into a distinct vibrational band with a maximum at about 3374 cm⁻¹ at 213 K while the main band redshifts by about 14 cm⁻¹. In the usual scenario where H-bonds are expected to become stronger with decreasing temperature, the OH associated bands intensify and redshift. However, the growth of a distinct band redshifted by ~175 cm⁻¹ clearly indicates the formation of another class of bound OH groups, with candidates in this case likely corresponding to the (c-a) to (c-c) interactions. We note that overtone or combination bands can be excluded in this frequency range.³⁴

Overall, the measured infrared spectra as a function of temperature are consistent with the formation of (c-c) hydrogen bonds, resulting in H-bonded clusters of like-charged ions. For the assignment of the measured IR spectra, we calculated two types of H-bonded clusters, (c-a) and (c-c), including up to four ion-pairs at the B3LYP-D3/6-31+G* level of theory.⁴⁷⁻⁵¹ These structures were fully optimized and only positive frequencies were found indicating true minimum structures on the potential energy surface. For (c-a) clusters, only OH frequencies from H-bonding between cation and anion are present. Although we observe minor cooperative effects with increasing cluster size from the (c-a) monomer to the (c-a) tetramer, the calculated frequencies range between 3480 cm⁻¹ and 3620 cm⁻¹ and are contained within the width of the high energy band envelope with maximum at 3549 cm⁻¹, which is therefore assigned to hydrogen bonding between cation and anion (see Fig. 2). As mentioned above, the OH frequencies are surprisingly high, considering that hydrogen bonding is enhanced by attractive Coulomb interaction between cation and anion. The doubly ionic hydrogen bond is not stronger than the H-bond of an alcohol dimer.⁴²⁻⁴⁶

The linear clusters (c-c) are characterized by hydrogen bonding between the cations with the terminal OH group interacting with one of the anions leading to structural motifs ⁺OH...⁺OH...BF₄⁻. The DFT-calculated frequencies of the

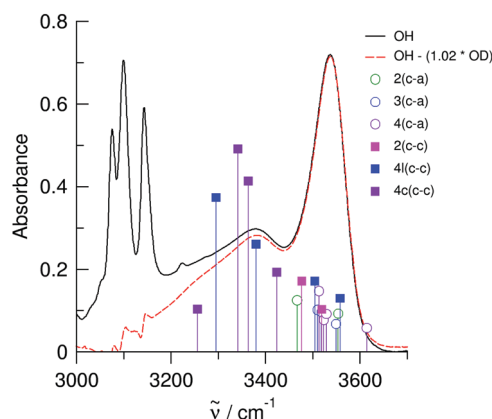


Fig. 2 Calculated frequencies [B3LYP-D3/6-31+G*, scaled by 0.985] of (c-a) (open symbols) and (c-c) (filled symbols) clusters, compared to the IR spectrum of [HEPy][BF₄] (solid black line) as well as the IR difference spectrum of IL-OH/IL-OD (red dashed line) at 213 K. Both linear and cyclic (c-c) configurations were considered. The (c-c) feature of the bulk liquid spectra is best represented by the cyclic tetramers (4c(c-c)).

2(c-c) dimer and the 4l(c-c) (linear (c-c)) tetramer reasonably describe the region of the broad redshifted vibrational band in the measured IR spectra with substantial intensity between 3200 cm⁻¹ and 3480 cm⁻¹. However, the measured spectral band is best described by the calculated frequencies of a cyclic (4c(c-c)) tetramer, showing all the features of cyclic tetramers that have been reported earlier for water and methanol.⁴²⁻⁴⁶ This agreement between the calculated frequencies of linear and cyclic (c-c) clusters with their neutral counterparts provides a compelling case that cyclic structural motifs are present in the ILs.

Enhanced cluster formation by adding the molecular liquid PhenEthOH

Next, we test the hypothesis that addition of the molecular liquid PhenEthOH to the [HEPy][BF₄] IL enhances the H-bonded domains. This was accomplished by monitoring the IR spectra resulting from various mixtures (0, 10, 20, 35 and 50 mol%) at *T* = 293 K, where only minor (c-c) cluster contributions are observed for the pure IL (see Fig. 1). The results are displayed in Fig. 3, demonstrating that the addition of PhenEthOH immediately results in substantial ⁺OH...⁺OH cluster formation, as evidenced by the rapid onset of the characteristic 3374 cm⁻¹ band observed earlier in the low temperature pure IL (Fig. 1). The calculated frequencies of the neutral tetramer clusters of the (c-c-m-m) and (c-m-c-m) configurations correspond well with this band region, with their structures displayed in Fig. S1 (ESI[†]). To provide more specific comparisons with the spectral signatures of these local motifs, we now turn to CIVP spectroscopy to establish the bands displayed by composition-selected cationic clusters of similar type.

Evidence for cyclic tetramers by means of cryogenic ion vibrational predissociation (CIVP) spectroscopy

The spectral signatures of various H-bonded motifs can be directly accessed by measuring the vibrational spectra of cold,

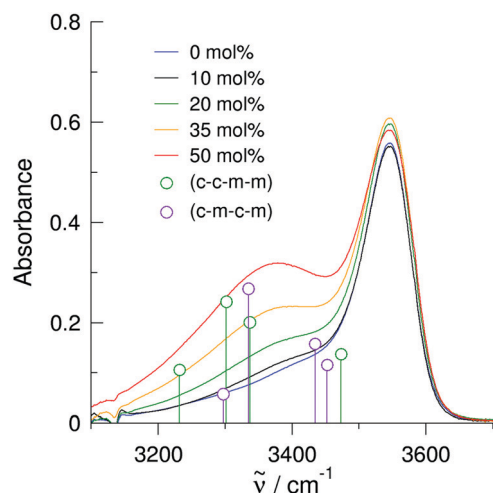


Fig. 3 Infrared spectra in the OH stretch region of [HEPy][BF₄]/PhenEthOH mixtures measured at different concentrations of 2-phenylethanol at 293 K. Calculated neutral tetramer cluster structures are provided in Fig. S1 (ESI†).

mass selected gas phase ions.³⁸ In the present case, we measured the spectra of the series (HEPy⁺)(PhenEthOH)_n, for comparison with the bands observed in the mixed IL/ML (Fig. 3).

The vibrational spectra of the mass selected ions were obtained using the so-called “messenger tagging” method.^{52,53} In that approach, linear absorption spectra are acquired by monitoring photoevaporation of a weakly interacting adduct, in this case N₂, using a double focusing, tandem time-of-flight photofragmentation mass spectrometer described in detail previously.^{54–57}

The spectral evolution of the cold (~35 K) (HEPy⁺)(PhenEthOH)_n complexes (*n* = 1–3) are compared with that of the isolated HEPy⁺ cation in Fig. 4. The doublet structure of the free OH peak is due to the perturbation by the N₂ adduct as discussed in detail in Fig. S2 (ESI†). The important result is that the free OH peaks in the bare cation and binary complex (Fig. 4a and b) are clearly absent for the *n* = 2 and 3 clusters (Fig. 4c and d), consistent with the formation of cyclic H-bond arrangements. Moreover, the band envelopes in the *n* = 2 and 3 spectra fall just on the low energy side of the redshifted transitions observed in both the bulk IL at 213 K (Fig. 4f) and in the [HEPy][BF₄]/PhenEthOH mixture at 293 K (Fig. 4e).

The important advantage of comparisons with cluster results is that the isolated, cold systems can be accurately treated with electronic structure methods. This allows us to extract detailed structural information about how the local interactions are reflected in the spectra. The calculated (B3LYP-D3/6-31+G*) structures and redshifts in the OH stretches of the (HEPy⁺)(PhenEthOH)_{n=0–4} clusters are presented in Fig. S3 and S5 (ESI†), respectively.^{47–51} These structures indeed correspond to homodromic H-bonded cyclic arrangements, which are analogous to those adopted by neutral cluster systems like methanol and water.^{58,59} Such cycles are known to exhibit increasingly redshifted OH stretching fundamentals with increasing size. The average (intensity-weighted) step-wise redshifts of the suite of OH vibrational transitions calculated for the cationic clusters are

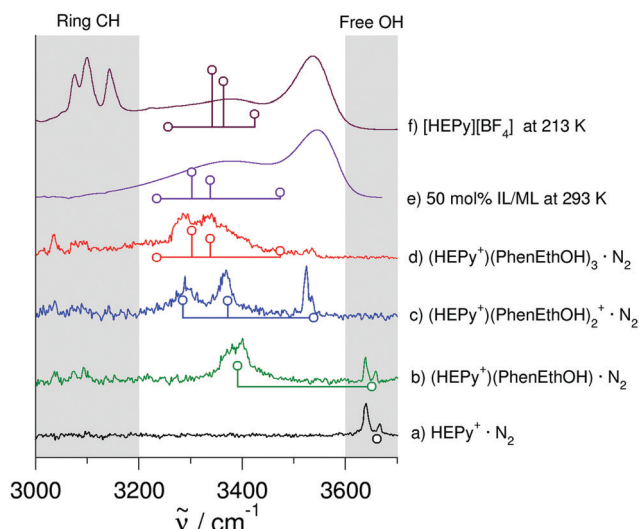


Fig. 4 Vibrational predissociation spectra of N₂-tagged cation HEPy⁺ (black) along with those of the (HEPy⁺)(PhenEthOH)_n clusters with *n* = 1 (green), *n* = 2 (blue) and *n* = 3 (red) at ~35 K. The bulk liquid IR spectra of the 50 mol% mixture of [HEPy][BF₄]/PhenEthOH at 293 K (purple) and the pure ionic liquid [HEPy][BF₄] at 213 K (teal). For comparison, the calculated frequencies of the monomer, dimer and the corresponding cyclic trimer and tetramers (see Scheme 1(a), (c) and (d)) are provided whereby the lowest intensities are set to zero.

compared with the experimentally observed band energies in Fig. 5. This behavior provides strong evidence that the observed low energy features in the bulk spectra are indeed assigned to the formation of extended, cyclic H-bonded motifs.

The H-bonding propensities in the cationic networks are interesting in that they raise the issue of whether binary interaction between a cationic OH group acts preferentially as an H-bond donor or acceptor when interacting with a neutral alcohol. This issue is directly addressed in the (HEPy⁺)(PhenEthOH) binary complex, where it can adopt two possible structures (⁺OH...OH vs. OH...⁺OH) which correspond to cationic H-bond donor and acceptor, respectively. The calculated bands of these combinations are compared to the neutral alcohol dimer, (PhenEthOH)₂ (Fig. 5). The ⁺OH...OH structural motif is characterized by significant charge transfer from the oxygen lone pair into the ⁺OH anti-bonding orbital, which is particularly strong here because the OH belongs to the positively charged, and hence more acidic cation. In contrast, the OH...⁺OH linkage is weakened because the oxygen lone pair on the cation is less basic. Thus, the ⁺OH...OH binary complex is the most energetically favorable configuration as opposed to OH...⁺OH, giving rise to a large redshift (260 cm^{−1}) and is detected in the gas phase (Fig. 4b).

The character of the binary ⁺OH...OH interaction has a profound impact on the spectrum of cyclic H-bonded networks that contain a single embedded cation, as the cation is a much better donor than it is an acceptor. This manifests as a splitting in the bands. Such an effect is illustrated by comparing the (HEPy⁺)(PhenEthOH)₃ system with the symmetric (neutral) ((PhenEthOH)₄) tetramer in Fig. 6. The single OH feature around 3340 cm^{−1} that is calculated for the (PhenEthOH)₄ tetramer

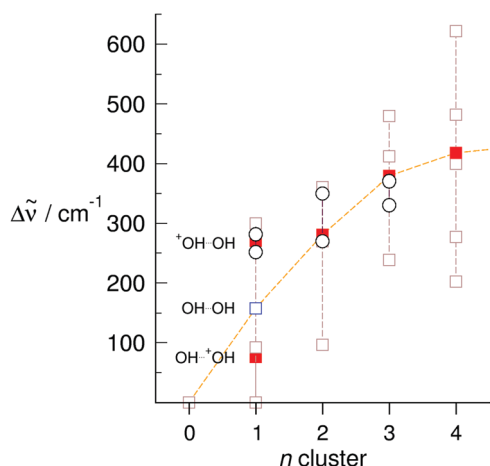


Fig. 5 Calculated vibrational redshifts for two kinds of binary complexes (HEPy⁺)(PhenEthOH) compared to the alcohol dimer (PhenEthOH)₂, and the cyclic clusters (HEPy⁺)(PhenEthOH)_n with $n = 2-4$. We calculated the shifts relative to the OH stretches of the bare cation HEPy⁺ (brown squares). The intensity weighted average frequencies (filled red squares) are guided by the dashed orange line. The single blue square symbolizes the OH red shift of the alcohol dimer (PhenEthOH)₂. The experimentally observed bands in the gas phase spectra appear at the frequencies calculated for the cyclic trimer (HEPy⁺)(PhenEthOH)₂ and cyclic tetramer (HEPy⁺)(PhenEthOH)₃ (black open circles).

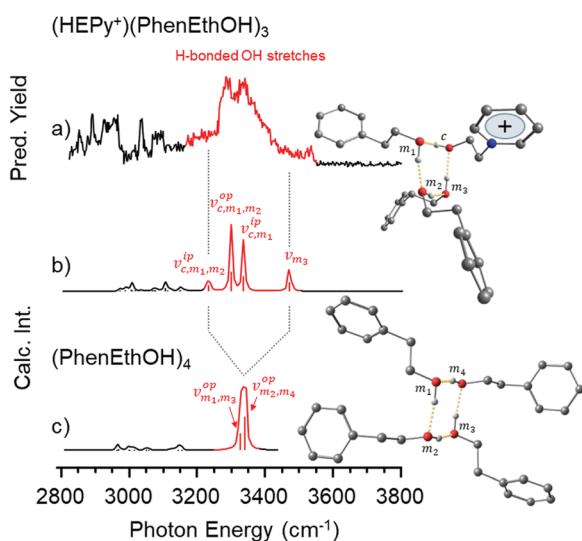


Fig. 6 Vibrational predissociation spectra of N₂-tagged (a) (HEPy⁺)(PhenEthOH)₃, compared to (b) its calculated spectrum. Calculated spectrum of (c) the cyclic molecular mimic tetramer (PhenEthOH)₄ is also presented for comparison. The superscripts 'ip' and 'op' in the band labels stands for 'in-plane' and 'out-of-plane' stretches, respectively. The structures are provided on the right of the figure and H-atoms connected to carbon atoms are omitted for clarity.

(Fig. 6c), splits into four distinct bands spanning a wide range between 3231–3470 cm⁻¹ (Fig. 6b). The lower energy bands correspond to displacement of the OH group on the cation, whereas the highest frequency transition belongs to the OH of the neutral molecule in the weak OH...OH⁺ linkage (labeled ν_{m_3} in Fig. 6b), discussed for the binary complex. Note that the

dominant bands in the experimental spectrum for this cluster covers the same frequency range as the broad redshifted OH vibrational band of the 50 mol% IL/ML mixture (Fig. 4e), but appears ~ 90 cm⁻¹ below that observed for the 213 K IL (Fig. 4f), which is also consistent with the elimination of the repulsive interactions in the gas phase species. Taken altogether, these observations provide compelling evidence for the formation of cyclic H-bonded domains in the bulk IL at low temperature (see Scheme 1), which would have been more challenging to accomplish by isolated, purely ionic complexes (Fig. S4, ESI[†]).

Conclusion

We analyzed liquid phase complexes and gaseous cationic clusters of [HEPy][BF₄] and the molecular mimic of its cation, 2-phenylethanol (PhenEthOH) by means of infrared spectroscopy, cryogenic ion vibrational predissociation spectroscopy, and quantum chemical calculations. Theoretical analysis of the resulting infrared spectra reveals the assignments of the OH stretching bands to the different binding motifs. Dimers, linear and cyclic tetramers with (c-c) cooperativity were inferred based on the vibrational spectra of neat ILs, but the spectra of ternary cationic complexes in the gas phase were dominated by bands characteristic of the ⁺OH...BF₄⁻ (c-a) interactions. However, replacing the ion-pairs with the molecular mimics of the IL cation yields features signalling OH network formation in both the positively charged cyclic tetramers (HEPy⁺)(PhenEthOH)₃ and in mixtures of the ionic and molecular liquids. Most importantly, the cationic cyclic tetramer (HEPy⁺)(PhenEthOH)₃ exhibits vibrational bands in the OH stretching region that are similar to those previously assigned³⁵ to cyclic tetramers in the broad liquid bands of the IL and the IL/ML mixtures. Our combined experimental and theoretical approach for the gas and the liquid phases thus provides a quantitative understanding of the competition between differently H-bonded and charged constituents in liquids.

Conflicts of interest

The authors declare no conflict of interest.

Acknowledgements

MAJ thanks the Department of Energy (DOE) under grant DE-FG02-06ER15800 for support of this work. The cryogenic ion spectrometer critical to these measurements was provided by the Air Force Office of Scientific Research (AFOSR) under grants FA9550-17-1-0267 (DURIP) and FA9550-18-1-0213. RL thanks for the financial support from the Deutsche Forschungsgemeinschaft (DFG) under grant LU 506/14-1. TN and AS thank the "HERMES-Forschungsförderung" and the "Frauenförderprogramm" of the University of Rostock for supporting their research stays at Yale University.

References

- 1 M. L. Huggins, *Science*, 1922, **55**, 459–460.
- 2 W. M. Latimer and W. H. Rodebush, *J. Am. Chem. Soc.*, 1920, **42**, 1419–1433.
- 3 M. L. Huggins, *Angew. Chem., Int. Ed. Engl.*, 1971, **10**, 147–152 (*Angew. Chem.*, 1971, **83**, 163–168).
- 4 L. Pauling, *The Nature of the Chemical Bond and the Structure of Molecules and Crystals: An Introduction to Modern Structural Chemistry*, Cornell University Press, Ithaca, NY, 1960.
- 5 G. A. Jeffrey, *An Introduction to Hydrogen Bonding*, Oxford University Press, New York, 1997.
- 6 G. Gilli and P. Gilli, *The Nature of the Hydrogen Bond: Outline of a Comprehensive Hydrogen Bond Theory*, Oxford University Press, Oxford, 2009.
- 7 G. R. Desiraju and T. Steiner, *The Weak Hydrogen Bond: In Structural Chemistry and Biology*, Oxford University Press, Oxford, 1999.
- 8 Y. Maréchal, *The Hydrogen Bond and the Water Molecule: The Physics and Chemistry of Water, Aqueous and Bio-Media*, Elsevier, Amsterdam, Boston, 2007.
- 9 T. Steiner, *Angew. Chem., Int. Ed.*, 2002, **41**, 48–76 (*Angew. Chem.*, 2002, **114**, 50–80).
- 10 A. C. Legon, *Chem. Soc. Rev.*, 1993, **22**, 153–163.
- 11 H. Weingärtner, *Angew. Chem., Int. Ed.*, 2008, **47**, 654–670 (*Angew. Chem.*, 2008, **120**, 664–682).
- 12 F. Endres and S. Z. El Abedin, *Phys. Chem. Chem. Phys.*, 2006, **8**, 2101–2116.
- 13 T. Welton, *Chem. Rev.*, 1999, **99**, 2071–2083.
- 14 N. V. Plechkova and K. R. Seddon, *Chem. Soc. Rev.*, 2008, **37**, 123–150.
- 15 S. P. M. Ventura, F. A. E. Silva, M. V. Quental, D. Mondal, M. G. Freire and J. A. P. Coutinho, *Chem. Rev.*, 2017, **117**, 6984–7052.
- 16 M. Galiński, A. Lewandowski and I. Stepniak, *Electrochim. Acta*, 2006, **51**, 5567–5580.
- 17 S. Menne, J. Pires, M. Anouti and A. Balducci, *Electrochem. Commun.*, 2013, **31**, 39–41.
- 18 K. Fumino and R. Ludwig, *J. Mol. Liq.*, 2014, **192**, 94–102.
- 19 K. Fumino, S. Reimann and R. Ludwig, *Phys. Chem. Chem. Phys.*, 2014, **16**, 21903–21929.
- 20 K. Fumino, A. Wulf and R. Ludwig, *Angew. Chem., Int. Ed.*, 2008, **47**, 8731–8734.
- 21 K. Fumino, T. Peppel, M. Geppert-Rybczyńska, D. H. Zaitsau, J. K. Lehmann, S. P. Verevkin, M. Köckerling and R. Ludwig, *Phys. Chem. Chem. Phys.*, 2011, **13**, 14064–14075.
- 22 P. A. Hunt, C. R. Ashworth and R. P. Matthews, *Chem. Soc. Rev.*, 2015, **44**, 1257–1288.
- 23 C. R. Ashworth, R. P. Matthews, T. Welton and P. A. Hunt, *Phys. Chem. Chem. Phys.*, 2016, **18**, 18145–18160.
- 24 R. Ozawa, S. Hayashi, S. Saha, A. Kobayashi and H. Hamaguchi, *Chem. Lett.*, 2003, **32**, 948–949.
- 25 H. Katayanagi, S. Hayashi, H. Hamaguchi and K. Nishikawa, *Chem. Phys. Lett.*, 2004, **392**, 460–464.
- 26 J. D. Holbrey, W. M. Reichert, M. Nieuwenhuyzen, S. Johnston, K. R. Seddon and R. D. Rogers, *Chem. Commun.*, 2003, 1636–1637.
- 27 A. Triolo, O. Russina, V. Arrighi, F. Juranyi, S. Janssen and C. M. Gordon, *J. Chem. Phys.*, 2003, **119**, 8549–8557.
- 28 R. W. Berg, M. Deetlefs, K. R. Seddon, I. Shim and J. M. Thompson, *J. Phys. Chem. B*, 2005, **109**, 19018–19025.
- 29 Y. Umebayashi, T. Fujimori, T. Sukizaki, M. Asada, K. Fujii, R. Kanzaki and S. Ishiguro, *J. Phys. Chem. B*, 2005, **109**, 8976–8982.
- 30 K. Fujii, T. Fujimori, T. Takamuku, R. Kanzaki, Y. Umebayashi, T. Sukizaki and R. S. Ishiguro, *J. Phys. Chem. B*, 2006, **110**, 8179–8183.
- 31 T. Köddermann, C. Wertz, A. Heintz and R. Ludwig, *ChemPhysChem*, 2006, **7**, 1944–1949.
- 32 A. Yokozeki, D. J. Kasprzak and M. B. Shiflett, *Phys. Chem. Chem. Phys.*, 2007, **9**, 5018–5026.
- 33 S. A. Katsyuba, M. V. Vener, E. E. Zvereva, Z. F. Fei, R. Scopelliti, G. Laurency, N. Yan, E. Paunescu and P. J. Dyson, *J. Phys. Chem. B*, 2013, **117**, 9094–9105.
- 34 A. Knorr and R. Ludwig, *Sci. Rep.*, 2015, **5**, 17505.
- 35 A. Knorr, P. Stange, K. Fumino, F. Weinhold and R. Ludwig, *ChemPhysChem*, 2016, **17**, 458–462.
- 36 A. Strate, T. Niemann, D. Michalik and R. Ludwig, *Angew. Chem., Int. Ed.*, 2017, **56**, 496–500.
- 37 T. Niemann, D. Zaitsau, A. Strate, A. Villinger and R. Ludwig, *Sci. Rep.*, 2018, **8**, 14753.
- 38 F. S. Menges, H. J. Zeng, P. J. Kelleher, O. Gorlova, M. A. Johnson, T. Niemann, A. Strate and R. Ludwig, *J. Phys. Chem. Lett.*, 2018, **9**, 2979–2984.
- 39 T. Niemann, A. Strate, R. Ludwig, H. J. Zeng, F. S. Menges and M. A. Johnson, *Angew. Chem., Int. Ed.*, 2018, **57**, 15364–15368 (*Angew. Chem.*, 2018, **130**, 15590–15594).
- 40 M. Fakhraee, B. Zandkarimi, H. Salari and M. R. Gholami, *J. Phys. Chem. B*, 2014, **118**, 14410–14428.
- 41 S. K. Panja, B. Haddad and J. Kiefer, *ChemPhysChem*, 2018, **19**, 3061–3068.
- 42 F. N. Keutsch and R. J. Saykally, *Proc. Natl. Acad. Sci. U. S. A.*, 2001, **98**, 10533–10540.
- 43 R. Ludwig, *Angew. Chem., Int. Ed.*, 2001, **40**, 1808–1827.
- 44 F. Huisken and M. Stemmler, *Chem. Phys. Lett.*, 1988, **144**, 391–395.
- 45 H. L. Han, C. Camacho, H. A. Witek and Y. P. Lee, *J. Chem. Phys.*, 2011, **134**, 144309.
- 46 P. Ayotte, G. H. Weddle and M. A. Johnson, *J. Chem. Phys.*, 1999, **110**, 7129–7132.
- 47 M. J. Frisch, G. W. Trucks, H. B. Schlegel, G. E. Scuseria, M. A. Robb, J. R. Cheeseman, G. Scalmani, V. Barone, B. Mennucci and G. A. Petersson, *et al.*, *Gaussian 09, Revision D.01*, 2016.
- 48 C. Möller and M. S. Plesset, *Phys. Rev.*, 1934, **46**, 618–622.
- 49 M. Head-Gordon, J. A. Pople and M. J. Frisch, *Chem. Phys. Lett.*, 1988, **153**, 503–506.
- 50 A. Strate, T. Niemann and R. Ludwig, *Phys. Chem. Chem. Phys.*, 2017, **19**, 18854–18862.
- 51 A. Strate, V. Overbeck, V. Lehde, J. Neumann, A. M. Bónsa, T. Niemann, D. Paschek, D. Michalik and R. Ludwig, *Phys. Chem. Chem. Phys.*, 2018, **20**, 5617–5625.

- 52 M. Okumura, L. I. Yeh, J. D. Myers and Y. T. Lee, *J. Phys. Chem.*, 1990, **94**, 3416–3427.
- 53 A. B. Wolk, C. M. Leavitt, E. Garand and M. A. Johnson, *Acc. Chem. Res.*, 2014, **47**, 202–210.
- 54 C. J. Johnson, J. A. Fournier, C. T. Wolke and M. A. Johnson, *J. Chem. Phys.*, 2013, **139**, 224305.
- 55 J. A. Fournier, C. T. Wolke, C. J. Johnson, A. B. McCoy and M. A. Johnson, *J. Chem. Phys.*, 2015, **142**, 064306.
- 56 S. M. Craig, F. S. Menges and M. A. Johnson, *J. Mol. Spectrosc.*, 2017, **332**, 117–123.
- 57 F. S. Menges, S. M. Craig, N. Totsch, A. Bloomfield, S. Ghosh, H. J. Kruger and M. A. Johnson, *Angew. Chem., Int. Ed.*, 2016, **55**, 1282–1285.
- 58 K. Liu, M. G. Brown, J. D. Cruzan and R. J. Saykally, *Science*, 1996, **271**, 62–65.
- 59 K. Nauta and R. E. Miller, *Science*, 2000, **287**, 293–295.

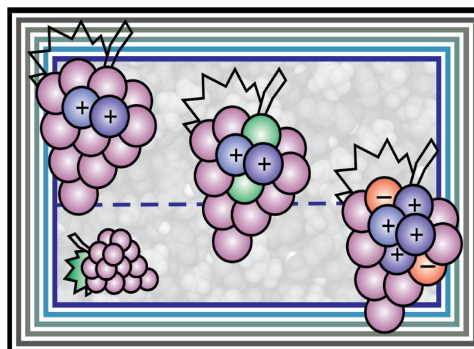
Controlling the Kinetic and Thermodynamic Stability of Cationic Clusters by the Addition of Molecules or Counterions

A. Strate (35 %), T. Niemann (30 %), R. Ludwig (35 %)

Phys. Chem. Chem. Phys., 19, 18854-18862, 2017

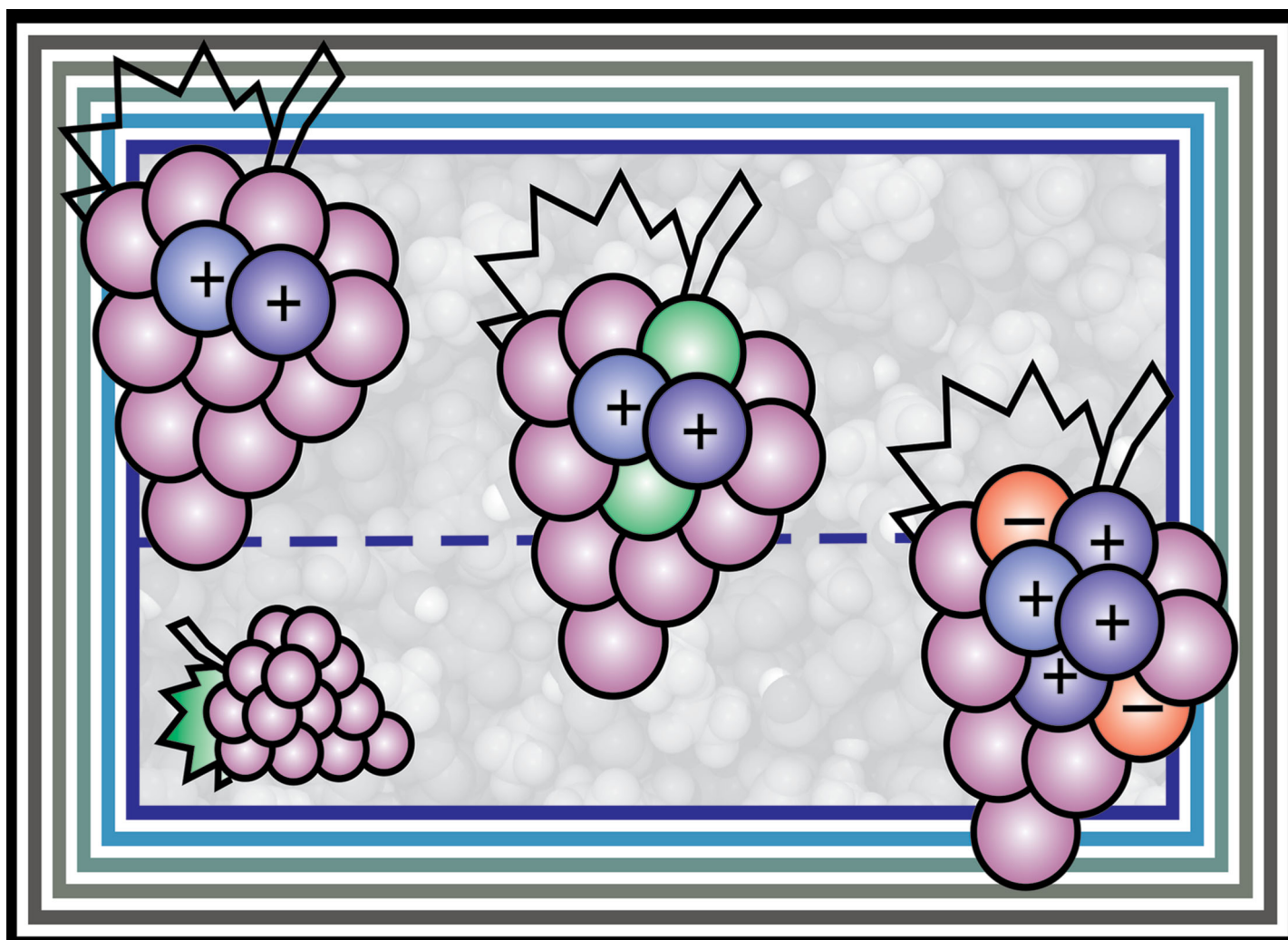
Content:

The charge, the size and the structural motives of cationic clusters in the gas phase are investigated. Compared to the neutral ionic liquids, the positive charges are not always fully balanced by anions in the gas phase.



Contributions to this work:

To this publication the authors contributed nearly equally. All three authors did some of the DFT calculations. Professor Ludwig wrote the manuscript, while Anne Strate and I got it for final corrections.



Showcasing work by Anne Strate, Thomas Niemann and Ralf Ludwig from Physical and Theoretical Chemistry at the University of Rostock, Germany

Controlling the kinetic and thermodynamic stability of cationic clusters by the addition of molecules or counterions

This paper reports the calculation of the kinetic and thermodynamic stability of cationic clusters with added molecules or counterions. These clusters of like-charged ions are stabilized by cooperative hydrogen bonding between hydroxyl groups overcoming the repulsive Coulomb forces. The cationic clusters show characteristic spectroscopic properties and some of them should be observable in demanding gas phase experiments.

As featured in:



See Ralf Ludwig et al.,
Phys. Chem. Chem. Phys.,
2017, 19, 18854.



Cite this: *Phys. Chem. Chem. Phys.*,
2017, 19, 18854

Controlling the kinetic and thermodynamic stability of cationic clusters by the addition of molecules or counterions

Anne Strate,^a Thomas Niemann^a and Ralf Ludwig  ^{*ab}

Whereas ion pairing is one of the most fundamental atomic interactions in chemistry and biology, pairing between like-charged ions remains an elusive concept. This phenomenon was only reported for large-scaled structures, assemblies or stabilizing frameworks. Recently, we could report the formation of cationic clusters in pure ionic liquids. In such structures like-charge repulsion is attenuated by cooperative hydrogen bonds. In the present work, we investigate the possible formation of cationic clusters in the gas phase beyond those found in the neutral ionic liquids wherein the positive charges are fully balanced by anions. Based on the ionic liquid (2-hydroxyethyl)trimethylammonium bis(trifluoromethylsulfonyl)imide we calculated differently charged cationic clusters including varying numbers of cation-like molecules (3-3-dimethyl-1-butanol) or ionic liquid anions (NTf₂). We give the number of molecules or anions which are needed to transfer the cationic clusters from the meta-stable into the thermodynamically stable regime. We analyze the charge, the size and the structural motif of these clusters. A particular focus we put on the cooperativity of hydrogen bonding and the role of dispersion forces for the cluster stability. We also show that interaction energies and charge transfer within the cationic clusters can be related to spectroscopic parameters such as NMR chemical shifts and IR vibrational frequencies. Finally, we suggest clusters which should be observable in demanding gas phase experiments.

Received 6th April 2017,
Accepted 21st June 2017

DOI: 10.1039/c7cp02227a

rsc.li/pccp

Ion pairing is one of the most fundamental atomic interactions in chemistry and biology. Ion pairs of electrostatically interacting cationic and anionic moieties are important for reaction mechanisms in solution, macromolecular catalysis, and biochemical hydrolysis.^{1–3} Different ionic species react with their own characteristic rate constants, resulting in a specific dynamic equilibrium. Ion pairing is also relevant for proteins and nucleic acids to perform their function.^{4–7} Thus, tremendous efforts have been made to understand the nature and kinetics of ion pairs. In contrast, establishing the theoretical foundation and experimental evidence for like-charge attraction in solution is a challenge. It seemingly contradicts conventional wisdom that like-charged ions can attract, despite the powerful opposing electrostatic forces: “Unlike charges attract, but like charges repel”. However, additional attractive forces between ions of like charge may attenuate the repulsive forces resulting in cationic or anionic clusters. Attractive interaction between ions of like charge has been observed for aqueous salt solutions of K/CsBr,⁸

for guanidinium ions in water,⁹ and in the micellation of tetraalkylammonium surfactants.¹⁰ Like-charge attraction is also reported for biomolecular systems, including oligopeptides and DNA.¹¹ Most recently, Gamrad *et al.* could report self-association of simple organic cations based on hydrogen bonding. Cation-cation pairing was detected in crystal structures *via* X-ray scattering.¹² Like-charge attraction is also reported from molecular dynamics simulations of aprotic ionic liquids and from hybrid quantum mechanics/molecular mechanics (QM/MM) simulations of guanidinium cations in aqueous solutions.¹³ Recently, Fatila *et al.* showed that hydrogen bonded anions can stabilize each other inside macrocyclic hosts.¹⁴ They claimed that these dimer salts only survive in supramolecular capsules but probably not in solution. So far, large-scale structures, assemblies or stabilizing frameworks are prerequisites for attractive interaction between like-charged ions. For smaller systems mediating solvent molecules such as water are required. In theoretical studies of like-charge attraction, Klein and Weinhold claimed that doubly-charged complexes [A-HB]^{2±} are manifestations of “anti-electrostatic” hydrogen bonds (AEHB), wherein the short-range donor-acceptor covalency forces overcome the powerful long-range electrostatic opposition to be expected between ions of like charge.^{15,16} Weinhold analyzed the potential energy curves for the ion-ion interactions which showed shallow

^a Universität Rostock, Institut für Chemie, Abteilung für Physikalische Chemie, Dr.-Lorenz-Weg 2, 18059, Rostock, Germany. E-mail: ralf.ludwig@uni-rostock.de; Tel: (+49) 381-498-6517

^b Leibniz-Institut für Katalyse an der Universität Rostock e.V., Albert-Einstein-Str. 29a, 18059, Rostock, Germany

local minima indicating hydrogen bonding between the like charged ions.

Recently, we could report the formation of clusters of like-charged ions in pure ionic liquids.^{17–20} Within the positively charged clusters the repulsive Coulomb interaction was attenuated by cooperative hydrogen bonds between the OH groups of the hydroxyethyl-methyl-imidazolium cations. The H-bonded clusters showed characteristic spectroscopic features. The OH proton chemical shifts were downfield shifted and the OH vibrational frequencies were red shifted compared to those observed for the OH bonds involved in common ion pairs formed by opposite charged ions.^{19,20} Meanwhile we could show that the size and the amount of cationic clusters can be controlled by different strong interacting anions.²⁰ In principle we followed a three-step strategy for supporting the cationic cluster formation in ILs. We introduced hydroxyl groups for possible hydrogen bonding as they are present in molecular clusters of water or alcohols.^{21–25} To overcome the repulsive forces between cations we selected weakly coordinating anions for maximum compensation of the delocalized positive charge in the aromatic imidazolium ring. Additionally we increased the distance between the positive charge and the functional OH group within the cation as shown for a cyclic tetramer in Scheme 1. This cyclic tetramer can only be formed due to cooperative hydrogen bonding within the ring structure and due to the weakly interacting anions. Meanwhile, this strategy could be significantly improved. ‘Kinetic trapping’ of meta-stable clusters is no longer required and thermodynamically stable cationic clusters can be observed already at room temperature.²⁰ So far we investigated pure ionic liquids or their mixtures, wherein the cationic clusters are fully solvated by counter ions resulting in neutral solvents.

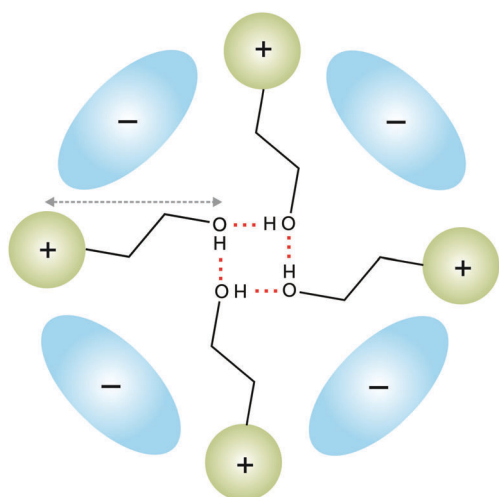
It is the purpose of the present work to investigate the possible formation of cationic clusters in the gas phase beyond those found in the neutral ionic liquids wherein the positive charges are fully balanced by anions. Meanwhile there are

several experimental setups which allow cryogenic cooling, mass selection and spectroscopic measurements of ionic clusters in the gas phase.^{26–30} In there, sufficiently cold ionic clusters are kinetically stable on the experimental time scale. The Johnson group showed cationic clusters $[\text{EMIM}]_2[\text{BF}_4]^+$ through cryogenic ion vibrational predissociation (CIVP) spectroscopy.^{27,28} We will address a number of relevant questions giving important hints whether these differently charged clusters can be observed experimentally.

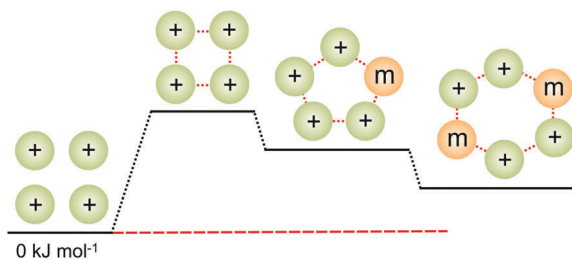
Is there a chance to find multiple positively charged clusters in gas phase experiments? Can we report the formation of a hydrogen bonded $[\text{O} \cdots \text{H}-\text{O}]^{2+}$ complex? How important is hydrogen bonding for the meta-stability of these clusters? What is the maximum size of pure cationic clusters wherein the repulsive Coulomb forces are attenuated by cooperative hydrogen bonds? Do the spectroscopic observables such as NMR chemical shifts and IR vibrational frequencies show the same behaviour for ionic and molecular clusters? How many molecules or counterions are needed to transfer the meta-stable clusters of like-charged ions into the thermodynamically stable regime? Is there a chance to observe these cationic clusters with charges up to plus four experimentally? And finally, are dispersion forces relevant for the stability of these pure or mixed cationic clusters?

We employed B3LYP/6-31+G* and B3LYP-D3/6-31+G* calculations performed with the Gaussian 09 program and analyzed with the NBO 6.0 program.^{31–33} For calculating all clusters at the same level of theory we have used the well-balanced, but small 6-31+G* basis set. It includes polarization as well as diffuse functions, and has been shown to be suitable for calculating hydrogen bonded clusters of like-charged ions.^{17–20} The usage of larger basis sets is limited by the frequency calculations on larger clusters such as hexamers. The 6-31+G* basis set is also chosen for better comparison with earlier studies of molecular and ionic clusters.^{17–20,23–25} As model cation we have chosen (2-hydroxyethyl)trimethylammonium well known as cholinium $[\text{Cho}]^+$. Combined with chloride as counteranion it forms choline which is a water soluble vitamin like substance and of relevance in bio chemical processes.³⁴ This cation is present in the ionic liquid $[\text{Cho}][\text{NTf}_2]$ which contains bis(trifluoromethylsulfonyl)imide as anion. The related neutral species to this cation is obtained by simply replacing the nitrogen in the ammonium cation by a carbon atom resulting into the alcohol 3-3-dimethyl-1-butanol DM1B. For the cationic clusters $[\text{Cho}]_x^{x+}$ (x) and the molecular clusters DM1B_x (my) linear and cyclic species up to hexamers were optimized. In a second step we added molecules or anions to the pure cationic clusters for stabilizing the overall cationic configurations. To give an example: If the cyclic cationic cluster c4c (4+) is meta-stable, we add successively molecules or counterions to strengthen kinetic stability or to achieve even thermodynamic stability. Our strategy is illustrated in Scheme 2 for adding molecules and in Scheme 3 for the addition of counterions. In the discussed clusters the overall charge 4+, 3+ or 2+ is preserved.

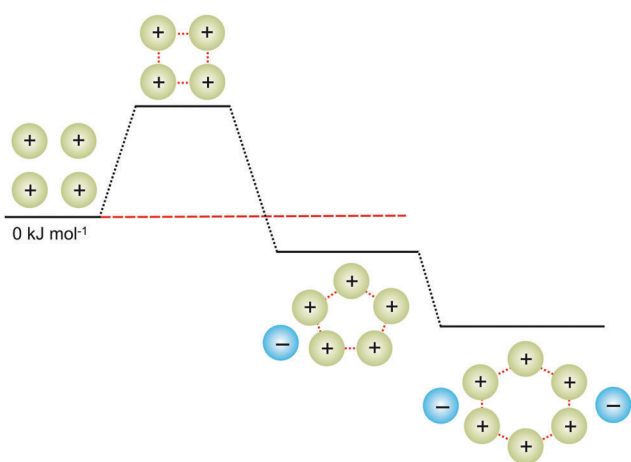
All the pure ionic and molecular clusters were fully optimized. The calculated vibrational frequencies were all positive showing that we calculated at least local minimum structures. Additionally, we calculated OH vibrational frequencies for the OH bonds, ν_{OH} , and the hydroxyl proton chemical shifts, $\delta^1\text{H}$,



Scheme 1 Strategy for supporting the formation of cationic clusters: (a) introduction of hydroxy groups for hydrogen bonding, (b) the use of weakly coordinating anions and (c) increasing the distance between the hydroxyl groups and the center of positive charge of the cation (as indicated by the dashed arrow).



Scheme 2 Strategy for supporting the formation of cationic clusters by adding neutral molecules. The energy of four isolated cations is set to 0 kJ mol⁻¹. The meta-stable cyclic tetramer c4c (4+) is enlarged to the cyclic pentamer c4-m1 and cyclic hexamer c4-m2 by the addition of one and two alcohol molecules, respectively. The positive charge 4+ is preserved for all clusters.



Scheme 3 Strategy for supporting the formation of cationic clusters by adding counterions. The energy of four isolated cations is set to 0 kJ mol⁻¹. The meta-stable cyclic tetramer c4c (4+) is enlarged to the cyclic pentamer c5c and cyclic hexamer c6c which become now thermodynamically stable by the addition of one and two anions, respectively. The positive charge 4+ is preserved for all clusters.

for each configuration. These spectroscopic observables are related to NBO calculated second order stabilization energy $\Delta E(2)_{n \rightarrow \sigma^*}$ and charge transfer, q_{CT} . Although the same procedure was applied to the clusters with molecules or counterions, only the interaction energies are discussed in respect to their kinetic or thermodynamic stability.

Cationic dimer: kinetic stability

For the dimer structure $[\text{Cho}]_2^{2+}$ (c2l) we calculated the relaxed-scan potential curve at the HF-6-31+G* (I), B3LYP-6-31+G* (II), B3LYP-D3-6-31+G* (III) and MP2-6-31+G* (IV) levels of theory. The local minimum structures were found at typical H-bond distances of $R_{O \cdots H} = 1.9415 \text{ \AA}$ and $R_{O \cdots H} = 1.9490 \text{ \AA}$ for III and IV, respectively. The B3LYP-6-31+G* calculated dimer shows a minimum at $R_{O \cdots H} = 2.0087 \text{ \AA}$, whereas the uncorrelated HF-level is even weaker bound and shows this minimum at large H-bond distances of $R_{O \cdots H} = 2.1574 \text{ \AA}$ and only a shallow local minimum (see Table 1). As shown in Fig. 1, a robust

Table 1 Calculated intermolecular distances $R(\text{O} \cdots \text{HO})$ and $R(\text{O} \cdots \text{O})$ as well as bond angles $\angle(\text{O} \cdots \text{HO})$ of the optimized dimer structures $[\text{Cho}]_2^{2+}$ using different theoretical methods but applying the same 6-31+G* basis set

Method	$R(\text{O} \cdots \text{HO})/\text{\AA}$	$R(\text{O} \cdots \text{O})/\text{\AA}$	$\angle(\text{O} \cdots \text{HO})/^\circ$
HF	2.1574	3.0768	162.06
B3LYP	2.0087	2.9507	161.42
B3LYP-D3	1.9415	2.8857	161.72
MP2	1.9490	2.8968	161.71

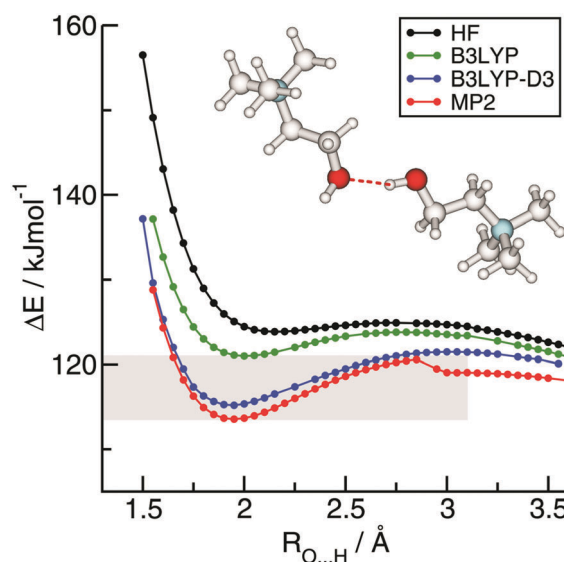


Fig. 1 Potential energy curves for $[\text{Cho}]_2^{2+}$ H-bonding (all at 6-31+G* basis level) as calculated with the uncorrelated HF (black), hybrid density functional B3LYP (green), hybrid density functional B3LYP-D3 including dispersion correction (blue), and *ab initio* MP2 (red) methods. The structures were relaxed for each bond length $R_{O \cdots H}$ which are given in Table 1.

kinetic stability with a clear dissociation barrier of 5–7 kJ mol⁻¹ is achieved for the B3LYP, B3LYP-D3 and the MP2 treatments. It is interesting to note that the MP2 calculations give the lowest energies and that the B3LYP calculations represent nearly the same potential energy curve if the D3 dispersion correction is taken into account.^{35–37} Thus doubly ionic hydrogen bonds between like-charged ions are well described by dispersion corrected DFT methods.^{38–43}

Larger cationic clusters $n = 3–6$

We optimized linear and cyclic cationic clusters of (2-hydroxyethyl)trimethylammonium from trimeric up to hexameric ($n = 3–6$) configurations. A linear cationic trimer is abbreviated by c3l, a cyclic trimer by c3c. The pure cationic clusters are kinetically stable for the cyclic trimers (c3c) and the cyclic tetramers (c4c), wherein cooperative H-bonding is maximized. Linear trimer (c3l) and tetramer (c4l) and larger cyclic clusters such as pentamers (c5c) or hexamers (c6c) are no longer meta-stable and dissociate during the geometry optimization procedure (see Fig. 2b). The meta-stable cationic clusters resemble the cyclic trimers and tetramers as known for alcohols and water.^{21–25} The detection and control of

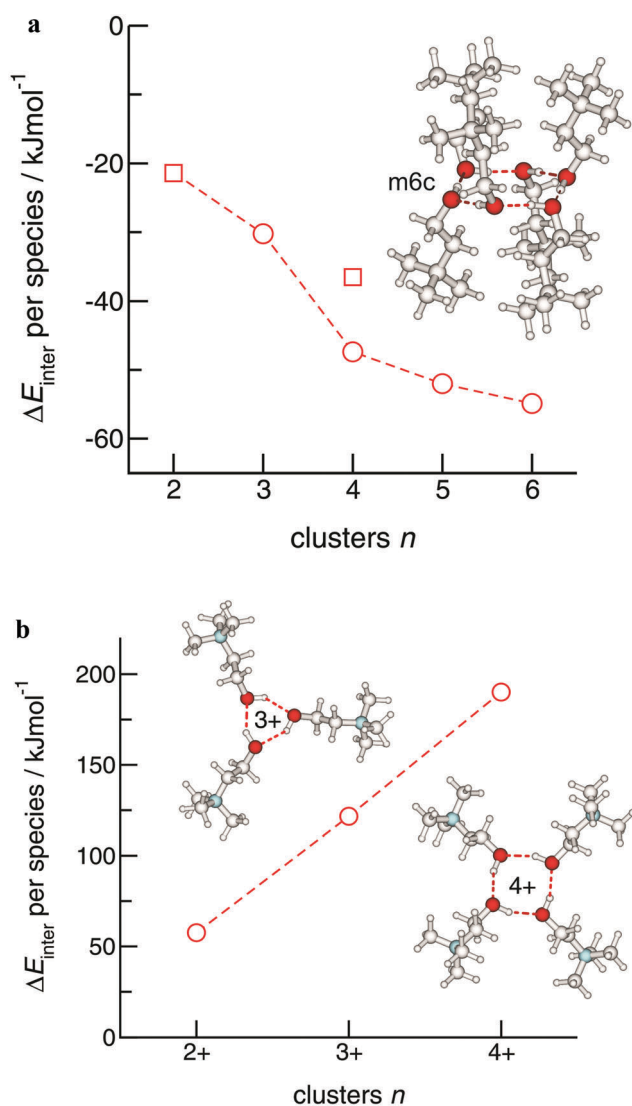


Fig. 2 (a) B3LYP-D3/6-31+G* calculated binding energies per species n for cyclic (circles) and linear (squares) clusters of the 3-3-dimethyl-1-butanol. For the alcohol clusters a strong lowering in energy is observed with increasing cluster size due to cooperative hydrogen bonding. Cooperativity is almost saturated with $n = 6$ similar to what is known for smaller alcohols and water.^{21–25} (b) B3LYP-D3/6-31+G* calculated binding energies per species n for clusters of the cation (2-hydroxyethyl)trimethylammonium. The cationic clusters $n = 2–4$ are meta-stable due to enhanced hydrogen bonding compensating the electrostatic repulsion. Sufficient cooperativity is only achieved if cyclic structures c3c and c4c are taken into account. Linear structure c3l and c4l as well as larger cyclic clusters c5c and c6c dissociate during the optimization procedure.

clusters of like-charged ions may be regarded as support for the “anti-electrostatic hydrogen bonds” (AEHB) as reported recently by Weinhold and Klein.^{15,16} Although Frenking and Head-Gordon could show that the local minimum structures for anionic dimers can be analyzed also by energy decomposition analysis (EDA) methods, AEHBs are supported by spectroscopic observables such as vibrational frequencies, ν_{OH} , and NMR chemical shifts, $\delta^1\text{H}$.^{45,46} Geometrical and spectroscopic properties of cationic and molecular clusters show similar behaviour. This will be shown in detail after discussing the neutral molecular clusters ($n = 1–6$) for DM1B.

What is the cause of the attractive forces between the like-charged ions? The B3LYP-D3/6-31+G* calculations suggest that the cation–cation $\text{OH} \cdots \text{OH}$ interaction is possible due to cooperative effects.^{24,25} Charge from the oxygen lone pair orbital of a first cation is donated into the OH anti-bond orbital of a second cation. The larger negative charge at the OH oxygen at the second cation can now be transferred into the OH anti-bond of another cation further enhancing hydrogen bonding. This process leads to even stronger cooperativity in the trimers and tetramers. This way the short-range donor–acceptor covalency forces can overcome the strong long-range electrostatic repulsive forces as expected for ions of like charge. These features can be rationalized in the framework of the natural bond orbital (NBO) analysis.^{15,16,32,33} The repulsive electrostatic forces are overcome by directional, cooperative H-bonds indicated by characteristic redshifts in the OH stretch region. NBO analysis shows typical strong $\text{n}_{\text{O}} \rightarrow \sigma^*_{\text{OH}}$ donor–acceptor interaction, corresponding to second order stabilization energies $\Delta E(2)_{\text{n} \rightarrow \sigma^*}$ and estimated total charge transfers of q_{TC} for the enhanced $\text{OH} \cdots \text{OH}$ hydrogen bonds, respectively.

Recently, Stone reported that the NBO properties are strongly overestimated and that hydrogen bonding is not dominated by the charge-transfer energy.⁴⁷ However, we still believe in the usefulness of the NBO concept. Although $\Delta E(2)_{\text{n} \rightarrow \sigma^*}$ and q_{TC} are overestimated, the changes in the charge-transfer energies can be nicely related to the shifts of spectroscopic observables. This has been shown in earlier studies for IR redshifts, $\Delta\nu_{\text{OH}}$, as well as for NMR downfield proton chemical shifts, $\delta^1\text{H}$, of water and alcohol clusters.^{23–25,42–44}

Molecular clusters $n = 1–6$

The DM1B clusters $n = 1–6$ show the typical enhanced interaction strength with increasing cluster size as known for molecular liquids.^{21–25} In Fig. 2a it is shown that the interaction energy per molecule is more than doubled in the cyclic tetramer, pentamer and hexamer compared to the alcohol dimer. This behaviour results from strong cooperative effects as discussed for the ionic clusters already. Strong $\text{n}_{\text{O}} \rightarrow \sigma^*_{\text{OH}}$ donor–acceptor interaction, related to second order stabilization energies $\Delta E(2)_{\text{n} \rightarrow \sigma^*}$ and estimated total charge transfers of q_{CT} from NBO analysis, perfectly enhance the $\text{OH} \cdots \text{OH}$ hydrogen bonds in the cyclic structural motifs. This is shown in Fig. 2a for the comparison of the linear m4l and cyclic tetramer m4c of DM1B. Although the linear cluster show enhanced interaction strength compared to the dimer and trimer cluster, cooperativity is maximized in the cyclic geometry. The enhanced H-bonding is reflected in the intra and intermolecular bond lengths as well as in the spectroscopic observables such as vibrational frequencies or NMR chemical shifts.

Bond lengths and spectroscopic observables in the cationic and molecular clusters

In the cationic clusters, the charge transfer from the oxygen lone pair orbital into the OH anti bond orbital results in hydrogen

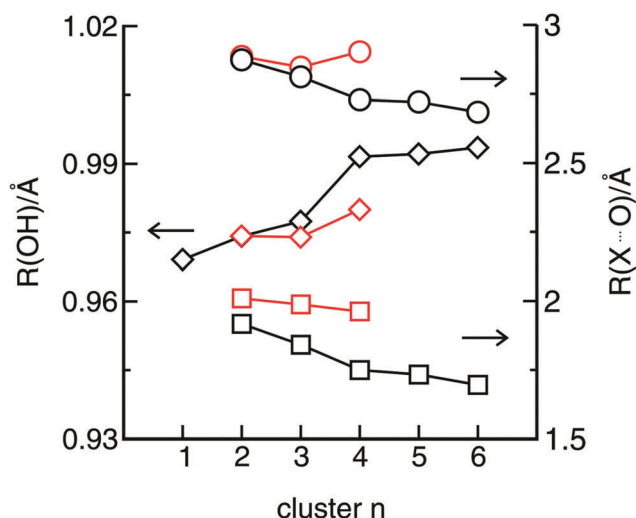


Fig. 3 The intramolecular bond lengths, $R(\text{OH})$, (left axis, diamonds) and the intermolecular bond distances, $R(\text{H}\cdots\text{O})$ (right axis, squares) and $R(\text{O}\cdots\text{O})$, (right axes, circles) are shown for the molecular (black open symbols) and pure cationic clusters (red open symbols), respectively. Enhanced hydrogen bonding with increasing cluster size is observed for all systems, indicated by lengthening of the OH bonds and shortening of the intermolecular bond distances.

bonding such as in molecular clusters but less pronounced. However, even in the four-fold H-bonded cationic cluster with net charge plus four, cooperative hydrogen bonding attenuates the repulsive Coulomb interaction resulting in longer intra- and shorter intermolecular bond lengths. Despite strong electrostatic opposition, the cationic clusters show typical H-bond distances and spectroscopic signatures as known for molecular liquids.

The intramolecular bond lengths, $R(\text{OH})$, and the intermolecular bond distances, $R(\text{H}\cdots\text{O})$ and $R(\text{O}\cdots\text{O})$, are shown in Fig. 3 for the pure cationic and the molecular clusters. Enhanced hydrogen bonding with increasing cluster size is observed. From the dimers to the cyclic tetramers, the intramolecular OH bonds are lengthened and the intermolecular distances $R(\text{H}\cdots\text{O})$ and $R(\text{O}\cdots\text{O})$ are shortened as expected for hydrogen bonding.^{24,25} Although both effects are less pronounced in the cationic clusters, cooperativity results in typical H-bond behaviour despite the strong repulsive forces in the cyclic cationic cluster (c4c).

Thus it is no surprise that the vibrational frequencies, ν_{OH} , and the proton chemical shifts, $\delta^1\text{H}$, for the hydroxyl groups in the cationic and molecular clusters reflect this behaviour in similar way. The OH frequencies in the cyclic structures of DM1B are substantially redshifted about 460 cm^{-1} as shown in Fig. 4. Although weaker, the redshift due to hydrogen bonding is also observed for the cationic clusters. The OH redshift of the 4+-charged tetramer is $\Delta\nu_{\text{OH}} = 150\text{ cm}^{-1}$ and thus comparable to that of the alcohol dimer. Again, cooperativity with increasing cluster size is also present for the cationic clusters. Similar behaviour is observed for the proton chemical shifts which are strongly downfield shifted (see Fig. 5) compared to the corresponding monomer values. In the DM1B clusters the hydroxyl protons are strongly deshielded resulting in downfield chemical

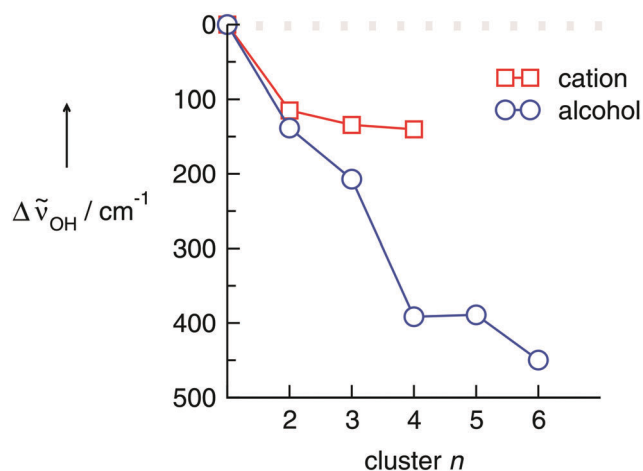


Fig. 4 Calculated O–H vibrational redshifts, $\Delta\nu_{\text{OH}}$, for the molecular (circles) and cationic clusters (squares) relative to the corresponding monomeric species (set to zero). Although less pronounced, the cationic clusters show similar redshifts as the molecular clusters with increasing cluster size. Cooperative hydrogen bonding is in particular strong in the cyclic cationic tetramer.

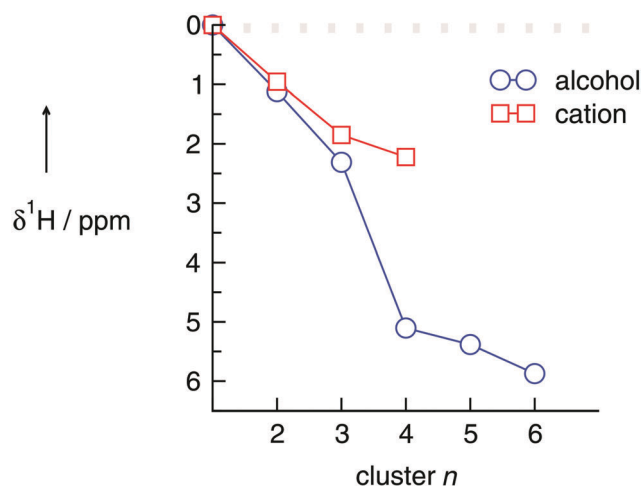


Fig. 5 Calculated down field chemical shifts for the molecular (circles) and cationic clusters (squares) relative to the value of tetramethylsilane (TMS, set to zero). Although less pronounced, the cationic clusters show similar downfield shifts as the molecular clusters with increasing cluster size. Cooperative hydrogen bonding is in particular strong in the cyclic cationic tetramer.

shifts between 5–6 ppm which is only slightly stronger than the values obtained for water and alcohols in their liquid phases.^{24,25,47} The downfield shift of the hydroxyl protons within the cationic clusters range up to 2 ppm for the cyclic tetramer. Such a chemical shift is clearly observable if such clusters are present in the gas or the liquid phase (see Fig. 5).

NBO parameters and spectroscopic observables of the cationic and molecular clusters

Now we check whether the second order stabilization energies, $\Delta E(2)_{n \rightarrow \sigma^*}$, and the charge transfer, q_{CT} , reflect the order of the

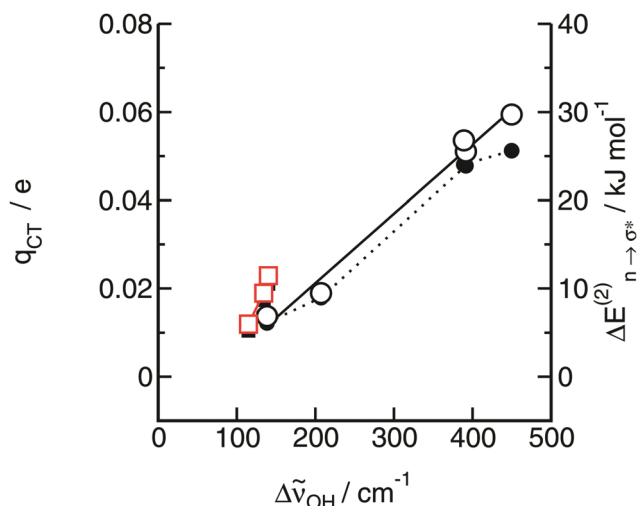


Fig. 6 NBO calculated second order stabilization energies $\Delta E(2)_{n \rightarrow \sigma^*}$ (open symbols) and estimated total charge transfers q_{CT} (closed symbols) for cationic (red) and molecular (black) clusters $n = 2-4$ plotted versus calculated redshifts of the average OH frequency, $\Delta\nu_{OH}$. The linear dependence indicates the strong relation between NBO stabilization energies and charge transfers with spectroscopic properties such as IR frequencies.

IR redshifts and NMR downfield shifts. For the cationic as well as for the molecular clusters, we plotted both NBO parameters versus the $\Delta\nu_{OH}$ redshifts (see Fig. 6) and to the δ^1H downfield chemical shifts (see Fig. 7). The spectroscopic features of the cationic clusters, wherein the strong repulsive Coulomb interaction is attenuated by hydrogen bonding, can be almost linearly related to the NBO parameters. Obviously, both properties characterize hydrogen bonding and cooperativity in a similar way. IR redshifts and downfield proton chemical shifts go along with

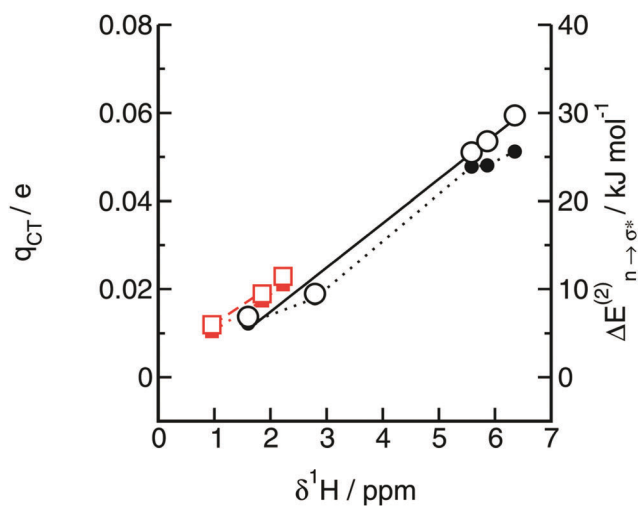


Fig. 7 NBO calculated second order stabilization energies $\Delta E(2)_{n \rightarrow \sigma^*}$ (open symbols) and estimated total charge transfers q_{CT} (closed symbols) for cationic (red) and molecular (black) clusters $n = 2-4$ plotted versus calculated average NMR proton chemical shifts, δ^1H (vs. TMS). The linear dependence indicates the strong relation between NBO stabilization energies and charge transfers with spectroscopic properties such as NMR chemical shifts.

increasing stabilization energies, $\Delta E(2)_{n \rightarrow \sigma^*}$, and enhanced charge transfer, q_{CT} .

That the strongest intermolecular stabilization energies are found for the cyclic structures is well correlated to the cooperative binding energies, frequencies and chemical shifts. These 'closed-CT' networks have highest stability resulting in strongest interaction, largest vibrational redshifts and strongest NMR downfield shifts.

Cationic clusters plus molecules ($[Chol_x[DM1B]_y]^{x+}$ ($cx-my$) with $x = 2-4$ and $y = 1-4$

For the cationic clusters the energies per species are positive in the dimer (c2l), the cyclic trimer (c3c) and the cyclic tetramer (c4c). As shown by the calculated frequencies which are positive throughout, these positively charged clusters present local minimum structures on the potential energy surface. They can be 'kinetically trapped', but are far away from thermodynamic stability. To achieve better kinetic stability or even thermodynamic stability for the positively charged clusters, we added neutral molecules as demonstrated in Scheme 2. As shown in Fig. 8, the dimer c2l (2+) can be stabilized by adding one DM1B molecule. However, thermodynamic stability can be only achieved if a second alcohol molecule is added resulting in the c2-m2 (2+) cyclic tetramer. By adding a third and fourth molecule we can further stabilize the 2+-charged clusters within

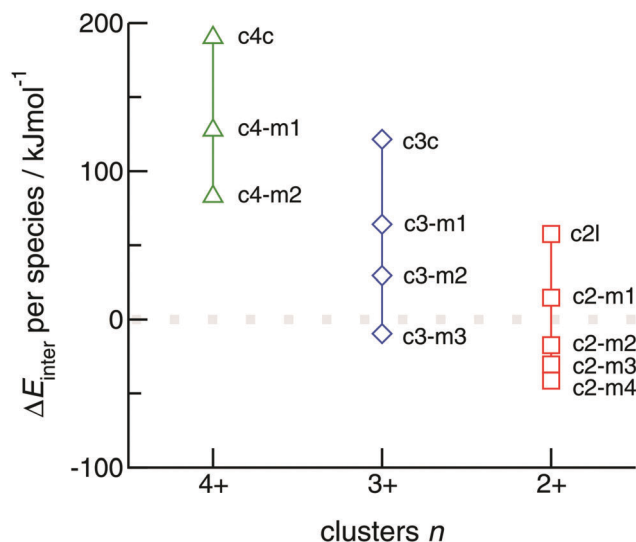


Fig. 8 B3LYP-D3/6-31+G* calculated binding energies per species for the cationic clusters c2l, c3c and c4c. To each of the 4+, 3+ and 2+ charged clusters 3-3-dimethyl-1-butanol molecules are added step by step leading to lower energies of the overall clusters. In principle the cationic clusters are meta-stable and exhibit positive energies. However, 3+ and 2+ charged clusters become also thermodynamically stable, if three molecules within a cyclic hexamer (c3-m3) or two molecules within a cyclic tetramer (c2-m2) are added. Larger cyclic clusters than hexamers were not taken into account because it is known from molecular clusters that cyclic heptamers and octamers do not show further increase of cooperativity but exhibit entropic penalties.²¹⁻²⁵

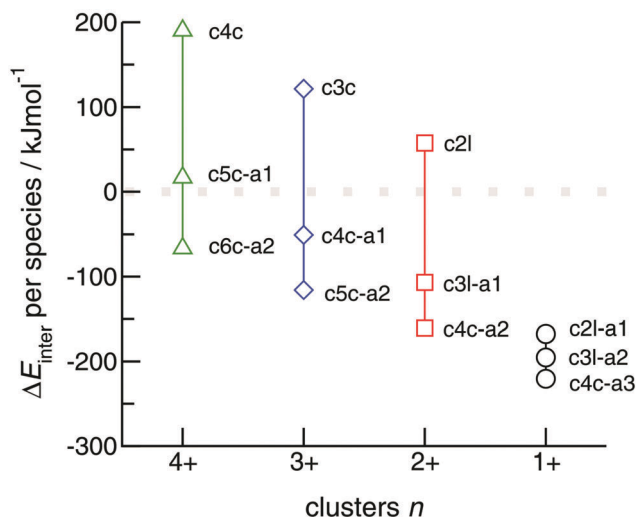


Fig. 9 B3LYP-D3/6-31+G* calculated binding energies per species for the cationic clusters c4c, c3c and c2l. To each of the 4+, 3+, 2+ and 1+ charged clusters counterions $[\text{NTf}_2]^-$ are added step by step leading to lower energies of the overall clusters. Except for the 4+ clusters it is shown that all positively charged clusters become thermodynamically stable by only adding one negative charge resulting in c4c-a1, c3l-a1 and c2l-a1 clusters, respectively. In principle cationic clusters up to 4+ should be observable in the experiment.

cyclic pentamers c2-m3 and cyclic hexamers c2-m4. With this procedure we change smoothly from the ionic to molecular systems by distributing the same positive charge over larger clusters. Two cations become thermodynamically stable if they are neighbored by only two neutral species and thus observable. Of course more molecules are needed to overcome the stronger repulsive Coulomb forces in the 3+-charged and 4+-charged configurations. One more namely three DM1B molecules are needed within a cyclic hexamer structure c3-m3 to achieve thermodynamic stability. Cooperative hydrogen bonds within this cyclic motif of the three-fold positively charged cluster are so strong that they overcome the repulsive forces between the three cations. Thermodynamic stability can

not be achieved for the 4-fold positively charged clusters. By adding one and two alcohol molecules 'kinetic stability' can be further improved within the cyclic pentamer c4-m1 and cyclic hexamer c4-m2 without approaching thermodynamic stability. In principle we could add more than two molecules to the c4c cluster. But then the ring structures exceed the size of the enthalpically and entropically favourable hexamer as known from studies of alcohol clusters. Cyclic heptamers and octamers show no further enhanced cooperativity which is required for increasing stability. It is interesting to note that cationic clusters with charge 3+ become thermodynamically stable by adding the same number of alcohol molecules. They are in particular stable if each cation is neighbored by molecules.

Cationic clusters plus anions $([\text{Chol}_x[\text{NTf}_2]_y]^{(x-y)+})^{(x-y)-}$ with $x = 2-4$ and $y = 1-3$

The situation becomes different if we add $[\text{NTf}_2]^-$ anions to the cationic clusters but remaining the 4+, 3+ and 2+ charged species. The single positively charged clusters c2l-a1, c3l-a2 and c4c-a3 are thermodynamically stable throughout (see Fig. 9). Thus these clusters should be observable in the experiment. Johnson *et al.* have shown that for the ionic liquid based clusters $[\text{EMIm}]_2[\text{BF}_4]^+$ with CIVP spectroscopy.^{27,28} Thus for the small clusters, additional strengthening due to cation-cation hydrogen bonding is not required. Also for the 2+-charged clusters only one additional anion is needed for thermodynamic stability. This is not surprising because each 'ion pair' in the c3l-a1 and c4c-a2 clusters contributes between 300 and 400 kJ mol^{-1} of binding energy which is well known from numerous calculations on smaller IL aggregates.³⁸⁻⁴³ Instead, it is remarkable that the H-bond ring in c4c-a2 is preserved during the optimization procedure and not tackled by the two weakly coordinating anions. That is even true for the 3+-charged clusters c4c-a1 and c5c-a2, wherein the cyclic cationic tetramer (c4c) and pentamer (c5c) survive. This behaviour

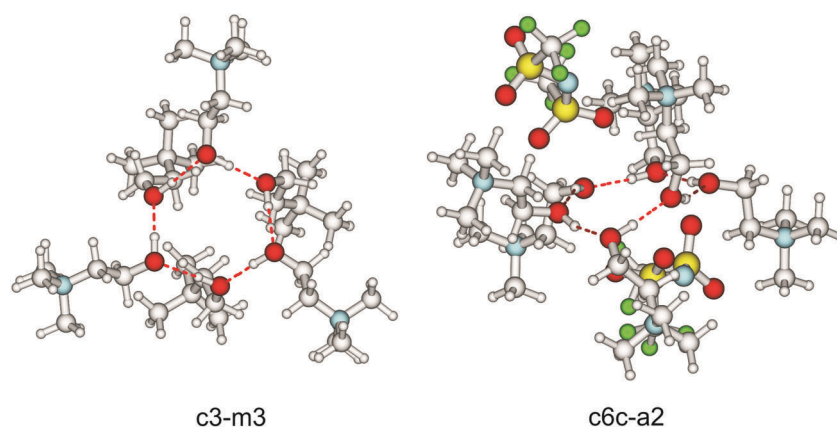


Fig. 10 The cationic clusters can be stabilized by (a) the addition of molecules or (b) the addition of counterions. For both cases, we show the thermodynamically stable clusters with the highest possible positive charges: c3-m3 (3+) and c6c-a2 (4+). Both clusters are stabilized by cooperative hydrogen bonding within the OH ring structures as indicated by the red dashed lines.

also holds for the 4+-charged clusters. Here, two counterions are needed to achieve thermodynamic stability. It is notable that the most favourable cyclic pentamer (c5c) and hexamer (c6c) keep their motif if one and two anions are coordinated as shown in Fig. 10.

Conclusion

In this work we showed that the addition of alcohol molecules (3-3-dimethyl-1-butanol) or counter ions (NTf_2^- anion) to pure cationic (cholinium) clusters results in enhanced 'kinetic stability' and in a few cases even in thermodynamic stability. Such clusters should be observable in sophisticated gas phase experiments such as CIVE spectroscopy.^{27,28} The pure cationic clusters c2l, c3c and c4c show 'kinetic stability' caused by cooperative hydrogen bonding which is in particular strong for cyclic structures. We showed for the cholinium dimer that the potential energy curves of the B3LYP and MP2 calculations become almost similar if the dispersion correction D3 for the DFT method is taken into account. However, the pure positive clusters cannot be observed experimentally even at low temperatures. In principle the cationic clusters can be stabilized by adding one or two alcohol molecules. Then the energy of the mixed, but still positively charged clusters can be lowered substantially. Despite strong cooperative hydrogen bonds and reduced like-charge repulsion the energies are still positive for most of the positively charged clusters. However, 'kinetic trapping' should be possible for all of them. It is remarkable that two- and threefold positively charged clusters become stable by adding two or three alcohol molecules resulting in c2-m2 (2+) and c3-m3 (3+) ring structures. Both configurations achieve highest stability if the cations are separated by neutral molecules. Two effects, enhanced hydrogen bonding and reduced Coulomb repulsion bring these clusters to thermodynamic stability.

Of course the strong like-charge repulsion can be easier overcome in the presence of compensating counterions. If the strong cooperative hydrogen bonds between the cations remain, only one anion is sufficient for achieving thermodynamic stability. Experimentally it should be possible to observe 2+, 3+ and 4+ charged clusters such as 3cl-a1 (2+), 4c-a1 (3+) and 5c-a1 (4+), respectively. Overall it can be concluded that multiple positively charged clusters should be detectable by experimental methods. The highest charged species which are thermodynamically stable is the c3-m3 (3+) cluster by the addition of three molecules and the c6c-a2 (4+) cluster by the addition of two anions. Both clusters are stable by the formation of cooperative hydrogen bonds within the cyclic structures.

Acknowledgements

This work has been supported by the DFG Research Grant LU-506/14-1 and partially by the DFG SPP 1807 "Control of London dispersion interactions in molecular chemistry".

References

- 1 J. Smid, *Angew. Chem., Int. Ed.*, 1972, **84**, 127–144 (*Angew. Chem., Int. Ed.*, 1972, **11**, 112–127).
- 2 C. Reichhardt, *Solvents and Solvent Effects in Organic Chemistry*, VCH, Weinheim, 1990.
- 3 Y. Marcus and G. Hefter, *Chem. Rev.*, 2006, **106**, 4585–4621.
- 4 J. Iwahara, A. Esadze and L. Zandarashvili, *Biomolecules*, 2015, **5**, 2435–2463.
- 5 (a) A. J. McCoy, V. Chandana Epa and P. M. Colman, *J. Mol. Biol.*, 1997, **268**, 570–584; (b) K. Nadassy, S. J. Wodak and J. Janin, *Biochemistry*, 1999, **38**, 1999–2017.
- 6 S. Jones, D. T. Daley, N. M. Luscombe, H. M. Berman and J. M. Thornton, *Nucleic Acids Res.*, 2001, **29**, 943–954.
- 7 B. D. Bax, P. F. Chan, D. S. Eggleston, A. Fosberry, D. R. Gentry, F. Gorrec, I. Giordano, M. M. Hann, A. Hennessy and M. Hibbs, *et al.*, *Nature*, 2010, **466**, 935–940.
- 8 M. Holz and K. J. Patil, *Ber. Bunsen-Ges.*, 1991, **95**, 107–113.
- 9 O. Shih, A. H. England, G. C. Dallinger, J. W. Smith, K. C. Duffey, R. C. Cohen, D. Prendergast and R. J. Saykally, *J. Chem. Phys.*, 2013, **139**, 035104.
- 10 M. Benrraou, B. L. Bales and R. Zana, *J. Phys. Chem. B*, 2003, **107**, 13432–13440, and references therein.
- 11 (a) A. E. Larsen and D. G. Grier, *Nature*, 1997, **385**, 230–233; (b) M. R. Caplan, P. N. Moore, S. Zhang, R. D. Kamm and D. A. Lauffenburger, *Biomacromolecules*, 2000, **1**, 627–631.
- 12 W. Gamrad, A. Dreier, R. Goddard and K.-R. Pörschke, *Angew. Chem., Int. Ed.*, 2015, **54**, 4482–4487.
- 13 (a) T. Inagaki, S. Aono, H. Nakano and T. Yamamoto, *J. Phys. Chem. B*, 2014, **118**, 5499–5508; (b) M. Fakhraee, B. Zandkarimi, H. Salari and M. R. Gholami, *J. Phys. Chem. B*, 2014, **118**, 14410–14428.
- 14 E. M. Fatila, E. B. Twum, A. Sengupta, M. Pink, J. A. Karty, K. Raghavachari and A. H. Flood, *Angew. Chem., Int. Ed.*, 2016, **55**, 14057–14062 (*Angew. Chem.*, 2016, **128**, 14263–14268).
- 15 (a) F. Weinhold and R. A. Klein, *Angew. Chem., Int. Ed.*, 2014, **126**, 11396–11399 (*Angew. Chem., Int. Ed.*, 2014, **53**, 11214–11217); (b) Corrigendum: F. Weinhold and R. A. Klein, *Angew. Chem., Int. Ed.*, 2014, **126**, 13207 (*Angew. Chem., Int. Ed.*, 2014, **53**, 12992).
- 16 F. Weinhold, C. R. Landis and E. D. Glendening, *Int. Rev. Phys. Chem.*, 2016, **35**, 399–440.
- 17 A. Knorr, K. Fumino, A.-M. Bonsa and R. Ludwig, *Phys. Chem. Chem. Phys.*, 2015, **17**, 30978–30982.
- 18 A. Knorr and R. Ludwig, *Sci. Rep.*, 2015, **5**, 17505.
- 19 A. Knorr, P. Stange, K. Fumino, F. Weinhold and R. Ludwig, *ChemPhysChem*, 2016, **17**, 458–462.
- 20 A. Strate, T. Niemann, P. Stange, D. Michalik and R. Ludwig, *Angew. Chem., Int. Ed.*, 2017, **56**, 496–500 (*Angew. Chem.*, 2017, **129**, 510–514).
- 21 K. M. Murdoch, T. D. Ferris, J. C. Wright and T. C. Farrar, *J. Chem. Phys.*, 2002, **116**, 5717.
- 22 F. Huisken, A. Kulcke, C. Laush and J. Lisy, *J. Chem. Phys.*, 1991, **95**, 3924–3929.
- 23 M. Huelsekopf and R. Ludwig, *J. Mol. Liq.*, 2002, **98–99**, 163–171.
- 24 R. Ludwig, F. Weinhold and T. C. Farrar, *Mol. Phys.*, 1999, **97**, 465–477.

- 25 R. Ludwig, *Phys. Chem. Chem. Phys.*, 2002, **4**, 5481–5487.
- 26 A. B. Wolk, C. M. Leavitt, E. Garand and M. A. Johnson, *Acc. Chem. Res.*, 2014, **47**, 202–210.
- 27 J. A. Fournier, C. T. Wolke, C. J. Johnson, A. B. McCoy and M. A. Johnson, *J. Chem. Phys.*, 2015, **142**, 064306.
- 28 C. J. Johnson, J. A. Fournier, C. T. Wolke and M. A. Johnson, *J. Chem. Phys.*, 2013, **139**, 224305.
- 29 N. C. Polfer and J. Comens, *Mass Spectrom. Rev.*, 2009, **28**, 468–494.
- 30 J. Lemaire, P. Boissel, M. Heninger, G. Mauclaire, G. Bellec, H. Mestdag, A. Simon, S. L. Caer, J. M. Ortega, F. Glotin and P. Maître, *Phys. Rev. Lett.*, 2002, **89**, 273002.
- 31 M. J. Frisch, G. W. Trucks, H. B. Schlegel, G. E. Scuseria, M. A. Robb, J. R. Cheeseman, G. Scalmani, V. Barone, G. A. Petersson, H. Nakatsuji, X. Li, M. Caricato, A. Marenich, J. Bloino, B. G. Janesko, R. Gomperts, B. Mennucci, H. P. Hratchian, J. V. Ortiz, A. F. Izmaylov, J. L. Sonnenberg, D. Williams-Young, F. Ding, F. Lipparini, F. Egidi, J. Goings, B. Peng, A. Petrone, T. Henderson, D. Ranasinghe, V. G. Zakrzewski, J. Gao, N. Rega, G. Zheng, W. Liang, M. Hada, M. Ehara, K. Toyota, R. Fukuda, J. Hasegawa, M. Ishida, T. Nakajima, Y. Honda, O. Kitao, H. Nakai, T. Vreven, K. Throssell, J. A. Montgomery, Jr., J. E. Peralta, F. Ogliaro, M. Bearpark, J. J. Heyd, E. Brothers, K. N. Kudin, V. N. Staroverov, T. Keith, R. Kobayashi, J. Normand, K. Raghavachari, A. Rendell, J. C. Burant, S. S. Iyengar, J. Tomasi, M. Cossi, J. M. Millam, M. Klene, C. Adamo, R. Cammi, J. W. Ochterski, R. L. Martin, K. Morokuma, O. Farkas, J. B. Foresman and D. J. Fox, *Gaussian 09, Revision A.02*, Gaussian, Inc., Wallingford CT, 2016.
- 32 E. D. Glendening, J. K. Badenhoop, A. E. Reed, J. E. Carpenter, J. A. Bohmann, C. M. Morales, C. R. Landis and F. Weinhold, *NBO 6.0.*, Theoretical Chemistry Institute, University of Wisconsin, Madison, 2013.
- 33 F. Weinhold and C. R. Landis, *Valency and Bonding A Natural Bond Orbital Donor–Acceptor Perspective*, Cambridge, University Press, Cambridge, 2005.
- 34 S. H. Zeisel and K.-A. da Costa, *Nutr. Rev.*, 2009, **67**, 615–623.
- 35 S. Grimme, J. Antony, S. Ehrlich and H. Krieg, *J. Chem. Phys.*, 2010, **132**, 154104.
- 36 S. Ehrlich, J. Moellmann, W. Reckien, T. Bredow and S. Grimme, *ChemPhysChem*, 2011, **12**, 3414–3420.
- 37 S. Grimme and A. Jansen, *Chem. Rev.*, 2016, **116**, 5105–5154.
- 38 P. A. Hunt, C. R. Ashworth and R. P. Matthews, *Chem. Soc. Rev.*, 2015, **44**, 1257–1288.
- 39 C. R. Ashworth, R. P. Matthews, T. Welton and P. A. Hunt, *Phys. Chem. Chem. Phys.*, 2016, **18**, 18145–18160.
- 40 E. Izgorodina, Z. L. Seeger, D. L. A. Scarborough and S. Y. S. Tan, *Chem. Rev.*, 2017, **117**, 6696–6754.
- 41 S. B. C. Lehmann, M. Roatsch, M. Schöppke and B. Kirchner, *Phys. Chem. Chem. Phys.*, 2010, **12**, 7473–7486.
- 42 K. Fumino and R. Ludwig, *J. Mol. Liq.*, 2014, **192**, 94–102.
- 43 K. Fumino, S. Reimann and R. Ludwig, *Phys. Chem. Chem. Phys.*, 2014, **40**, 21903–21929.
- 44 G. Frenking and G. F. Caramori, *Angew. Chem.*, 2015, **126**, 2632–2635 (*Angew. Chem., Int. Ed.*, 2015, **54**, 2596–2599).
- 45 P. R. Horn, Y. Mao and M. Head-Gordon, *Phys. Chem. Chem. Phys.*, 2016, **18**, 23067–23079.
- 46 A. J. Stone, *J. Chem. Chem. A*, 2017, 1531–1534.
- 47 R. Ludwig, *ChemPhysChem*, 2005, **6**, 1369–1375.

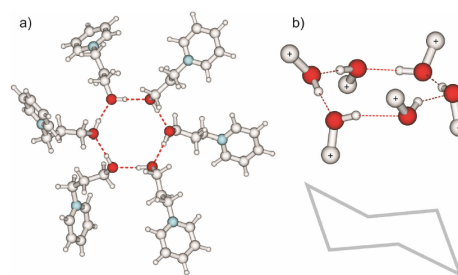
Like-likes-Like: Cooperative Hydrogen Bonding Overcomes Coulomb Repulsion in Cationic Clusters with Net Charges up to $Q=+6e$

T. Niemann (40 %), A. Strate (15 %), P. Stange (15 %), R. Ludwig (30 %)

ChemPhysChem, 19, 1691-1695, 2018

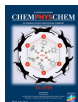
Content:

It was shown that clusters of monovalent cations with net charges up to $Q = +6e$ are kinetically stable. Quantum chemical calculations suggest that hydrogen bonds can make (c-c) structural features possible despite the repulsive COULOMB force. Cooperative hydrogen bonding is in particular strong in cyclic clusters, which look similar to well-known structural motives for water or alcohols.



Contributions to this work:

For this publication I have done some of the DFT calculations and I wrote the first draft. I have discussed the results with Anne Strate. Peter Stange contributed to this work with corrections on the initial draft. Professor Ludwig has done the other part of the DFT calculations and got the manuscript for the final corrections.



Like-likes-Like: Cooperative Hydrogen Bonding Overcomes Coulomb Repulsion in Cationic Clusters with Net Charges up to $Q = +6e$

Thomas Niemann,^[a] Peter Stange,^[a] Anne Strate,^[a] and Ralf Ludwig^{*,[a, b]}

Quantum chemical calculations have been employed to study kinetically stable cationic clusters, wherein the monovalent cations are trapped by hydrogen bonding despite strongly repulsive electrostatic forces. We calculated linear and cyclic clusters of the hydroxy-functionalized cation N-(3-hydroxypropyl) pyridinium, commonly used as cation in ionic liquids. The largest kinetically stable cluster was a cyclic hexamer that very much resembles the structural motifs of molecular clusters, as known for water and alcohols. Surprisingly, strong cooperative hydrogen bonds overcome electrostatic repulsion and result in cationic clusters with a high net charge up to $Q = +6e$. The structural, spectroscopic, and electronic signatures of the cationic and related molecular clusters of 3-phenyl-1-propanol could be correlated to NBO parameters, supporting the existence of “anti-electrostatic” hydrogen bonds (AEHB), as recently suggested by Weinhold. We also showed that dispersion forces enhance the cationic cluster formation and compensate the electrostatic repulsion of one additional positive charge.

In contrast to ion pairing between ions of opposite charge, the clustering of like-charged ions seems to be an elusive concept.^[1,2] It contradicts the tenet of classical electrostatics that like charges repel each other. Meanwhile, theoretical and experimental evidence is available showing the importance of this counterintuitive phenomenon in the gaseous and condensed phase.^[3–11] Cationic and anionic dimers are kinetically stabilized by hydrogen bonding, opposing a “Coulomb explosion” to separate the ions. In theoretical studies of like-charge attraction, Klein and Weinhold claimed that doubly-charged complexes $[A-HB]^{2\pm}$ are manifestations of “anti-electrostatic” hydrogen bonds (AEHB), wherein the short-range donor-acceptor or covalency forces overcome the powerful long-range electro-

static opposition to be expected between ions of like charge.^[3–5] Weinhold analyzed the potential energy curves for the ion-ion interactions which showed shallow local minima indicating hydrogen bonding between the like-charged ions and kinetic stabilization. However, like-charge attraction in “real systems” could be only observed for large-scale structures, assemblies or stabilizing frameworks.^[6–9] In solution, solvent molecules like water are required to attenuate the Coulomb repulsion.^[10,11] Recently, the formation of clusters of like-charged ions in pure ionic liquids has been observed. Cationic clusters are kinetically stabilized by cooperative hydrogen bonds between the OH groups of the hydroxy-functionalized ammonium and imidazolium cations.^[12–18] However, to large extent the cationic cluster formation is supported by weakly coordinating anions, which compensate for the positively charged centers of the cations and allow for counterion-mediated attraction between the likes.^[17,18]

It is the purpose of the present work to study kinetically stable cationic clusters, wherein, in the absence of any mediating “solvent effects” by molecules or counterions, the repulsive Coulomb forces can be compensated merely by cooperative hydrogen bonding between the cations. We particularly want to show that like-charge attraction also exists for cationic clusters that are much larger than the reported dimers with net charge $Q = \pm 2e$.^[3,4] Braga and coworkers already questioned anion-anion interaction from molecular electrostatic potential considerations and concluded that it is instead a “tugboat interaction”, controlling anion aggregation and minimizing anion-anion repulsions.^[19] They claimed that the anionic dimer would fall apart if the counterions are removed. However, Head-Gordon and Frenking showed that the local minimum structures for anionic dimers can be also analyzed by electronic decomposition analysis (EDA) methods.^[20,21] Nevertheless, larger cationic clusters are not expected within electrostatic conception due to strongly increasing repulsive interaction with each additional positive charge.

Here, we show that larger clusters of monovalent cations up to net charges $Q = +6e$ can be kinetically trapped by cooperative hydrogen bonding. No mediating molecules, counterions or screening effects are needed to overcome the repulsive Coulomb forces. The structural, spectroscopic and electronic signatures of the cationic and related molecular clusters could be related to NBO parameters, supporting the existence of “anti-electrostatic” hydrogen bonds (AEHB) as recently suggested by Weinhold.^[3–5] We also show that dispersion forces enhance the cationic cluster formation and compensate the long-range electrostatic repulsion. Overall,

[a] T. Niemann, P. Stange, Dr. A. Strate, Prof. Dr. R. Ludwig
Universität Rostock, Institut für Chemie, Abteilung für Physikalische und Theoretische Chemie,
Dr.-Lorenz-Weg 2, 18059, Rostock (Germany)
E-mail: ralf.ludwig@uni-rostock.de

[b] Prof. Dr. R. Ludwig
Leibniz-Institut für Katalyse an der Universität Rostock e.V., Albert-Einstein-Str. 29a, 18059 Rostock (Germany)

Supporting Information for this article is available on the WWW under <https://doi.org/10.1002/cphc.201800293>

© 2018 The Authors. Published by Wiley-VCH Verlag GmbH & Co. KGaA.
This is an open access article under the terms of the Creative Commons Attribution Non-Commercial NoDerivs License, which permits use and distribution in any medium, provided the original work is properly cited, the use is non-commercial and no modifications or adaptations are made.

dispersion interactions shift the kinetic stability from a cyclic pentamer to a cyclic hexamer.

For that purpose we have chosen the hydroxy-functionalized cation N-(3-hydroxypropyl) pyridinium [HPPy⁺] and its molecular mimic 3-phenyl-1-propanol [3-Phe-1-Pr] as model systems. We calculated linear clusters up to tetramers ($n=4$) and cyclic clusters up to hexamers ($n=6$). The hydroxy groups on the cations form hydrogen bonds and promote the aggregation into highly charged cationic clusters. We employed B3LYP/6-31 + G* and B3LYP-D3/6-31 + G* calculations performed with the Gaussian 09 program and analyzed with the NBO 6.0 program.^[22–27] For calculating all cationic and molecular clusters at the same level of theory, we have used the well-balanced, but small 6-31 + G* basis set. It includes polarization as well as diffuse functions, and has been shown to be suitable for calculating hydrogen-bonded clusters of like-charged ions.^[14–18] The 6-31 + G* basis set is also chosen for better comparison with earlier studies of molecular and ionic clusters.^[28–31] We also show that the salient properties of these clusters can be robustly calculated with both smaller and larger basis sets. This is demonstrated for the features of the largest cationic cluster found here (see calculated cyclic hexamers revealed from B3LYP-D3 calculations at 3-21G, 6-31 + G* and 6-311 + + G** basis sets (see SI). All the pure cationic clusters [HPPy⁺]_n and molecular clusters [3-Phe-1-Pr]_n were fully optimized. The calculated vibrational frequencies were all positive, showing that we calculated at least local minimum structures. Additionally, we calculated OH vibrational frequencies for the OH bonds, ν_{OH} and the hydroxy proton chemical shifts, $\delta^1\text{H}$, for each configuration. These spectroscopic observables are related to NBO-calculated second order stabilization energy $\Delta E(2)_{n \rightarrow o^*}$ and charge transfer, q_{CT} .

Kinetically Stabilized Dimers [HPPy⁺]₂: For the dimer structure [HPPy⁺]₂ we calculated the fully relaxed-scan potential curve at the HF/6-31 + G* (I), B3LYP/6-31 + G* (II), B3LYP-D3/6-31 + G* (III) and MP2/6-31 + G* (IV) levels of theory. The local minimum structures were found at typical H-bond distances of $R_{\text{O} \cdots \text{H}} = 2.0706 \text{ \AA}$, $R_{\text{O} \cdots \text{H}} = 1.9546 \text{ \AA}$, $R_{\text{O} \cdots \text{H}} = 1.9124 \text{ \AA}$ and $R_{\text{O} \cdots \text{H}} = 1.9175 \text{ \AA}$, for the dimers I–IV (see Table 1, SI). As shown in Figure 1, a robust kinetic stability with a clear dissociation barrier of 12–13 kJ mol^{−1} is achieved for the B3LYP-D3 and the MP2 treatments. It is interesting to note that the MP2 calculations give the lowest energies and that the B3LYP calculations represent nearly the same potential energy curve if the D3 dispersion correction is taken into account.^[25–27] Thus hydrogen bonds between like-charged ions are well described by dispersion-corrected DFT methods. Therefore, a cheaper

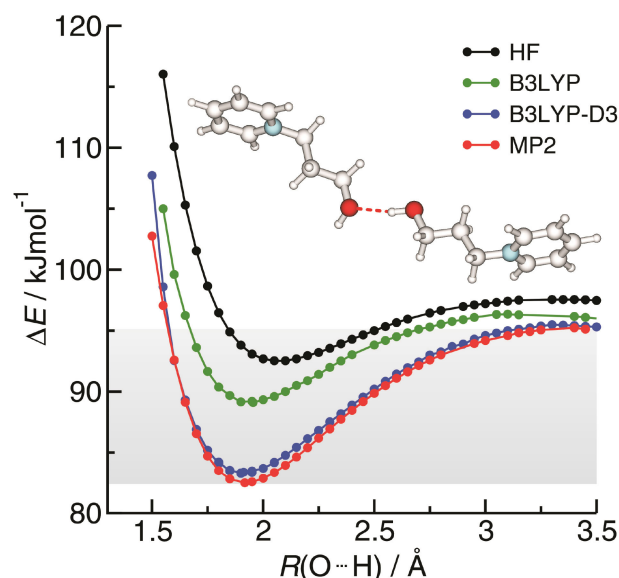


Figure 1. Potential energy curves for [HPPy⁺]₂ H-bonding (all at 6-31 + G* basis level) as calculated with the HF (black), hybrid density functional B3LYP (green), hybrid density functional B3LYP-D3 including dispersion correction (blue), and ab initio MP2 (red) methods. The structures were relaxed for each bond length $R(\text{O} \cdots \text{H})$. The bond lengths $R(\text{O} \cdots \text{H})$ at lowest energy are given in Table 1.

than MP2 level of theory can be used to describe the essential structural and energetic properties of cationic clusters without significant loss of accuracy.

Cyclic Clusters up to Net Charge $Q = +6e$: We then optimized linear and cyclic cationic clusters of [HPPy⁺]_n and [3-Phe-1-Pr]_n from trimers up to hexamers ($n=3–6$) (see SI). For both the exotic ionic species as well as the familiar neutral analogues, the starting geometries of linear trimers and tetramers were optimized towards cyclic clusters, wherein cooperative H-bonding is maximized. By taking Grimme's D3 dispersion correction into account, we obtained intrinsic (meta) stable cyclic hexamers [HPPy⁺]_{6c} which exhibit a net charge of $Q = +6e$.^[25–27] The meta-stable cationic clusters resemble the cyclic hexamer of [3-Phe-1-Pr] and those known for other alcohols and water.^[14–18] Without including dispersion forces these highly charged hexamers show “Coulomb explosion” and dissociate during the optimization procedure. Ignoring dispersion forces leads to cyclic pentamers as largest kinetically stable ionic clusters (see SI).

The detection and control of clusters of like-charged ions may be regarded as support for the “anti-electrostatic” hydrogen bonds (AEHB) as reported recently by Weinhold and Klein.^[3,4] Although Frenking and Head-Gordon could show that the local minimum structures for anionic dimers can be analyzed also by electronic decomposition analysis (EDA) methods, AEHBs are supported by spectroscopic observables, such as vibrational frequencies, ν_{OH} and NMR chemical shifts, $\delta^1\text{H}$.^[20,21] Geometrical and spectroscopic properties of cationic and molecular clusters show similar behavior.

Bond Lengths and Spectroscopic Observables of the Cationic and Molecular Clusters: In the cationic clusters, the charge transfer from the oxygen lone pair orbital into the OH

Table 1. Calculated intermolecular distances $R(\text{O} \cdots \text{HO})$ and $R(\text{O} \cdots \text{O})$ as well as bond angles $\angle(\text{O} \cdots \text{HO})$ of the optimized dimer structures [HPPy⁺]₂ using different theoretical methods but applying the same 6-31 + G* basis set.

Method	$R(\text{O} \cdots \text{HO})$	$R(\text{O} \cdots \text{O})$	$\angle(\text{O} \cdots \text{HO})$
HF	2.0706	3.0096	168.68
B3LYP	1.9546	2.9084	164.60
B3LYP-D3	1.9124	2.8716	166.32
MP2	1.9175	2.8807	166.58

antibonding orbital results in hydrogen bonding such as in molecular clusters but less pronounced. However, even in the six-fold H-bonded cationic cluster with $Q = +6e$, cooperative hydrogen bonding attenuates the repulsive Coulomb interaction, resulting in longer intra- and shorter intermolecular bond lengths. Despite strong electrostatic opposition, the cationic clusters show typical H-bond distances and spectroscopic signatures as known for molecular liquids. The intramolecular bond lengths, $R(\text{OH})$, and the intermolecular bond distances, $R(\text{H}\cdots\text{O})$ and $R(\text{O}\cdots\text{O})$, are shown in Figure 2 for the pure cationic

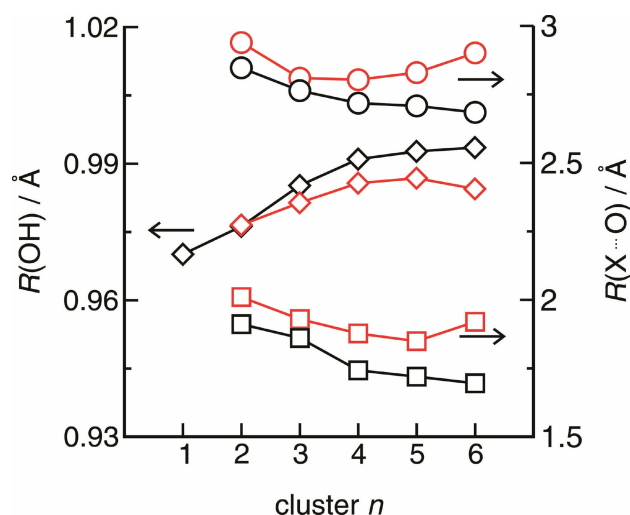
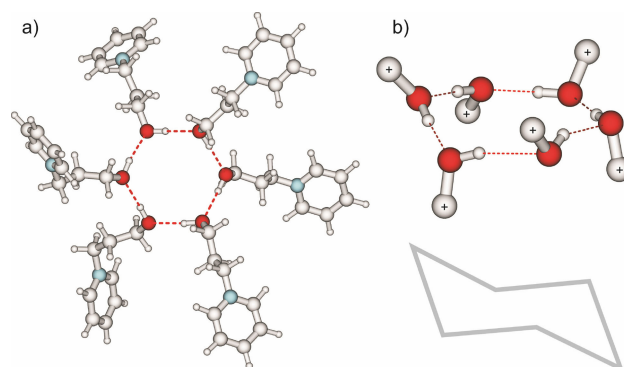


Figure 2. The intramolecular bond lengths, $R(\text{OH})$, (left axis, diamonds) and the intermolecular bond distances, $R(\text{H}\cdots\text{O})$ (right axis, squares) and $R(\text{O}\cdots\text{O})$, (right axes, circles) are shown for the molecular (black open symbols) and pure cationic clusters (red open symbols), respectively. Enhanced hydrogen bonding with increasing cluster size is observed for all systems, indicated by lengthening of the OH bonds and shortening of the intermolecular bond distances.

and the molecular clusters. Enhanced hydrogen bonding with increasing cluster size is observed. From the dimers to the cyclic tetramers, the intramolecular OH bonds are lengthened and the intermolecular distances $R(\text{H}\cdots\text{O})$ and $R(\text{O}\cdots\text{O})$ are shortened as expected for enhanced hydrogen bonding.^[28–32] Although both effects are less pronounced in the cationic clusters, cooperativity results in typical H-bond behavior despite the strong repulsive forces.

It is interesting to note that the cationic clusters show weaker cooperativity from the cyclic tetramer on. In the higher charged cationic clusters the electrostatic repulsion becomes stronger with each additional positive charge which cannot be fully compensated by cooperative hydrogen bonding. However, also the molecular clusters show weaker cooperativity with increasing cluster size. Therein, dispersion forces strengthen the attractive interaction between the phenyl groups and indirectly weaken the hydrogen bonds of the cyclic pentamers and hexamers compared to those of the cyclic tetramer. To illustrate these effects we show the cationic hexamer in Scheme 1. The ring structure $[\text{HPPy}^+]_6$ resembles that of the water hexamer which has served for analyzing the hydrogen bond in ice. The B3LYP-D3/6-31 + G* optimal geometry has an almost S_6 symme-



Scheme 1. Kinetically stable cationic hexamer $[\text{HPPy}^+]_6$: a) the cyclic cluster in the supervision and b) the enlarged hydrogen bonding motif of the cluster showing a “chair” configuration.

try with four oxygen atoms lying in plane. The two remaining oxygen atoms lie on either side of this plane giving rise to a “chair” configuration.^[32]

The vibrational frequencies, ν_{OH} , and the proton chemical shifts, $\delta^1\text{H}$, for the hydroxy groups in the cationic and molecular clusters reflect this behavior in a similar way. The OH frequencies in the cyclic structures of [3-Phe-1-Pr] are substantially redshifted up to 460 cm^{-1} as shown in Figure 3a. Although weaker, the redshift due to hydrogen bonding is also observed for the cationic clusters. The OH redshift of the hexamer with $Q = +6e$ is $\Delta\nu_{\text{OH}} = 280\text{ cm}^{-1}$ and thus stronger than for the neutral [3-Phe-1-Pr] trimer. Again, cooperativity with increasing clusters size is also present for the cationic clusters. Similar behavior is observed for the proton chemical shifts which are strongly shifted downfield (see Figures 3b) compared to the corresponding monomer values. In the [3-Phe-1-Pr] clusters the hydroxy protons are strongly de-shielded, resulting in downfield chemical shifts between 5–6 ppm which is only slightly stronger than the values obtained for water and alcohols in their liquid phases.^[28–30] The downfield shift of the hydroxy protons within the cationic clusters range up to 4 ppm for the cyclic pentamer/hexamer. Overall, such significant vibrational redshifts and downfield chemical shifts should be clearly observable in gas phase experiments.^[33,34]

NBO Parameters and Spectroscopic Observables of the Cationic and Molecular Clusters: The B3LYP-D3/6-31 + G* calculations suggest that the cation-cation interaction via the $\text{OH}\cdots\text{OH}$ hydrogen bond is possible due to cooperative effects.^[18] Electron density from the oxygen lone pair orbital of a first cation is donated into the OH antibonding orbital of a second cation. The resulting larger negative charge at the OH oxygen at the second cation can now be transferred into the OH antibonding orbital of another cation, further enhancing hydrogen bonding. This process leads to even stronger cooperativity in the cyclic structures such as tetramers, pentamers and hexamers. This way, the short-range donor-acceptor covalency forces can overcome the strong long-range electrostatic repulsive forces as expected for ions of like charge. These features can be rationalized in the framework of the natural bond orbital (NBO) analysis.^[23,24] NBO analysis shows

typical strong $n_o \rightarrow \sigma^*_{OH}$ donor-acceptor interaction, corresponding to second order stabilization energies $\Delta E(2)_{n \rightarrow \sigma^*}$ and estimated total charge transfers of q_{CT} for the enhanced OHLudwigOH hydrogen bonds, respectively. These typical NBO descriptors are plotted versus $\Delta\nu_{OH}$ redshifts (see Figure 4) and δ^1H downfield chemical shifts (see Figure 5). The spectroscopic features of the cationic clusters, wherein the strong repulsive Coulomb interaction is attenuated by hydrogen bonding, can be almost linearly related to the NBO descriptors. Obviously, both properties characterize hydrogen bonding and cooperativity in a similar way. IR redshifts and downfield proton chemical shifts go along with increasing stabilization energies, $\Delta E(2)_{n \rightarrow \sigma^*}$, and enhanced charge transfer, q_{CT} . That the strongest intermolecular stabilization energies are found for the cyclic structures is well correlated to the cooperative binding energies, frequencies and chemical shifts. These "closed-CT" networks have highest stability, resulting in strongest inter-

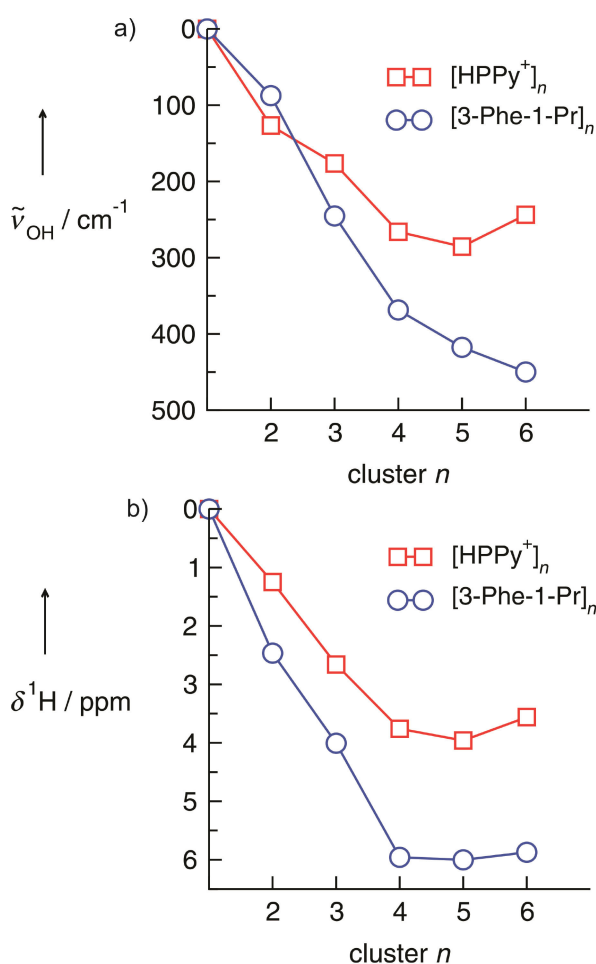


Figure 3. a) Calculated O–H vibrational redshifts, $\Delta\nu_{OH}$, for the molecular (circles) and the cationic clusters (squares) relative to the monomer values of both species. Although less pronounced, the cationic clusters show similar redshifts as the molecular clusters with increasing cluster size. Cooperative hydrogen bonding is in particular strong in the cyclic cationic tetramer. b) Calculated δ^1H downfield shifts for the molecular (circles) and cationic clusters (squares) relative to the monomer values of both species. Although less pronounced, the cationic clusters show similar downfield shifts as the molecular clusters with increasing cluster size. Cooperative hydrogen bonding is in particular strong in the cyclic cationic pentamer.

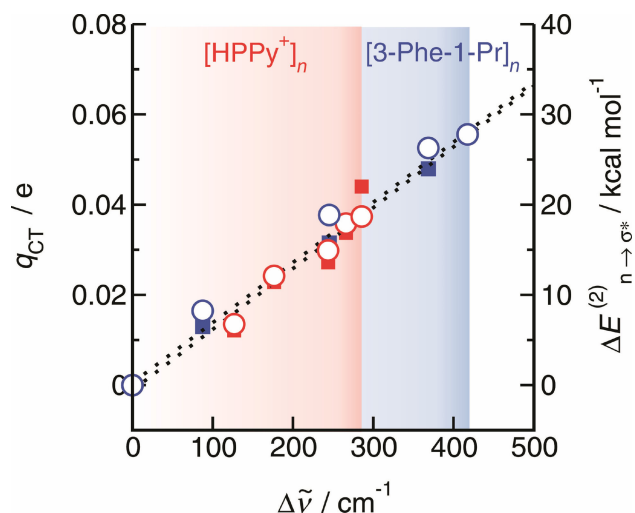


Figure 4. NBO-calculated second-order stabilization energies $\Delta E(2)_{n \rightarrow \sigma^*}$ (open circles) and estimated total charge transfers q_{CT} (closed squares) for cationic (red) and molecular (blue) clusters $n=2-6$ plotted versus redshifts of the average OH frequency, $\Delta\nu_{OH}$, of the monomeric cation and molecule. The linear dependence indicates the strong relation between NBO stabilization energies and charge transfers with spectroscopic properties such as IR frequencies. The largest redshifts for the cationic and molecular clusters are indicated by the red and blue areas.

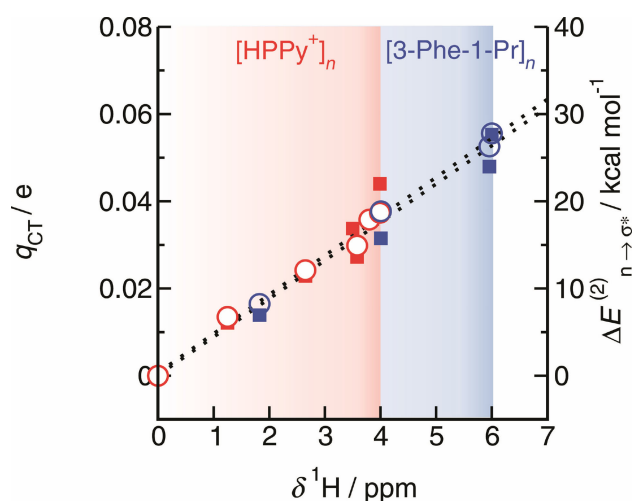


Figure 5. NBO-calculated second-order stabilization energies $\Delta E(2)_{n \rightarrow \sigma^*}$ (open circles) and estimated total charge transfers q_{CT} (closed squares) for cationic (red) and molecular (blue) clusters $n=2-6$ plotted versus calculated average NMR proton chemical shifts, δ^1H , of the monomeric cation and molecule. The linear dependence indicates the strong relation between NBO stabilization energies and charge transfers with spectroscopic properties, such as NMR chemical shifts. The largest redshifts for the cationic and molecular clusters are indicated by the red and blue areas.

action, largest vibrational redshifts and strongest NMR downfield shifts.

In this work, we show that clusters of monovalent cations with net charges up to $Q = +6e$ are kinetically stable. Quantum chemical calculations suggest that hydrogen bonds overcome the repulsive Coulomb forces. Cooperative hydrogen bonding is in particular strong in cyclic clusters, which look similar to well-known structural motifs for water or alcohols. Coopera-

tivity is reflected in redshifted vibrational frequencies and downfield NMR chemical shifts. The cooperative effect with increasing cluster size in the cationic clusters is less pronounced, but similar to that observed in molecular clusters. Both spectroscopic probes for hydrogen bonding are linearly related to NBO-calculated interaction energies and charge transfer. This strong correlation suggests the existence of “anti-electrostatic” hydrogen bonds (AEHB) as recently introduced by Weinhold and Klein and confirmed experimentally. The present study shows that these AEHBs do not allow only the formation of ionic dimers but larger cyclic clusters with high net charges, wherein attractive short-range hydrogen bonds successfully compete with long-range repulsive Coulomb forces. Introducing dispersion forces additionally strengthens the attractive interaction and allows for the formation of cyclic hexamers with exceptionally high charge.

Acknowledgements

This work has been supported by the DFG Research Grant LU-506/14-1.

Conflict of Interest

The authors declare no conflict of interest.

Keywords: hydrogen bonding • ionic bonding • natural bond orbital analysis • spectroscopy • theoretical chemistry

- [1] J. Smid, *Angew. Chem.* **1972**, *84*, 127–144; *Angew. Chem. Int. Ed.* **1972**, *11*, 112–127.
- [2] Y. Marcus, G. Hefter, *Chem. Rev.* **2006**, *106*, 4585–4621.
- [3] F. Weinhold, R. A. Klein, *Angew. Chem. Int. Ed.* **2014**, *53*, 11214–11217; *Angew. Chem.* **2014**, *126*, 11396–11399.
- [4] F. Weinhold, *Angew. Chem. Int. Ed.* **2017**, *56*, 14577–14581; *Angew. Chem.* **2017**, *129*, 14769–14773.
- [5] F. Weinhold, *Inorg. Chem.* **2018**, *57*, 2035–2044.
- [6] E. M. Fatila, E. B. Twum, A. Sengupta, M. Pink, J. A. Karty, K. Raghavachari, A. H. Flood, *Angew. Chem. Int. Ed.* **2016**, *55*, 14057–14062; *Angew. Chem.* **2016**, *128*, 14263–14268.
- [7] W. Zhao, B. Qiao, C.-H. Chen, A. H. Flood, *Angew. Chem. Int. Ed.* **2017**, *56*, 13083–13087; *Angew. Chem.* **2017**, *129*, 13263–13267.
- [8] E. M. Fatila, E. B. Twum, J. A. Karty, A. H. Flood, *Chem. Eur. J.* **2017**, *23*, 10652–10662.
- [9] W. Gamrad, A. Dreier, R. Goddard, K.-R. Pörschke, *Angew. Chem. Int. Ed.* **2015**, *54*, 4482–4487.
- [10] O. Shih, A. H. England, G. C. Dallinger, J. W. Smith, K. C. Duffey, R. C. Cohen, D. Prendergast, R. J. Saykally, *J. Chem. Phys.* **2013**, *139*, 035104.
- [11] T. Inagaki, S. Aono, H. Nakano, T. Yamamoto, *J. Phys. Chem. B* **2014**, *118*, 5499–5508.
- [12] S. A. Katsyuba, M. V. Vener, E. E. Zvereva, Z. Fei, R. Scopelliti, G. Laurenczy, N. Yan, E. Paunescu, P. J. Dyson, *J. Phys. Chem. B* **2013**, *117*, 9094–9105.
- [13] M. Fakhraee, B. Zandkarimi, H. Salari, M. R. Gholami, *J. Phys. Chem. B* **2014**, *118*, 14410–14428.
- [14] A. Knorr, K. Fumino, A.-M. Bansa, R. Ludwig, *Phys. Chem. Chem. Phys.* **2015**, *17*, 30978–30982.
- [15] A. Knorr, R. Ludwig, *Sci. Rep.* **2015**, *5*, 17505.
- [16] A. Knorr, P. Stange, K. Fumino, F. Weinhold, R. Ludwig, *ChemPhysChem* **2016**, *17*, 458–462.
- [17] A. Strate, T. Niemann, P. Stange, D. Michalik, R. Ludwig, *Angew. Chem. Int. Ed.* **2017**, *56*, 496–500; *Angew. Chem.* **2017**, *129*, 510–514.
- [18] A. Strate, T. Niemann, R. Ludwig, *Phys. Chem. Chem. Phys.* **2017**, *19*, 18854–18862.
- [19] D. Braga, F. Grepioni, J. J. Novoa, *Chem. Commun.* **1998**, 1959–1960.
- [20] G. Frenking, G. F. Caramori, *Angew. Chem.* **2015**, *126*, 2632–2635; *Angew. Chem. Int. Ed.* **2015**, *54*, 2596–2599.
- [21] P. R. Horn, Y. Mao, M. Head-Gordon, *Phys. Chem. Chem. Phys.* **2016**, *18*, 23067–23079.
- [22] Gaussian 09, Revision A.02, M. J. Frisch, G. W. Trucks, H. B. Schlegel, G. E. Scuseria, M. A. Robb, J. R. Cheeseman, G. Scalmani, V. Barone, G. A. Petersson, H. Nakatsuji, X. Li, M. Caricato, A. Marenich, J. Bloino, B. G. Janesko, R. Gomperts, B. Mennucci, H. P. Hratchian, J. V. Ortiz, A. F. Izmaylov, J. L. Sonnenberg, D. Williams-Young, F. Ding, F. Lipparini, F. Egidi, J. Goings, B. Peng, A. Petrone, T. Henderson, D. Ranasinghe, V. G. Zakrzewski, J. Gao, N. Rega, G. Zheng, W. Liang, M. Hada, M. Ehara, K. Toyota, R. Fukuda, J. Hasegawa, M. Ishida, T. Nakajima, Y. Honda, O. Kitao, H. Nakai, T. Vreven, K. Throssell, J. A. Montgomery, Jr., J. E. Peralta, F. Ogliaro, M. Bearpark, J. J. Heyd, E. Brothers, K. N. Kudin, V. N. Staroverov, T. Keith, R. Kobayashi, J. Normand, K. Raghavachari, A. Rendell, J. C. Burant, S. S. Iyengar, J. Tomasi, M. Cossi, J. M. Millam, M. Klene, C. Adamo, R. Cammi, J. W. Ochterski, R. L. Martin, K. Morokuma, O. Farkas, J. B. Foresman, D. J. Fox, Gaussian, Inc., Wallingford CT, **2016**.
- [23] E. D. Glendening, J. K. Badenhoop, A. E. Reed, J. E. Carpenter, J. A. Bohmann, C. M. Morales, C. R. Landis, F. Weinhold, *Theoretical Chemistry Institute, University of Wisconsin, Madison*, **2013**.
- [24] F. Weinhold, C. R. Landis, *Valency and Bonding A Natural Bond Orbital Donor-Acceptor Perspective*, Cambridge, University Press, Cambridge, **2005**.
- [25] S. Grimme, J. Antony, S. Ehrlich, H. Krieg, *J. Chem. Phys.* **2010**, *132*, 154104.
- [26] S. Ehrlich, J. Moellmann, W. Reckien, T. Bredow, S. Grimme, *ChemPhysChem* **2011**, *12*, 3414–3420.
- [27] S. Grimme, A. Jansen, *Chem. Rev.* **2016**, *116*, 5105–5154.
- [28] R. Ludwig, *Phys. Chem. Chem. Phys.* **2002**, *4*, 5481–5487.
- [29] K. M. Murdoch, T. D. Ferris, J. C. Wright, T. C. Farrar, *J. Chem. Phys.* **2002**, *116*, 5717.
- [30] R. Ludwig, *ChemPhysChem* **2005**, *6*, 1369–1375.
- [31] K. Fumino, S. Reimann, R. Ludwig, *Phys. Chem. Chem. Phys.*, **2014**, *40*, 21903–21929.
- [32] S. S. Xantheas, T. H. Dunning, *J. Chem. Phys.* **1993**, *99*, 8774–8792.
- [33] A. B. Wolk, C. M. Leavitt, E. Garand, M. A. Johnson, *Acc. Chem. Res.* **2014**, *47*, 202–210.
- [34] J. A. Fournier, C. T. Wolke, C. J. Johnson, A. B. McCoy, M. A. Johnson, *J. Chem. Phys.* **2015**, *142*, 064306.

Manuscript received: April 3, 2018

Accepted Article published: April 6, 2018

Version of record online: April 26, 2018

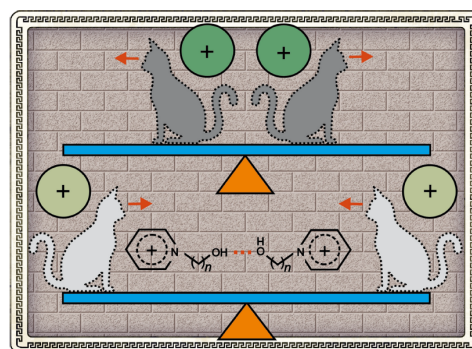
When hydrogen bonding overcomes Coulomb repulsion: from kinetic to thermodynamic stability of cationic dimers

T. Niemann (40 %), A. Strate (15 %), P. Stange (15 %), R. Ludwig (30 %)

Phys. Chem. Chem. Phys., 21, 8215-8220, 2019

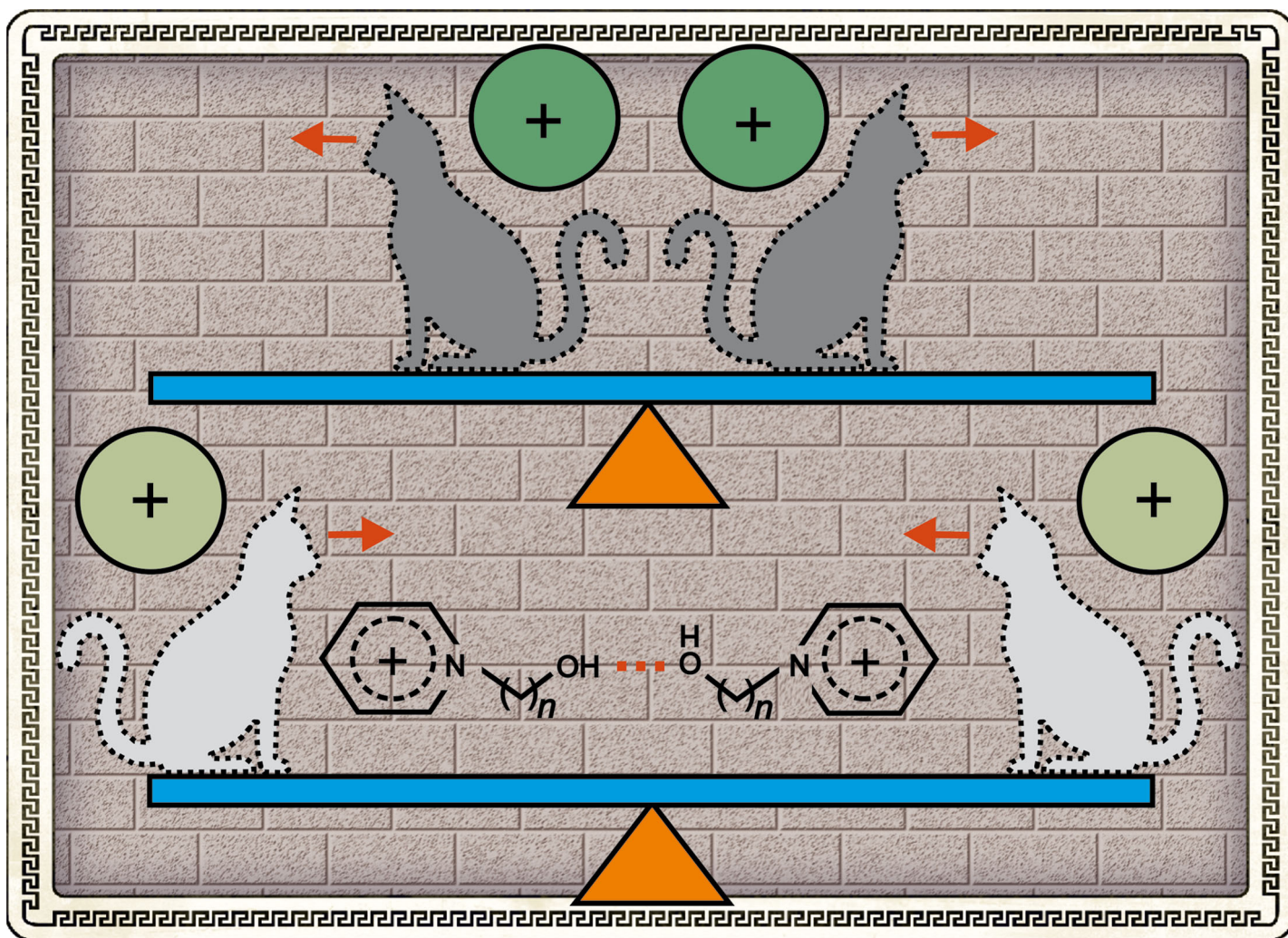
Content:

Quantum chemical calculations of the dimer $[\text{Py}-(\text{CH}_2)_n\text{-OH}^+]_2$ at the MP2 level of theory suggest that short-range and directional hydrogen bonds attenuate the long-range repulsive COULOMB forces preventing the dimers from dissociation and providing a robust kinetic stability. For $n \geq 15$ the initially kinetic stability turns into a thermodynamic stability.



Contributions to this work:

I had the initial idea for this publication and have done some of the DFT calculations and I wrote the first draft. I have discussed the results with Anne Strate. Peter Stange contributed to this work with corrections on the initial draft. Professor Ludwig has done most of the DFT calculations and got the manuscript for the final corrections.



A paper by Thomas Niemann, Peter Stange, Anne Strate, and Ralf Ludwig from Physical and Theoretical Chemistry at the University of Rostock, Germany

When hydrogen bonding overcomes Coulomb repulsion: from kinetic to thermodynamic stability of cationic dimers

This paper reports quantum chemical calculations of the kinetic and thermodynamic stability of cationic dimers. With increasing alkyl chain length, cooperative hydrogen bonds overcome the repulsive Coulomb forces. The cationic dimers with longer alkyl chains should be observable in gas phase experiments at low temperatures.

As featured in:



See R. Ludwig et al.,
Phys. Chem. Chem. Phys.,
2019, 21, 8215.



Cite this: *Phys. Chem. Chem. Phys.*,
2019, 21, 8215

When hydrogen bonding overcomes Coulomb repulsion: from kinetic to thermodynamic stability of cationic dimers†

T. Niemann,^a P. Stange,^a A. Strate^a and R. Ludwig^{id} *^{abc}

Quantum chemical calculations have been employed to study the kinetic and thermodynamic stability of hydroxy-functionalized 1-(3-hydroxyalkyl)pyridinium cationic dimers. For $[\text{Py}-(\text{CH}_2)_n-\text{OH}^+]_2$ structures with $n = 2-17$ we have calculated the robust local minima with clear dissociation barriers preventing their "Coulomb explosion" into separated cations. For $n = 15$ hydrogen bonding and dispersion forces fully compensate for the repulsive Coulomb forces between the cations allowing for the quantification of the pure hydrogen bond in the order of 20 kJ mol^{-1} . The increasing kinetic stability even turns to thermodynamic stability with further elongated hydroxyalkyl chains. Now, quantum-type short-range attraction wins over classical long-range electrostatic repulsion resulting in negative binding energies and providing the first thermodynamically stable cationic dimers. The electronic, structural and spectroscopic signatures of the cationic dimers could be correlated to NBO parameters, supporting the existence of anti-electrostatic hydrogen bonds (AEHB) as recently suggested by Weinhold. In principle, these pure cationic dimers should be detectable in gas-phase experiments at low temperatures without the need of mediating molecules or counteranions.

Received 15th October 2018,
Accepted 14th January 2019

DOI: 10.1039/c8cp06417b

rsc.li/pccp

Weinhold and Klein recently predicted the existence of dimers of like-charged ions. Such cationic and anionic dimers are kinetically stabilized by hydrogen bonding, opposing their "Coulomb explosion" into separated ions.¹⁻³ These findings strongly challenged the claim of Braga and co-workers that anionic dimers would fall apart if the counteranions are removed.⁴ And indeed, experimental evidence for cationic or anionic dimers is only provided for systems wherein the repulsive Coulomb forces are mediated by molecules or counterions.⁵⁻¹⁴ Most similar to pure cationic dimers are isolated ion clusters in the gas phase consisting of two cations and one anion, as recently reported by Menges *et al.*¹⁵ For ternary $(\text{HEMIm}^+)_2\text{NTf}_2^-$ complexes consisting of two 1-(2-hydroxyethyl)-3-methylimidazolium cations and one weakly interacting bis(trifluoromethylsulfonyl)imide anion, two isomers could be isolated by cryogenic ion vibrational pre-dissociation spectroscopy combined with double resonance techniques.^{15,16} One (2,1) complex was identified to exhibit direct contact between the cations. Therein, the OH group of one cation binds to the OH group of the other, which then

attaches to the basic nitrogen atom of the NTf_2^- anion.¹⁵ That was the first experimental evidence for cation-cation hydrogen bonds in small isolated clusters of ionic liquids (ILs). Still, we cannot ignore the mediation role of the counteranion so far. Nevertheless, for the doubly hydrogen bonded hydrogen sulfate dimer $(\text{HSO}_4^-)_2$, Weinhold calculated a potential energy curve with a remarkably deep potential well of about $\Delta E^* = 13.5 \text{ kJ mol}^{-1}$.³ However, these anionic dimers still exhibit positive energies lying at approximately $\Delta E = 164.84 \text{ kJ mol}^{-1}$ above the asymptotic limit of infinitely separated ions ($\Delta E = 0$). The meta-stable dimers are still far away from thermodynamic stability. Recently, we could show that dimers of hydroxy-functionalized cations also exhibit robust kinetic stability.¹⁷ Ammonium-, imidazolium- and pyridinium-based cations with hydrogen bonding hydroxyethyl groups are well-known constituents of ionic liquids. In such cationic dimers, hydrogen bonding opposes the repulsive Coulomb forces between the positive charges.¹⁸⁻²³ In principle, the Coulomb repulsion can be further attenuated by elongation of the hydroxyalkyl chain, thus increasing the distance between the positively charged centres of the cations.²⁴ This way, robust kinetically stable complexes should exist without altering the dielectric environment. An ultimate goal would be the prediction of a cationic dimer exhibiting negative binding energies that should be observable in sophisticated gas phase experiments.

It is the aim of this work to show that the interplay between attractive short-range hydrogen bonds and repulsive long-range

^a Universität Rostock, Institut für Chemie, Abteilung für Physikalische Chemie, Dr.-Lorenz-Weg 2, 18059, Rostock, Germany. E-mail: ralf.ludwig@uni-rostock.de

^b Department LL&M, University of Rostock, Albert-Einstein-Str. 25, 18059, Rostock, Germany

^c Leibniz-Institut für Katalyse an der Universität Rostock e.V., Albert-Einstein-Str. 29a, 18059 Rostock, Germany

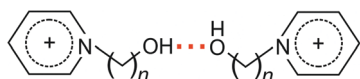
† Electronic supplementary information (ESI) available. See DOI: 10.1039/c8cp06417b

Coulomb forces provides kinetic well-depths and barrier widths for simple cationic dimers with net charge $Q = +2e$. We demonstrate that hydrogen-bonded dimers of hydroxy-functionalized 1-(3-hydroxyalkyl)pyridinium cations exhibit substantial kinetic stability without being embedded in a dielectric medium by adding molecules or counterions.¹⁷ We show that with increasing length of the hydroxyalkyl chain tether even absolute thermodynamic stability is achieved. In these cationic species, hydrogen bonding does not only attenuate, but also overcomes the repulsive Coulomb forces. Then, the hydrogen bond strength and geometry in the cationic dimer approach those of familiar molecular species such as water and alcohols. Thus, there is a good chance for finding these like-charged dimers in gas phase experiments at low temperatures.

Kinetically stabilized dimers $[\text{Py}-(\text{CH}_2)_n-\text{OH}^+]_2$ with $n = 2-6$

For that purpose we calculated the potential energy curves for dimers of the hydroxy-functionalized cations 1-(3-hydroxyalkyl)pyridinium $[\text{Py}-(\text{CH}_2)_n-\text{OH}^+]_2$ with $n = 2-6$ at the unrestricted second-order Møller-Plesset perturbation theory (UMP2) by using the well-balanced but small 6-31+G* basis set as implemented in the Gaussian 09 program (Scheme 1).²⁵ The methylene (CH_2) groups in the alkyl chains of the cations are all kept in *trans* position to the hydroxy functional group $-\text{OH}$. Analytical positive frequencies were obtained for all species $n = 2-6$ to verify the local stability of each optimized structure. The optimized geometries and frequencies for the dimers $n = 2-6$ are given in the ESI.†

For the cationic dimers $[\text{Py}-(\text{CH}_2)_n-\text{OH}^+]_2$ with $n = 2-6$ we calculated relaxed potential energy curves by varying the $\text{H}\cdots\text{O}$ intermolecular distance and optimizing all other geometrical variables at each step of the scan. The resulting potential energy curves for each dimers $[\text{Py}-(\text{CH}_2)_n-\text{OH}^+]_2$ with $n = 2-6$ are shown in Fig. 1a. For each curve, we show the net energy release ΔE and the activation barrier height ΔE^* for the dissociation potentials of the cationic dimers. Additionally, we indicated the optimized equilibrium H-bond distances $R_{(\text{H}\cdots\text{O})}$. Table 1 lists all these energetic and geometric parameters. As shown in Fig. 1a, robust kinetic stabilities with clear dissociation barriers are achieved for the UMP2 treatment. As an example we first discuss the potential energy curve for the smallest cationic dimer $[\text{Py}-(\text{CH}_2)_2-\text{OH}^+]_2$ dissociated along the $R_{(\text{H}\cdots\text{O})}$ H-bond stretching coordinate with respect to the energy of the isolated cations at $\Delta E = 0$. In Fig. 1c the vertical arrow at $R_{(\text{H}\cdots\text{O})} = 1.9994 \text{ \AA}$ shows the calculated $\Delta E = 136.4 \text{ kJ mol}^{-1}$ equilibrium well depth at this level of theory. The effective well depth is measured with respect to the transition state (near $R_{(\text{H}\cdots\text{O})} = 3.0 \text{ \AA}$) that signals descent toward separated cations,



Scheme 1 1-(3-Hydroxyalkyl)pyridinium dimer $[\text{Py}-(\text{CH}_2)_n-\text{OH}^+]_2$.

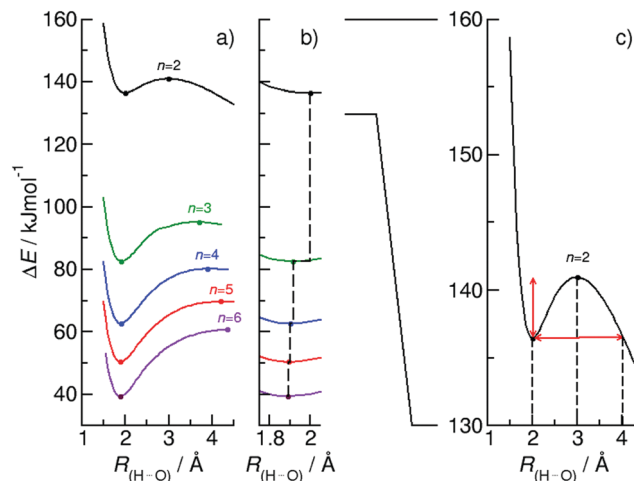


Fig. 1 (a) The potential energy curves for the cationic dimers $[\text{Py}-(\text{CH}_2)_n-\text{OH}^+]_2$ with $n = 2-6$ were calculated at the UMP2/6-31+G* basis level of theory relaxing the structures for each bond length $R_{\text{H}\cdots\text{O}}$. The dissociative energy profiles show pronounced binding wells with respect to the dissociated cations and effective equilibrium well depths with respect to the transition state. (b) The bond lengths $R_{(\text{H}\cdots\text{O})}$ at the minima shift to shorter distances due to increasing hydrogen bonding. (c) The potential energy curve for the $[\text{Py}-(\text{CH}_2)_2-\text{OH}^+]_2$ dimer shows a pronounced binding well at $136.4 \text{ kJ mol}^{-1}$ with respect to the dissociated cations, an effective equilibrium well depth of 3.6 kJ mol^{-1} with respect to the transition state, and an energy barrier width of about 2 \AA , respectively.

Table 1 Calculated intermolecular distances $R_{(\text{H}\cdots\text{O})}$ and $R_{(\text{O}\cdots\text{O})}$ along with the energies relative to the asymptotic dissociated ions, ΔE , and the binding energies, ΔE^* of the optimized dimer structures $[\text{Py}-(\text{CH}_2)_n-\text{OH}^+]_2$ with $n = 2-17$ calculated at the UMP2/6-31+G* level of theory

n	$R_{(\text{H}\cdots\text{O})}/\text{\AA}$	$R_{(\text{O}\cdots\text{O})}/\text{\AA}$	$\Delta E/\text{kJ mol}^{-1}$	$\Delta E^*/\text{kJ mol}^{-1}$
2	1.9994	2.8807	136.43	4.52
3	1.9174	2.8808	82.51	12.54
4	1.9015	2.8661	62.62	17.59
5	1.8949	2.8670	50.28	19.33
6	1.8906	2.8638	39.31	21.27
7	1.8892	2.8642	31.46	
8	1.8871	2.8624	24.42	
9	1.8859	2.8617	19.31	
10	1.8850	2.8608	14.83	
11	1.8874	2.8603	10.76	
12	1.8835	2.8599	7.50	
13	1.8824	2.8592	4.64	
14	1.8820	2.8592	2.71	
15	1.8814	2.8584	0.0	
16	1.8818	2.8588	-1.89	
17	1.8826	2.8595	-3.61	

corresponding to an activation barrier height of $\Delta E^* = 4.52 \text{ kJ mol}^{-1}$. In the following section we discuss the energetic and geometric parameters for the larger dimers with hydroxyalkyl tethers $n = 3-6$. The ΔE values drop from $136.4 \text{ kJ mol}^{-1}$ for $n = 2$ down to 39.3 kJ mol^{-1} for $n = 6$ as shown in Fig. 1a. Thus, the equilibrium energy for the cationic dimer $[\text{Py}-(\text{CH}_2)_6-\text{OH}^+]_2$ is only moderately above that of the isolated cations. The stronger attractive interaction with increasing tether length is also reflected in shortened hydrogen bond distances $R_{(\text{H}\cdots\text{O})}$,

changing from 1.9994 Å for $n = 2$ down to 1.891 Å for $n = 6$, as indicated by the dots at the potential minima in Fig. 1a. Similarly, the deep potential wells ΔE^* increase from 4.5 to 20 kJ mol⁻¹, exceeding significantly the values reported for other cationic and anionic dimers.^{1–3} Fig. 1 also displays the extreme breadth of the potential barrier through which the dimeric species must tunnel to reach the lower energy of long-range dissociation. This barrier breadth already increases from $R_{(\text{H}\cdots\text{O})} = 2.0$ Å to $R_{(\text{H}\cdots\text{O})} = 4.5$ Å by adding only one methylene group to the hydroxyalkyl chain tether of the cationic dimer $[\text{Py}-(\text{CH}_2)_2-\text{OH}^+]_2$, resulting in $[\text{Py}-(\text{CH}_2)_3-\text{OH}^+]_2$. The full potential barrier for the dimer $[\text{Py}-(\text{CH}_2)_n-\text{OH}^+]_2$ with $n = 6$ could not be calculated at the demanding UMP2 level of theory in reasonable time. At this point we conclude that elongation of the hydroxyalkyl chain tether up to $n = 6$ leads to cationic dimer energies of only 40 kJ mol⁻¹ above those of the dissociated cations, and to energetic barriers of about 20 kJ mol⁻¹.

Kinetically and thermodynamically stabilized dimers $[\text{Py}-(\text{CH}_2)_n-\text{OH}^+]_2$ with $n = 7–17$

The cationic dimers $[\text{Py}-(\text{CH}_2)_n-\text{OH}^+]_2$ including longer hydroxyalkyl chain tethers $n = 7–16$ were fully optimized at the MP2/6-31+G*. Unfortunately, frequencies and potential energy curves could not be obtained at this demanding level of theory. For these cationic dimers we calculated the net energy release relative to the dissociated cations, ΔE , the potential energy and the $R_{(\text{H}\cdots\text{O})}$ distances that are shown along with the properties of $[\text{Py}-(\text{CH}_2)_n-\text{OH}^+]_2$ with $n = 2–6$ in Fig. 2 and 3. In Fig. 2 we show the calculated energies ΔE for all dimers $[\text{Py}-(\text{CH}_2)_n-\text{OH}^+]_2$ which decrease from 136.4 kJ mol⁻¹ for $n = 2$ via 39.3 kJ mol⁻¹ for $n = 6$ down to -3.6 kJ mol⁻¹ for $n = 17$, respectively. With increasing hydroxyalkyl chain length, a robust kinetic stability switches to weak thermodynamic stability. For $[\text{Py}-(\text{CH}_2)_n-\text{OH}^+]_2$ with $n = 16, 17$ the binding energies are slightly negative. The hydrogen bond overcomes the repulsive Coulomb forces that are attenuated by the elongated alkyl chains. The quantum chemical calculations tell us that about ninety percent of the positive charge is located on the pyridinium rings (see ESI†). Putting +0.9e charges at the centres of both rings and using the calculated ring–ring distances, we can estimate the Coulomb energies for all dimers. They are shown in comparison to the calculated MP2/6-31+G* energies in Fig. 2. For the cationic dimers $[\text{Py}-(\text{CH}_2)_{15}-\text{OH}^+]_2$ the energy release is zero ($\Delta E = 0$). At a ring–ring distance of about 42 Å, the energy of the cationic dimer is exactly the same as that of the isolated cations. In this case, the repulsive Coulomb forces are fully counter-balanced by the attractive H \cdots O hydrogen bond and dispersion forces that are both described reasonably well by the MP2 method. For dissecting the amount of stabilizing energy of about 26.8 kJ mol⁻¹ into hydrogen bonding and dispersion contributions, we performed additional B3LYP/6-31+G* calculations on the MP2/6-31+G* optimized geometries with and without including dispersion forces. This is realized by using Grimme's D3-method^{26–28} The B3LYP-D3/6-31+G* calculated energy on the

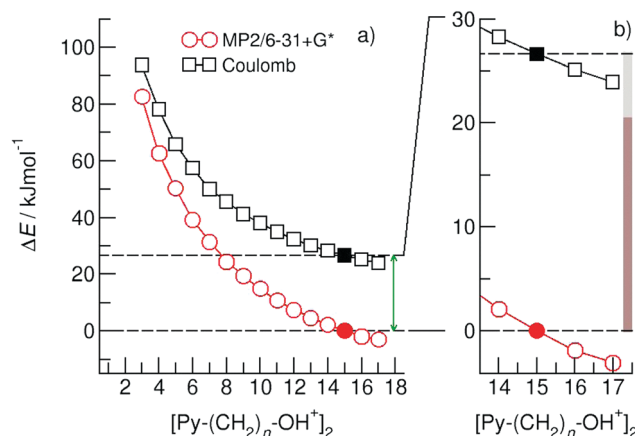


Fig. 2 (a) The binding energies for all cationic dimers $[\text{Py}-(\text{CH}_2)_n-\text{OH}^+]_2$ with $n = 2–17$ were calculated at the UMP2/6-31+G* basis level of theory (circles). They are compared to the long-range e^2/R behavior of idealized Coulomb electrostatic repulsion assuming positive charges $q = +0.9e$ on the pyridinium ring (squares). (b) For the $[\text{Py}-(\text{CH}_2)_{15}-\text{OH}^+]_2$ dimer the Coulomb repulsion is perfectly counter-balanced by the attractive hydrogen bond and dispersion forces resulting in $\Delta E = 0$ (filled symbols). The energy difference represents the sum of the H-bond and dispersion energy as indicated by the brown and grey bars, respectively.

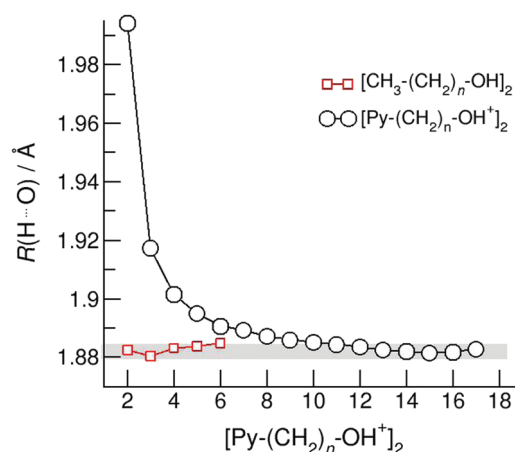


Fig. 3 The inter-molecular hydrogen bond distances, $R_{(\text{H}\cdots\text{O})}$ for the equilibrium structures of $[\text{Py}-(\text{CH}_2)_n-\text{OH}^+]_2$ with $n = 2–17$ decrease with increasing hydroxyalkyl chain length. Each additional (CH_2) group attenuates the Coulomb repulsion and results in enhanced hydrogen bonding as indicated by shorter H-bond lengths. If hydrogen bonding is maximized at about $n = 15$, no further shortening of $R_{(\text{H}\cdots\text{O})}$ is observed. Then the $R_{(\text{H}\cdots\text{O})}$ distances agree with those obtained for calculated n -alcohol dimers with $n = 2–6$ (red squares).

UMP2/6-31+G* optimized geometries $\Delta E = 1.42$ kJ mol⁻¹ is only slightly above $\Delta E = 0$ kJ mol⁻¹, justifying the applied approach. Overall, the calculated dispersion energy stabilizes the cation–cation interaction by 6.7 kJ mol⁻¹. Now we are able to dissect the overall attractive interaction energy of about 26.8 kJ mol⁻¹. The energy difference of about 20.1 kJ mol⁻¹ can be referred to the pure H \cdots O hydrogen bond in the cationic dimer. Such a H-bond energy is typical for hydrogen-bonded dimers of water and alcohols.^{29–34}

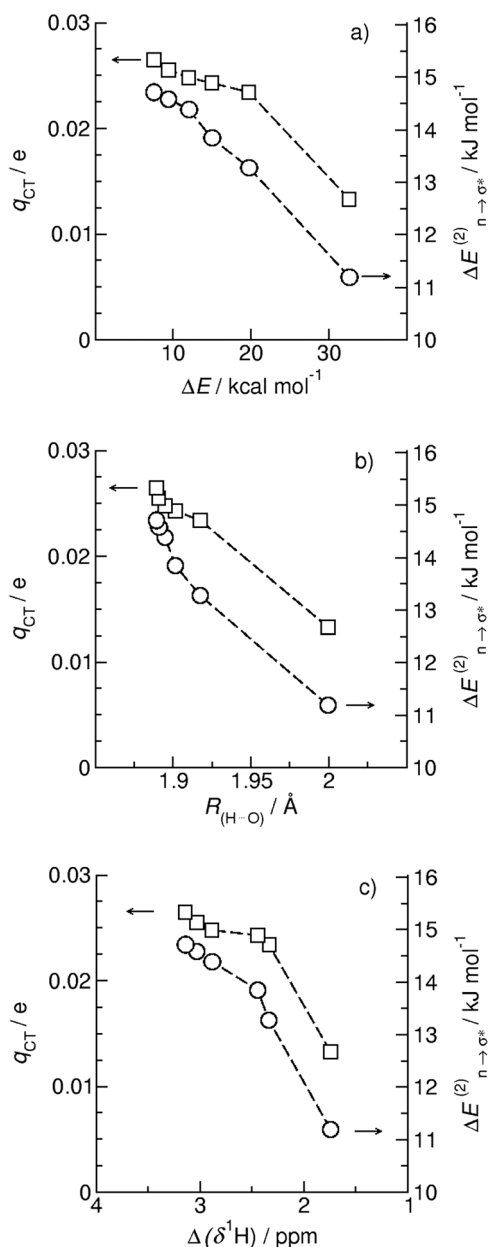


Fig. 4 NBO calculated second order stabilization energies $\Delta E_{n \rightarrow \sigma^*}^{(2)}$ (open circles) and estimated total charge transfers q_{CT} (closed squares) for cationic dimers with $n = 2-6$ plotted versus calculated (a) energies ΔE , (b) intermolecular hydrogen bond distances, $R_{(H \cdots O)}$ and (c) proton chemical shifts differences between the H-bonded and free OH of the dimers, $\Delta(\delta^1H)$. The linear dependence indicates the strong relation between NBO stabilization energies and charge transfers with energetic, geometric and spectroscopic properties of the cationic dimers.

Remarkably, the energies of the cationic dimers $[\text{Py}-(\text{CH}_2)_n-\text{OH}^+]_2$ with $n > 15$ dip below the asymptotic limit of cationic dissociation, thereby achieving thermodynamic as well as kinetic stability (see Fig. 3). Such surprising thermodynamic stability suggests that $[\text{Py}-(\text{CH}_2)_{17}-\text{OH}^+]_2$, once formed, should be observable in gas phase experiments already at moderate temperatures. The energies become negative because attractive hydrogen bonding overcomes the Coulomb repulsion. Following

Coulomb's law, the repulsive interaction is getting weaker with $1/r$, whereas the attractive forces seem to maximize. This is best observed for the optimized H-bond distances $R_{(H \cdots O)}$ with increasing hydroxyalkyl chain length in Fig. 3. From $n = 2$ to $n = 17$ the equilibrium distances are shortened due to enhanced hydrogen bonding while the Coulomb repulsion is constantly weakened. It seems that hydrogen bonding is maximized in $[\text{Py}-(\text{CH}_2)_{16}-\text{OH}^+]_2$ indicated by constant H-bond distances $R_{(H \cdots O)}$. The hydrogen bond is fully relaxed and no longer competes with stronger repulsive Coulomb forces. For the largest cationic dimer the H-bond length is 1.882 Å, in good agreement with values calculated for methanol and ethanol dimers at the same level of theory.²⁹⁻³⁴

NBO parameter versus energy, H-bond distances and NMR proton chemical shifts

The H-bonded cationic dimers demonstrate that the short-range donor-acceptor covalent forces compete with the powerful long-range electrostatic repulsions.^{1-3,17} Characteristic covalency features of $\text{H} \cdots \text{O}$ hydrogen bonds can be readily recognized in the framework of the natural bond orbital (NBO) analysis as distinctive $\text{n}_\text{O} \rightarrow \sigma_{\text{OH}^*}$ donor-acceptor interactions expressed by the second order stabilization energies $\Delta E_{n \rightarrow \sigma^*}^{(2)}$ and estimated total charge transfers q_{CT} for the enhanced $\text{OH} \cdots \text{OH}$ hydrogen bonds, respectively.^{35,36} Charge from the oxygen lone pair orbital of a first cation is donated into the OH anti-bond orbital of second cation. This way the short-range donor-acceptor covalent forces overcome the strong long-range electrostatic repulsive forces as expected for ions of like charge. In Fig. 4 the NBO energy descriptors are plotted versus binding energies ΔE , H-bond distances $R_{(H \cdots O)}$ and proton chemical shifts differences between the H-bonded and free OH of the dimers, $\Delta(\delta^1H)$. As shown in Fig. 4, the second order stabilization energies $\Delta E_{n \rightarrow \sigma^*}^{(2)}$ and the total charge transfers, q_{CT} are strongly correlated to the enhanced H-bond strength in the order from $n = 2$ to $n = 6$. This behavior is reflected as lower energies ΔE , shorter H-bond distances $R_{(H \cdots O)}$ and larger proton chemical shift differences $\Delta(\delta^1H)$. The NBO parameters strongly indicate the covalent and anti-electrostatic character of hydrogen bonding also in dimers of like-charged ions.

Conclusion

In this work we employed quantum chemistry for calculating the kinetic and thermodynamic stability of hydroxy-functionalized 1-(3-hydroxyalkyl)pyridinium cationic dimers. The meta-stable dimers $[\text{Py}-(\text{CH}_2)_n-\text{OH}^+]_2$ with $n = 2-6$ provide net energy releases from 136 down to 39 kJ mol^{-1} , and activation barrier heights from 6 up to 20 kJ mol^{-1} , respectively. Quantum chemical calculations at the MP2 level of theory suggest that short-range and directional hydrogen bonds attenuate the long-range repulsive Coulomb

forces preventing the dimers from dissociation and providing robust kinetic stability. For the cationic dimer $[\text{Py}-(\text{CH}_2)_{15}-\text{OH}^+]_2$ the energy release is zero and the repulsive Coulomb forces are fully counter-balanced by attractive hydrogen bonding and dispersion forces. B3LYP calculations with and without considering dispersion forces allow dissecting the pure hydrogen bond energy in the cationic dimer. The H-bond energy is 20 kJ mol^{-1} and thus comparable to those known for water and methanol dimers. The attenuation of the repulsive Coulomb forces with elongation of the hydroxyalkyl chain tethers leads to enhanced hydrogen bonding as expressed by substantial shortening of the H-bond length of about 0.1 \AA . Further lengthening of the hydroxyalkyl chain length changes the cationic dimers from intrinsically meta-stable to thermodynamically stable complexes. These cationic dimers should be observable in gas phase experiments at lower temperatures.

Conflicts of interest

There are no conflicts to declare.

Acknowledgements

This work has been supported by the DFG Research Grant LU-506/14-1.

References

- (a) F. Weinhold and R. A. Klein, *Angew. Chem., Int. Ed.*, 2014, **53**, 11214–11217 (*Angew. Chem.*, 2014, **126**, 11396–11399); (b) Corrigendum: F. Weinhold and R. A. Klein, *Angew. Chem., Int. Ed.*, 2014, **53**, 12992 (*Angew. Chem.*, 2014, **126**, 13207).
- F. Weinhold, *Angew. Chem., Int. Ed.*, 2017, **56**, 14577–14581 (*Angew. Chem.*, 2017, **129**, 14769–14773).
- F. Weinhold, *Inorg. Chem.*, 2018, **57**, 2035–2044.
- D. Braga, F. Grepioni and J. J. Novoa, *Chem. Commun.*, 1998, 1959–1960.
- M. Holz and K. J. Patil, *Ber. Bunsen-Ges.*, 1991, **95**, 107–113.
- O. Shih, A. H. England, G. C. Dallinger, J. W. Smith, K. C. Duffey, R. C. Cohen, D. Prendergast and R. J. Saykally, *J. Chem. Phys.*, 2013, **139**, 035104.
- A. E. Larsen and D. G. Grier, *Nature*, 1997, **385**, 230–233.
- M. R. Caplan, P. N. Moore, S. Zhang, R. D. Kamm and D. A. Lauffenburger, *Biomacromolecules*, 2000, **1**, 627–631.
- W. Gamrad, A. Dreier, R. Goddard and K.-R. Pörschke, *Angew. Chem., Int. Ed.*, 2015, **54**, 4482–4487 (*Angew. Chem.*, 2015, **127**, 4564–4569).
- T. Inagaki, S. Aono, H. Nakano and T. Yamamoto, *J. Phys. Chem. B*, 2014, **118**, 5499–5508.
- M. Fakhraee, B. Zandkarimi, H. Salari and M. R. Gholami, *J. Phys. Chem. B*, 2014, **118**, 14410–14428.
- E. M. Fatila, E. B. Twum, A. Sengupta, M. Pink, J. A. Karty, K. Raghavachari and A. H. Flood, *Angew. Chem., Int. Ed.*, 2016, **55**, 14057–14062 (*Angew. Chem.*, 2016, **128**, 14263–14268).
- W. Zhao, B. Qiao, C.-H. Chen and A. H. Flood, *Angew. Chem., Int. Ed.*, 2017, **56**, 13083–13087 (*Angew. Chem.*, 2017, **129**, 13263–13267).
- E. M. Fatila, E. B. Twum, J. A. Karty and A. H. Flood, *Chem. – Eur. J.*, 2017, **23**, 10652–10662.
- F. S. Menges, H. J. Zeng, P. J. Kelleher, O. Gorlova, M. A. Johnson, T. Niemann, A. Strate and R. Ludwig, *J. Phys. Chem. Lett.*, 2018, **9**, 2979–2984.
- A. B. Wolk, C. M. Leavitt, E. Garand and M. A. Johnson, *Acc. Chem. Res.*, 2014, **47**, 202–210.
- A. Strate, T. Niemann and R. Ludwig, *Phys. Chem. Chem. Phys.*, 2017, **19**, 18854–18862.
- A. Knorr, K. Fumino, A.-M. Bónsa and R. Ludwig, *Phys. Chem. Chem. Phys.*, 2015, **17**, 30978–30982.
- A. Knorr and R. Ludwig, *Sci. Rep.*, 2015, **5**, 17505.
- A. Knorr, P. Stange, K. Fumino, F. Weinhold and R. Ludwig, *ChemPhysChem*, 2016, **17**, 458–462.
- A. Strate, T. Niemann, P. Stange, D. Michalik and R. Ludwig, *Angew. Chem., Int. Ed.*, 2017, **56**, 496–500 (*Angew. Chem.*, 2017, **129**, 510–514).
- T. Niemann, P. Stange, A. Strate and R. Ludwig, *ChemPhysChem*, 2018, **19**, 1691–1695.
- T. Niemann, D. Zaitsau, A. Strate, A. Villinger and R. Ludwig, *Sci. Rep.*, 2018, **8**, 14753.
- T. Niemann, A. Strate, R. Ludwig, H. J. Zeng, F. S. Menges and M. A. Johnson, *Angew. Chem., Int. Ed.*, 2018, **57**, 15364–15368 (*Angew. Chem.*, 2018, **130**, 15590–15594).
- M. J. Frisch, G. W. Trucks, H. B. Schlegel, G. E. Scuseria, M. A. Robb, J. R. Cheeseman, G. Scalmani, V. Barone, G. A. Petersson, H. Nakatsuji, X. Li, M. Caricato, A. Marenich, J. Bloino, B. G. Janesko, R. Gomperts, B. Mennucci, H. P. Hratchian, J. V. Ortiz, A. F. Izmaylov, J. L. Sonnenberg, D. Williams-Young, F. Ding, F. Lipparini, F. Egidi, J. Goings, B. Peng, A. Petrone, T. Henderson, D. Ranasinghe, V. G. Zakrzewski, J. Gao, N. Rega, G. Zheng, W. Liang, M. Hada, M. Ehara, K. Toyota, R. Fukuda, J. Hasegawa, M. Ishida, T. Nakajima, Y. Honda, O. Kitao, H. Nakai, T. Vreven, K. Throssell, J. A. Montgomery, Jr., J. E. Peralta, F. Ogliaro, M. Bearpark, J. J. Heyd, E. Brothers, K. N. Kudin, V. N. Staroverov, T. Keith, R. Kobayashi, J. Normand, K. Raghavachari, A. Rendell, J. C. Burant, S. S. Iyengar, J. Tomasi, M. Cossi, J. M. Millam, M. Klene, C. Adamo, R. Cammi, J. W. Ochterski, R. L. Martin, K. Morokuma, O. Farkas, J. B. Foresman and D. J. Fox, *Gaussian 09, Revision A.02*, Gaussian, Inc., Wallingford CT, 2016.
- S. Grimme, J. Antony, S. Ehrlich and H. Krieg, *J. Chem. Phys.*, 2010, **132**, 154104.
- S. Ehrlich, J. Moellmann, W. Reckien, T. Bredow and S. Grimme, *ChemPhysChem*, 2011, **12**, 3414–3420.
- S. Grimme and A. Jansen, *Chem. Rev.*, 2016, **116**, 5105–5154.
- K. M. Murdoch, T. D. Ferris, J. C. Wright and T. C. Farrar, *J. Chem. Phys.*, 2002, **116**, 5717.

- 30 F. Huisken, A. Kulcke, C. Laush and J. Lisy, *J. Chem. Phys.*, 1991, **95**, 3924–3929.
- 31 M. Hulsekopf and R. Ludwig, *J. Mol. Liq.*, 2002, **98–99**, 163–171.
- 32 R. Ludwig, F. Weinhold and T. C. Farrar, *Mol. Phys.*, 1999, **97**, 465–477.
- 33 R. Ludwig, *Chem. Phys. Chem.*, 2000, **1**, 53–56.
- 34 R. Ludwig, *Phys. Chem. Chem. Phys.*, 2002, **4**, 5481–5487.
- 35 E. D. Glendening, J. K. Badenhoop, A. E. Reed, J. E. Carpenter, J. A. Bohmann, C. M. Morales, C. R. Landis and F. Weinhold, *NBO 6.0*, Theoretical Chemistry Institute, University of Wisconsin, Madison, 2013.
- 36 F. Weinhold and C. R. Landis, *Valency and Bonding A Natural Bond Orbital Donor-Acceptor Perspective*, Cambridge, University Press, Cambridge, 2005.

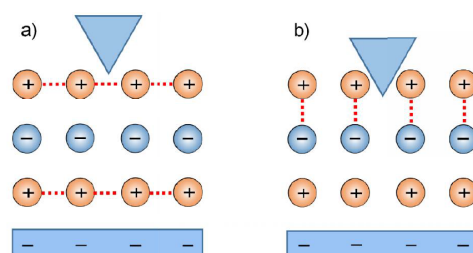
Influence of hydrogen bonding between ions of like charge on the ionic liquid interfacial structure at a mica surface

T. Niemann (65 %), H. Li (5 %), G. G. Warr (10 %), R. Ludwig (10 %), R. Atkin (10 %)

submitted to *J. Phys. Chem. Lett.*

Content:

With a large number of different ILs categorized in four subsets the influence of like-charge attraction on the near surface structures at the mica/IL interface was shown by means of AFM. It could be shown that enhanced H-bonding between the cations increases the number and strength of layers formed at the above surface.



Contributions to this work:

I have synthesized all ILs investigated in this work and I have done all AFM and density measurements. Hua Li introduced me to the methodology of the AFM and its evaluation. I wrote the first draft of the paper. After corrections from Professor Ludwig, Professor Warr and Professor Atkin I made it to the final manuscript. Professor Atkin has submitted the final manuscript.

Influence of hydrogen bonding between ions of like charge on the ionic liquid interfacial structure at a mica surface

Thomas Niemann,^{1,2} Hua Li,³ Gregory G. Warr,⁴ Ralf Ludwig,^{1,2,5} Rob Atkin,^{3,*}

¹ Universität Rostock, Institut für Chemie, Abteilung für Physikalische Chemie, Dr.-Lorenz-Weg 2, 18059, Rostock, Germany

² Department LL&M, University of Rostock, Albert-Einstein-Str. 25, 18059, Rostock, Germany

³ School of Molecular Sciences, The University of Western Australia, Perth, Western Australia 6009, Australia

⁴ School of Chemistry and Sydney Nano Institute, The University of Sydney, NSW 2006, Australia

⁵ Leibniz-Institut für Katalyse an der Universität Rostock e.V., Albert-Einstein-Str. 29a, 18059 Rostock, Germany

Ionic liquids (ILs) are attract increasing interest in science and technology due to their remarkable properties, which can be tuned via varying ion structures to control the relative strengths of Coulomb interactions, hydrogen bonding and dispersion forces. Here we use atomic force microscopy (AFM) to probe the interfacial nanostructures of hydroxyl-functionalized ILs at negatively charged mica surfaces. Hydrogen bonding between hydroxyl functionalised cations (c-c) produces cation clusters and stronger interfacial nanostructure. Hydrogen bond stabilised cation clusters form despite opposing electrostatic repulsions between charge groups, cation – anion electrostatic attractions, and (c-a) hydrogen bonds. Comparison of ILs with and without OH functionalised cations shows directional hydrogen bonding enhances interfacial structure more strongly than the dispersion forces between the alkyl groups. These findings reveal a new means of control ionic liquid interfacial nanostructure via hydrogen bonding between like charged ions, which will impact diverse areas including electrochemical charge storage (batteries and catalysis), electrodeposition, catalysis, and lubrication, etc.

In recent years, ionic liquids (ILs) have attracted increasing interest in science and technology owing to their unique properties, which often includes a wide electrochemical window, [1] [2] very low vapour pressure, [3] [4] and high thermal stability. [5] Per definition, a salt can be called an IL if it melts at low temperature and a room temperature ionic liquid (RTIL) if the melting point is below 25 °C. As ionic liquids consist entirely of ions, Coulomb forces are ubiquitous, but properties are governed by a subtle balance of electrostatics, hydrogen bonding and dispersion forces. [6] [7] In particular, local and directional hydrogen bonding has significant influence on IL behaviour. [8] [9] [10]

In hydroxyl-functionalized ILs two main types of hydrogen bonding are generally possible. One involves the Coulomb-enhanced interaction between a cation and an anion (c-a), and the other between ions of like charge, which in the present case involves the positively charged cations (c-c). In ILs bulk, (c-c) hydrogen bonds might not appear to be important drivers of local structures because they have to compete with the strong repulsive Coulomb forces between the cations as well as with the Coulomb-enhanced (c-a) hydrogen bonds. Despite this expectation, however, structural motifs involving H-bonded cationic clusters were observed in the bulk liquid phase. [11] [12] [13] [14] [15] FT-IR measurements clearly showed two distinct hydrogen bonded species, and that (c-c) hydrogen bonds are stronger (c-a) hydrogen bonds as indicated by the magnitudes of the redshifts of their vibrational bands. [11] [12] [13] [14] [15] The formation of these (c-c) clusters is mediated by surrounding counterions and was observed to become more prominent at lower temperature (ca. 213 K).

The diffuse nature of the bulk IL vibrational bands only provides a qualitative picture of the local interaction. To compensate, gas phase isolated +1 charged clusters were investigated. Chain-like dimeric and trimeric species, where two or three OH groups of the cations form a linear hydrogen-bonded chain from the OH group of one cation to the OH group of the next cation, were identified. The chain is terminated by an H-bond from the terminal OH group to an anion. [16] [17] [18]

Very recently neutron diffraction experiments, supported by MD simulations and DFT calculations, elucidated the bulk nanostructure of the hydroxyl functionalised IL [HOC₄Py][NTf₂]. It was found that (c-c) H-bonds are significantly stronger (shorter and straighter) than then for (c-a), and that (c-c) H-bonds account for ~20% of the h-bonds present. [19] [20] While the structure of cation clusters in [HOC₄Py][NTf₂] is well characterised, the effect of variations ion species and structure on (c-c) H-bonds is heretofore poorly understood, and the nanostructure of ILs which form cationic clusters near solid surfaces has not previously been probed. As the presence of a macroscopic interfaces enforces different ion arrangements near the surface compared to the bulk, the forces between the ions differs. Thus deep understanding of ion arrangements is critical for IL applications involving solid interfaces for potential IL applications like heterogeneous catalysis, [21] wood treatment, [22] lubrication , [23] [24] and electrochemistry, [25] [26] [27] [28] and charge storage [29]. Here we use atomic force microscopy (AFM) to compare the interfacial nanostructure of conventional and OH-functionalized ILs near a mica surface (a model anionic substrate). We show that AFM can easily detect the presence of cationic clusters, and

probe the effect of varying the anion, the polarizability of the cation, and the length of the hydroxyalkyl functional, and conventional, cation chain.

From our bulk phase studies we know that the formation of cationic clusters is governed by three structural factors that act to enhance (c-c) interactions: (1) weakly interacting anions to attenuate the (c-a) interaction, (2) polarisable cations with only one interaction site (in this case OH functional groups) to better compensate for the negative charge of the anion, and (3) large distances between the OH functional group and the positive charge centre of the cation to weaken the like-charge repulsion. [13] [14] [15] [16] [17] [18] To address the effects of all these dependencies on the formation of (c-c) hydrogen bonding and its influence on the near surface structures, we developed a set comprised of nine ILs in total, which can be divided into four subsets (see **Table 1**): in the first subset we address the chain length dependence by enlarging the chain length of the 1-(x-hydroxyalkyl)pyridinium-bis(trifluoromethanesulfonyl)imide ($[\text{HOC}_x\text{Py}][\text{NTf}_2]$) ILs sequentially from ethyl to butyl. The second set utilizes the 1-(x-hydroxyalkyl)methylpiperidinium cation ($[\text{HOC}_x\text{MPip}]^+$) which possesses a localized charge on the nitrogen, contrary to the delocalized charge of the pyridinium cation of subset 1. The anions are the same in both subsets. By comparing the second subset with the first one we investigate the influence of the polarisability of the cation. The third subset contains the same $[\text{HOC}_x\text{Py}]^+$ cation as subset one, but instead of the $[\text{NTf}_2]^-$ anion we use the methanesulfonate ($[\text{OMs}]^-$) anion which is known to suppress (c-c) hydrogen bonding because of its strong coordination strength to the OH group, which leads to (c-a) hydrogen bonding exclusively. For the fourth set the IL 1-penthyropyridinium-bis(trifluoromethanesulfonyl)imide ($[\text{C}_5\text{Py}][\text{NTf}_2]$) is chosen to compare the most promising IL for (c-c) hydrogen bonding $[\text{HOC}_4\text{Py}][\text{NTf}_2]$ to an unfunctionalized one with same shape and molecular volume.

ILs were synthesized at Universität Rostock. Synthesis details are provided in the supporting materials (SI). The ILs were dried under vacuum to a water content below 10 ppm H_2O , determined by Karl-Fischer titration. To obtain the force curves in the AFM experiments a Nanoscope IV multimode AFM (Bruker Instruments) in contact mode with a sharpened Si_3N_4 tip. The spring constant was 0.06 N/m. The ILs were held in an AFM fluid cell, sealed by a silicone O-ring. These were cleaned by rinsing several times with Milli-Q water, followed by rinsing several times with ethanol and then dried using filtered nitrogen. The cantilever was carefully rinsed with ethanol and irradiated with ultraviolet light for 10 min prior to every experiment to avoid contaminations. A fresh mica surface was obtained for each experiment

by removing the top layer of a mica wafer with an adhesive tape. The mica surface thus obtained is clean and atomically smooth. After filling the AFM cell with IL, the system was equilibrated for at least 1 h. The scan rate was 0.2 Hz and the scan size was 50 nm, resulting in a tip velocity of 20 nm/s. All experiments were performed at room temperature and repeated at least three times. The experimental conditions only allow the investigation of RTILs which makes it impossible for us to study $[\text{HOC}_2\text{Py}][\text{NTf}_2]$, $[\text{C}_3\text{Py}][\text{NTf}_2]$ and $[\text{C}_4\text{Py}][\text{NTf}_2]$, which are solid at room temperature.

Figure 1 a) shows the effect of alkyl chain length on the force separation profiles (FSPs) for the $[\text{HOC}_x\text{Py}][\text{NTf}_2]$ series. During the approach of the tip to the surface the force acting on the tip remains constant at separations greater than 4 nm. This force is set to zero and indicates bulk structure. At smaller separations the force on the tip increases abruptly, then the tip jumps inward as it encounters a series of regularly-spaced, repulsive barriers. These periodic force repulsions indicate the bulk structure has transitioned into a more ordered layered structure near the negatively-charged mica surface (see **Scheme 1**). When the tip encounters the outermost detectable interfacial layer, it pushes against it, leading to a repulsive force. Once the force is sufficiently high, breaks through the layer and “jumps” to the next one, whereupon the force increases again and the process repeats. The closer the tip is to the surface, the more structured the interfacial layers and the higher the break through force.

The jump distance is the interfacial layer thickness ($\Delta_{sep.}$). In previous studies, $\Delta_{sep.}$ has been shown to be well-approximated by the ion pair diameter, D_m , which is calculated simply from the macroscopic density and the molecular weight, assuming a cubic packing geometry. [30] [31] [32] [33] The agreement here is also quite good, c.f. Table 1.

The number of detectable layers increases with chain length of the $[\text{HOC}_x\text{Py}][\text{NTf}_2]$ ILs in **Figure 1 a)**, from three for $[\text{HOC}_2\text{Py}][\text{NTf}_2]$ to five for $[\text{HOC}_4\text{Py}][\text{NTf}_2]$. The break through forces increase markedly from $[\text{HOC}_2\text{Py}][\text{NTf}_2]$ to $[\text{HOC}_3\text{Py}][\text{NTf}_2]$, then more modestly to $[\text{HOC}_4\text{Py}][\text{NTf}_2]$. This is because the stabilizing effect of enhanced hydrogen bonding between the cations on the interfacial layers as the separation between OH and cation charge centres increases, as illustrated in **Scheme 1 a)**. These findings are in good agreement with the studies of bulk phase of OH-functionalized cationic clusters. The non-vertical repulsions indicate layer compressibility due to the flexibility in the underlying structure, which deforms before it finally ruptures.

The importance of c-c hydrogen bonds is immediately clear from comparing forces in [HOC₄Py][NTf₂] with the unfunctionalized IL [C₅Py][NTf₂] (see **Fig. 1 b**). [C₅Py][NTf₂] and [HOC₄Py][NTf₂] have similar molecular volumes and ion pair diameters, D_m (0.792 nm and 0.788 nm, respectively) and differ only in that the -OH functional group in [HOC₄Py]⁺ is replaced by a -CH₃ group in [C₅Py]⁺ cation which prevents it from forming (c-c) hydrogen bonds. In the force curves it can be seen that the interfacial layer thicknesses ($\Delta sep = 0.79$ nm) are also identical, but the break through forces are much higher in the functionalized IL (8.0 nN vs. 2.1 nN). The interfacial layers of [HOC₄Py][NTf₂] are stabilized by H-bonding between the cations, whereas the interfacial layers of the IL [C₅Py][NTf₂] can only be stabilized by weaker, non-directional van der Waals interactions between the unfunctionalized cation alkyl chains.

Figure 1 c) shows the effect of reducing cation charge delocalisation (polarizability) on the layer integrity for three [HOC_xMPip][NTf₂] ILs. Although periodic repulsions are again observed, the break through forces are lower than those of the corresponding [HOC_xPy][NTf₂] ILs by a factor of between four and 10. The strongly localized charge on the nitrogen of the saturated N-methylpiperidinium ring of the [HOC_xMPip]⁺ cations is less able to compensate for the weakly coordinating [NTf₂]⁻ anions than is the delocalized charge on the [HOC_xPy]⁺ cations. [15] This leads to a significant decrease of (c-c) H-bonding caused by increased Coulomb repulsion, and to layers weakened to such an extent that [HOC₄Py]⁺ is comparable to the non-H-bonding [C₅Py]⁺.

Careful comparison of measured Δsep to the calculated D_m in these series reveals some systematic deviations (**Fig. 2**). These most likely result from the assumption the calculated D_m of isotropic packing, whereas the ion pair volume of these ILs investigated here is expected to be anisotropic because of the cation chains. We observe a small but significant odd-even alternation in Δsep with increasing cation chain length, which is larger for ILs with even numbers of carbons in the alkyl chain and smaller for ILs with an odd number. This suggests that, on average, the anisotropic ion pairs tend to orient their long axes (d_{max}) normal to the surface in the even cases and parallel in the odd cases (see SI **Scheme S1**). Odd-even effects are known for many ILs and molecular salts, and their special structural features influence properties like glass transition temperatures, viscosities and electrical conductivities, [34] [35] [36] [37] but have not previously been observed at IL interfaces. To study this effect in greater detail, ILs with even longer chain length would be necessary. The interfacial layer

thickness ($\Delta sep.$) is also systematically slightly higher for the piperidinium-based IL, which is also reflected in the calculated ion pair diameters (D_m).

Replacing the weakly-coordinating $[NTf_2]^-$ anion with $[OMs]^-$ while keeping the $[HOC_xPy]^+$ cation virtually eliminates all near-surface order in the ILs. The force-separation profiles of $[HOC_3Py][OMs]$ and $[HOC_4Py][OMs]$ show only a single, weak layer adjacent to the mica surface (**Fig. 1 d**). From bulk phase IR studies it is known that the $[OMs]^-$ anion is strongly coordinated to the OH functional group of the cations, resulting in strong, Coulomb enhanced anion-cation H-bonds, and the almost complete absence of stabilizing c-c hydrogen bonds. [13] [14] The resultant ion pairs are much more mobile than the bigger H-bonded cationic clusters, which means that they can be displaced easily by the AFM tip, as illustrated in **Scheme 1 b**). Only the first two cation layers above the surface are bound strongly enough to the mica surface to form detectable interfacial layers. The interfacial layer thickness (Δsep) of the $[HOC_xPy][OMs]$ ILs is significantly smaller than $[HOC_xPy][NTf_2]$ ILs. This is primarily due to the much smaller $[OMs]^-$ anion. (As the sole detectable layer is probably cation-enriched due to the negative mica charge, we cannot infer other details of near-surface ion-pair arrangements.)

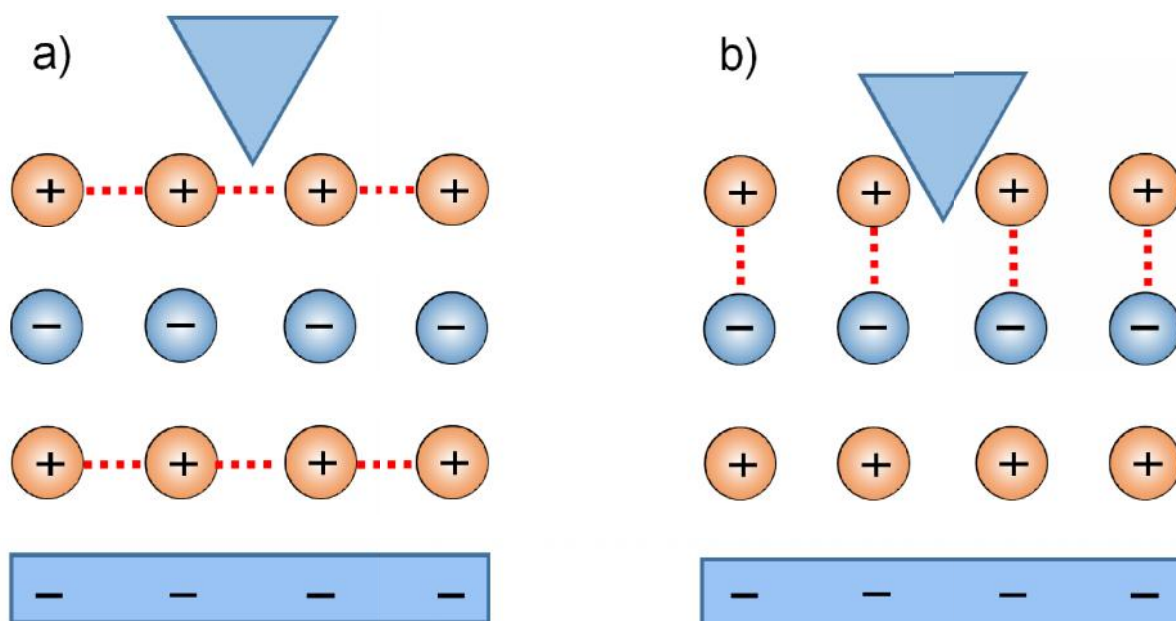
In summary, we have used atomic force microscopy measurements to characterize the nanoscale forces at the solid/IL interface. In particular, we have shown that the formation of (c-c) hydrogen bonds can increase the near-surface structuring of ILs and stabilize the layers, and the effect of the chain length of the hydroxyalkyl group on the formation of ion-enriched layers at a mica surface. Enhanced H-bonding is due to a reduced Coulomb repulsion, which is caused by a larger distance between the OH group and the positive charge, which means interfacial layers are stabilized. However, a localized positive charge on the cation destabilizes the H-bonding between the cations, due to enhanced Coulomb repulsion. By changing the weakly coordinating $[NTf_2]^-$ anion to the strongly coordinating $[OMs]^-$ anion, we revealed the effect of the anion on the near-surface structures. The results suggest that strongly coordinating anions form almost entirely anion-cation pairs via (a-c) H-bonds which can be moved easily by the AFM tip, leading to a decrease of the number of interfacial layers. Finally, we point out the stabilizing effect of H-bonding between the functionalized cations by comparing the force separation profile of the IL $[HOC_4Py][NTf_2]$, which shows the most structuring and the highest break through forces, with the force separation profile of the unfunctionalized IL $[C_5Py][NTf_2]$, in which the ions are almost identical in size and shape. In conclusion, ionic liquids interfacial nanostructure can be controlled by hydrogen bonding

between ions of like-charge, the cation polarizability, the anion interaction strength, and hydroxyl-alkyl chains length.

Literature

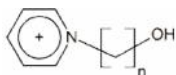
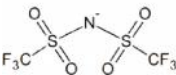
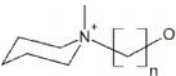
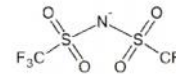
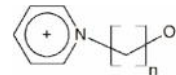
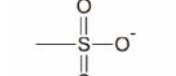
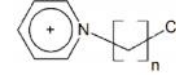
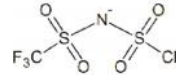
- [1] F. Endres, *Chem. Ing. Tech.*, **2011**, 83, 1485-1492.
- [2] F. Endres, N. Borisenko, R. Al Salman, M. Al Zoubi, A. Prowald, T. Carstens und S. Z. El Abedin, *Ionic Liquids Uncoiled*, **2012**, 1-27.
- [3] M. Freemantle, *Chem. Eng. News*, **1998**, 76, 32-37.
- [4] J. S. Wilkes, *Green Chem.*, **2002**, 4, 73-80.
- [5] T. Welton, *Chem. Rev.*, **1999**, 99, 2071-2083.
- [6] K. Fumino und R. Ludwig, *J. Mol. Liq.*, **2014**, 192, 94-102.
- [7] K. Fumino, S. Reimann und S. Ludwig, *Phys. Chem. Chem. Phys.*, **2014**, 16, 21903-21929.
- [8] K. Fumino, A. Wulf und R. Ludwig, *Angew. Chem. Int. Ed.*, **2018**, 47, 8731-8734.
- [9] K. Fumino, A. Wulf und R. Ludwig, *Angew. Chem.*, **2008**, 120, 8859-8862.
- [10] K. Fumino, T. Peppel, M. Geppert-Rybczynska, D. H. Zaitsau, J. K. Lehmann, S. P. Verevkin, M. Köckerling und R. Ludwig, *Phys. Chem. Chem. Phys.*, **2011**, 13, 14064-14075.
- [11] A. Knorr und R. Ludwig, *Sci. Rep.*, **2015**, 5, 17505.
- [12] A. Knorr, P. Stange, K. Fumino, F. Weinhold und R. Ludwig, *ChemPhysChem*, **2016**, 17, 458-462.
- [13] A. Strate, T. Niemann, D. Michalik und R. Ludwig, *Angew. Chem. Int. Ed.*, **2017**, 56, 496-500.
- [14] A. Strate, T. Niemann, D. Michalik und R. Ludwig, *Angew. Chem.*, **2017**, 129, 510-514.
- [15] T. Niemann, D. Zaitsau, A. Strate, A. Villinger und R. Ludwig, *Sci. Rep.*, **2018**, 8, 14753.
- [16] F. S. Menges, H. J. Zeng, P. J. Kelleher, O. Gorlova, M. A. Johnson, T. Niemann, A. Strate und R. Ludwig, *J. Phys. Chem. Lett.*, **2018**, 9, 2979-2984.
- [17] T. Niemann, A. Strate, R. Ludwig, H. J. Zeng., F. S. Menges und M. A. Johnson, *Angew. Chem. Int. Ed.*, **2018**, 57, 15364-15368.
- [18] T. Niemann, A. Strate, R. Ludwig, H. J. Zeng., F. S. Menges und M. A. Johnson, *Angew. Chem.*, **2018**, 130, 15590-15594.
- [19] T. Niemann, J. Neumann, P. Stange, S. Gärtner, T. G. A. Youngs, D. Paschek, G. G. Warr, R. Atkin und R. Ludwig, *Angew. Chem. Int. Ed.*, **2019**, DOI: 10.1002/anie.201904712.
- [20] T. Niemann, J. Neumann, P. Stange, S. Gärtner, T. G. A. Youngs, D. Paschek, G. G. Warr, R. Atkin

- und R. Ludwig, *Angew. Chem.*, **2019**, DOI: 10.1002/ange.201904712.
- [21] Y. Gu und G. Li, *Adv. Synth. Catal.*, **2009**, 351, 817-847.
- [22] S. Morales-delaRosa, J. M. Compos-Martin und J. L. G. Fierro, *Catal. Today*, **2018**, 302, 87-93.
- [23] A. Elbourne, J. Sweeney, E. J. Wanless, G. B. Webber, G. G. Warr, M. W. Rutland und R. Atkin, *Chem. Comm.*, **2013**, 49, 6797-6799.
- [24] A. Elbourne, J. Sweeney, G. B. Webber, E. J. Wanless, G. G. Warr, M. W. Rutland und R. Atkin, *Chem. Commun.*, **2013**, 49, 6797-6799.
- [25] M. G. Li, L. Chen, Y. X. Zhong, Z. B. Chen, J. W. Yan und B. W. Mao, *Electrochimica Acta*, **2016**, 197, 282-289.
- [26] Y. Zhang, B. Dyatkin und P. Cummings, *J. Phys. Chem. C*, **2019**, 123, 12583-12591.
- [27] Q. Zhang, Q. Wang, S. Zhang, X. Lu und X. Zhang, *ChemPhysChem*, **2016**, 17, 335-351.
- [28] A. J. Page, A. Elbourne, R. Stefanovic, M. A. Addicoat, G. G. Warr, K. Voitchowsky und R. Atkin, *Nanoscale*, **2014**, 6, 8100.
- [29] X. Mao, P. Brown, C. Červinka, G. Hazell, H. Li, Y. Ren, D. Chen, R. Atkin, J. Eastoe, I. Grillo, A. A. H. Padua, M. F. C. Gomes und T. A. Hatton, *Nat. Mater.*, **2019**, DOI: 10.1038/s41563-019-0449-6.
- [30] R. Horn, D. F. Evans und B. W. Ninham, *J. Phys. Chem.*, **1988**, 92, 3531-3537.
- [31] R. G. Horn und J. N. Israelachvili, *J. Chem. Phys.*, **1981**, 75, 1400-1413.
- [32] M. Antognozzi, A. D. Humphris und M. J. Miles, *J. Appl. Phys. Lett.*, **2001**, 78, 300-302.
- [33] R. Hayes, S. Z. El Abedin und R. Atkin, *J. Phys. Chem. B*, **2009**, 113, 7049-7052.
- [34] G. Adamová, J. N. Canongia Lopes, L. P. N. Rebelo, L. M. N. B. Santos, K. R. Seddon und K. Shimizu, *Phys. Chem. Chem. Phys.*, **2014**, 16, 4033-4038.
- [35] M. A. A. Rocha, C. M. S. S. Neves, M. G. Freire, O. Russina, A. Triolo, J. A. P. Coutinho und L. M. N. B. F. Santos, *J. Phys. Chem. B*, **2013**, 117, 10889-10897.
- [36] N. A. S. White und H. A. Ellis, *J. Mol. Struct.*, **2008**, 888, 386-393.
- [37] C. Shen, Q. Zhao und C. M. Evans, *Mol. Syst. Des. Eng.*, **2019**, 4, 332-341.
- [38] B. McLean, H. Li, R. Stefanovic, R. J. Wood, G. B. Webber, K. Ueno, M. Watanabe, G. G. Warr, A. Page und R. Atkin, *Phys. Chem. Chem. Phys.*, **2015**, 17, 325-333.



Scheme 1: Simplified illustration of possible local structures at a negatively charged interface. The cation-enriched layers are shown as entirely cationic and the anion-enriched layers are depicted as entirely anionic for the sake of simplicity. **a)** illustrates the stabilizing effect of enhanced H-bonding between the cations on the interfacial layer formation. The tip pushes against the layer during the approach to the surface. **b)** illustration of the exclusive occurrence of anion-cation H-bonds and the absence of cation-cation H-bonds. The ion pairs thus obtained can easily move together and be displaced by the tip without facing a significantly higher force than in the bulk phase.

Table 1: Name, Abbreviation, Structure, Molecular Weight (M), Density (ρ), Ion pair diameter (D_m) and measured separation layer thicknesses Δ_{sep} .

IL	Abbreviation	Structure	M [g]	ρ [g cm ⁻³]	D_m [nm]	Δ_{sep} [nm]
1-(2-hydroxyethyl)pyridinium-bis(trifluoromethanesulfonyl)imide	[HOC ₂ Py] [NTf ₂]		404.31	1.595	0.749	0.770
1-(3-hydroxypropyl)pyridinium-bis(trifluoromethanesulfonyl)imide	[HOC ₃ Py] [NTf ₂]		418.34	1.557	0.764	0.756
1-(4-hydroxybutyl)pyridinium-bis(trifluoromethanesulfonyl)imide	[HOC ₄ Py] [NTf ₂]		432.37	1.520	0.779	0.794
1-(2-hydroxyethyl)methylpiperidinium-bis(trifluoromethanesulfonyl)imide	[HOC ₂ MPip] [NTf ₂]		424.39	1.500	0.777	0.780
1-(3-hydroxypropyl)methylpiperidinium-bis(trifluoromethanesulfonyl)imide	[HOC ₃ MPip] [NTf ₂]		438.41	1.470	0.791	0.763
1-(4-hydroxybutyl)methylpiperidinium-bis(trifluoromethanesulfonyl)imide	[HOC ₄ MPip] [NTf ₂]		452.44	1.444	0.804	0.804
1-(3-hydroxypropyl)pyridinium-methanesulfonate	[HOC ₃ Py] [OMs]		233.29	1.297	0.668	0.564
1-(4-hydroxybutyl)pyridinium-methanesulfonate	[HOC ₄ Py] [OMs]		247.32	1.310	0.679	0.687
1-pentylpyridinium-bis(trifluoromethanesulfonyl)imide	[C ₅ Py] [NTf ₂]	 	430.39	1.436	0.792	0.790

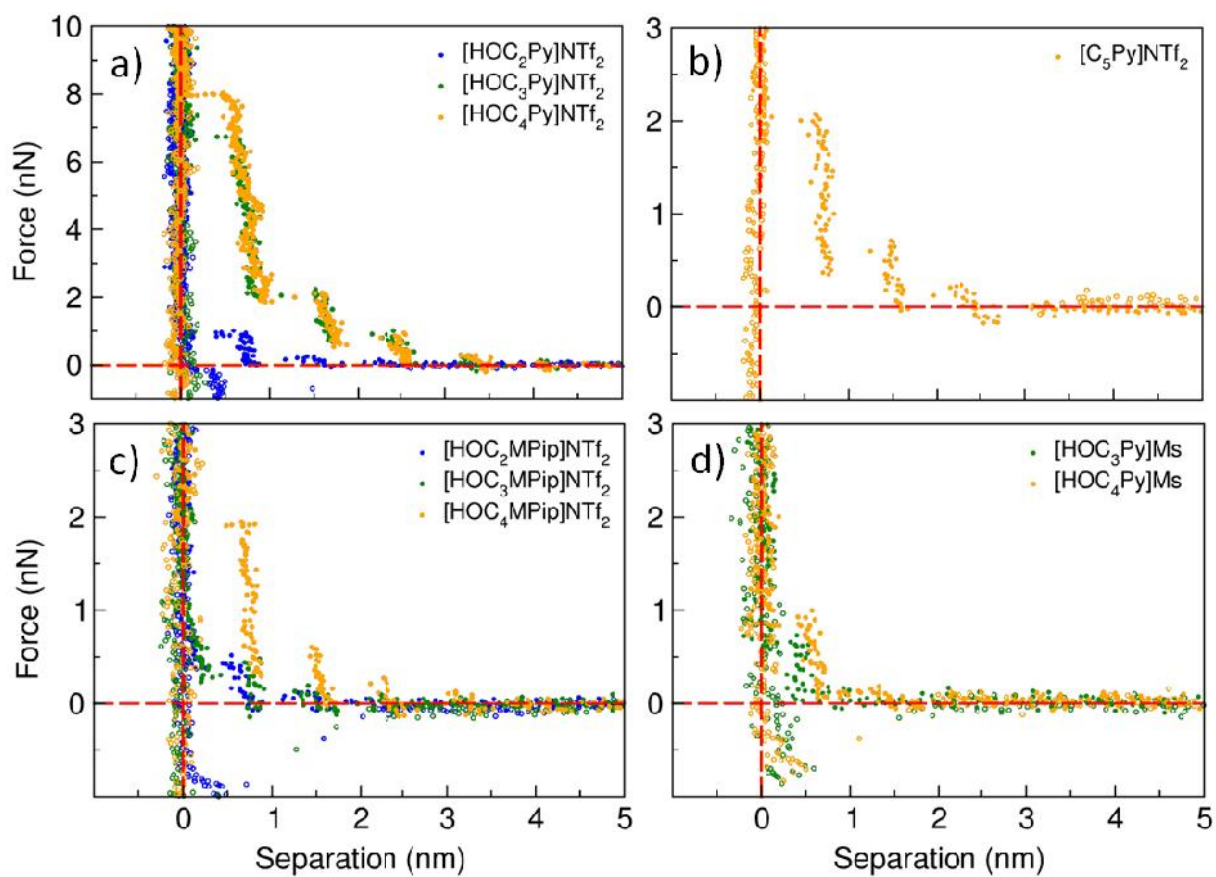


Figure 1: Force separation profiles for the subsets: **a)** $[\text{HOC}_n\text{Py}][\text{NTf}_2]$ **b)** $[\text{HOC}_n\text{MPip}][\text{NTf}_2]$ **c)** $[\text{HOC}_n\text{MPip}][\text{OMs}]$ and **d)** $[\text{C}_5\text{Py}][\text{NTf}_2]$. All profiles show the approach (filled circles) of the AFM tip to the mica surface as well as the retraction (open circles).

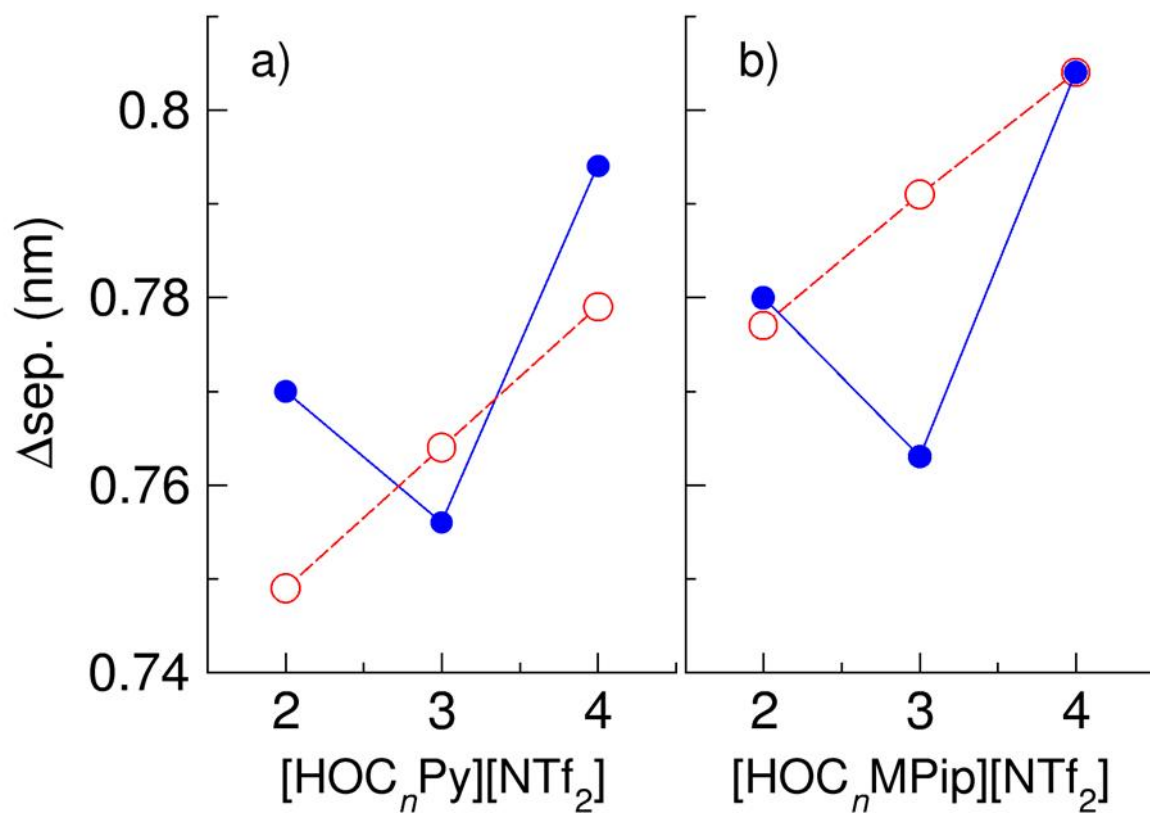


Figure 2: The interfacial layer thickness ($\Delta_{sep.}$) (blue) and the ion pair diameter, D_m , calculated from the macroscopic density and the molecular weight (red) in dependence of the number of carbons in the hydroxyalkyl chain for the ILs: **a)** $[HOC_nPy][NTf_2]$ and **b)** $[HOC_nMPip][NTf_2]$.

A. Appendix

Table A.1.: Cation dependence for the Bis(trifluoromethylsulfonyl)imide $[\text{NTf}_2]^-$ anion

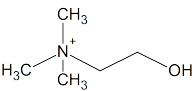
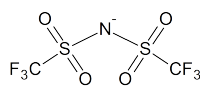
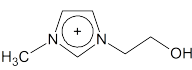
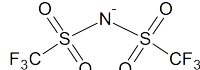
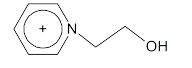
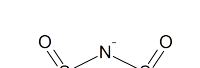
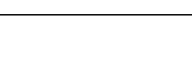
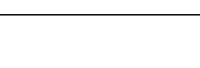
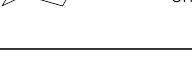
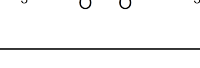
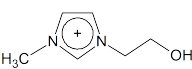
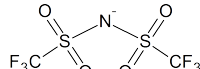
No.	IL	Cation	Anion
1	$[\text{HOC}_2\text{TMA}][\text{NTf}_2]$ Hydroxyethyltrimethylammonium bis(trifluoromethanesulfonyl)imide		
2	$[\text{HOC}_2\text{MIm}][\text{NTf}_2]$ Hydroxyethylmethylimidazolium bis(trifluoromethanesulfonyl)imide		
3	$[\text{HOC}_2\text{Py}][\text{NTf}_2]$ Hydroxyethylpyridinium bis(trifluoromethanesulfonyl)imide		
4	$[\text{HOC}_2\text{MPip}][\text{NTf}_2]$ Hydroxyethylmethylpiperidinium bis(trifluoromethanesulfonyl)imide		
5	$[\text{HOC}_2\text{MPyr}][\text{NTf}_2]$ Hydroxyethylmethylpyrrolidinium bis(trifluoromethanesulfonyl)imide		

Table A.2.: Anion dependence for the 1-(2-hydroxyethyl)-3-methylimidazolium cation

No.	IL	Cation	Anion
2	$[\text{HOC}_2\text{MIm}][\text{NTf}_2]$ Hydroxyethylmethylimidazolium bis(trifluoromethanesulfonyl)imide		

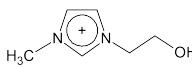
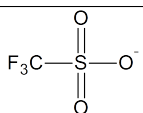
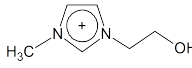
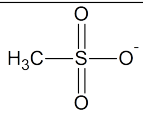
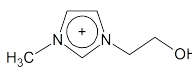
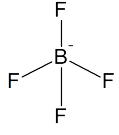
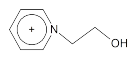
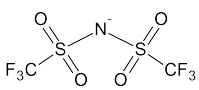
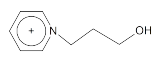
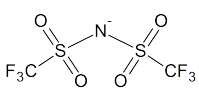
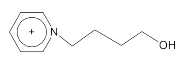
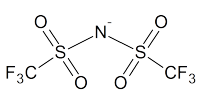
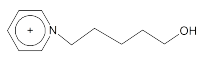
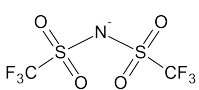
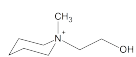
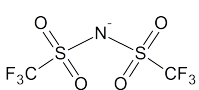
6	[HOC ₂ MIm][OTf] Hydroxyethylmethylimidazolium trifluoromethanesulfonate		
7	[HOC ₂ MIm][OMs] Hydroxyethylmethylimidazolium methanesulfonate		
8	[HOC ₂ MIm][BF ₄] Hydroxyethylmethylimidazolium tetrafluoroborate		

Table A.3.: Chain length dependence of the cluster formation

No.	IL	Cation	Anion
3	[HOC ₂ Py][NTf ₂] Hydroxyethylpyridinium bis(trifluoromethanesulfonyl)imide		
9	[HOC ₃ Py][NTf ₂] Hydroxypropylpyridinium bis(trifluoromethanesulfonyl)imide		
10	[HOC ₄ Py][NTf ₂] Hydroxybutylpyridinium bis(trifluoromethanesulfonyl)imide		
11	[HOC ₅ Py][NTf ₂] Hydroxypentylpyridinium bis(trifluoromethanesulfonyl)imide		
4	[HOC ₂ MPip][NTf ₂] Hydroxypentylmethylpiperidinium bis(trifluoromethanesulfonyl)imide		

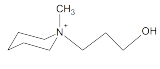
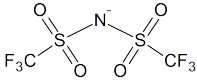
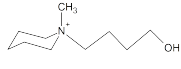
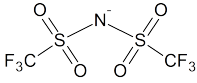
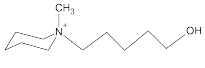
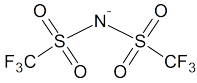
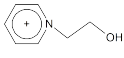
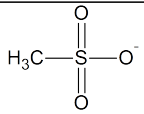
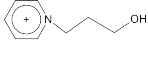
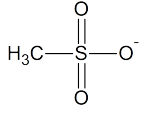
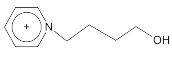
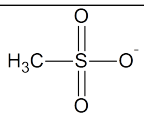
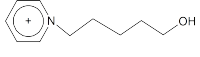
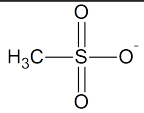
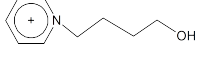
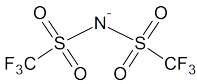
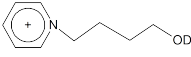
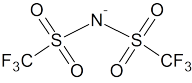
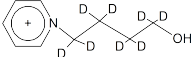
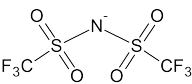
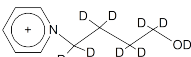
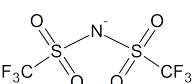
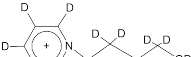
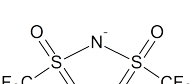
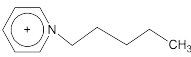
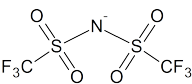
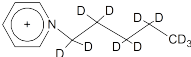
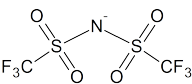
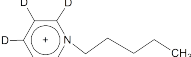
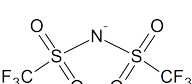
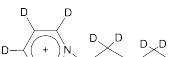
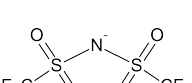
12	[HOC ₃ MPip][NTf ₂] Hydroxypropylmethylpiperidinium bis(trifluoromethanesulfonyl)imide		
13	[HOC ₄ MPip][NTf ₂] Hydroxybutylmethylpiperidinium bis(trifluoromethanesulfonyl)imide		
14	[HOC ₅ MPip][NTf ₂] Hydroxypentylmethylpiperidinium bis(trifluoromethanesulfonyl)imide		
15	[HOC ₂ Py][Ms] Hydroxyethylpyridinium methanesulfonate		
16	[HOC ₃ Py][Ms] Hydroxypropylpyridinium methanesulfonate		
17	[HOC ₄ Py][Ms] Hydroxybutylpyridinium methanesulfonate		
18	[HOC ₅ Py][Ms] Hydroxypentylpyridinium methanesulfonate		

Table A.4.: List of partially deuterated ionic liquids for neutron diffraction measurements

No.	IL	Cation	Anion
10	[HOC ₄ Py][NTf ₂] Hydroxybutylpyridinium bis(trifluoromethanesulfonyl)imide		

19	[HOC ₄ Py][NTf ₂]-d1 Hydroxybutylpyridinium bis(trifluoromethanesulfonyl)imide-d1		
20	[HOC ₄ Py][NTf ₂]-d8 Hydroxybutylpyridinium bis(trifluoromethanesulfonyl)imide-d8		
21	[HOC ₄ Py][NTf ₂]-d9 Hydroxybutylpyridinium bis(trifluoromethanesulfonyl)imide-d9		
22	[HOC ₄ Py][NTf ₂]-d14 Hydroxybutylpyridinium bis(trifluoromethanesulfonyl)imide-d14		
23	[C ₅ Py][NTf ₂] Pentylpyridinium bis(trifluoromethanesulfonyl)imide		
24	[C ₅ Py][NTf ₂]-d11 Pentylpyridinium bis(trifluoromethanesulfonyl)imide-d11		
25	[C ₅ Py][NTf ₂]-d5 Pentylpyridinium bis(trifluoromethanesulfonyl)imide-d5		
26	[C ₅ Py][NTf ₂]-d16 Pentylpyridinium bis(trifluoromethanesulfonyl)imide-d16		

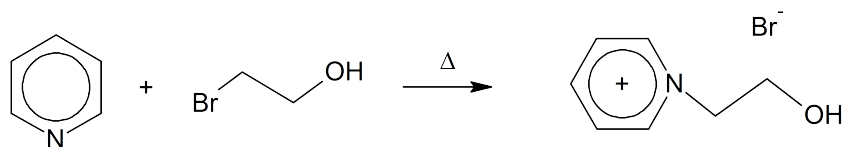
A.1. Preparation of the Compounds

Apart from the reactions in aqueous solutions all reactions were performed in a moisture-guarded assembly and reflux condenser was used while heating. The glassware used was alternately heated 3 times with a hot air blower at 630 °C and vented with dry argon as common for SCHLENK technique. The used solvents were dried with molecular sieves to a water content less than 50 ppm and distilled freshly. The solid starting materials were dried for several hours at elevated temperature in a high vacuum. Solvents and liquid starting materials were transferred to the respective reaction vessels with disposable syringes. The disposable syringes were previously purged 3 times with argon. All sources and made purification of starting materials are summarized in table A.1. The ionic liquids 1-(2-hydroxyethyl)-3-methylimidazolium-tetrafluoroborate, 1-(2-hydroxyethyl)-3-methylimidazolium-bis(trifluoromethanesulfonyl)imide, 1-(2-hydroxyethyl)-3-methylimidazolium-trifluoromethanesulfonate and, 1-(2-hydroxyethyl)-3-methylimidazolium-methanesulfonate and 1-(2-hydroxyethyl)-1,1,1-trimethylammonium-bis(trifluoromethanesulfonyl)imide were purchased from IoLiTec.

Table A.5.: List of chemicals, their provider, purification and drying method

Substances	Provider	Purification	Drying
Pyridine 99,5	Merck	distilled	Molecular sieves 4 Å
Pyridine- ₅ 99,5 %	Deutero	distilled	Molecular sieves 4 Å
2-Bromoethanol 95 %	distilled	destilliert	Molecular sieves 4 Å
N-Methylpiperidine 99 %	ALDRICH Chemistry	distilled	Molecular sieves 4 Å
N-Methylpyrrolidine 95 %	ALDRICH Chemistry	distilled	Molecular sieves 4 Å
Acetonitrile 99 %	Sigma-Aldrich	distilled	Molecular sieves 4 Å
Methanesulfonic acid 99,5 %	Sigma-Aldrich	-	-
Silver nitrate per analysis per analysis	VEB Feinchemie Sebnitz	- -	- -
Litium-bis(trifluoromethan- sulfonylimide 99 %	Sigma-Aldrich	-	-
3-Chloropropanol 95 %	Sigma-Aldrich	distilled	Molecular sieves 4 Å
Acetone 99 %	Sigma-Aldrich	distilled	Molecular sieves 4 Å
Tetrahydrofuran 99 %	Sigma-Aldrich	distilled	Sodium
Tetrahydrofuran-d ₈ 99,5 %	Deutero	distilled	Molecular sieves 4 Å
Bromotrimethylsilane 97 %	Sigma-Aldrich	distilled	Molecular sieves 4 Å
Iodotrimethylsilane 97 %	Sigma-Aldrich	distilled	Molecular sieves 4 Å
Deuterium oxide 99 %	Sigma-Aldrich	-	-
Tetrahydropyran 99 %	Merck	distilled	Molecular sieves 4 Å

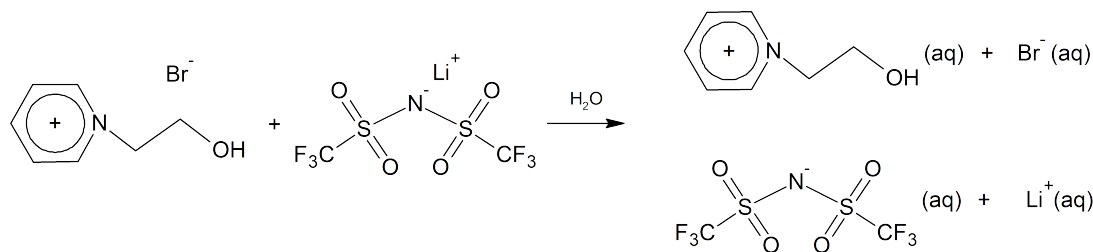
A.1.1. Synthesis of 1-(2-Hydroxyethyl)pyridinium-bromide [HOC₂Py]Br (**3 (a)**)



At room temperature equimolar amounts of pyridine (8.977 g; 113 mmol; 9.6 ml) and 2-bromoethanol (14.929 g; 113 mmol; 14.9 ml) were mixed and heated slowly up to 110 °C. When the reaction begins, the solution turns brown and starts to crystallize. The mixture was cooled to room temperature. The crude product was recrystallized from about 330 ml acetonitrile. The product (**3 (a)**) was obtained as rod-shaped colorless crystals. Yield 89 %.

EA % calc. (det.): C 41.20 (41.22); H 4.94 (4.92); N 6.86 (6.76). ¹H-NMR(298.2 K, DMSO-d₆, 300.13 MHz, [ppm]): δ = 3.86 (dd, 2H, CH₂-CH₂-OH); 4.67-4.74 (m, 2H, CH₂-CH₂-OH); 5.25(t, 1H, OH); 8.14-8.21 (m, 2H, *m*-CH); 8.60-8.67 (m, 1H, *p*-CH); 9.03-9.09 (m, 2H, *o*-CH). ¹³C-NMR(298 K, DMSO-d₆, 75.46 MHz, [ppm]): δ = 59.98 (s, CH₂-CH₂-OH); 63.04 (s, CH₂-CH₂-OH); 127.67 (s, *m*-CH); 145.15 (s, *p*-CH); 145.53 (s, *o*-CH).

A.1.2. Synthesis of 1-(2-Hydroxyethyl)pyridinium-bis(trifluoromethylsulfonyl)imide [HOC₂Py]NTf₂ (**3**)

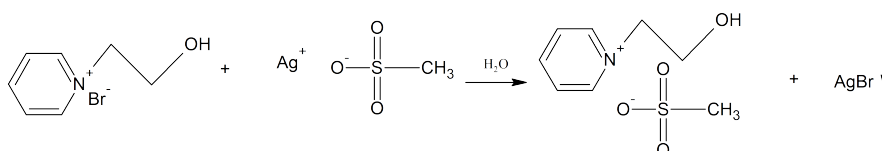


3.220 g ([HEPy]Br) (16 mmol) solved in 2 ml H₂O were added to a solution of 4.576 g lithium-bis(trifluoromethylsulfonyl)imide LiNTf₂ (16 mmol) in 2.5 ml H₂O. The mixture was stirred for 1 h. Two phases were obtained, the lower one was washed several times with water until no residual bromine could be detected with silver nitrate solution. The obtained colorless liquid of (**3**) was dried for 8 h in vacuum at 60 °C. Yield 57 %.

EA % calc. (det.): C 26.73 (26.14); H 2.49 (2.41); N 6.93 (6.54); S 15.86 (15.50). ¹H-NMR(298.2 K, DMSO-d₆, 300.13 MHz, [ppm]): δ = 3.88 (dd, 2H, CH₂-CH₂-OH); 4.65-4.71 (m, 2H, CH₂-CH₂-OH); 5.22(t, 1H, OH); 8.12-8.20 (m, 2H, *m*-CH); 8.57-8.64 (m, 1H, *p*-CH); 9.00-9.05 (m, 2H, *o*-CH). ¹³C-NMR(298 K, DMSO-d₆, 75.46 MHz, [ppm]): δ = 59.95 (s, CH₂-CH₂-OH); 63.01 (s, CH₂-CH₂-OH); 119.43 (q, CF₃); 127.65 (s, *m*-CH); 145.12 (s, *p*-CH); 145.50 (s, *o*-CH). ¹⁹F-NMR(298

K, DMSO- d_6 , 282.40 MHz, [ppm]): $\delta = -78.81$ (s, CF_3). **IR** (Transm., CaF_2 -window, 12 μm -spacer, 20 °C, 128 Scans, $[cm^{-1}]$): 3528 (vw); 3141 (vw); 3097 (vw); 3074 (vw); 2972 (vw); 2951 (vw); 2893 (vw); 2857 (vw); 1936 (vw); 1850 (vw); 1741 (vw); 1638 (w); 1585 (vw); 1502 (vw); 1491 (m); 1451 (vw); 1352 (vs); 1200 (s); 1136 (s); 1060 (s).

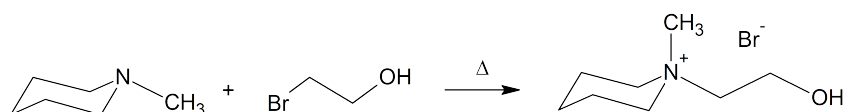
A.1.3. Synthesis of 1-(2-Hydroxyethyl)pyridinium-methanesulfonate [HOC₂Py]OMs (15)



10.000 g ([HOC₂Py][Br]) (49 mmol) dissolved in 300 ml H₂O were titrated dropwise with the equimolar amount of an aqueous silver-methanesulfonate solution. The equivalence point is reached as soon as an additional drop of silver-methanesulfonate solution no longer leads to precipitation. To remove the precipitated AgBr the suspension was then filtered. Small volumes of the resulting colourless solution were then tested with AgNO₃ and NaCl solution, the absence of any precipitation indicates that there are no residual educts. The water in the remaining solution was then removed with the help of a rotary evaporator. The obtained colourless liquid of ([HOC₂Py][OMs]) was dried for 8 h in vacuum at 60 °C. Yield 90 %.

¹H-NMR(298.2 K, DMSO- d_6 , 300.13 MHz, [ppm]): $\delta = 2.33$ (s, 3H, SO₃CH₃); 3.86 (dd, 2H, CH₂–CH₂–OH); 4.66-4.70 (m, 2H, CH₂–CH₂–OH); 5.19(t, 1H, OH); 8.12-8.22 (m, 2H, *m*-CH); 8.59-8.67 (m, 1H, *p*-CH); 9.00-9.07 (m, 2H, *o*-CH). ¹³C-NMR(298 K, DMSO- d_6 , 75.46 MHz, [ppm]): $\delta = 39.77$ (s, SO₃CH₃); 60.11 (s, CH₂–CH₂–OH); 63.11 (s, CH₂–CH₂–OH); 127.67 (s, *m*-CH); 145.22 (s, *p*-CH); 145.52 (s, *o*-CH).

A.1.4. Synthesis of 1,1-(2-Hydroxyethyl)methylpiperidinium-bromide [HOC₂MPip]Br (4 (a))

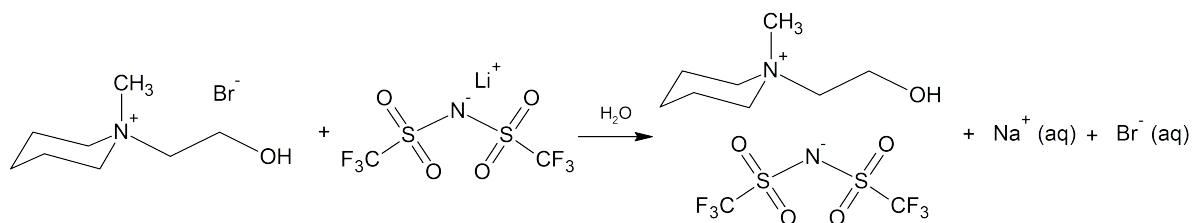


32.661 g of 2-bromoethanol (261 mmol, 19 ml) were added to a solution of 16.378 g of N-methylpiperidine (165 mmol, 20 ml) and 40 ml ethanol at room temperature. The mixture was refluxed for 2 h. After cooling to room temperature, the ethanol and the residual 2-bromoethanol were removed in vacuum. The liquid crude product begins to crystallize by addition of 40 ml of acetone. The white precipitate was washed three times with dry acetone. The product was dried for 4 h in vacuum at 60 °C. **4 (a)** was

obtained in 89 % yield.

EA % calc. (det.): C 42.87 (42.65); H 8.10 (8.06); N 6.25 (6.11). ¹H-NMR(298.2 K, DMSO-d₆, 300.13 MHz, [ppm]): δ = 1.48-1.58 (m, 2H, C(4)H₂); 1.74-1.84 (m, 4H, C(2; 6)H₂); 3.08 (s, 3H, CH₃); 3.30-3.47 (m, 6H, C(3; 5)H₂ + CH₂-CH₂-OH); 3.81-3.88 (m, 2H, CH₂-CH₂-OH), 5.26 (t, 1H, OH). ¹³C-NMR(298 K, DMSO-d₆, 75.46 MHz, [ppm]): δ = 20.48 (s, C(4)); 19.24 (s, C(3; 5)); 48.07 – 48.27 (m, CH₃); 54.49 (s, CH₂-CH₂-OH); 60.77 – 60.92 (m, CH₂-CH₂-OH); 63.72 – 63.93 (m, C(2; 6)).

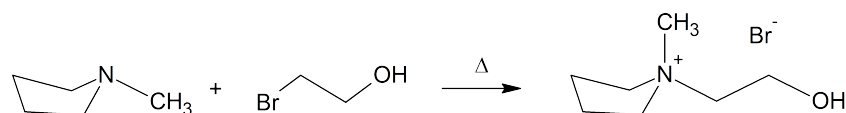
A.1.5. Synthesis of 1,1-(2-Hydroxyethyl)methylpiperidinium-bis(trifluoromethylsulfonyl)imide [HOC₂MPip]NTf₂ (**4**)



9.030 g **4** (**a**) (40 mmol) were solved in 10 ml H₂O and added to a solution of 11.518 g LiNTf₂ (40 mmol) in 10 ml H₂O. The mixture was stirred for 1 h. During this time two phases were formed. The lower phase was washed several times with water until no residual bromine could be detected with silver nitrate solution. The thus obtained colorless liquid (**4**) was dried for 6 h at 110°C in vacuum. Yield: 68 %.

¹H-NMR(300 K, DMSO-d₆, 250.13 MHz, [ppm]): δ = 1.46-1.57 (m, 2H, C(4)H₂); 1.71-1.82 (m, 4H, C(2; 6)H₂); 3.05 (s, 3H, CH₃); 3.26-3.44 (m, 6H, C(3; 5)H₂ + CH₂-CH₂-OH); 3.78-3.86 (m, 2H, CH₂-CH₂-OH), 5.24 (t, 1H, OH). ¹³C-NMR(298 K, DMSO-d₆, 75.46 MHz, [ppm]): δ = 20.48 (s, C(4)); 19.24 (s, C(3; 5)); 48.07 – 48.27 (m, CH₃); 54.49 (s, CH₂-CH₂-OH); 60.77 – 60.92 (m, CH₂-CH₂-OH); 63.72 – 63.93 (m, C(2; 6)); 119.43 (q, CF₃). ¹⁹F-NMR(300 K, DMSO-d₆, 235.36 MHz, [ppm]): δ = –78.79 (s, CF₃). IR (Transm., CaF₂-Window, 12 μm-spacer, 20°C, 128 scans, [cm⁻¹]): 3536 (w); 2958 (w); 2882 (w); 1846 (vw); 1797 (vw); 1471 (w); 1349 (s); 1332 (m); 1195 (s); 1138 (s); 1086 (w); 1056 (s); 986 (w).

A.1.6. Synthesis of 1,1-(2-Hydroxyethyl)methylpyrrolidinium-bromide [HOC₂MPyrro]Br (**5** (**a**))

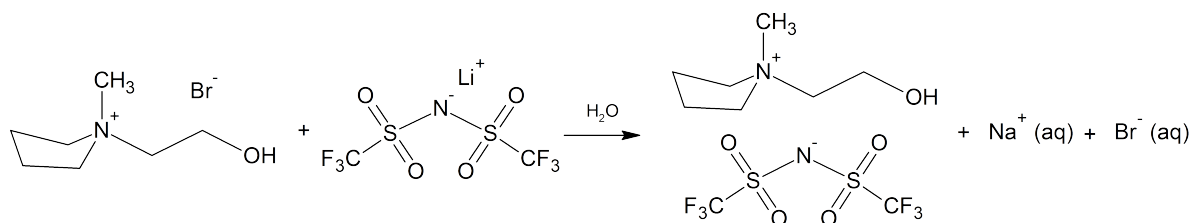


15.732 g N-Methylpyrrolidine (185 mmol; 20 ml) were mixed with 35.732 g 2-bromoethanol (286 mmol; 20 ml) at room temperature. The mixture was heated slowly

up to 100 °C. When the reaction begins, the mixture turns brown. After 1 h at this temperature, the mixture was allowed to cool down. Excess 2-bromoethanol and unreacted N-Methylpyrrolidine are then removed in vacuum. The brownish crystalline crude product was recrystallized from 1400 ml of an acetone/acetonitrile mixture 3:1. The colourless product (**5 (a)**) is obtained in the form of needle-shaped crystals. Yield 66,4 %.

EA % calc. (det.): C 40.01 (39.64); H 7.68 (7.75); N 6.67 (6.46). **¹H-NMR**(298.2 K, DMSO-d₆, 300.13 MHz, [ppm]): δ = 2.03-2.13 (m, 4H, C(3; 4)H₂); 3.06 (s, 3H, CH₃); 3.43-3.48 (m, 2H, CH₂-CH₂-OH); 3.49-3.56 (m, 4H, C(2; 5)H₂); 3.79-3.87 (m, 2H, CH₂-CH₂-OH), 5.27 (t, 1H, OH). **IR** (ATR, 30 °C, 128 scans, [cm⁻¹]): 3326 (vs); 3280 (vs); 3013 (m); 2963 (w); 2941 (w); 2887 (w); 1460 (m); 1395 (w); 1371 (w); 1305 (w); 1238 (w); 1179 (vw); 1081 (m); 1037 (w); 996 (m); 954 (w); 936 (m); 900 (w); 873 (w); 814 (w).

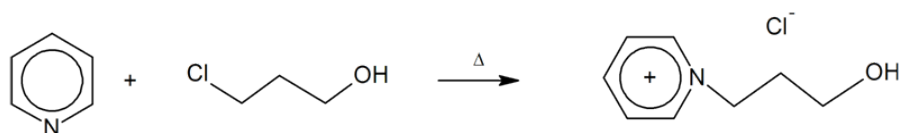
A.1.7. Synthesis of 1,1-(2-Hydroxyethyl)methylpyrrolidinium-bis(trifluoromethylsulfonyl)imide [HOC₂MPip]NTf₂ (**5**)



4.201 g (**7**) (20 mmol) dissolved in 10 ml H₂O were mixed with 5.739 g LiNTf₂ (20 mmol) dissolved in 10 ml H₂O. The mixture was stirred for 1 h. During this time two phases were formed. The lower one was washed several times with water until no residual bromine could be detected with silver nitrate solution. The thus obtained colorless liquid was (**5**) dried 6 h at 110 °C in vacuum. Yield: 63 %.

¹H-NMR(298.2 K, DMSO-d₆, 300.13 MHz, [ppm]): δ = 2.02-2.13 (m, 4H, C(3; 4)H₂); 3.06 (s, 3H, CH₃); 3.39-3.45 (m, 2H, CH₂-CH₂-OH); 3.49-3.56 (m, 4H, C(2; 5)H₂); 3.79-3.87 (m, 2H, CH₂-CH₂-OH), 5.26 (t, 1H, OH). **¹⁹F-NMR**(298,2 K, DMSO-d₆, 282.40 MHz, [ppm]): δ = -78.73 (s, CF₃). **IR** (Transm., CaF₂-window, 12 μm-spacer, 20 °C, 128 scans, [cm⁻¹]): 3539 (w); 3044 (vw); 2980 (w); 2903 (w); 1849 (vw); 1799 (vw); 1701 (vw); 1470 (w); 1431 (w); 1355 (vs); 1355 (m); 1199 (vs); 1138 (s); 1054 (s); 998 (w); 986 (w).

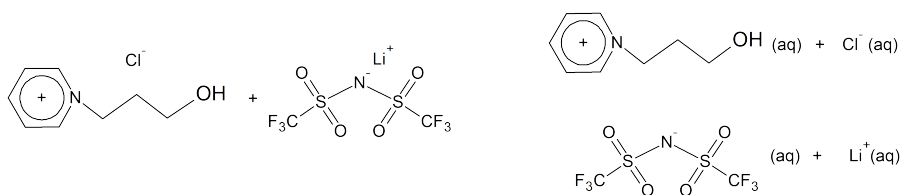
A.1.8. Synthesis of 1-(3-Hydroxypropyl)pyridinium-chloride [HOC₃Py]Cl (**9 a**)



At room temperature equimolar amounts of pyridine (12.231 g; 155 mmol; 13.1 ml) and 3-chloropropanol (14.600 g; 154 mmol; 12.9 ml) were mixed and heated slowly up to 100 °C. When the reaction begins, the solution turns slightly brown and starts to crystallize upon cooling to room temperature. The crude product was recrystallized from about 450 ml acetonitrile. The product was obtained as rod-shaped colorless crystals. Yield 92 %.

¹H-NMR(298.2 K, DMSO-d₆, 300.13 MHz, [ppm]): δ = 2.03-2.13 (tt, 2H, CH₂-CH₂-CH₂-OH); 3.38-3.45 (dt, 2H, CH₂-CH₂-CH₂-OH); 4.76 (t, 2H, CH₂-CH₂-CH₂-OH); 5.12 (t, 1H, OH); 8.13-8.19 (m, 2H, *m*-CH); 8.58-8.65 (m, 1H, *p*-CH); 9.25-9.29 (m, 2H, *o*-CH). ¹³C-NMR(298.2 K, DMSO-d₆, 75.46 MHz, [ppm]): δ = 33.46 (s, CH₂-CH₂-CH₂-OH); 56.88 (s, CH₂-CH₂-CH₂-OH); 58.42 (s, CH₂-CH₂-CH₂-OH); 127.87 (s, *m*-CH); 145.05 (s, *p*-CH); 145.38 (s, *o*-CH). IR (ATR, 30 °C, 128 scans, [cm⁻¹]): 3277 (m); 3128 (w); 3093 (w); 3071 (w); 3043 (w); 3019 (w); 2969 (w); 2939 (w); 2905 (w); 2868 (w); 2804 (w); 1636 (w); 1626 (m); 1579 (vw); 1505 (w); 1484 (s); 1470 (m); 1421 (w); 1379 (vw); 1360 (w); 1304 (m); 1265 (w); 1233 (w); 1174 (m); 1150 (w); 1083 (m); 1050 (s); 957 (w); 934 (m); 872 (vw); 819 (w); 774 (s); 685 (vs); 638 (s).

A.1.9. Synthesis of 1-(3-Hydroxypropyl)pyridinium-bis(trifluoromethylsulfonyl)imide [HOC₃Py]NTf₂ (9)

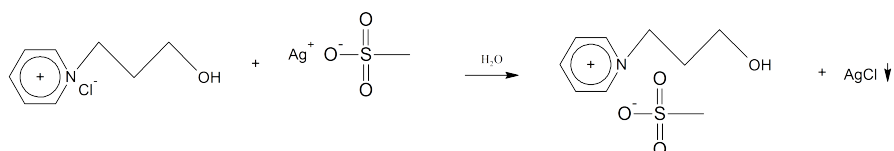


9.653 g ([HOC₃Py][Cl]) (56 mmol) solved in 10 ml H₂O were added to a solution of 16.125 g lithium- bis(trifluoromethylsulfonyl)imide LiNTf₂ (56 mmol) in 10 ml H₂O. The mixture was stirred for 1 h. Two phases were obtained, the lower one was washed several times with water until no residual chlorine could be detected with silver nitrate solution. The obtained colorless liquid of ([HOC₃Py][NTf₂]) was dried for 8 h in vacuum at 60 °C. Yield 77 %.

¹H-NMR(298.2 K, DMSO-d₆, 300.13 MHz, [ppm]): δ = 2.03-2.13 (tt, 2H, CH₂-CH₂-CH₂-OH); 3.38-3.45 (dt, 2H, CH₂-CH₂-CH₂-OH); 4.76 (t, 2H, CH₂-CH₂-CH₂-OH); 5.12 (t, 1H, OH); 8.13-8.19 (m, 2H, *m*-CH); 8.58-8.65 (m, 1H, *p*-CH); 9.25-9.29 (m, 2H, *o*-CH). ¹³C-NMR(298.2 K, DMSO-d₆, 75.46 MHz, [ppm]): δ = 33.46 (s, CH₂-CH₂-CH₂-OH); 56.88 (s, CH₂-CH₂-CH₂-OH); 58.42 (s, CH₂-CH₂-CH₂-OH); 119.43 (q, C F₃); 127.87 (s, *m*-CH); 145.05 (s, *p*-CH); 145.38 (s, *o*-CH). IR (ATR, 30 °C, 128 scans, [cm⁻¹]): 3277 (m); 3128 (w); 3093 (w); 3071 (w); 3043 (w); 3019 (w); 2969 (w); 2939 (w); 2905 (w); 2868 (w); 2804 (w); 1636 (w); 1626 (m); 1579 (vw); 1505 (w); 1484 (s); 1470 (m); 1421 (w); 1379 (vw); 1360 (w); 1304

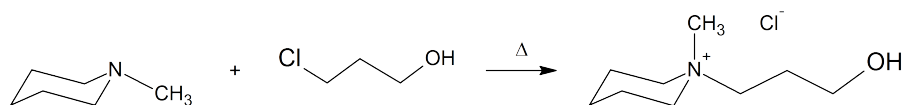
(m); 1265 (w); 1233 (w); 1174 (m); 1150 (w); 1083 (m); 1050 (s); 957 (w); 934 (m); 872 (vw); 819 (w); 774 (s); 685 (vs); 638 (s).

A.1.10. Synthesis of 1-(3-Hydroxypropyl)pyridinium-methanesulfonate [HOC₃Py]OMs (16)



12.268 g ([HOC₃Py][Cl]) (71 mmol) solved in 300 ml H₂O were titrated dropwise with the equimolar of an aqueous silver-methanesulfonate solution. The equivalence point is reached as soon as an additional drop of silver-methanesulfonate solution no longer leads to precipitation. To remove the precipitated AgCl the suspension was then filtered. Small volumes of the resulting colorless solution were then tested with AgNO₃ and NaCl solution, the absence of any precipitation indicates that there are no residual educts. The water in the remaining solution was then removed with the help of a rotation evaporator. The obtained colorless liquid of ([HOC₃Py][OMs]) was dried for 8 h in vacuum at 60 °C. Yield 92 %. ¹H-NMR(298.2 K, DMSO-d₆, 300.13 MHz, [ppm]): δ = 2.08 (tt, 2H, CH₂-CH₂-CH₂-OH); 2.35 (s, 3H, SO₃CH₃); 3.45 (dt, 2H, CH₂-CH₂-CH₂-OH); 4.69 (t, 2H, CH₂-CH₂-CH₂-OH); 5.42 (t, 1H, OH); 8.15 (m, 2H, *m*-CH); 8.60 (m, 1H, *p*-CH); 9.10 (m, 2H, *o*-CH). ¹³C-NMR(298.2 K, DMSO-d₆, 75.46 MHz, [ppm]): δ = 33.76 (s, CH₂-CH₂-CH₂-OH); 40.24(s, SO₃CH₃); 57.69 (s, CH₂-CH₂-CH₂-OH); 59.18(s, CH₂-CH₂-CH₂-OH); 128.45 (s, *m*-CH); 145.53 (s, *p*-CH); 145.93 (s, *o*-CH).

A.1.11. Synthesis of 1-(3-Hydroxypropyl)methylpiperidinium-chloride [HOC₃MPip]Cl (12 (a))

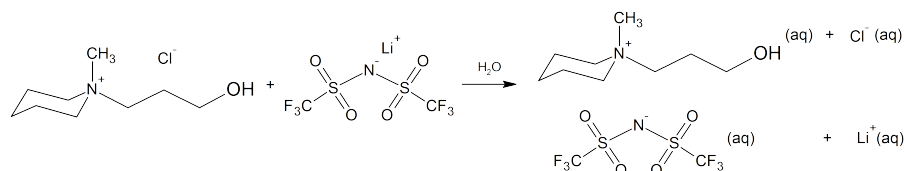


At room temperature equimolar amounts of N-methylpiperidine (8.286 g; 105 mmol; 8.9 ml) and 3-chloropropanol (14.600 g; 105 mmol; 8.8 ml) were mixed and heated slowly up to 110 °C. When the reaction begins, the solution turns yellow and starts to crystallize upon cooling to room temperature. The crude product was recrystallized from about 400 ml of an acetonitrile/acetone mixture. The product was obtained as needle-shaped colorless crystals. Yield 87 %.

¹H-NMR(298.2 K, DMSO-d₆, 300.13 MHz, [ppm]): δ = 1.48-1.58 (m, 2H, C(4)H₂); 1.71-1.88 (m, 4H, C(2; 6)H₂ + 2H, CH₂-CH₂-OH); 3.01 (s, 3H, CH₃); 3.28-3.43 (m, 6H,

C(3; 5) H_2 + $CH_2-CH_2-CH_2-OH$); 3.47 (td, 2H, $CH_2-CH_2-CH_2-OH$); 5.06 (t, 1H, OH). $^{13}C-NMR$ (298.2 K, DMSO- d_6 , 75.46 MHz, [ppm]): δ = 19.27 (s, C(3; 5)); 20.58 (s, C(4)); 24.59 (s, CH_2-CH_2-OH); 47.07 (s, CH_3); 57.58 (s, CH_2-CH_2-OH); 59.87 (s, C(2; 6)) 60.24 (s, $CH_2-CH_2-CH_2-OH$).

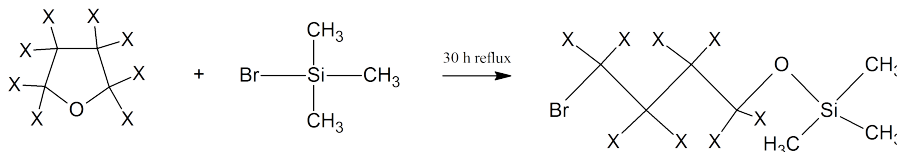
A.1.12. Synthesis of 1-(3-Hydroxypropyl)methylpiperidinium-bis(trifluoromethylsulfonyl)imide [HOC₃MPip]NTf₂ (12)



10 g ([HPMPip][Cl]) (52 mmol) were solved in 10 ml H_2O and added to a solution of 14.821g LiNTf₂ (52 mmol) and 10 ml H_2O . The mixture was stirred for 1h. During this time two phases were formed. The lower phase was washed several times with water until no residual chlorine could be detected with silver nitrate solution. The thus obtained colourless liquid was dried for 6 h at 110 °C in vacuum. Yield: 74 %.

^1H-NMR (298.2 K, DMSO- d_6 , 300.13 MHz, [ppm]): δ = 1.48-1.58 (m, 2H, C(4) H_2); 1.71-1.88 (m, 4H, C(2; 6) H_2 + 2H, CH_2-CH_2-OH); 3.01 (s, 3H, CH_3); 3.28-3.43 (m, 6H, C(3; 5) H_2 + $CH_2-CH_2-CH_2-OH$); 3.47 (td, 2H, $CH_2-CH_2-CH_2-OH$); 5.06 (t, 1H, OH). $^{13}C-NMR$ (298.2 K, DMSO- d_6 , 75.46 MHz, [ppm]): δ = 19.27 (s, C(3; 5)); 20.58 (s, C(4)); 24.59 (s, CH_2-CH_2-OH); 47.07 (s, CH_3); 57.58 (s, CH_2-CH_2-OH); 59.87 (s, C(2; 6)) 60.24 (s, $CH_2-CH_2-CH_2-OH$); 119.43 (q, CF_3). $^{19}F-NMR$ (298,2 K, DMSO- d_6 , 282.40 MHz, [ppm]): δ = -78.79 (s, CF_3). IR (Transm., CaF₂-window, 12 μm -spacer, 20°C, 128 scans, [cm⁻¹]): 3539 (w); 2952 (w); 2882 (w); 1841 (vw); 1800 (vw); 1470 (w); 1349 (s); 1332 (m); 1194 (s); 1136 (s); 1086 (w); 1056 (s); 985 (w).

A.1.13. Synthesis of 4-Bromo-1-trimethylsiloxybutane- d_x TMSOC₄Br- d_x



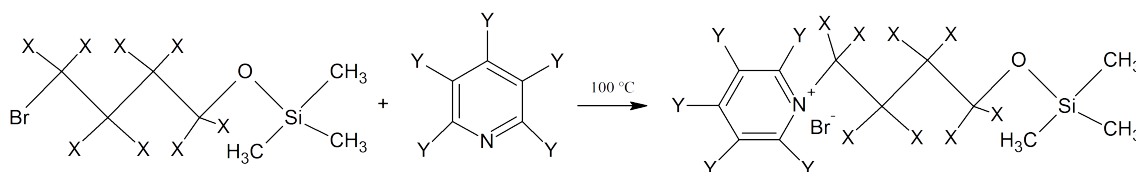
A mixture of equimolar amounts of dry tetrahydrofuran- d_x and bromotrimethylsilane was refluxed for 30 h and the crude product was then isolated by distillation in vacuum (78 °C; 17 mbar). The product was obtained as a colourless liquid. Yield 80 %.

4-Bromo-1-trimethylsiloxybutane- d_0 (10 (a)); (19 (a)): ^1H-NMR (298.2 K, DMSO- d_6 , 300.13 MHz, [ppm]): δ = 0.05 (s, 9H, -Si(CH_3)₃); 1.52 (tt, 2H, CH_2-CH_2-O); 1.84 (tt, 2H, Br- CH_2-CH_2 -); 3.41 (t, 2H, CH_2-CH_2-O); 3.53 (t, 2H, Br- CH_2-CH_2 -).

^{13}C -NMR(298 K, DMSO- d_6 , 75.46 MHz, [ppm]): δ = 2.05 (s, $-\text{Si}(\text{CH}_3)_3$); 29.24 (s, $\text{CH}_2\text{-CH}_2\text{-O-}$); 31.01 (s, $\text{Br-CH}_2\text{-CH}_2\text{-}$); 35.28 (s, $\text{Br-CH}_2\text{-CH}_2\text{-}$); 59.82 (s, $\text{CH}_2\text{-CH}_2\text{-O-}$).

4-Bromo-1-trimethylsiloxybutane- d_8 (20 (a)); (21 (a)); (22 (a)): ^1H -NMR(298.2 K, DMSO- d_6 , 300.13 MHz, [ppm]): δ = 0.05 (s, 9H, $-\text{Si}(\text{CH}_3)_3$). ^{13}C -NMR(298 K, DMSO- d_6 , 75.46 MHz, [ppm]): δ = 2.05 (s, $-\text{Si}(\text{CH}_3)_3$); 24.28 (quint, $\text{CD}_2\text{-CD}_2\text{-O-}$); 29.90 (quint, $\text{Br-CD}_2\text{-CD}_2\text{-}$); 33.34 (quint, $\text{Br-CD}_2\text{-CD}_2\text{-}$); 66.39 (quint, $\text{CD}_2\text{-CD}_2\text{-O-}$).

A.1.14. Synthesis of 1-(4-Trimethylsiloxybutyl)-pyridinium-bromide- d_{x+y} [TMSOC $_4$ Py]Br- d_{x+y}



Equimolar amounts of pyridine- d_y and 4-Bromo-1-trimethylsiloxybutane- d_x were mixed at room temperature and heated slowly up to round about 100 °C - 110 °C. When the reaction begins, the solution starts to cloud. After a few minutes two phases are formed, the lower one is yellow and the upper one is colourless. After about 5 h only one yellow phase is obtained. All volatiles were removed in vacuum. The crude product was cooled to room temperature whereby it starts to crystallize. Yield 75 %.

1-(4-Trimethylsiloxybutyl)-pyridinium-bromide- d_0 (10 (b)); (19 (b)): ^1H -NMR(298.2 K, DMSO- d_6 , 300.13 MHz, [ppm]): δ = 0.05 (s, 9H, $-\text{Si}(\text{CH}_3)_3$); 1.41 (tt, 2H, $\text{CH}_2\text{-CH}_2\text{-O-}$); 1.96 (tt, 2H, $\text{Br-CH}_2\text{-CH}_2\text{-}$); 3.41 (t, 2H, $\text{CH}_2\text{-CH}_2\text{-O-}$); 4.68 (t, 2H, $\text{N-CH}_2\text{-CH}_2\text{-}$); 8.14-8.21 (m, 2H, $m\text{-CH}$); 8.60-8.67 (m, 1H, $p\text{-CH}$); 9.03-9.09 (m, 2H, $o\text{-CH}$). ^{13}C -NMR(298 K, DMSO- d_6 , 75.46 MHz, [ppm]): δ = 2.05 (s, $-\text{Si}(\text{CH}_3)_3$); 26.36 (s, $\text{CH}_2\text{-CH}_2\text{-O-}$); 27.34 (s, $\text{N-CH}_2\text{-CH}_2\text{-}$); 58.96 (s, $\text{N-CH}_2\text{-CH}_2\text{-}$); 60.19 (s, $\text{CH}_2\text{-CH}_2\text{-O-}$); 127.67 (s, $m\text{-CH}$); 144.65 (s, $p\text{-CH}$); 145.46 (s, $o\text{-CH}$).

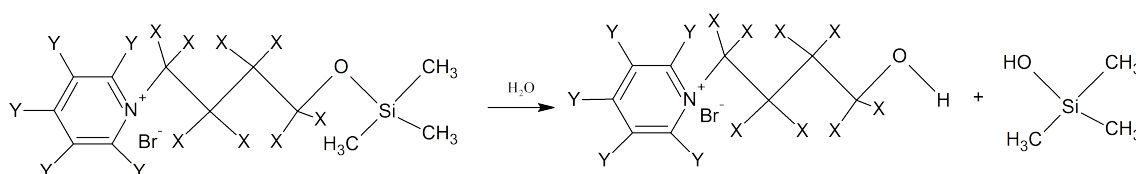
1-(4-Trimethylsiloxybutyl)-pyridinium-bromide- d_5 : ^1H -NMR(298.2 K, DMSO- d_6 , 300.13 MHz, [ppm]): δ = 0.05 (s, 9H, $-\text{Si}(\text{CH}_3)_3$); 1.41 (tt, 2H, $\text{CH}_2\text{-CH}_2\text{-O-}$); 1.96 (tt, 2H, $\text{Br-CH}_2\text{-CH}_2\text{-}$); 3.41 (t, 2H, $\text{CH}_2\text{-CH}_2\text{-O-}$); 4.68 (t, 2H, $\text{N-CH}_2\text{-CH}_2\text{-}$). ^{13}C -NMR(298 K, DMSO- d_6 , 75.46 MHz, [ppm]): δ = 2.05 (s, $-\text{Si}(\text{CH}_3)_3$); 26.36 (s, $\text{CH}_2\text{-CH}_2\text{-O-}$); 27.34 (s, $\text{N-CH}_2\text{-CH}_2\text{-}$); 58.96 (s, $\text{N-CH}_2\text{-CH}_2\text{-}$); 60.19 (s, $\text{CH}_2\text{-CH}_2\text{-O-}$); 126.76-128.00 (m, $m\text{-CD}$); 143.53-145.57 (m, $p\text{-CH} + o\text{-CH}$).

1-(4-Trimethylsiloxybutyl)-pyridinium-bromide- d_8 (20 (b)): ^1H -NMR(298.2 K, DMSO- d_6 , 300.13 MHz, [ppm]): δ = 0.05 (s, 9H, $-\text{Si}(\text{CH}_3)_3$); 8.14-8.21 (m, 2H, $m\text{-CH}$); 8.60-8.67 (m, 1H, $p\text{-CH}$); 9.03-9.09 (m, 2H, $o\text{-CH}$). ^{13}C -NMR(298 K, DMSO- d_6 , 75.46 MHz, [ppm]): δ = 2.05 (s, $-\text{Si}(\text{CH}_3)_3$); 26.18-28.21 (m, $\text{CD}_2\text{-CD}_2\text{-O-} + \text{N-CD}_2\text{-CD}_2\text{-}$); 58.86-61.27 (m, $\text{N-CD}_2\text{-CD}_2\text{-} + \text{CD}_2\text{-CD}_2\text{-O-}$); 127.67 (s, $m\text{-CH}$); 144.65 (s, $p\text{-CH}$); 145.46 (s, $o\text{-CH}$).

1-(4-Trimethylsiloxybutyl)-pyridinium-bromide- d_{13} (22 (b)): ^1H -NMR(298.2

K, DMSO-d₆, 300.13 MHz, [ppm]): $\delta = 0.05$ (s, 9H, -Si(CH₃)₃). ¹³C-NMR(298 K, DMSO-d₆, 75.46 MHz, [ppm]): $\delta = 2.05$ (s, -Si(CH₃)₃; 26.18-28.21 (m, CD₂-CD₂-O- + N-CD₂-CD₂-); 58.86-61.27 (m, N-CD₂-CD₂- + CD₂-CD₂-O-); 126.76-128.00 (m, *m*-CD); 143.53-145.57 (m, *p*-CH + *o*-CH).

A.1.15. Synthesis of 1-(4-Hydroxybutyl)-pyridinium-bromide-d_{x+y} [HOC₄Py]Br-d_{x+y}



1-(4-Trimethylsiloxybutyl)-pyridinium-bromide-d_{x+y} was dissolved in a tenfold excess of H₂O. The solution was stirred for 4 h at 80 °C. Two phases were formed. All volatiles were removed in vacuum. The procedure was repeated to remove all trimethylsilyl residuals. The crude product was cooled to room temperature whereby it starts to crystallize. The almost colourless crystalline crude product was recrystallized from a small amount of acetonitrile. Yield 80 %.

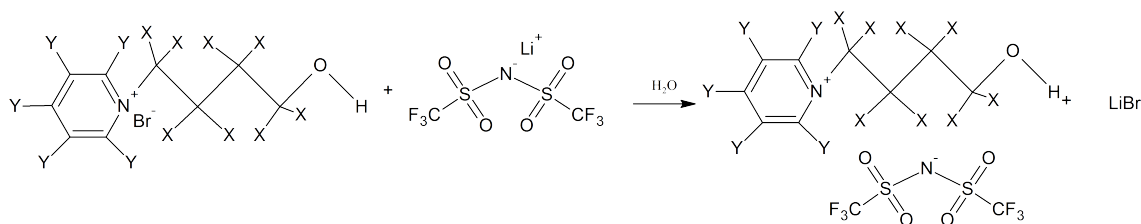
1-(4-Hydroxybutyl)-pyridinium-bromide-d₀ (10 (c)): ¹H-NMR(298.2 K, DMSO-d₆, 300.13 MHz, [ppm]): $\delta = 1.41$ (tt, 2H, CH₂-CH₂-O-); 1.96 (tt, 2H, N-CH₂-CH₂-); 3.41 (t, 2H, CH₂-CH₂-O-); 4.13 (s, 1H, -OH); 4.68 (t, 2H, N-CH₂-CH₂-); 8.14-8.21 (m, 2H, *m*-CH); 8.60-8.67 (m, 1H, *p*-CH); 9.03-9.09 (m, 2H, *o*-CH). ¹³C-NMR(298 K, DMSO-d₆, 75.46 MHz, [ppm]): $\delta = 26.36$ (s, CH₂-CH₂-O-); 27.34 (s, N-CH₂-CH₂-); 58.96 (s, N-CH₂-CH₂-); 60.19 (s, CH₂-CH₂-O-); 127.67 (s, *m*-CH); 144.65 (s, *p*-CH); 145.46 (s, *o*-CH).

1-(4-Hydroxybutyl)-pyridinium-bromide-d₅: ¹H-NMR(298.2 K, DMSO-d₆, 300.13 MHz, [ppm]): $\delta = 1.41$ (tt, 2H, CH₂-CH₂-O-); 1.96 (tt, 2H, N-CH₂-CH₂-); 3.41 (t, 2H, CH₂-CH₂-O-); 4.13 (s, 1H, -OH); 4.68 (t, 2H, N-CH₂-CH₂-). ¹³C-NMR(298 K, DMSO-d₆, 75.46 MHz, [ppm]): $\delta = 26.36$ (s, CH₂-CH₂-O-); 27.34 (s, N-CH₂-CH₂-); 58.96 (s, N-CH₂-CH₂-); 60.19 (s, CH₂-CH₂-O-); 126.76-128.00 (m, *m*-CD); 143.53-145.57 (s, *p*-CD + *o*-CD).

1-(4-Hydroxybutyl)-pyridinium-bromide-d₈ (20 (c)): ¹H-NMR(298.2 K, DMSO-d₆, 300.13 MHz, [ppm]): $\delta = 4.13$ (s, 1H, -OH); 8.14-8.21 (m, 2H, *m*-CH); 8.60-8.67 (m, 1H, *p*-CH); 9.03-9.09 (m, 2H, *o*-CH). ¹³C-NMR(298 K, DMSO-d₆, 75.46 MHz, [ppm]): $\delta = 26.18$ -28.21 (s, CD₂-CD₂-O- + N-CD₂-CD₂-); 58.86-61.27 (m, N-CD₂-CD₂- + CD₂-CD₂-O-); 127.67 (s, *m*-CH); 144.65 (s, *p*-CH); 145.46 (s, *o*-CH).

1-(4-Hydroxybutyl)-pyridinium-bromide-d₁₃ (22 (b)): ¹H-NMR(298.2 K, DMSO-d₆, 300.13 MHz, [ppm]): $\delta = 4.13$ (s, 1H, -OH). ¹³C-NMR(298 K, DMSO-d₆, 75.46 MHz, [ppm]): $\delta = 26.18$ -28.21 (s, CD₂-CD₂-O- + N-CD₂-CD₂-); 58.86-61.27 (m, N-CD₂-CD₂- + CD₂-CD₂-O-); 126.76-128.00 (m, *m*-CH); 143.53-145.57 (m, *p*-CH + *o*-CH).

A.1.16. Synthesis of 1-(4-Hydroxybutyl)-pyridinium-bis(trifluoromethylsulfonyl)imide- d_{x+y} [HOC₄Py]NTf₂- d_{x+y}



1-(4-Hydroxybutyl)-pyridinium-bromide- d_{x+y} was solved in a few milliliters H₂O. This solution was added to an equimolar aqueous solution of LiNTf₂. The mixture was stirred for 1h. During this time two phases were formed. The lower phase was washed several times with water until no residual bromine could be detected with silver nitrate solution. The thus obtained colorless liquid was dried for 6 h at 60 °C in vacuum ($1 \cdot 10^{-6}$ mbar). Yield: 90 %.

1-(4-Hydroxybutyl)-pyridinium-bis(trifluoromethylsulfonyl)imide- d_0 (10):

¹H-NMR(298.2 K, DMSO- d_6 , 300.13 MHz, [ppm]): δ = 1.41 (tt, 2H, CH₂-CH₂-O-); 1.96 (tt, 2H, N-CH₂-CH₂-); 3.41 (t, 2H, CH₂-CH₂-O-); 4.13 (s, 1H, -OH); 4.68 (t, 2H, N-CH₂-CH₂-); 8.14-8.21 (m, 2H, *m*-CH); 8.60-8.67 (m, 1H, *p*-CH); 9.03-9.09 (m, 2H, *o*-CH). ¹³C-NMR(298 K, DMSO- d_6 , 75.46 MHz, [ppm]): δ = 26.36 (s, CH₂-CH₂-O-); 27.34 (s, N-CH₂-CH₂-); 58.96 (s, N-CH₂-CH₂-); 60.19 (s, CH₂-CH₂-O-); 119.43 (q, C F₃); 127.67 (s, *m*-CH); 144.65 (s, *p*-CH); 145.46 (s, *o*-CH).

1-(4-Hydroxybutyl)-pyridinium-bis(trifluoromethylsulfonyl)imide- d_5 :

¹H-NMR(298.2 K, DMSO- d_6 , 300.13 MHz, [ppm]): δ = 1.41 (tt, 2H, CH₂-CH₂-O-); 1.96 (tt, 2H, N-CH₂-CH₂-); 3.41 (t, 2H, CH₂-CH₂-O-); 4.13 (s, 1H, -OH); 4.68 (t, 2H, N-CH₂-CH₂-). ¹³C-NMR(298 K, DMSO- d_6 , 75.46 MHz, [ppm]): δ = 26.36 (s, CH₂-CH₂-O-); 27.34 (s, N-CH₂-CH₂-); 58.96 (s, N-CH₂-CH₂-); 60.19 (s, CH₂-CH₂-O-); 119.43 (q, C F₃); 126.76-128.00 (m, *m*-CD); 143.53-145.57 (s, *p*-CD + *o*-CD).

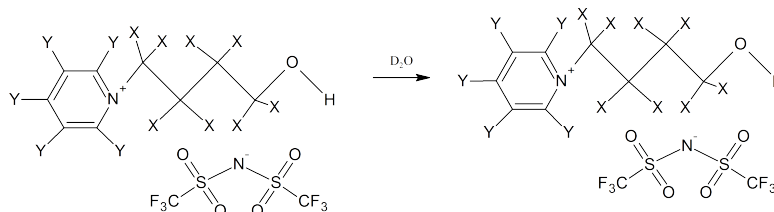
1-(4-Hydroxybutyl)-pyridinium-bis(trifluoromethylsulfonyl)imide- d_8 (20):

¹H-NMR(298.2 K, DMSO- d_6 , 300.13 MHz, [ppm]): δ = 4.13 (s, 1H, -OH); 8.14-8.21 (m, 2H, *m*-CH); 8.60-8.67 (m, 1H, *p*-CH); 9.03-9.09 (m, 2H, *o*-CH). ¹³C-NMR(298 K, DMSO- d_6 , 75.46 MHz, [ppm]): δ = 26.18-28.21 (s, CD₂-CD₂-O- + N-CD₂-CD₂-); 58.86-61.27 (m, N-CD₂-CD₂- + CD₂-CD₂-O-); 119.43 (q, C F₃); 127.67 (s, *m*-CH); 144.65 (s, *p*-CH); 145.46 (s, *o*-CH).

1-(4-Hydroxybutyl)-pyridinium-bis(trifluoromethylsulfonyl)imide- d_{13} (22):

¹H-NMR(298.2 K, DMSO- d_6 , 300.13 MHz, [ppm]): δ = 4.13 (s, 1H, -OH). ¹³C-NMR(298 K, DMSO- d_6 , 75.46 MHz, [ppm]): δ = 26.18-28.21 (s, CD₂-CD₂-O- + N-CD₂-CD₂-); 58.86-61.27 (m, N-CD₂-CD₂- + CD₂-CD₂-O-); 119.43 (q, C F₃); 126.76-128.00 (m, *m*-CH); 143.53-145.57 (m, *p*-CH + *o*-CH).

A.1.17. Synthesis of 1-(4-Hydroxybutyl)-pyridinium-bis(trifluoromethylsulfonyl)imide- d_{x+y} [HOC₄Py]NTf₂- d_{x+y+1}



1-(4-Hydroxybutyl)-pyridinium-bromide- d_{x+y} was solved in a few milliliters H₂O. This solution was added to an equimolar aqueous solution of LiNTf₂. The mixture was stirred for 1h. During this time two phases were formed. The lower phase was washed several times with water until no residual bromine could be detected with silver nitrate solution. The thus obtained colourless liquid was dried for 6 h at 60 °C in vacuum ($1 \cdot 10^{-6}$ mbar). Yield: 90 %.

1-(4-Hydroxybutyl)-pyridinium-bis(trifluoromethylsulfonyl)imide- d_1 (19):

¹H-NMR(298.2 K, DMSO- d_6 , 300.13 MHz, [ppm]): δ = 1.41 (tt, 2H, CH₂-CH₂-O-); 1.96 (tt, 2H, N-CH₂-CH₂-); 3.41 (t, 2H, CH₂-CH₂-O-); 4.68 (t, 2H, N-CH₂-CH₂-); 8.14-8.21 (m, 2H, *m*-CH); 8.60-8.67 (m, 1H, *p*-CH); 9.03-9.09 (m, 2H, *o*-CH). ¹³C-NMR(298 K, DMSO- d_6 , 75.46 MHz, [ppm]): δ = 26.36 (s, CH₂-CH₂-O-); 27.34 (s, N-CH₂-CH₂-); 58.96 (s, N-CH₂-CH₂-); 60.19 (s, CH₂-CH₂-O-); 119.43 (q, C F₃); 127.67 (s, *m*-CH); 144.65 (s, *p*-CH); 145.46 (s, *o*-CH).

1-(4-Hydroxybutyl)-pyridinium-bis(trifluoromethylsulfonyl)imide- d_6 :

¹H-NMR(298.2 K, DMSO- d_6 , 300.13 MHz, [ppm]): δ = 1.41 (tt, 2H, CH₂-CH₂-O-); 1.96 (tt, 2H, N-CH₂-CH₂-); 3.41 (t, 2H, CH₂-CH₂-O-); 4.68 (t, 2H, N-CH₂-CH₂-). ¹³C-NMR(298 K, DMSO- d_6 , 75.46 MHz, [ppm]): δ = 26.36 (s, CH₂-CH₂-O-); 27.34 (s, N-CH₂-CH₂-); 58.96 (s, N-CH₂-CH₂-); 60.19 (s, CH₂-CH₂-O-); 119.43 (q, C F₃); 126.76-128.00 (m, *m*-CD); 143.53-145.57 (s, *p*-CD + *o*-CD).

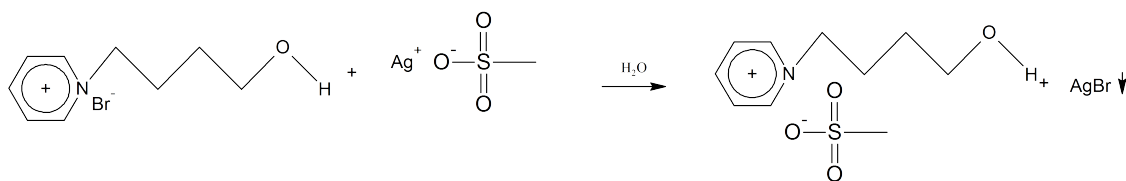
1-(4-Hydroxybutyl)-pyridinium-bis(trifluoromethylsulfonyl)imide- d_9 (21):

¹H-NMR(298.2 K, DMSO- d_6 , 300.13 MHz, [ppm]): δ = 8.14-8.21 (m, 2H, *m*-CH); 8.60-8.67 (m, 1H, *p*-CH); 9.03-9.09 (m, 2H, *o*-CH). ¹³C-NMR(298 K, DMSO- d_6 , 75.46 MHz, [ppm]): δ = 26.18-28.21 (s, CD₂-CD₂-O- + N-CD₂-CD₂-); 58.86-61.27 (m, N-CD₂-CD₂- + CD₂-CD₂-O-); 119.43 (q, C F₃); 127.67 (s, *m*-CH); 144.65 (s, *p*-CH); 145.46 (s, *o*-CH).

1-(4-Hydroxybutyl)-pyridinium-bis(trifluoromethylsulfonyl)imide- d_{14} (22):

¹³C-NMR(298 K, DMSO- d_6 , 75.46 MHz, [ppm]): δ = 26.18-28.21 (s, CD₂-CD₂-O- + N-CD₂-CD₂-); 58.86-61.27 (m, N-CD₂-CD₂- + CD₂-CD₂-O-); 119.43 (q, C F₃); 126.76-128.00 (m, *m*-CH); 143.53-145.57 (m, *p*-CH + *o*-CH).

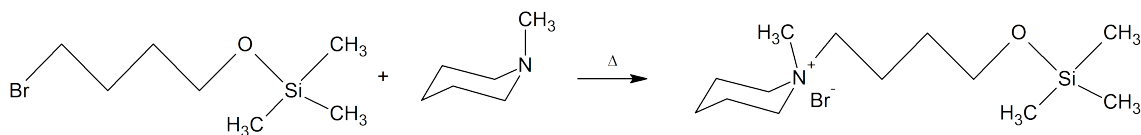
A.1.18. Synthesis of 1-(4-Hydroxybutyl)-pyridinium-methanesulfonate [HOC₄Py]OMs (17)



10.021 g ([HOC₄Py][Br]) (43 mmol) solved in 300 ml H₂O were titrated dropwise with the equimolar of an aqueous silver-methanesulfonate solution. The equivalence point is reached as soon as an additional drop of silver-methanesulfonate solution no longer leads to precipitation. To remove the precipitated AgBr the suspension was then filtered. Small volumes of the resulting colorless solution were then tested with AgNO₃ and NaCl solution, the absence of any precipitation indicates that there are no residual educts. The water in the remaining solution was then removed with the help of a rotation evaporator. The obtained colourless liquid of ([HOC₄Py][OMs]) was dried for 8 h in vacuum at 60 °C. Yield 94 %.

¹H-NMR(298.2 K, DMSO-d₆, 300.13 MHz, [ppm]): δ = 1.41 (tt, 2H, CH₂-CH₂-O-); 1.96 (tt, 2H, N-CH₂-CH₂-); 2.33 (s, 3H, SO₃CH₃); 3.42 (t, 2H, CH₂-CH₂-O-); 4.58 (s, 1H, -OH); 4.64 (t, 2H, N-CH₂-CH₂-); 8.14-8.21 (m, 2H, *m*-CH); 8.60-8.67 (m, 1H, *p*-CH); 9.03-9.09 (m, 2H, *o*-CH). ¹³C-NMR(298 K, DMSO-d₆, 75.46 MHz, [ppm]): δ = 27.77 (s, CH₂-CH₂-O-); 28.67 (s, N-CH₂-CH₂-); 39.76(s, SO₃CH₃); 59.88 (s, N-CH₂-CH₂-); 60.69 (s, CH₂-CH₂-O-); 128.08 (s, *m*-CH); 144.81 (s, *p*-CH); 145.46 (s, *o*-CH).

A.1.19. Synthesis of 1-(4-Trimethylsiloxybutyl)-methylpiperidinium-bromide [TMSOC₄MPip]Br (13 (a))

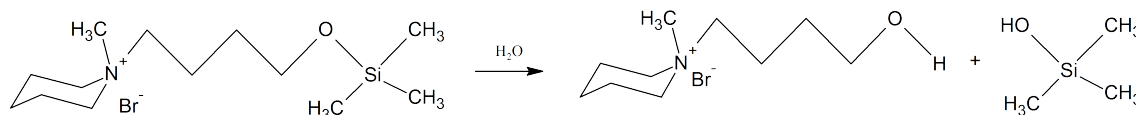


17.386 g of N-methylpiperidine (175 mmol) and 39.481 g of 4-Bromo-1-trimethylsiloxybutane (175 mmol) were mixed at room temperature and heated slowly up to round about 100 °C - 110 °C. When the reaction begins, the solution starts to cloud. After a few minutes two phases are formed, the lower one is yellow and the upper one is colorless. After about 5 h only one yellow phase is obtained. All volatiles were removed in vacuum. The crude product was cooled to room temperature whereby it starts to crystallize. Yield 70 %.

¹H-NMR(298.2 K, DMSO-d₆, 300.13 MHz, [ppm]): δ = 0.08 (s, 9H, -Si(CH₃)); 1.41-1.58 (m, 4H, N-C₂-CH₂-CH₂-); 1.61-1.72 (m, 2H, C(4)H₂); 1.72-1.84 (m, 4H, C(3);

5) H_2); 3.01 (s, 3H, CH_3); 3.30-3.43 (m, 6H, $C(2; 6)H_2 + N-CH_2-C_2-$); 3.58 (td, 2H, C_2-CH_2-O-).

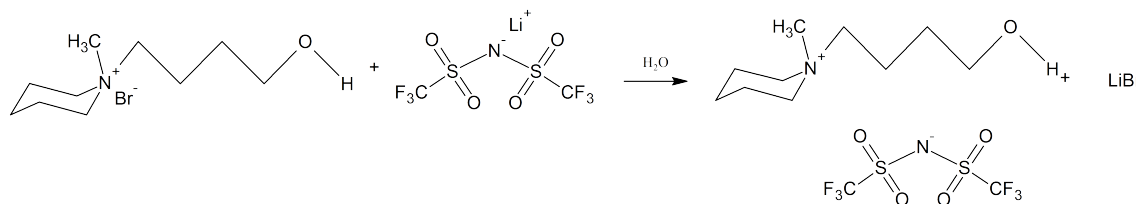
A.1.20. Synthesis of 1-(4-Hydroxybutyl)-methylpiperidinium-bromide [HOC_4MPip]Br (13 (b))



1-(4-Trimethylsiloxybutyl)-1-methylpiperidinium-bromide was dissolved in a tenfold excess of H_2O . The solution was stirred for 4 h at 80 °C. Two phases were formed. All volatiles were removed in vacuum. The procedure was repeated to remove all trimethylsilyl residuals. The crude product was cooled to room temperature whereby it starts to crystallize. The almost colourless crystalline crude product was recrystallized from a small amount of an 1:1 acetonitrile:acetone mixture. Yield 85 %.

1H -NMR(298.2 K, $DMSO-d_6$, 300.13 MHz, [ppm]): δ = 1.38-1.58 (m, 4H, $N-C_2-CH_2-CH_2-$); 1.63-1.73 (m, 2H, $C(4)H_2$); 1.72-1.83 (m, 4H, $C(3; 5)H_2$); 3.00 (s, 3H, CH_3); 3.30-3.39 (m, 6H, $C(2; 6)H_2 + N-CH_2-C_2-$); 3.44 (td, 2H, C_2-CH_2-OH); 4.57 (t, 1H, C_2-C_2-OH). ^{13}C -NMR(298 K, $DMSO-d_6$, 75.46 MHz, [ppm]): δ = 17.93 (s, $N-C_2-C_2-$); 19.25 (s, $C(3; 5)$); 20.66 (s, $C(4)$); 29.13 (s, C_2-C_2-OH); 47.01 (s, CH_3); 51.88 (s, C_2-C_2-OH); 59.84 (s, $C(2; 6)$); 62.16 (s, $N-C_2-C_2-$).

A.1.21. Synthesis of 1-(4-Hydroxybutyl)-methylpiperidinium-bis(trifluoromethylsulfonyl)imide [HOC_4MPip]NTf₂ (13 (c))

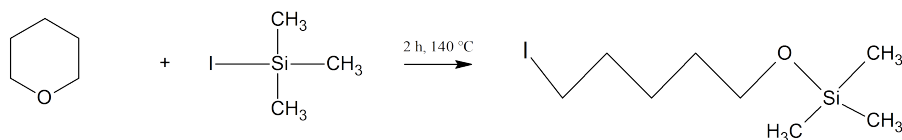


1-(4-Hydroxybutyl)-1-methylpiperidinium-bromide was dissolved in a few milliliters H_2O . This solution was added to an equimolar aqueous solution of $LiNTf_2$. The mixture was stirred for 1h. During this time two phases were formed. The lower phase was washed several times with water until no residual bromine could be detected with silver nitrate solution. The thus obtained colourless liquid was dried for 6 h at 60 °C in vacuum ($1 \cdot 10^{-6}$ mbar). Yield: 93 %.

1H -NMR(298.2 K, $DMSO-d_6$, 300.13 MHz, [ppm]): δ = 1.38-1.58 (m, 4H, $N-CH_2-CH_2-CH_2-$); 1.63-1.73 (m, 2H, $C(4)H_2$); 1.72-1.83 (m, 4H, $C(3; 5)H_2$); 2.97 (s, 3H, CH_3);

3.25-3.39 (m, 6H, C(2; 6) H_2 + N- CH_2 - CH_2 -); 3.39-3.50 (m, 2H, CH_2 - CH_2 -OH); 4.56 (t, 1H, CH_2 - CH_2 -OH. ^{13}C -NMR(298 K, DMSO- d_6 , 75.46 MHz, [ppm]): δ = 17.93 (s, N- CH_2 - CH_2 -); 19.25 (s, C(3; 5)); 20.66 (s, C(4)); 29.13 (s, CH_2 - CH_2 -OH); 47.01 (s, CH_3); 51.88 (s, CH_2 - CH_2 -OH); 59.84 (s, C(2; 6)); 62.16 (s, N- CH_2 - CH_2 -); 119.54 (q, CF_3). ^{19}F -NMR(298,2 K, DMSO- d_6 , 282.40 MHz, [ppm]): δ = -78.79 (s, CF_3).

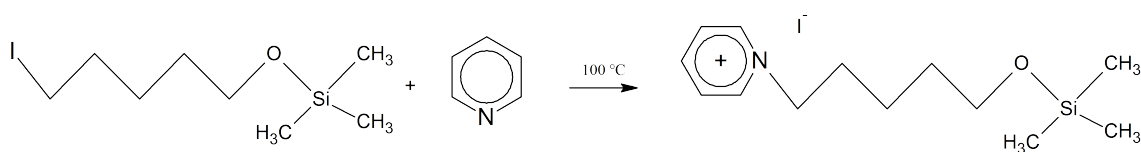
A.1.22. Synthesis of 5-Iodo-1-trimethylsiloxypentane TMSOC₅I (11 (a))



50 g Iodotrimethylsilane (250 mmol) and 21.523 g Tetrahydropyran were mixed at room temperature. The mixture was heated up to 140 °C and kept at this temperature for two hours. Within this time the solution turns reddish. The mixture was cooled to room temperature. The thus obtained crude product was then purified by distillation in vacuum (3 mbar; 87 °C). The product was obtained as a pale yellowish liquid. Yield 81 %.

1H -NMR(298.2 K, DMSO- d_6 , 300.13 MHz, [ppm]): δ = 0.06 (s, 9H, -Si(CH_3)₃); 1.23-1.53 (m, 4H, - CH_2 - CH_2 - CH_2 -O); 1.64-1.86 (m, 2H, I- CH_2 - CH_2 -); 3.19-3.58 (m, 4H, CH_2 - CH_2 -O- + I- CH_2 - CH_2 -). ^{13}C -NMR(298 K, DMSO- d_6 , 75.46 MHz, [ppm]): δ = 1.96 (s, -Si(CH_3)₃); 8.96 (s, - CH_2 - CH_2 - CH_2 -O); 26.51 (s, CH_2 - CH_2 -O-); 31.32 (s, I- CH_2 - CH_2 -); 32.79 (s, I- CH_2 - CH_2 -); 60.45 (s, CH_2 - CH_2 -O-).

A.1.23. Synthesis of 1-(5-Trimethylsiloxypentyl)-pyridinium-iodide [TMSOC₅Py]⁺I⁻ (11 (b))

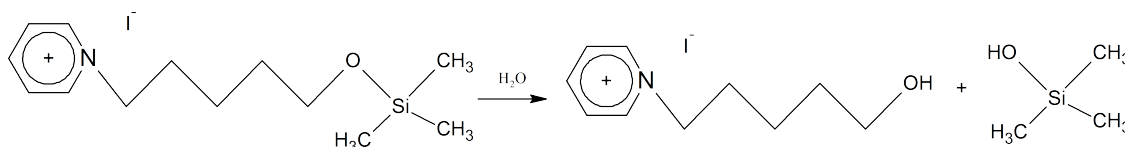


Equimolar amounts of pyridine (7.3586 g; 93 mmol) and 5-Iodo-1-trimethylsiloxypentane (26.6267 g; 93 mmol) were mixed at room temperature and heated slowly up to round about 100 °C - 110 °C. When the reaction begins, the solution starts to cloud. After a few minutes two phases are formed, the lower one is yellow and the upper one is colourless. After about 4 h only one yellow phase is obtained. All volatiles were removed in vacuum. The crude product was cooled to room temperature. Yield 89 %.

1H -NMR(298.2 K, DMSO- d_6 , 300.13 MHz, [ppm]): δ = 0.03 (s, 9H, -Si(CH_3)₃); 1.23-1.35 (m, 2H, - CH_2 - CH_2 - CH_2 -O); 1.37-1.50 (m, 2H, - CH_2 - CH_2 - CH_2 -O); 1.86-2.00

(m, 2H, N-CH₂-CH₂-); 3.37 (t, 2H, CH₂-CH₂-O-); 4.62 (t, 2H, N-CH₂-CH₂-); 8.13-8.21 (m, 2H, *m*-CH); 8.58-8.66 (m, 1H, *p*-CH); 9.09-9.17 (m, 2H, *o*-CH). ¹³C-NMR(298 K, DMSO-d₆, 75.46 MHz, [ppm]): δ = 1.96 (s, -Si(CH₃)₃); 21.98 (s, -CH₂-CH₂-CH₂-O); 30.47 (s, CH₂-CH₂-O-); 31.62 (s, I-CH₂-CH₂-); 60.16 (s, N-CH₂-CH₂-); 60.70 (s, CH₂-CH₂-O-); 128.04 (s, *m*-CH); 144.62 (s, *p*-CH); 145.41 (s, *o*-CH).

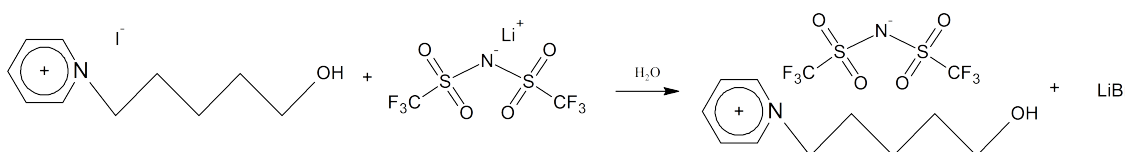
A.1.24. Synthesis of 1-(5-Hydroxypentyl)-pyridinium-iodide [HOC₅Py]I (11 (c))



1-(5-Trimethylsiloxy)pentyl-pyridinium-iodide was dissolved in a tenfold excess of H₂O. The solution was stirred for 4 h at 80 °C. Two phases were formed. All volatiles were removed in vacuum. The procedure was repeated to remove all trimethylsilyl residuals. The crude product was cooled to room temperature whereby it starts to crystallize. The yellowish crystalline crude product was recrystallized from an 1:2 acetonitrile/acetone mixture. Yield 77 %.

¹H-NMR(298.2 K, DMSO-d₆, 300.13 MHz, [ppm]): δ = 1.23-1.35 (m, 2H, -CH₂-CH₂-CH₂-O); 1.37-1.50 (m, 2H, -CH₂-CH₂-CH₂-O); 1.86-2.00 (m, 2H, N-CH₂-CH₂-); 3.37 (t, 2H, CH₂-CH₂-O-); 4.35 (t, 1H, -OH); 4.62 (t, 2H, N-CH₂-CH₂-); 8.13-8.21 (m, 2H, *m*-CH); 8.58-8.66 (m, 1H, *p*-CH); 9.09-9.17 (m, 2H, *o*-CH). ¹³C-NMR(298 K, DMSO-d₆, 75.46 MHz, [ppm]): δ = 21.98 (s, -CH₂-CH₂-CH₂-O); 30.47 (s, CH₂-CH₂-O-); 31.62 (s, N-CH₂-CH₂-); 60.16 (s, N-CH₂-CH₂-); 60.70 (s, CH₂-CH₂-O-); 128.04 (s, *m*-CH); 144.62 (s, *p*-CH); 145.41 (s, *o*-CH).

A.1.25. Synthesis of 1-(5-Hydroxypentyl)-pyridinium-bis(trifluoromethylsulfonyl)imide [HOC₅Py]NTf₂ (11)

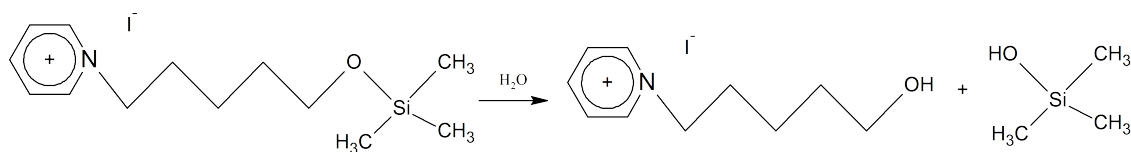


10.021 g ([HOC₄Py][Cl]) (43 mmol) solved in 300 ml H₂O were titrated dropwise with the equimolar of an aqueous silver-methanesulfonate solution. The equivalence point is reached as soon as an additional drop of silver-methanesulfonate solution no longer leads to precipitation. To remove the precipitated AgCl the suspension was then filtered. Small volumes of the resulting colourless solution were then tested with

AgNO₃ and NaCl solution, the absence of any precipitation indicates that there are no residual educts. The water in the remaining solution was then removed whit the help of a rotation evaporator The obtained colourless liquid of ([HOC₄Py][OMs]) was dried for 8 h in vacuum at 60 °C. Yield 89 %.

¹H-NMR(298.2 K, DMSO-d₆, 300.13 MHz, [ppm]): δ = 1.23-1.35 (m, 2H, -CH₂-CH₂-CH₂-O); 1.37-1.50 (m, 2H, -CH₂-CH₂-CH₂-O); 1.86-2.00 (m, 2H, N-CH₂-CH₂-); 3.37 (t, 2H, CH₂-CH₂-O-); 4.39 (t, 1H, -OH); 4.62 (t, 2H, N-CH₂-CH₂-); 8.13-8.21 (m, 2H, *m*-CH); 8.58-8.66 (m, 1H, *p*-CH); 9.09-9.17 (m, 2H, *o*-CH). ¹³C-NMR(298 K, DMSO-d₆, 75.46 MHz, [ppm]):δ = 21.98 (s, -CH₂-CH₂-CH₂-O); 30.47 (s, CH₂-CH₂-O-); 31.62 (s, N-CH₂-CH₂-); 60.16 (s, N-CH₂-CH₂-); 60.70 (s, CH₂-CH₂-O-); 119.43 (q, C F₃); 128.04 (s, *m*-CH); 144.62 (s, *p*-CH); 145.41 (s, *o*-CH).

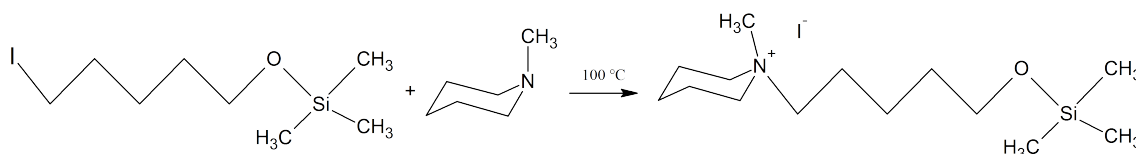
A.1.26. Synthesis of 1-(5-Hydroxypentyl)-pyridinium-methanesulfonate [HOC₅Py]OMs (18)



15.531 g ([HOC₅Py][I]) (53 mmol) dissolved in 300 ml H₂O were titrated dropwise with the equimolar of an aqueous silver-methanesulfonate solution. The equivalence point is reached as soon as an additional drop of silver-methanesulfonate solution no longer leads to precipitation. To remove the precipitated AgI the suspension was then filtered. Small volumes of the resulting colourless solution were then tested with AgNO₃ and NaCl solution, the absence of any precipitation indicates that there are no residual educts. The water in the remaining solution was then removed whit the help of a rotation evaporator The obtained colourless liquid of ([HOC₅Py][OMs]) was dried for 8 h in vacuum at 60 °C. Yield 94 %.

¹H-NMR(298.2 K, DMSO-d₆, 300.13 MHz, [ppm]): δ = 1.23-1.37 (m, 2H, -CH₂-CH₂-CH₂-O); 1.37-1.50 (m, 2H, -CH₂-CH₂-CH₂-O); 1.86-2.00 (m, 2H, N-CH₂-CH₂-); 2.33 (s, 3H, SO₃CH₃); 3.37 (t, 2H, CH₂-CH₂-O-); 4.35 (t, 1H, -OH); 4.62 (t, 2H, N-CH₂-CH₂-); 8.13-8.21 (m, 2H, *m*-CH); 8.58-8.66 (m, 1H, *p*-CH); 9.09-9.17 (m, 2H, *o*-CH). ¹³C-NMR(298 K, DMSO-d₆, 75.46 MHz, [ppm]):δ = 22.05 (s, -CH₂-CH₂-CH₂-O); 30.53 (s, CH₂-CH₂-O-); 31.67 (s, N-CH₂-CH₂-); 39.76(s, SO₃CH₃); 60.20 (s, N-CH₂-CH₂-); 60.73 (s, CH₂-CH₂-O-); 128.08 (s, *m*-CH); 144.69 (s, *p*-CH); 145.46 (s, *o*-CH).

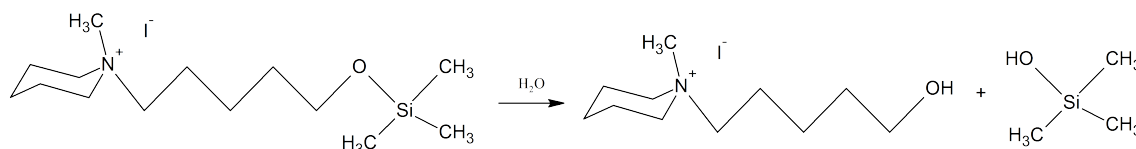
A.1.27. Synthesis of 1-(5-Trimethylsiloxypentyl)-methylpiperidinium-iodide [TMSOC₅MPip]I (14 (b))



Equimolar amounts of N-methylpiperidine (15.859 g; 160 mmol) and 5-Iodo-1-trimethylsiloxypentane (45.770 g; 160 mmol) were mixed at room temperature and heated slowly up to round about 140 °C. When the reaction begins, the solution starts to cloud. After a few minutes two phases are formed, the lower one is yellow and the upper one is colorless. After about 1 h only one yellow phase is obtained. While cooling to room temperature the crude product starts to crystallize. Yield 96 %.

¹H-NMR(298.2 K, DMSO-d₆, 300.13 MHz, [ppm]): δ = 0.07 (s, 9H, -Si(CH₃)₃); 1.27-1.35 (m, 2H, -CH₂-CH₂-CH₂-O); 1.43-1.50 (m, 2H, -CH₂-CH₂-CH₂-O); 1.49-1.59 (m, 2H, N-CH₂-CH₂-); 1.61-1.71 (m, 2H, C(4)H₂); 1.73-1.83 (m, 4H, C(3; 5)H₂); 3.00 (s, 3H, CH₃); 3.27-3.35 (m, 6H, C(2; 6)H₂ + N-CH₂-CH₂-); 3.40 (t, 2H, CH₂-CH₂-O-).

A.1.28. Synthesis of 1-(5-Hydroxypentyl)-methylpiperidinium-iodide [HOC₅MPip]I (14 (c))

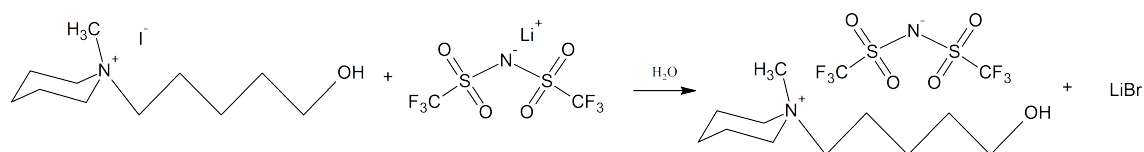


1-(5-Trimethylsiloxypentyl)-methylpiperidinium-iodide was dissolved in a tenfold excess of H₂O. The solution was stirred for 4 h at 80 °C. Two phases were formed. All volatiles were removed in vacuum. The procedure was repeated to remove all trimethylsilyl residuals. The crude product was dried for 6 h at 60 °C in vacuum (1 · 10⁻⁶ mbar). The yellowish crude product was obtained in 77 % yield.

¹H-NMR(298.2 K, DMSO-d₆, 300.13 MHz, [ppm]): δ = 1.27-1.35 (m, 2H, -CH₂-CH₂-O); 1.43-1.50 (m, 2H, -CH₂-CH₂-CH₂-O); 1.49-1.59 (m, 2H, N-CH₂-CH₂-); 1.61-1.71 (m, 2H, C(4)H₂); 1.73-1.83 (m, 4H, C(3; 5)H₂); 3.00 (s, 3H, CH₃); 3.27-3.35 (m, 6H, C(2; 6)H₂ + N-CH₂-CH₂-); 3.40 (t, 2H, CH₂-CH₂-O-); 4.35 (t, 1H, -OH).

¹³C-NMR(298 K, DMSO-d₆, 75.46 MHz, [ppm]): δ = 19.23 (s, C(3; 5)); 20.63 (s, C(4)); 20.79 (s, -CH₂-CH₂-CH₂-O); 22.46 (s, CH₂-CH₂-O-); 31.78 (s, N-CH₂-CH₂-); 46.99 (s, CH₃); 59.87 (s, N-CH₂-CH₂-); 60.22 (s, CH₂-CH₂-O-); 62.38 (s, C(2; 6)).

A.1.29. Synthesis of 1-(5-Hydroxypentyl)-methylpiperidinium-bis(trifluoromethylsulfonyl)imide [HOC_5Py] NTf_2 (14)



17.16 g 1-(5-Hydroxypentyl)-methylpiperidinium-iodide (44.52 mmol) were solved in a few milliliters H_2O . This solution was added to an equimolar aqueous solution of LiNTf_2 (12.783 g; 44.52 mmol). The mixture was stirred for 1 h. During this time two phases were formed. The lower phase was washed several times with water until no residual iodine could be detected with silver nitrate solution. The thus obtained pale yellowish liquid was dried for 6 h at 60 °C in vacuum ($1 \cdot 10^{-6}$ mbar). Yield: 82 %.

$^1\text{H-NMR}$ (298.2 K, DMSO-d_6 , 300.13 MHz, [ppm]): δ = 1.27-1.35 (m, 2H, $-\text{CH}_2-\text{CH}_2-\text{O}$); 1.43-1.50 (m, 2H, $-\text{CH}_2-\text{CH}_2-\text{CH}_2-\text{O}$); 1.49-1.59 (m, 2H, $\text{N-CH}_2-\text{CH}_2-$); 1.61-1.71 (m, 2H, C(4)H_2); 1.73-1.83 (m, 4H, C(3; 5)H_2); 3.00 (s, 3H, CH_3); 3.27-3.35 (m, 6H, $\text{C(2; 6)H}_2 + \text{N-CH}_2-\text{CH}_2-$); 3.40 (t, 2H, $\text{CH}_2-\text{CH}_2-\text{O}-$); 4.39 (t, 1H, $-\text{OH}$).
 $^{13}\text{C-NMR}$ (298 K, DMSO-d_6 , 75.46 MHz, [ppm]): δ = 19.23 (s, C(3; 5)); 20.63 (s, C(4)); 20.79 (s, $-\text{CH}_2-\text{CH}_2-\text{CH}_2-\text{O}$); 22.46 (s, $\text{CH}_2-\text{CH}_2-\text{O}-$); 31.78 (s, $\text{N-CH}_2-\text{CH}_2-$); 46.99 (s, CH_3); 59.87 (s, $\text{N-CH}_2-\text{CH}_2-$); 60.22 (s, $\text{CH}_2-\text{CH}_2-\text{O}-$); 62.38 (s, C(2; 6)); 119.43 (q, C F_3).

Bibliography

- [1] F. Endres. Ionische flüssigkeiten in der elektrochemischen abscheidung – potenzial und herausforderungen. *Chem. Ing. Tech.*, 83:1485–1492, 2011.
- [2] F. Endres, N. Borisenko, R. Al Salman, M. Al Zoubi, A. Prowald, T. Carstens, and S. Z. El Abedin. *Electrodeposition from Ionic Liquids: Interface Processes, Ion Effects, and Macroporous Structures*, chapter 1, pages 1–27. John Wiley & Sons, Ltd, 2012.
- [3] J. S. Wilkes. A short history of ionic liquids—from molten salts to neoteric solvents. *Green Chem.*, 4:73–80, 2002.
- [4] T. Welton. Room-temperature ionic liquids. solvents for synthesis and catalysis. *Chem. Rev.*, 99:2071–2084, 1999.
- [5] K. Fumino and R. Ludwig. Analyzing the interaction energies between cation and anion in ionic liquids: The subtle balance between coulomb forces and hydrogen bonding. *J. Mol. Liq.*, 192:94 – 102, 2014.
- [6] K. Fumino, S. Reimann, and R. Ludwig. Probing molecular interaction in ionic liquids by low frequency spectroscopy: Coulomb energy, hydrogen bonding and dispersion forces. *Phys. Chem. Chem. Phys.*, 16:21903–21929, 2014.
- [7] K. Fumino, A. Wulf, and R. Ludwig. Strong, localized, and directional hydrogen bonds fluidize ionic liquids. *Angew. Chem. Int. Ed.*, 47:8731–8734, 2008.
- [8] K. Fumino, A. Wulf, and R. Ludwig. Starke, lokalisierte und gerichtete h-brücken machen ionische flüssigkeiten beweglicher. *Angew. Chem.*, 120:8859–8862, 2008.
- [9] K. Fumino, T. Peppel, M. Geppert-Rybczyńska, D. H. Zaitsau, J. K. Lehmann, S. P. Verevkin, M. Köckerling, and R. Ludwig. The influence of hydrogen bonding on the physical properties of ionic liquids. *Phys. Chem. Chem. Phys.*, 13:14064–14075, 2011.
- [10] J. Smid. Structure of ion pair solvation complexes. *Angew. Chem. Int. Ed.*, 11:112–127, 1972.
- [11] J. Smid. Die struktur solvatisierter ionenpaare. *Angew. Chem.*, 84:127–144, 1972.
- [12] C. Reichardt and T. Welton. *Solvents and Solvent Effects in Organic Chemistry*. Wiley-VCH, oct 2010.

- [13] Y. Marcus and G. Hefter. Ion pairing. *Chem. Rev.*, 106:4585–4621, 2006.
- [14] M. Holz and K. J. Patil. Cation-cation association of tetramethylammonium ions in aqueous mixed electrolyte solutions. *Ber. Bunsenges. Phys. Chem.*, 95:107–113, 1991.
- [15] O. Shih, A. H. England, G. C. Dallinger, J. W. Smith, K. C. Duffey, R. C. Cohen, D. Prendergast, and R. J. Saykally. Cation-cation contact pairing in water: Guanidinium. *J. Chem. Phys.*, 139:035104, 2013.
- [16] M. Benrraou, B. L. Bales, and R. Zana. Effect of the nature of the counterion on the properties of anionic surfactants. 1. cmc, ionization degree at the cmc and aggregation number of micelles of sodium, cesium, tetramethylammonium, tetraethylammonium, tetrapropylammonium, and tetrabutylammonium dodecyl sulfates. *J. Phys. Chem. B*, 107:13432–13440, 2003.
- [17] A. E. Larsen and D. G. Grier. Like-charge attractions in metastable colloidal crystallites. *Nature*, 385:230–233, 1997.
- [18] M. R. Caplan, P. N. Moore, S. Zhang, R. D. Kamm, and D. A. Lauffenburger. Self-assembly of a β -sheet protein governed by relief of electrostatic repulsion relative to van der waals attraction. *Biomacromolecules*, 1:627–631, 2000.
- [19] M. Kuron and A. Arnold. Role of geometrical shape in like-charge attraction of dna. *Eur. Phys. J. E Soft Matter*, 38:20, 2015.
- [20] S. B. C. Lehmann, M. Roatsch, M. Schöppke, and B. Kirchner. On the physical origin of the cation–anion intermediate bond in ionic liquids part i. placing a (weak) hydrogen bond between two charges. *Phys. Chem. Chem. Phys.*, 12:7473–7486, 2010.
- [21] A. S. Pensado, M. F. C. Gomes, J. N. C. Lopes, P. Malfreyt, and A. A. H. Pádua. Effect of alkyl chain length and hydroxyl group functionalization on the surface properties of imidazolium ionic liquids. *Phys. Chem. Chem. Phys.*, 13:13518–13526, 2011.
- [22] P. A. Hunt, C. R. Ashworth, and R. P. Matthews. Hydrogen bonding in ionic liquids. *Chem. Soc. Rev.*, 44:1257–1288, 2015.
- [23] C. R. Ashworth, R. P. Matthews, T. Welton, and P. A. Hunt. Doubly ionic hydrogen bond interactions within the choline chloride–urea deep eutectic solvent. *Phys. Chem. Chem. Phys.*, 18:18145–18160, 2016.
- [24] A. Knorr, K. Fumino, A.-M. Bónsa, and R. Ludwig. Spectroscopic evidence of ‘jumping and pecking’ of cholinium and h-bond enhanced cation–cation interaction in ionic liquids. *Phys. Chem. Chem. Phys.*, 17:30978–30982, 2015.

- [25] A. Knorr and R. Ludwig. Cation-cation clusters in ionic liquids: Cooperative hydrogen bonding overcomes like-charge repulsion. *Sci. Rep.*, 5:17505, 2015.
- [26] A. Knorr, P. Stange, K. Fumino, F. Weinhold, and R. Ludwig. Spectroscopic evidence for clusters of like-charged ions in ionic liquids stabilized by cooperative hydrogen bonding. *ChemPhysChem*, 17:458–462, 2016.
- [27] A. Strate, T. Niemann, and R. Ludwig. Controlling the kinetic and thermodynamic stability of cationic clusters by the addition of molecules or counterions. *Phys. Chem. Chem. Phys.*, 19:18854–18862, 2017.
- [28] P. Walden. Ueber die molekulargroesse und elektrische leitfaehigkeit einiger geschmolzenen salze. *Bull. Acad. Imper. Sci.*, 8:405, 1914.
- [29] J. Verron, J.-M. Joerger, M. Pucheault, and M. Vaultier. Task specific onium salts (tsoss) as efficient soluble supports for zard radical addition to olefins. *Tetrahedron Lett.*, 48:4055 – 4058, 2007.
- [30] A. S. Shaplov, E. I. Lozinskaya, D. O. Ponkratov, I. A. Malyshkina, F. Vidal, P.-H. Aubert, O. V. Okatova, G. M. Pavlov, L. I. Komarova, C. Wandrey, and Y. S. Vygodskii. Bis(trifluoromethylsulfonyl)amide based “polymeric ionic liquids”: Synthesis, purification and peculiarities of structure–properties relationships. *Electrochim. Acta*, 57:74 – 90, 2011.
- [31] X. Yang, N. Yan, Z. Fei, R. M. Crespo-Quesada, G. Laurenczy, L. Kiwi-Minsker, Y. Kou, Y. Li, and P. J. Dyson. Biphasic hydrogenation over pvp stabilized rh nanoparticles in hydroxyl functionalized ionic liquids. *Inorg. Chem.*, 47:7444–7446, 2008.
- [32] J. H. Davis Jr., C. M. Gordon, C. Hilgers, and P. Wasserscheid. *Synthesis and Purification of Ionic Liquids*, chapter 2, pages 7–40. John Wiley & Sons, Ltd, 2003.
- [33] F. Deng, Z. K. Reeder, and K. M. Miller. 1,3-bis(2-hydroxyethyl)imidazolium ionic liquids: correlating structure and properties with anion hydrogen bonding ability. *J. Phys. Org. Chem.*, 27:2–9, 2014.
- [34] E. M. Erdni-Goryaev, A. Y. Alent’ev, A. S. Shaplov, D. O. Ponkratov, and E. I. Lozinskaya. New membrane materials based on crosslinked poly(ethylene glycols) and ionic liquids for separation of gas mixtures containing co₂. *Polym. Sci. Ser. B*, 56:900–908, 2014.
- [35] M. Koufaki, V. Polychroniou, T. Calogeropoulou, A. Tsotinis, M. Drees, H. H. Fiebig, S. LeClerc, H. R. Hendriks, and A. Makriyannis. Alkyl and alkoxyethyl antineoplastic phospholipids. *J. Med. Chem.*, 39:2609–2614, 1996.

- [36] Y. Dong, J. Holm, J. Kärkkäinen, J. Nowicki, and U. Lassi. Dissolution and hydrolysis of fibre sludge using hydroxyalkylimidazolium hydrogensulphate ionic liquids. *Biomass Bioenergy*, 70:461 – 467, 2014.
- [37] G. J. Navathe, D. S. Patil, P. R. Jadhav, D. V. Awale, A. M. Teli, S. C. Bhise, S. S. Kolekar, M. M. Karanjkar, J. H. Kim, and P. S. Patil. Rapid synthesis of nanostructured copper oxide for electrochemical supercapacitor based on novel [hpmim][cl] ionic liquid. *J. Electroanal. Chem.*, 738:170 – 175, 2015.
- [38] H. R. Kricheldorf, G. Mörber, and W. Regel. Syntheses of alkyl bromides from ethers and bromotrimethylsilane. *Synthesis*, 1981:383–384, 1981.
- [39] U. Krüerke. Halogen-austausch an chlorsilanen und die tetrahydrofuran-spaltung durch brom-und jodsilane. *Chem. Ber.*, 95:174–182, 1962.
- [40] S. Kirpichenko, L. Tolstikova, E. Suslova, A. Albanov, and M. Voronkov. Regioselectivity of radical cyclization of unsaturated organosilicon thiols. *PHOSPHORUS SULFUR.*, 106:47–53, 1995.
- [41] J. Ohshita, A. Iwata, F. Kanetani, A. Kunai, Y. Yamamoto, and C. Matui. Ring-opening iodo- and bromosilation of cyclic ethers by treatment with iodo- and bromotrialkylsilane equivalents. *J. Org. Chem.*, 64:8024–8026, 1999.
- [42] H. Poleschner, M. Heydenreich, and D. Martin. Cyclische ether als edukte zur synthese von schmetterlings-pheromonen. *Synthesis*, 1991:1231–1235, 1991.
- [43] S. Zhang, N. Sun, X. He, X. Lu, and X. Zhang. Physical properties of ionic liquids: Database and evaluation. *J. Phys. Chem. Ref. Data*, 35:1475–1517, 2006.
- [44] L. Cammarata, S. G. Kazarian, P. A. Salter, and T. Welton. Molecular states of water in room temperature ionic liquids. *Phys. Chem. Chem. Phys.*, 3:5192–5200, 2001.
- [45] J. S. Wilkes and M. J. Zaworotko. Air and water stable 1-ethyl-3-methylimidazolium based ionic liquids. *J. Chem. Soc., Chem. Commun.*, pages 965–967, 1992.
- [46] E. Leete. 2,3-dehydrococaine: Not a direct precursor of cocaine in erythroxylum coca. *J. Nat. Prod.*, 50:30–35, 1987.
- [47] A. Lewandowski and M. Galiński. Carbon–ionic liquid double-layer capacitors. *J. Phys. Chem. Solids*, 65:281 – 286, 2004.
- [48] E. J. Sekabunga, M. L. Smith, T. R. Webb, and W. E. Hill. Coordination chemistry of silver(i) with the nitrogen-bridged ligands: The effect of alkylating the nitrogen bridge on ligand bridging versus chelating behavior. *Inorg. Chem.*, 41:1205–1214, 2002.

- [49] P. Bonhôte, A. P. Dias, N. Papageorgiou, K. Kalyanasundaram, and M. Grätzel. Hydrophobic, highly conductive ambient-temperature molten salts. *Inorg. Chem.*, 35:1168–1178, 1996.
- [50] J. G. Huddleston, H. D. Willauer, R. P. Swatloski, A. E. Visser, and R. D. Rogers. Room temperature ionic liquids as novel media for ‘clean’ liquid–liquid extraction. *Chem. Commun.*, pages 1765–1766, 1998.
- [51] M. Blesic, M. Swadźba-Kwaśny, T. Belhocine, H. Q. N. Gunaratne, J. N. C. Lopes, M. F. C. Gomes, A. A. H. Pádua, K. R. Seddon, and L. P. N. Rebelo. 1-alkyl-3-methylimidazolium alkanesulfonate ionic liquids, [ch₂+1mim][ch₂+1so₃]: synthesis and physicochemical properties. *Phys. Chem. Chem. Phys.*, 11:8939–8948, 2009.
- [52] B.C. Smith. *Fundamentals of fourier transform infrared spectroscopy, second edition*. Theophanides, 01 2011.
- [53] G. Wedler and H.J. Freund. *Lehrbuch der Physikalischen Chemie*. Number Bd. 1 in Wiley VCH Lehrbuchkollektion 1. Wiley-VCH, 2012.
- [54] P. Nockemann, K. Binnemans, B. Thijs, T. N. Parac-Vogt, K. Merz, A.-V. Mudring, P. C. Menon, R. N. Rajesh, G. Cordoyiannis, J. Thoen, J. Leys, and C. Glorieux. Temperature-driven mixing-demixing behavior of binary mixtures of the ionic liquid choline bis(trifluoromethylsulfonyl)imide and water. *J. Phys. Chem. B*, 113:1429–1437, 2009.
- [55] P. G. Debenedetti and F. H. Stillinger. Supercooled liquids and the glass transition. *Nature*, 410:259–267, 2001.
- [56] A. K. Soper. *GudrunN and GudrunX Programs for correcting raw neutron and x-ray total scattering data to differential cross section*. ISIS, Rutherford Appleton Laboratory, Didcot, U. K., 2012.
- [57] M. A. Howe, R. L. McGreevy, and W. S. Howells. The analysis of liquid structure data from time-of-flight neutron diffractometry. *J. Phys.: Condens. Matter*, 1:3433–3451, 1989.
- [58] A. K. Soper. On the uniqueness of structure extracted from diffraction experiments on liquids and glasses. *J. Phys.: Condens. Matter*, 19:415108, 2007.
- [59] P. Schuster, G. C. Maitland, M. Rigby, E. B. Smith, and W. A. Wakeham. Intermolecular forces – their origin and determination. *Ber. Bunsenges. Phys. Chem.*, 87:291–292, 1983.
- [60] J. L. Calais. Theory of molecular fluids. volume 1: Fundamentals. by c. g. gray and k. e. gubbins, the clarendon press, oxford university press, new york, 1984. *Int. J. Quantum Chem.*, 38:497–497, 1990.

- [61] W. G. Hoover. Canonical dynamics: Equilibrium phase-space distributions. *Phys. Rev. A*, 31:1695–1697, 1985.
- [62] H. J. C. Berendsen, J. P. M. Postma, W. F. van Gunsteren, A. DiNola, and J. R. Haak. Molecular dynamics with coupling to an external bath. *J. Chem. Phys.*, 81:3684–3690, 1984.
- [63] S. Nosé. A molecular dynamics method for simulations in the canonical ensemble. *Mol. Phys.*, 52:255–268, 1984.
- [64] M. Parrinello and A. Rahman. Polymorphic transitions in single crystals: A new molecular dynamics method. *J. Appl. Phys.*, 52:7182–7190, 1981.
- [65] S. Nosé and M. L. Klein. Constant pressure molecular dynamics for molecular systems. *Mol. Phys.*, 50:1055–1076, 1983.
- [66] A. K. Soper. Partial structure factors from disordered materials diffraction data: An approach using empirical potential structure refinement. *Phys. Rev. B*, 72:104204, 2005.
- [67] S. E. Norman, A. H. Turner, and T. G. A. Youngs. Structure of ionic liquids with amino acid anions via neutron diffraction. *RSC Adv.*, 5:67220–67226, 2015.
- [68] A. K. Soper. *Empirical Potential Structure Refinement - A User's Guide*. ISIS, Rutherford Appleton Laboratory, Didcot, U. K., 2006.
- [69] C. J. Benmore and A. K. Soper. *The SANDALS Manual: A Guide to Performing Experiments on the Small Angle Neutron Diffractometer for Amorphous and Liquid Samples at ISIS.*, version1.0, ral technical reports, ral-tr-1998-1006 edition, 1998.
- [70] A. K. Soper, W. S. Howells, and A. C. Hannon. *ATLAS-Analysis of Time-of-Flight Diffraction Data from Liquid and Amorphous Samples*, ral-89-046 1989 edition, 1989.
- [71] R. Kanzaki, T. Mitsugi, S. Fukuda, K. Fujii, M. Takeuchi, Y. Soejima, T. Takamuku, T. Yamaguchi, Y. Umebayashi, and S. i. Ishiguro. Ion-ion interaction in room temperature ionic liquid 1-ethyl-3-methylimidazolium tetrafluoroborate studied by large angle x-ray scattering experiment and molecular dynamics simulations. *J. Mol. Liq.*, 147:77 – 82, 2009.
- [72] G. Ferru, L. Berthon, O. Diat, P. Bauduin, and P. Guilbaud. Elucidation of the structure of organic solutions in solvent extraction by combining molecular dynamics and x-ray scattering. *Angew. Chem. Int. Ed.*, 53:5346–5350, 2014.
- [73] G. Ferru, L. Berthon, O. Diat, P. Bauduin, and P. Guilbaud. Elucidation of the structure of organic solutions in solvent extraction by combining molecular dynamics and x-ray scattering. *Angew. Chem.*, 126:5450–5454, 2014.

- [74] K. M. Murdoch, T. D. Ferris, J. C. Wright, and T. C. Farrar. Infrared spectroscopy of ethanol clusters in ethanol–hexane binary solutions. *J. Chem. Phys.*, 116:5717–5724, 2002.
- [75] F. Huisken, A. Kulcke, C. Laush, and J. M. Lisy. Dissociation of small methanol clusters after excitation of the o–h stretch vibration at $2.7\ \mu$. *J. Chem. Phys.*, 95:3924–3929, 1991.
- [76] M. Hulsekopf and R. Ludwig. Hydrogen bonding in a sterically hindered alcohol. *J. Mol. Liq.*, 98-99:163 – 171, 2002.
- [77] R. Ludwig, F. Weinhold, and T. C. Farrar. Quantum cluster equilibrium theory of liquids: temperature dependent chemical shifts, quadrupole coupling constants and vibrational frequencies in liquid ethanol. *Mol. Phys.*, 97:479–486, 1999.
- [78] R. Ludwig, F. Weinhold, and T. C. Farrar. Quantum cluster equilibrium theory of liquids: molecular clusters and thermodynamics of liquid ethanol. *Mol. Phys.*, 97:465–477, 1999.
- [79] R. Ludwig. Hexamers: From covalently bound organic structures to hydrogen bonded water clusters. *ChemPhysChem*, 1:53–56, 2000.
- [80] R. Ludwig. The effect of hydrogen bonding on the thermodynamic and spectroscopic properties of molecular clusters and liquids. *Phys. Chem. Chem. Phys.*, 4:5481–5487, 2002.
- [81] A. B. Wolk, C. M. Leavitt, E. Garand, and M. A. Johnson. Cryogenic ion chemistry and spectroscopy. *Acc. Chem. Res.*, 47:202–210, 2014.
- [82] M. Z. Kamrath, E. Garand, P. A. Jordan, C. M. Leavitt, A. B. Wolk, M. J. Van Stipdonk, S. J. Miller, and M. A. Johnson. Vibrational characterization of simple peptides using cryogenic infrared photodissociation of h2-tagged, mass-selected ions. *J. Am. Chem. Soc.*, 133:6440–6448, 2011.
- [83] L. Drahos and K. Vékey. Masskinetics: a theoretical model of mass spectra incorporating physical processes, reaction kinetics and mathematical descriptions. *J. Mass Spectrom.*, 36:237–263, 2001.
- [84] C. M. Leavitt, A. B. Wolk, J. A. Fournier, M. Z. Kamrath, E. Garand, M. J. Van Stipdonk, and M. A. Johnson. Isomer-specific ir-ir double resonance spectroscopy of d2-tagged protonated dipeptides prepared in a cryogenic ion trap. *J. Phys. Chem. Lett.*, 3:1099–1105, 2012.
- [85] J. W. DePalma, P. J. Kelleher, L. C. Tavares, and M. A. Johnson. Coordination-dependent spectroscopic signatures of divalent metal ion binding to carboxylate head groups: H2- and he-tagged vibrational spectra of $m2+\cdot rco2-$ ($m = mg$ and ca , $r = -cd3$, $-cd2cd3$) complexes. *J. Phys. Chem. Lett.*, 8:484–488, 2017.

- [86] J. R. Roscioli, E. G. Diken, M. A. Johnson, S. Horvath, and A. B. McCoy. Prying apart a water molecule with anionic h-bonding: A comparative spectroscopic study of the x-h₂o (x = oh, o, f, cl, and br) binary complexes in the 600-3800 cm⁻¹ region. *J. Phys. Chem. A*, 110:4943–4952, 2006.
- [87] O. Gorlova, J. W. DePalma, C. T. Wolke, A. Brathwaite, T. T. Odbadrakh, K. D. Jordan, A. B. McCoy, and M. A. Johnson. Characterization of the primary hydration shell of the hydroxide ion with h₂ tagging vibrational spectroscopy of the oh-(h₂o)_{n=2,3} and od- (d₂o)_{n=2,3} clusters. *J. Chem. Phys.*, 145:134304, 2016.
- [88] W. H. Robertson, G. H. Weddle, J. A. Kelley, and M. A. Johnson. Solvation of the cl-h₂o complex in ccl₄ clusters: The effect of solvent-mediated charge redistribution on the ionic h-bond. *J. Phys. Chem. A*, 106:1205–1209, 2002.
- [89] W. H. Robertson, K. Karapetian, P. Ayotte, K. D. Jordan, and M. A. Johnson. Infrared predissociation spectroscopy of i-(ch₃oh)_n, n=1,2: Cooperativity in asymmetric solvation. *J. Chem. Phys.*, 116:4853–4857, 2002.
- [90] W. H. Robertson, E. G. Diken, E. A. Price, J. W. Shin, and M. A. Johnson. Spectroscopic determination of the oh- solvation shell in the oh·-(h₂o)_n clusters. *Science*, 299:1367–1372, 2003.
- [91] R. S. Booth, C. J. Annesley, J. W. Young, K. M. Vogelhuber, J. A. Boatz, and J. A. Stearns. Identification of multiple conformers of the ionic liquid [emim][tf₂n] in the gas phase using ir/uv action spectroscopy. *Phys. Chem. Chem. Phys.*, 18:17037–17043, 2016.
- [92] R. Cooper, A. M. Zolot, J. A. Boatz, D. P. Sporleder, and J. A. Stearns. Ir and uv spectroscopy of vapor-phase jet-cooled ionic liquid emim+tf₂n⁻: Ion pair structure and photodissociation dynamics. *J. Phys. Chem. A*, 117:12419–12428, 2013.
- [93] E. I. Obi, C. M. Leavitt, P. L. Raston, C. P. Moradi, S. D. Flynn, G. L. Vaghjiani, J. A. Boatz, S. D. Chambreau, and G. E. Douberly. Helium nanodroplet isolation and infrared spectroscopy of the isolated ion-pair 1-ethyl-3-methylimidazolium bis(trifluoromethylsulfonyl)imide. *J. Phys. Chem. A*, 117:9047–9056, 2013.
- [94] A. E. Khudozhitkov, P. Stange, B. Golub, D. Paschek, A. G. Stepanov, D. I. Kolokolov, and R. Ludwig. Characterization of doubly ionic hydrogen bonds in protic ionic liquids by nmr deuteron quadrupole coupling constants: Differences to h-bonds in amides, peptides, and proteins. *Angew. Chem. Int. Ed.*, 56:14310–14314, 2017.
- [95] E.K. Plyler. Infrared spectra of methanol, ethanol, and n-propanol. *J. Res. Natl. Bur. Stand.*, 48:281–286, 1952.
- [96] K. Liu, M. G. Brown, J. D. Cruzan, and R. J. Saykally. Vibration-rotation tunneling spectra of the water pentamer: Structure and dynamics. *Science*, 271:62–64, 1996.

- [97] K. Nauta and R. E. Miller. Formation of cyclic water hexamer in liquid helium: The smallest piece of ice. *Science*, 287:293–295, 2000.
- [98] *Elementary Quantum Chemistry*, chapter 1, pages 3–18. John Wiley & Sons, Ltd, 2001.
- [99] *Electron Density and Hole Functions*, chapter 2, pages 19–28. John Wiley & Sons, Ltd, 2001.
- [100] K. Burke. Perspective on density functional theory. *J. Chem. Phys.*, 136:150901, 2012.
- [101] P. Hohenberg and W. Kohn. Inhomogeneous electron gas. *Phys. Rev.*, 136:B864–B871, 1964.
- [102] R. D. Johnson, K. K. Irikura, R. N. Kacker, and R. Kessel. Scaling factors and uncertainties for ab initio anharmonic vibrational frequencies. *J. Chem. Theory Comput.*, 6:2822–2828, 2010.
- [103] T. M. Klapötke and A. Schulz. *Quantenmechanische Methoden in der Hauptgruppenchemie*, chapter 6, pages 101–108. Spektrum Akademischer Verlag, 1996.
- [104] F. Weinhold. Natural bond orbital analysis: A critical overview of relationships to alternative bonding perspectives. *J. Comput. Chem.*, 33:2363–2379, 2012.
- [105] F. Weinhold and C. R. Landis. *Hybrids and Bonds in Molecules*, chapter 4, pages 51–91. John Wiley & Sons, Ltd, 2016.
- [106] F. Weinhold and C. R. Landis. *Intermolecular Interactions*, chapter 9, pages 209–230. John Wiley & Sons, Ltd, 2016.
- [107] A. J. Stone. Natural bond orbitals and the nature of the hydrogen bond. *J. Phys. Chem. A*, 121:1531–1534, 2017.
- [108] F. Weinhold, C. R. Landis, and E. D. Glendening. What is nbo analysis and how is it useful? *Int. Rev. Phys. Chem.*, 35:399–440, 2016.
- [109] E. I. Izgorodina, Z. L. Seeger, D. L. A. Scarborough, and S. Y. S. Tan. Quantum chemical methods for the prediction of energetic, physical, and spectroscopic properties of ionic liquids. *Chem. Rev.*, 117:6696–6754, 2017.
- [110] F. Weinhold and R. A. Klein. Anti-electrostatic hydrogen bonds. *Angew. Chem. Int. Ed.*, 53:11214–11217, 2014.
- [111] F. Weinhold and R. A. Klein. Addendum: Anti-electrostatic hydrogen bonds. *Angew. Chem. Int. Ed.*, 53:12992–12992, 2014.

- [112] P. R. Horn, Y. Mao, and M. Head-Gordon. Probing non-covalent interactions with a second generation energy decomposition analysis using absolutely localized molecular orbitals. *Phys. Chem. Chem. Phys.*, 18:23067–23079, 2016.
- [113] F. Weinhold. Polyion covalency: Exotic species from the unexplored world of electrostatically shielded molecular ion chemistry. *Angew. Chem. Int. Ed.*, 56:14577–14581, 2017.
- [114] F. Weinhold. Polyion covalency: Exotic species from the unexplored world of electrostatically shielded molecular ion chemistry. *Angew. Chem.*, 129:14769–14773, 2017.
- [115] F. Weinhold. Theoretical prediction of robust second-row oxyanion clusters in the metastable domain of antielectrostatic hydrogen bonding. *Inorg. Chem.*, 57:2035–2044, 2018.
- [116] M. J. E. A. Frisch, G. W. Trucks, H. B. Schlegel, G. E. Scuseria, M. A. Robb, J. R. Cheeseman, G. Scalmani, V. Barone, B. Mennucci, and G. Petersson. Gaussian 09, revision a. 02, gaussian. *Inc., Wallingford, CT*, 200:28, 2009.
- [117] E. D. Glendening, J. K. Badenhoop, A. E. Reed, J. E. Carpenter, J. A. Bohmann, C. M. Morales, and F. Weinhold. Theoretical chemistry institute. *University of Wisconsin, Madison*, 2001.
- [118] F. Weinhold and C. R. Landis. *Valency and Bonding: A Natural Bond Orbital Donor-Acceptor Perspective*. Cambridge University Press, 2005.
- [119] S. Grimme, J. Antony, S. Ehrlich, and H. Krieg. A consistent and accurate ab initio parametrization of density functional dispersion correction (dft-d) for the 94 elements h-pu. *J. Chem. Phys.*, 132:154104, 2010.
- [120] S. Ehrlich, J. Moellmann, W. Reckien, T. Bredow, and S. Grimme. System-dependent dispersion coefficients for the dft-d3 treatment of adsorption processes on ionic surfaces. *ChemPhysChem*, 12:3414–3420, 2011.
- [121] S. Grimme, A. Hansen, J. G. Brandenburg, and C. Bannwarth. Dispersion-corrected mean-field electronic structure methods. *Chem. Rev.*, 116:5105–5154, 2016.
- [122] G. Meyer and N. M. Amer. Novel optical approach to atomic force microscopy. *Appl. Phys. Lett.*, 53:1045–1047, 1988.
- [123] S. Alexander, L. Helleman, O. Marti, J. Schneir, V. Elings, P. K. Hansma, M. Longmire, and J. Gurley. An atomic-resolution atomic-force microscope implemented using an optical lever. *J. Appl. Phys.*, 65:164–167, 1989.
- [124] F. Moreno-Herrero and J. Gomez-Herrero. *AFM: Basic Concepts*, chapter 1, pages 1–34. John Wiley & Sons, Ltd, 2012.

- [125] F. Moreno-Herrero, P. J. de Pablo, J. Colchero, J. Gómez-Herrero, and A. M. Baró. The role of shear forces in scanning force microscopy: a comparison between the jumping mode and tapping mode. *Surf. Sci.*, 453:152 – 158, 2000.
- [126] R. G. Horn, D. F. Evans, and B. W. Ninham. Double-layer and solvation forces measured in a molten salt and its mixtures with water. *J. Phys. Chem.*, 92:3531–3537, 1988.
- [127] R. G. Horn and J. N. Israelachvili. Direct measurement of structural forces between two surfaces in a nonpolar liquid. *J. Chem. Phys.*, 75:1400–1411, 1981.
- [128] M. Antognozzi, A. D. L. Humphris, and M. J. Miles. Observation of molecular layering in a confined water film and study of the layers viscoelastic properties. *Appl. Phys. Lett.*, 78:300–302, 2001.
- [129] R. Hayes, S. Z. El Abedin, and R. Atkin. Pronounced structure in confined aprotic room-temperature ionic liquids. *J. Phys. Chem. B*, 113:7049–7052, 2009.